The Development of a Test Rig to Determine Fouling Factors of Feedwater Heaters

Prepared by:

Nicolaas Hallatt

HLLNIC025

Department of Mechanical Engineering

University of Cape Town

Supervisor:

A/Prof Wim Fuls

March 2019

Submitted to the Department of Mechanical Engineering at the University of Cape Town in partial fulfilment of the academic requirements for a Masters of Science degree in Mechanical Engineering

Key Words: Feedwater Heater, Fouling Factors, Test Rig

Abstract

Feedwater heaters are large shell and tube heat exchangers. They from part of the Rankine cycle used in coal fired power plants with the main purpose being the improvement of the overall cycle efficiency. Like most heat exchangers, feedwater heaters suffer from fouling.

Fouling is defined as “any undesirable deposit on heat exchanger surfaces that increases resistance to heat transmission”. In the design of heat exchangers, fouling is accommodated by adding additional surface area to the heat exchanger. The amount of additional area is determined by the use of fouling factors. Although this is the only wide-spread method accepted in industry, the fouling factors in use are outdated, generally considered conservative and lead to oversized heat exchangers.

The purpose of this study was to design and build a test rig that can accurately measure fouling factors of feedwater heater tubes that has been in service for a full life cycle. A comprehensive literature study was performed to decide on the most effective test method, as well as the required instrument type and accuracy. The best method was found to be where the overall heat transfer coefficient for a fouled tube, outside cleaned tube (half clean) and clean tube was measured. The measured values are then converted to the internal, external and overall fouling factors.

Validation test were done on the test rig. These included energy balance tests, theoretical comparison tests and repeatability tests. The results of all tests were acceptable and within measurement uncertainty limits.

Five sample test tubes, obtained from a 30 year old LP heater at an Eskom power station, were tested. The results indicated that the average measured fouling factors were less than 20% of the commonly used HEI fouling factors. This is significantly lower and confirms that the fouling factors in use for this specific case are conservative.

The test rig proved to be accurate and effective in measuring the fouling factors. Although the tests shows promising results, the small amount of tubes tested from only one heat exchanger are not sufficient to make meaningful conclusions. The test rig is now ready for a future study where a large sample of tubes can be tested.

Declaration

I, Nicolaas Johannes Hallatt, hereby declare the work contained in this dissertation to be my own. All information which has been gained from various journal articles, text books or other sources has been referenced accordingly. I have not allowed, and will not allow, anyone to copy my work with the intention of passing it off as their own work or part thereof.

This thesis/dissertation has been submitted to the Turnitin module and I confirm that my supervisor has seen my report and any concerns revealed by such have been resolved with my supervisor.

Signed by candidate

_____

Nicolaas Johannes Hallatt

Acknowledgements

The acknowledgements will be done in Afrikaans, the mother tongue of the student.

Ek wil eerstens dankie sê vir ons hemelse Vader vir die geleentheid, talente en gawes uit Sy hand ontvang. Sonder Hom is niks moontlik nie.

Die Eskom RT&D flowlab personeel, spesifiek Ferdi Liebenberg. Sonder sy hulp, raad en motivering sou die projek nie moontlik gewees het nie. Na die projek is ek nie net ‘n uitstekende mentor nie, maar ook ‘n kollega en goeie vriend ryker.

Eskom se EPPEI program, vir die wonderlike geleentheid.

My mentors in die projek, A/Prof Wim Fuls en Dr. Francois du Preez, dankie vir die raad, opinies en leiding, dit word opreg wardeer.

Carl Kohrs en Ockert Augustyn, kollegas en buurmanne in die kantoor. Dankie vir die klankbord, opinies en gedagtes wissel. Dit was baie waardevol.

My vrou Suret en ons twee pragtige kinders Nico (4) en Anke (2). Julle is en sal vir altyd die belangrikste mense in my lewe bly. Alles wat ek doen is direk of indirek vir julle.

Table of Contents

List of Figures

List of Tables

List of Nomenclature

General Symbols

A	Area [m²]
b_R	Systematic Uncertainty of the result
$b_{R,Cal}$	Systematic standard uncertainty of the calibration standard. It is the combination of the calibration standard's systematic and random uncertainties into the systematic uncertainty of the instrument under calibration
b_{sd}	The systematic standard uncertainty of the calibration standard
$b_{\bar{X}}$	Systematic Standard Uncertainty
$B_{\bar{X}}$	Systematic Uncertainty
C_p	Specific heat [kJ/kg.K]
d	Diameter [m]
f	Darcy Friction Factor
g	Gravitational acceleration [m/s²]
h	Enthalpy [kJ/kg]
h	Heat Transfer Coefficient [W/m².K]
k	Conductivity [W/m.K]
L	Length [m]
$LMTD$	Log Mean temperature difference [°C]
$\dot{m}$	Mass flow rate [kg/s]
N_{cal}	Number of data points in the calibration line fit
Nu	Nusselt Number
P	Pressure [kPa]
Pr	Prandtl Number
Q	Heat Transfer [kW]
R	Heat Transfer Resistance [m².K/W]
r	Radius [m]
Ra	Raleigh Number
Re	Reynolds Number
R_f	Overall Fouling Factor [m².K/W]
R_i	Internal Fouling Factor [m².K/W]
R_o	External Fouling Factor [m².K/W]

s_R	Random Uncertainty of the result
$s_{R,cal}$	Standard deviation of calibration data
$s_{\bar{R},cal}$	Random standard uncertainty of the calibration
$S_{\bar{X}}$	Random Uncertainty
$s_{\bar{X}}$	Random Standard Uncertainty
s_X	Sample standard deviation
t	Students Multiplier / Coverage Factor
T	Temperature [°C]
U	Overall Heat Transfer Coefficient [W/m².K]
U_I	Manufacturers quoted instrument uncertainty or accuracy specification for the instrument under calibration. It is assumed to be 95% with infinite degrees of freedom
U_R	Expanded Uncertainty of the result
u_R	Combined Uncertainty of the Result
$U_{\bar{X}}$	Expanded Uncertainty
$u_{\bar{X}}$	Combined Uncertainty
$U_{95,Cal}$	Simplified calibration uncertainty for the instrument
$U_{95,IS}$	In-Spec Calibrated Uncertainty
v	Velocity [m/s]
X	Measured value
$\bar{X}$	Sample mean

Greek symbols

α	Thermal diffusivity $= \frac{k}{\rho C_p}$ [m²/s]
β	volumetric thermal expansion coefficient [1/K]
δ	Total Error
μ	Dynamic Viscosity [Pa.s]
ν	Kinematic Viscosity $= \frac{\mu}{\rho}$ [m²/s]
ε	Relative pipe roughness
ε	Emissivity
ρ	Density [kg/m³]
σ	Stefan Boltzmann constant [W/m²K⁴]

Subscripts

ann	annulus
b	bulk
c	cold
CL	cold Loop
clean	no fouling
fouled	fouled on the internal and the external surface
h	hot
h	hydraulic
half clean	fouled on the internal surface only
HL	hot loop
i	inlet / internal
m	medium
o	outlet / external
out	outer surface
r	radiation
s	surface
w	wall
∞	surroundings

Acronyms and Abbreviations

ASME	American Society of Mechanical Engineers
ASTM	America Society for Testing and Materials
BS	British Standards
DIN	Deutsches Institut für Normung
EN	European Stanards
GNP	Gross National Product
HEI	Heat Exchanger Institute
HPWJ	High Pressure Water Jet
NB	Nominal Bore
NIST	National Institute of Standards and Technology
OD	Outer Diameter
P&ID	Piping and Instrumentation Diagram
PER	Pressure Equipment Regulations
PN	Pressure Nominal

PTFE	Polytetrafluoroethylene
RT&D	Eskom Research Testing and Development
RTD	Resistance Temperature Detectors
SEE	Standard Estimate of Error
TEMA	Tubular Exchangers Manufacturers Association
T/C	Thermocouples
TTD	Terminal Temperature Difference

1.Introduction

1.1 Background

Feedwater heaters are large shell and tube heat exchangers. The main purpose of feedwater heaters is to increase the thermal efficiency of the Rankine cycle used in coal-fired and nuclear power stations. During operation, a number of mechanisms can cause scaling or deposition on the inside and outside of the tubes. This deposit is called fouling.

1.2 Problem description

The thermal conductivity and hence the resistance to heat transfer of the fouling layers is significantly higher than that of the tube material as can be seen in Table 1-1. Due to this low conductivity, a thin fouling layer can cause a significant decrease in the thermal performance of heat exchangers.

Table 1-1: Thermal Conductivity of some fouling layers and heat exchanger tubes materials [1]–[4]

Typical Fouling Deposits	Conductivity [W/m.K]	Typical Heater Exchanger Tube Materials	Conductivity [W/m.K]
Sodium aluminium silicate	0.2–0.4	Carbon Steel (EN 10028 P265 GH)	55.2
Hematite (iron oxide)	0.6	Stainless Steel (AISI 304)	14.9
Magnetite (iron oxide)	2.9	EN 10028 16Mo3	49.5
Biofilm	0.7	EN 10028 10CrMo9-10	37.09
Calcite (boiler deposit)	0.9	Brass (70% Cu, 30% Zn)	110
Calcium sulphate	2.3	Pure Aluminium	237
Calcium carbonate	2.9	Aluminium Alloy 2024-T6	177

A recent investigation done by the author on a feedwater heater in the Eskom fleet showed how severe the decrease in performance can be. For this specific feedwater heater fouling layers consisting of a combination of hematite and magnetite measuring between 0.1 mm - 0.5 mm thick was observed [5]. If the worst case of a 0.5 mm thick layer is used in the thermal analysis of the heater it results in a decrease of up to 20°C in the feedwater outlet temperature. That is more than 50% of the total temperature rise across the heat exchanger. Figure 1-1 below shows the effect on the thermal performance for the heater in question for different fouling layer thicknesses. The calculation was done for full load conditions. The thermal conductivity of the fouling was determined using a combination of 15% magnetite and 85% hematite with the conductivity values as given in Table 1-1 above. Note that Terminal temperature difference (TTD) on secondary axis is defined in section 2.2.4.

Additional area is added when the feedwater heaters are designed to ensure that even with a certain amount of fouling, the feedwater heater can still perform according to its design parameters. This does lead to larger heat exchanger when compared to the design case or the so-called “clean condition”.

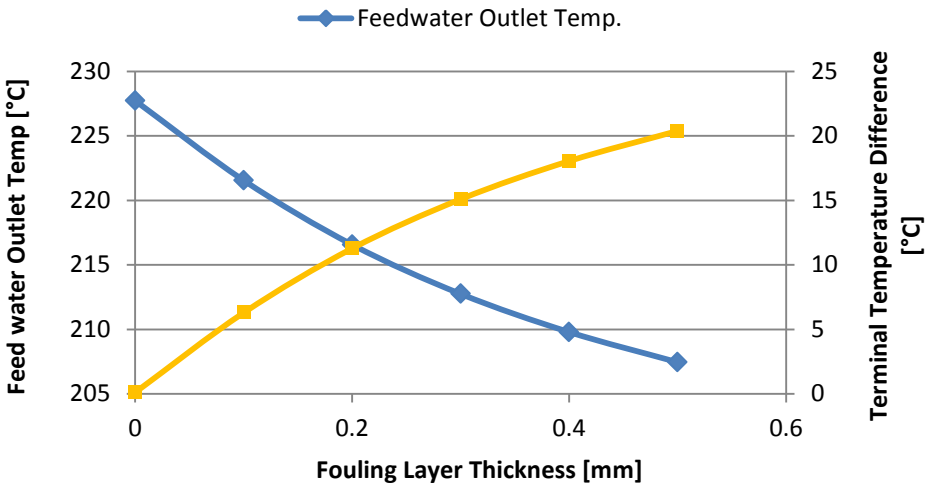

Figure 1-1: Effect of fouling on Feedwater heater performance

The amount of additional heat transfer surface area is determined by fouling factors found in heat exchanger standards used in industry. The fouling factor adds additional resistance to heat transfer when the required area is calculated. These fouling factors are generally considered conservative and can lead to oversized heat exchangers that increase costs unnecessarily. An example of this can be seen in Figure 1-2 below. The blue bar indicates the required heat transfer surface area for the different zones as well as the total area for the specific feedwater heater in the clean condition. The red bar indicates the same when the commonly used Heat Exchanger Institute (HEI) [6] fouling factors are used. In this example, the fouling case represents an increase of up to 20% in the area. For feedwater heaters in general, the value is typically 10% - 20%.

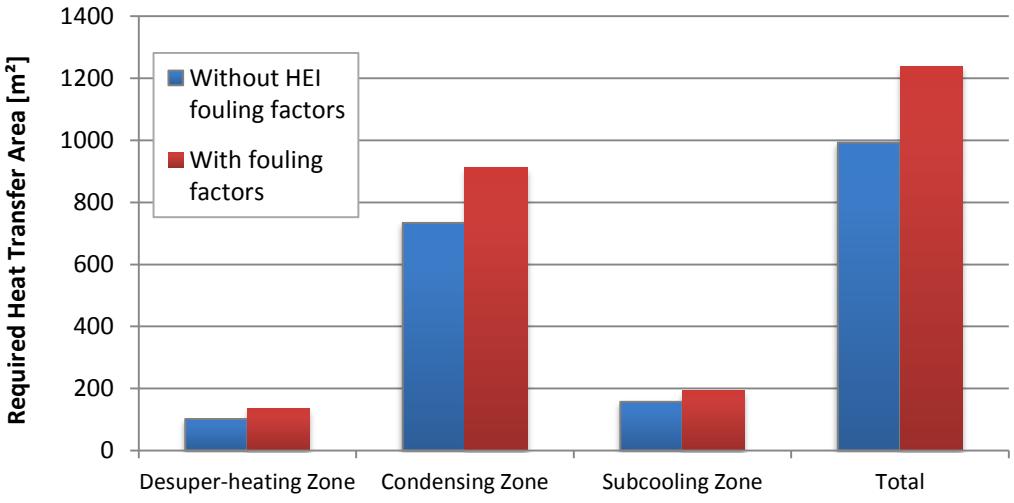

Figure 1-2: Comparison of required heat transfer surface area in clean and fouled conditions

When considering general industry this value increases significantly. Muller-Steinhagen reported in [7] that the practice of specifying fouling resistances increases heat transfer areas by 20-300%. The results of the study are presented graphically in Figure 1-3.

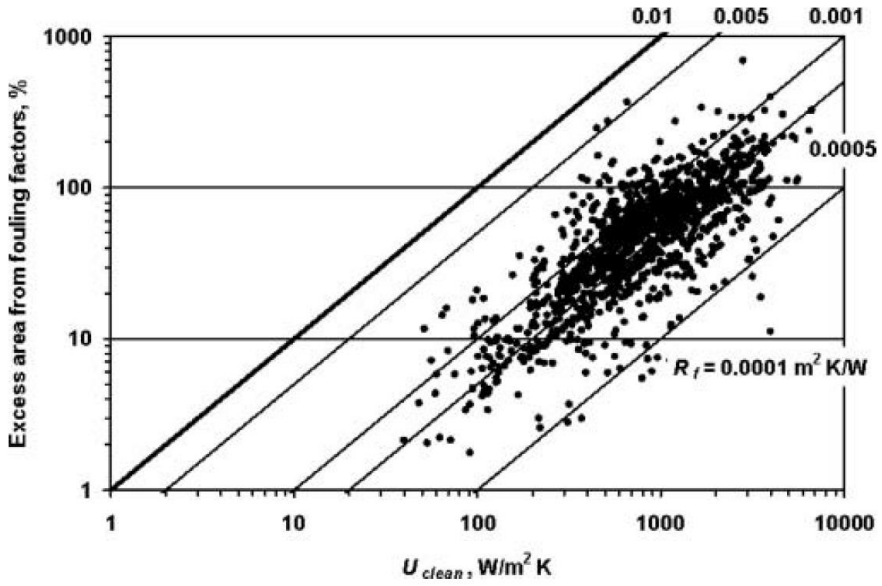

Figure 1-3: Impact of fouling factors on the design of 2000 heat exchangers [7]

1.3 Opportunity to determine actual fouling

Eskom has an installed capacity in excess of 40 000 MW. The majority of this is coal and nuclear Power stations. Both these types of power stations make use of the Regenerative Rankine Cycle and thus feedwater heaters. When Medupi and Kusile are completed there will be more than 700 feedwater heaters installed in Eskom.

A number of these feedwater heaters are nearing the end of their life and are being replaced. Currently, six power stations are busy with projects to replace feedwater heaters. Since it is very difficult and thus very expensive to remove feedwater heater tubes from heaters in operation, sample tubes can only be obtained when heaters reach the end of their life and are scrapped and replaced with new ones. In the foreseeable future, a large number of feedwater heater tubes that have been in service for a full heater life cycle of approximately 30 years will become available.

This puts Eskom in a position to determine the amount of fouling that has actually occurred on feedwater heater tubes in a full lifecycle under Eskom operating conditions. Although the amount of fouling is dependent on a number of variables, most importantly the cycle chemistry, these are controlled according to the same specifications throughout the Eskom fleet.

The fouling factor of the fouling that has occurred can be determined. This can be accomplished by designing and building a heat transfer test facility or test rig that can accurately measure the amount of heat transfer through the tubes.

1.4 Research questions and hypothesis

1.4.1 Research Questions

1. How is fouling included in the design of heat exchangers in industry?
2. What fouling factors are prescribed in literature and are used in industry for feedwater heaters?
3. What are the actual fouling factors found on feedwater heater tubes samples?
    - What is the optimum way to test heat transfer of feedwater heater tubes?
    - What are the requirements and specification for a test facility to test heat transfer through tubes?
    - How accurate must the test facility be?
    - What are the uncertainties associated with the result obtained by the test facility?

1.4.2 Hypotheses

Given a well-designed test facility with adequate instrumentation the fouling factors found on sample feedwater heater tubes can be measured with acceptable accuracy.

1.5 Purpose of the study

The above-mentioned problem, research questions and hypothesis lead to the formulation of a study that can investigate the problem, utilise the opportunity and answer the research questions.

The purpose of the study is as follows:

- To design and construct a test rig that can accurately measure the heat transfer and determine the fouling factors on sample feedwater heater tubes.

To achieve this purpose the following activities will be investigated and undertaken:

- Review heat transfer calculation methodology.
- Investigate different types of fouling found on heat exchanger and specifically on feedwater heater tubes.
- Investigate different methodologies used in heat exchanger design to accommodate and minimise fouling.
- Investigate Heat transfer measurement methodology.
- Investigate and evaluate similar test facilities designed and used by others.
- Develop a specification for the test facility.
- Design the test facility that complies with the specification.
- Determine the required uncertainty for the testing facility.
- Determine what types of instrumentation must be used that will provide acceptable accuracy and uncertainty.

- Build the test facility at the Eskom RT&D facilities in Rosherville, Johannesburg.
- Demonstrate that the test rig can measure fouling factors of available feedwater heater tubes samples with the required accuracy.
- Determine the uncertainties of measurement and propagate those to determine the uncertainty associated with the results.

1.6 Scope limitations

The following are excluded from the scope of this study

- The purpose of the test rig is to test tubes that are removed from service and are already in a fouled condition. No fouling growth tests will be done.
- The scope of the study includes the design, manufacture, and commissioning of the test rig. The amount of actual testing will be limited. Most of the actual testing will be done by a future study.
- No correlation will be made between the chemistry under which the tubes operated and the actual amount of fouling that have occurred.
- The actual fouling and reasons for fouling will not be investigated, nor will an attempt be made to suggest new or alternative methods to reduce the formation of fouling.

1.7 Outline

Chapter 1: Introduction

This chapter provides the background and introduction to the problem that leads to the purpose of the study and what the study aims to achieve. The limitations imposed on the study are provided.

Chapter 2: Theory

Relevant theory that provides background on feedwater heaters and typical process calculations that are used in the design of heat exchangers and the test rig are reviewed in this chapter.

Chapter 3: Literature review

A detailed literature review is done in this chapter. The definition of fouling, the cost of fouling, the different types of fouling and the effect of different process parameters on fouling are covered. The different methods to design heat exchangers for fouling are considered. The chapter then continues to identify numerous methods and experimental facilities that can measure heat transfer in different geometries. Uncertainty analysis is reviewed in detail. Different methods used in industry for flow and temperature measurement are reviewed and the advantages and

disadvantages considered. The chapter ends with an overview of calibration of these types of instruments.

Chapter 4: Experimental facility

This chapter start with an explanation of the fouling factor test methodology. A technical specification is then developed for the test rig. The best concept from the different available methods for heat transfer measurement is selected. The process design and mechanical design in the form of component selection are provided. The budget and manufacturing are discussed. Details of the calibration done on the different instruments are provided. The chapter end with notes and issues experienced during commissioning.

Chapter 5: Experimental Work

In this chapter, the validation tests and results are discussed. The actual test methodology and the results of the sample tubes that were tested are provided. Results of the uncertainty analysis are provided.

Chapter 6: Discussion and conclusion

This chapter discusses the performance of test rig and provide improvement that can be considered going forward. The results that were obtained from the tested sample tubes are discussed and recommendations made on the initial proposed theory regarding the conservativeness of the fouling factor used and the need for testing to be continued. The chapter ends with a discussion on the uncertainty of the test rig and improvements thereof.

2. Theory

The purpose of this section is to give the necessary theory and background that is required and will be used to carry out the work. It will give an overview of the Rankine cycle and feedwater heaters and discuss the basic flow mechanics and heat transfer theory.

2.1 The Rankine cycle

The Rankine cycle is used in most thermo-electric power plants to convert the heat energy from a coal combustion process or a nuclear fission process to rotational mechanical energy. The rotational mechanical energy is then converted to electrical energy and supplied to the power grid. The main components of the simple Rankine cycle are the turbine, condenser, pump and steam generator or boiler. These are connected as shown in Figure 2-1. Water and steam are used as the flow medium.

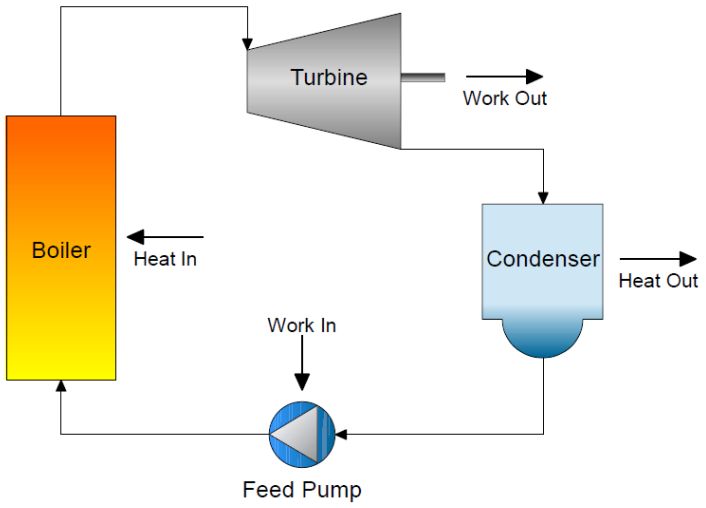

Figure 2-1: Simple Rankine Cycle

The efficiency of the basic Rankine cycle can be improved in a number of ways [8]. This includes:

- Reducing Condenser Pressure.
- Increasing Boiler Pressure and Temperature.
- Using Superheat.
- Using Reheat.
- Using Feedwater Heaters.

A schematic of a typical coal power plant is shown in Figure 2-2. All the main components of a simple and improved Rankine cycle are shown. Figure 2-3 shows the T-s Diagram for the main

processes of the Rankine cycle. The numbers and letters correspond to the number and letters in Figure 2-2. The addition of feedwater heaters makes the process a Regenerative Rankine Cycle.

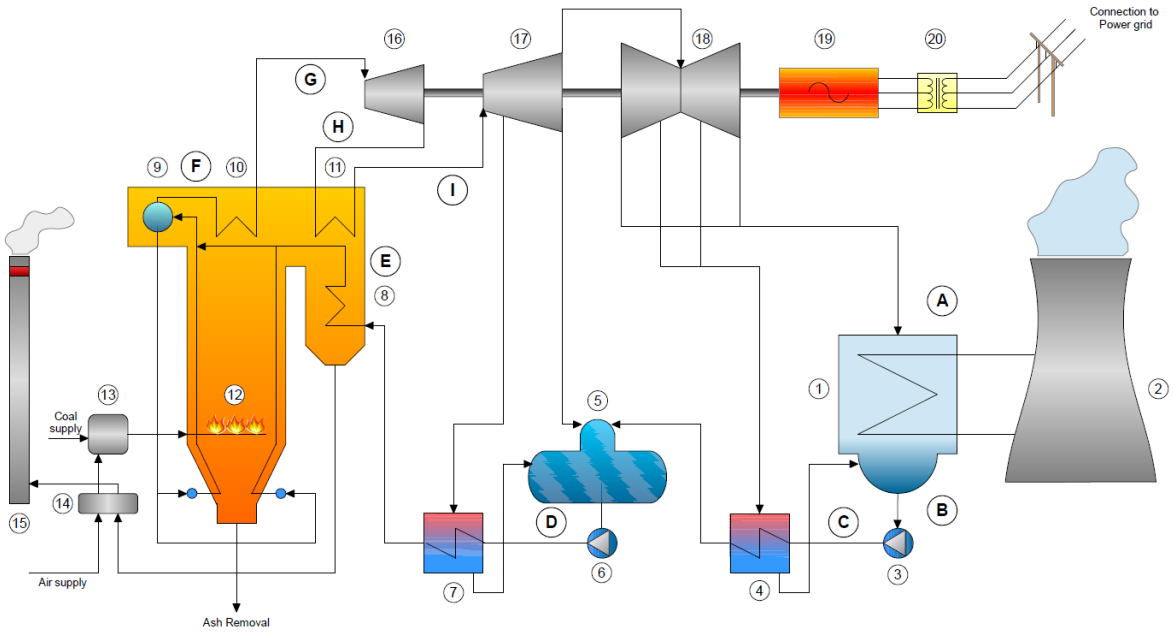

1. Condenser	6. Boiler Feed Pump	11. Re-heater	16. High-Pressure Turbine
2. Cooling Tower	7. High-Pressure Feedwater Heaters	12. Burners	17. Intermediate Pressure Turbine
3. Condensate Extraction Pump	8. Economiser	13. Mills	18. Low Pressure Turbine
4. Low-Pressure Feedwater Heaters	9. Boiler Drum	14. Air Heater	19. Generator
5. Feedwater Storage Tank	10. Superheater	15. Smoke Stack	20. Transformer

Figure 2-2: Basic Coal-Fired Power plant schematic

The section below will give a high-level overview of the cycle and the main components. Since it is a closed loop cycle any point can be used as the starting point. For this explanation, the condenser inlet (A) is used.

Wet steam enters the condenser (A) (1) where the latent heat is removed by cooling water from the cooling towers (2) and condensed to saturated liquid (B). From here it is pumped by the Condensate Extraction pumps (C) (3) through the Low-Pressure heaters (4) where extraction steam from the LP turbine (18) are used to heat the water to the Feedwater storage tank (5).

The water is fed to boiler feedwater pumps (D) (6) where it is pumped through the High-Pressure heaters (7) that are heated with extraction steam from the Intermediate Pressure turbine (17) to the boiler economiser (E) (8). From the economiser the flow is directed to the boiler drum (9) where it is heated by the boiler side walls to boiling point (F). Saturated steam from the boiler drum is taken to the superheater (10) where the steam is heated to superheated steam (G).

The steam is expanded through the High-Pressure turbine (H) (16) and converts the thermal energy to mechanical energy. The steam is heated again in the re-heater (I) (11) and expanded

through the Intermediate pressure and Low-Pressure turbines (17) (18). The Low-Pressure turbine exhaust to the Condenser (A) (1) and the cycle repeats itself.

The Rankine cycle as depicted in Figure 2-2 is plotted on a Temperature-Entropy (T-s) diagram below. The temperature increase across the pumps (C & D) is exaggerated to allow it to be visually observable. All other values are based on the full load heat balance for a specific 600 MW Eskom Power station.

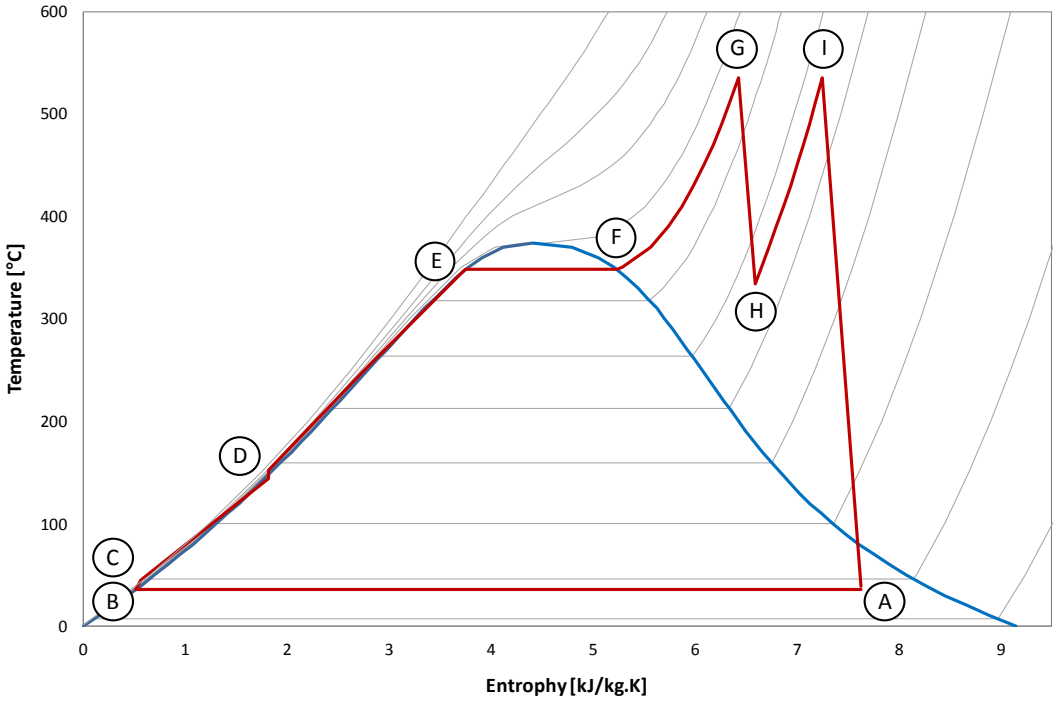

Figure 2-3: Modified Rankine Cycle is shown on T-s diagram for typical coal power plant

In 2009, thermoelectric power plants using the Rankine cycle in the US generated almost 90% of all power [9]. In Eskom, the situation is similar with 89.47% (38301 MW) of total nominal capacity [10] of which the majority is coal-fired. For the overall South African power grid, the percentage of thermo-electric power plants using the Rankine cycle is 83.8% [10].

2.2 Feedwater heaters

2.2.1 Purpose of feedwater heaters

A large inefficiency in the overall Rankine cycle is the irreversibility in the economiser associated with the addition of heat at a high-temperature differential [8]. Feedwater heating is used to reduce this temperature differential. Steam is extracted from the turbine at various positions and used to pre-heat the feedwater before it enters the boiler. The steam is condensed in the feedwater heaters. This recovers the latent heat in the steam that would otherwise be lost in the condenser and cooling towers if the steam passed through the complete turbine.

Naga Raju et al. [11] did a study on two power plant units of 210 MW. They showed that the unit efficiency can be increased from 36.03% to 42.6% with the addition of feedwater heaters.

Grosser and Bouwer [12] compared the heat rate of a modern large capacity turbine generator plant involving seven stages of feed heating with a hypothetical plant of the same generating capacity. The heat rate of the plant with feedwater heaters was found to be 0.86 of that of the hypothetical plant without feedwater heaters. If the heat rate from the heat balance diagram of the station in question is used this represents an increase in efficiency of approximately 6%.

All of these examples represent a significant increase in efficiency. A rule of thumb mentioned regularly in industry is that a 1 percentage point efficiency increase can be observed for each stage of feedwater heating. This amount is however limited, as there is a diminishing return on investment for each added feedwater heater.

2.2.2 Types of feedwater heaters

All closed feedwater heaters are shell and tube type heat exchangers. Two different technologies are used in the construction of feedwater heaters. This results in two main types of feedwater heaters. These are tube sheet and header type feedwater heaters.

The tube sheet type heaters (Figure 2-4) are characterised by a thick tube sheet that divides the water box or water side of the heater and the shell or steam side of the heater. The feedwater is fed through the tubes and the extraction steam from the turbine are cooled and condensed in the shell. Tubes are attached to the tube sheet by various means that include expansion and welding and are normally in a two-pass configuration. Tube sheet type heaters are generally considered smaller and less expensive than header type heaters for similar heat loads. They can suffer from reliability issues when subjected to a high amount of start-up and shut down cycles. This is mainly due to the high and varying temperature differentials across the tube sheet.

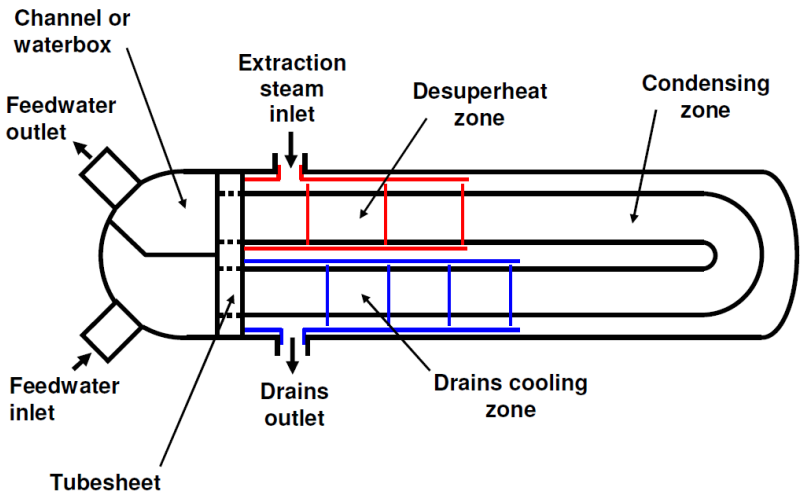

Figure 2-4: Tube sheet type feedwater heater [8]

Header type heaters (Figure 2-5) are based on the same technology used for the large flow distribution headers found in power utility scale boilers. Thick-walled cylindrical headers are used to divide the water side and shell side of header heaters. Tubes are welded to nipples that are in turn welded to the headers. Separate headers are used for the water inlet and water outlet. The headers penetrate the shell to connect feedwater piping and allow for maintenance access. Header type heaters are not so sensitive to cyclic loads and generally give higher reliability and longer life than tube sheet heaters. This does however come at an increase in price and higher maintenance costs due to the difficulty in accessing the headers which are typically 450 mm in diameter.

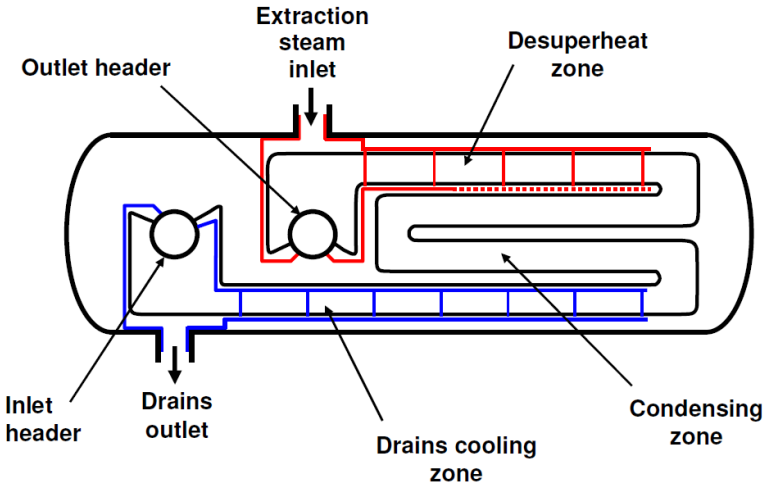

Figure 2-5: Header type feedwater heater [8]

In Eskom the use of the different types of heaters are as follows:

- All low-pressure heaters are tube sheet type.
- High-pressure heaters for all stations built before 1979 was originally fitted with tube sheet heaters. The last station fitted with tube sheet heaters in 1976 was later changed to header heaters due to reliability issues experienced with the tube sheet heaters.
- High-pressure heaters for all stations built after 1979 including the new built projects are fitted with header type high-pressure heaters.

2.2.3 Different zones in feedwater heaters

Feedwater heaters can consist of different zones within one shell. These are typically referred to as the De-superheating zone, the Condensing zone and the drains cooling zone.

The reason for the different zones is that the heat exchanger design is highly dependent on the fluid phase and properties that participate in the heat transfer. On the shell side of a feedwater heater, the heating medium sometimes starts off as superheated steam. The first section of the

heat exchanger is thus to remove the superheat from the steam. In the second part condensation takes place and in the third part, the condensed steam is subcooled. For each of these sections, a different optimal arrangement is required.

The different zones can be seen in Figure 2-4 and Figure 2-5 where the de-superheating zone is indicated in red and the subcooling zone in blue. The remainder of the heater is the condensing zone. The condensing zone is typically significantly larger than the other two zones as can be seen in Figure 1-2 above. This was confirmed by the work done by Hussaini et al. [13] that confirmed that the maximum heat duty was found in the condensing zone for all cases studied.

The difference in heat duty and temperature changes of a typical three-zone feedwater can be presented graphically [8] as can be seen in Figure 2-6. The blue line represents the feedwater flow with the inlet on the right of the figure and outlet on the left. The red line represents the steam with the inlet on the left and the outlet on the right.

2.2.4 Performance measurement of feedwater heaters

A number of different parameters are used as input to the design and to determine or measure the performance of feedwater heaters. are given below as defined in [8]:

- Terminal Temperature Difference (TTD): Temperature difference between the saturation temperature in the heater and the feedwater temperature at the heater outlet.
- Drains Cooler Approach (DCA): Temperature difference between the feedwater temperature at the heater inlet and the temperature of the outgoing distillate drains.

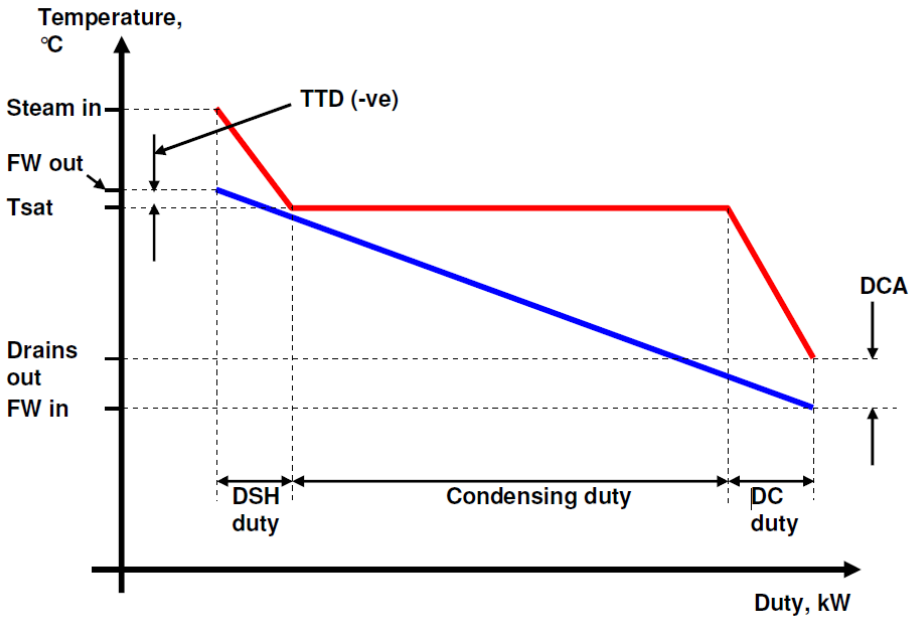

Figure 2-6: Temperature Profile in a 3 zone feedwater heater [8]

2.3 Mechanics of fluids

2.3.1 Pressure drop in pipes

For all piping pressure drop calculations the well-known and widely used Darcy-Weisbach equations will be used. This can be given in head loss or pressure loss form. The pressure loss form is given below:

$$\Delta P = f\frac{L}{d}\frac{\rho v^2}{2} \tag{2-1}$$

2.3.2 Friction factor correlations

The friction factor is an essential variable used in a variety of industrial applications. For this work, it is used in both the Darcy-Weisbach pressure drop equation for flow in pipes as well as the Gnielinski correlation for the heat transfer inside a pipe and an annulus. The accepted method for calculating the friction factor is the implicit Colebrook White equation. In [14] it is given as:

$$\frac{1}{\sqrt{f}} = -2log\left(\frac{2.51}{Re\sqrt{f}} + \frac{\varepsilon}{3.7}\right) \tag{2-2}$$

Due to the implicit nature of the Colebrook White Equation, it was plotted on what is now the well-known *Moody Chart.* The implicit form of the equation makes quick calculation difficult. For these reasons, a large number of approximations have been proposed. A very good and thorough overview, as well as a statistical analysis of these, are given by Genic et al. in [14]. The approximation that is recommended by Genic et al. and that will be used for this work is that of Zigrang and Sylvester [15] which was proposed in 1982. It is as follows:

$$f = \left\{-2log\left[\frac{\varepsilon}{3.7} - \frac{5.02}{Re}log\left(\varepsilon - \frac{5.02}{Re}log\left(\frac{\varepsilon}{3.7} + \frac{13}{Re}\right)\right)\right]\right\}^{-2} \qquad \begin{matrix} Re = \ 4000 - \ 10^8 \\ \varepsilon = \ 0.00004 - 0.05 \end{matrix} \tag{2-3}$$

2.4 Heat transfer analysis

The purpose of this section is to give the required theory to simulate and model heat exchangers. The following sections are discussed specifically for a counter flow heat exchanger that will be used in the experimental work as shown in Figure 2-7 below.

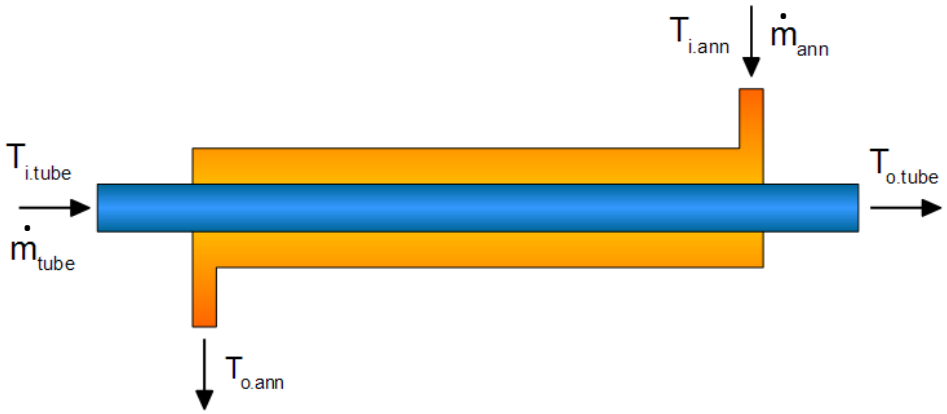

Figure 2-7: Counterflow heat exchanger

2.4.1 Governing equations

The governing equation for heat transfer as given in [16] is:

$$Q = UA(T_1 - T_2) \tag{2-4}$$

U is the overall heat transfer coefficient between two points where the temperatures are T_1 and T_2 respectively with *A* being the heat transfer surface area.

If applied to heat exchangers, equation (2-4) becomes [1]:

$$Q = U_{out}A_{out}LMTD \tag{2-5}$$

In Equation (2-5) the outside tube area is typically used as reference area as well as reference for the overall heat transfer coefficient.

The following can be written for the hot side of the heat exchanger:

$$Q_h = \dot{m}_h C_p\left(T_{h,i} - T_{h,o}\right) = \dot{m}\left(h_{h,i} - h_{h,o}\right) \tag{2-6}$$

And similar for the cold side:

$$Q_c = \dot{m}_c C_p\left(T_{c,o} - T_{c,i}\right) = \dot{m}\left(h_{c,o} - h_{c,i}\right) \tag{2-7}$$

The total heat transferred in the heat exchanger is equal to the energy gained by the cold stream and the energy lost by the hot stream:

$$Q = Q_h = Q_c \tag{2-8}$$

When analysing a counter flow heat exchanger as shown in Figure 2-7 above with the inlet conditions and the area known, equation (2-5), (2-6) and (2-7) needs to be solved simultaneously to solve for Q, $T_{h,o}$ and $T_{c,o}$.

2.4.2 Log mean temperature difference

The Log Mean Temperature Difference or LMTD gives the temperature driving force for heat transfer in a heat exchanger. It is a function of the inlet and outlet temperatures of both streams and is determined differently for parallel-flow and counter-flow heat exchangers. It is given in [1] as:

$$LMTD = \frac{\Delta T_2 - \Delta T_1}{\ln(\frac{\Delta T_2}{\Delta T_1})} = \frac{\Delta T_1 - \Delta T_2}{\ln(\frac{\Delta T_1}{\Delta T_2})} \tag{2-9}$$

For a parallel flow heat exchanger:

$$\begin{aligned} \Delta T_1 &= T_{h,i} - T_{c,i} \\ \Delta T_2 &= T_{h,o} - T_{c,o} \end{aligned} \tag{2-10}$$

For a counter flow heat exchanger:

$$\begin{aligned} \Delta T_1 &= T_{h,i} - T_{c,o} \\ \Delta T_2 &= T_{h,o} - T_{c,i} \end{aligned} \tag{2-11}$$

2.4.3 Overall Heat transfer coefficient

The overall heat transfer coefficient is defined in terms of total thermal resistance between the two fluids in the heat exchanger [1]. The total thermal resistance is the sum of a number of resistances. This includes:

- Inside film boundary layer resistance $(R_{h,i})$.
- Inside fouling resistance $(R_{F,i})$ or (R_i).
- Conduction through tube wall resistance (R_W).
- Outside fouling resistance $(R_{F,o})$ or (R_o).
- Outside film boundary layer resistance $(R_{h,o})$.

The different resistances and associated temperatures indicated as T_1 to T_6 can be seen in Figure 2-8.

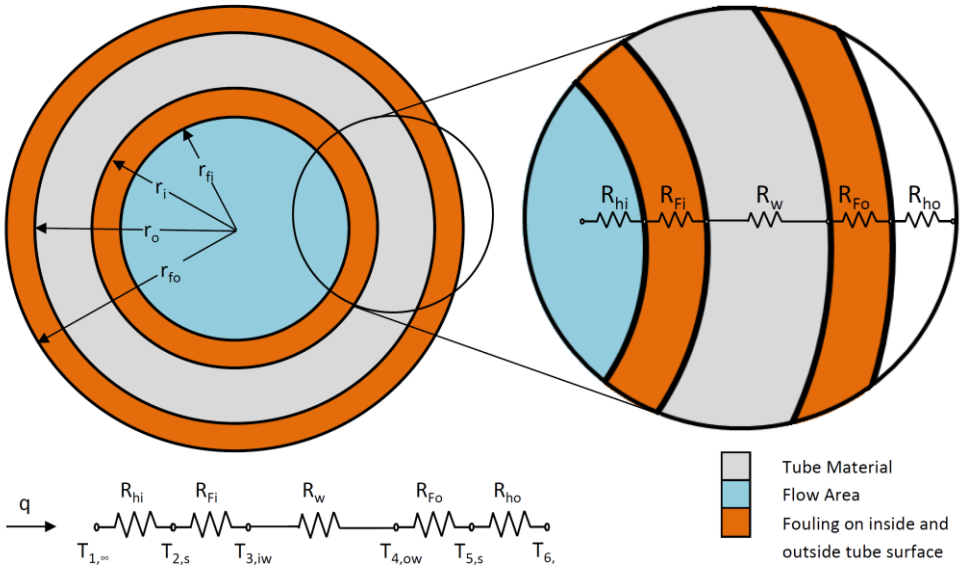

Figure 2-8: Resistance to heat transfer of a single tube with fouling layers on the inside and outside of the tube

The Overall heat transfer coefficient is typically given in the following form for clean tubes [1]:

$$\frac{1}{U_{clean}A} = \frac{1}{U_{i,clean}A_i} = \frac{1}{U_{o,clean}A_o} = \frac{1}{h_i A_i} + \frac{\ln\frac{d_o}{d_i}}{2\pi k_w l} + \frac{1}{h_o A_o} \tag{2-12}$$

The equation can also be written to include allowances for fouling [1].

$$\frac{1}{U_{fouled}A} = \frac{1}{U_{i,fouled}A_i} = \frac{1}{U_{o,fouled}A_o} = \frac{1}{h_i A_i} + \frac{R_i}{A_i} + \frac{\ln\frac{d_o}{d_i}}{2\pi k_w l} + \frac{R_o}{A_o} + \frac{1}{h_o A_o} \tag{2-13}$$

This can be easily be rewritten in a more useful form without the area that can be used in heat exchanger design or analysis.

For clean tubes:

$$\frac{1}{U_{o,clean}} = \frac{r_o}{h_i r_i} + \frac{r_0 \ln\frac{r_o}{r_i}}{k_w} + \frac{1}{h_o} \tag{2-14}$$

And for fouled tubes:

$$\frac{1}{U_{o,fouled}} = \frac{r_o}{h_i r_i} + \frac{R_i r_o}{r_i} + \frac{r_0 \ln\frac{r_o}{r_i}}{k_w} + R_0 + \frac{1}{h_o} \tag{2-15}$$

Note the fouling resistances (R_i , R_o) used in equation (2-13) and (2-15). These are added resistances of zero thickness that account for fouling on the inside and outside of the tube. These fouling resistances or so-called fouling factors are the most common way to include fouling in heat exchangers designs.

2.4.4 Fouling factor definition

This section discusses the definition of the fouling factor from a thermal and heat transfer point of view. For the history and development of the fouling refer to section 3.5.2.

Fischer et al. [17] defined the fouling factor as given in (2-19). The derivation is as follows:

If one combines the fouling on the outside and inside of the tubes as one resistance with

$$R_f = \frac{R_i r_o}{r_i} + R_0 \tag{2-16}$$

Equation (2-15) can be written as:

$$\frac{1}{U_{o,fouled}} = \frac{r_o}{h_i r_i} + \frac{r_0 \ln\frac{r_o}{r_i}}{k_w} + \frac{1}{h_o} + R_f \tag{2-17}$$

Writing in terms of R_f:

$$R_f = \frac{1}{U_{o,fouled}} - \left(\frac{r_o}{h_i r_i} + \frac{r_0 \ln\frac{r_o}{r_i}}{k_w} + \frac{1}{h_o} \right) \tag{2-18}$$

The term in brackets in equation (2-18) is the same as the left-hand side of equation (2-14). When substituting the overall fouling factor R_f becomes:

$$R_f = \frac{1}{U_{o,fouled}} - \frac{1}{U_{o,clean}} \tag{2-19}$$

Equation (2-19) can also be written as the overall heat transfer coefficient between the wall surface temperature and bulk fluid temperatures [18] if local resistance is considered.

$$R_f = \left(\frac{T_s - T_b}{Q/A}\right)_{fouled} - \left(\frac{T_s - T_b}{Q/A}\right)_{clean} \tag{2-20}$$

Up two now two different overall heat transfer coefficients were used. One is for a clean tube and the other for a fouled tube. This allows calculation of the combined fouling factor, R_f. To be able to differentiate between the internal (R_i) and external (R_o) fouling factors a third overall heat transfer coefficient is required. This can be in the form of either the internal or external part of the tube cleaned. For the purposes of this work, the externally clean condition will be used and it will be referred to the as the “half clean” condition. By using the “half clean” overall heat transfer coefficient one can derive (R_i).

The starting point will be equation (2-15) as given above.

$$\frac{1}{U_{o,fouled}} = \frac{r_o}{h_i r_i} + \frac{R_i r_o}{r_i} + \frac{r_0 \ln \frac{r_o}{r_i}}{k_w} + R_0 + \frac{1}{h_o} \quad (2\text{-}21)$$

In this case however, it will have been cleaned on the outside thus R_0 is equal to 0.

$$\frac{1}{U_{o,halfclean}} = \frac{r_o}{h_i r_i} + \frac{R_i r_o}{r_i} + \frac{r_0 \ln \frac{r_o}{r_i}}{k_w} + \frac{1}{h_o} \quad (2\text{-}22)$$

Re-writing:

$$\frac{1}{U_{o,halfclean}} - \frac{R_i r_o}{r_i} = \frac{r_o}{h_i r_i} + \frac{r_0 \ln \frac{r_o}{r_i}}{k_w} + \frac{1}{h_o} \quad (2\text{-}23)$$

Again the left hand to the equation is equal to the left hand of equation (2-14) and can be substituted:

$$\frac{1}{U_{o,halfclean}} - \frac{R_i r_o}{r_i} = \frac{1}{U_{o,clean}} \quad (2\text{-}24)$$

Re-writing in terms of R_i :

$$\frac{R_i r_o}{r_i} = \frac{1}{U_{o,halfclean}} - \frac{1}{U_{o,clean}} \quad (2\text{-}25)$$

This is now in the form that R_i appears in the typical overall heat transfer coefficient equations. The $\frac{r_o}{r_i}$ term is used to convert it to the tube outside area. The internal fouling factor is however typically given in terms of the tube inside area as a standalone value.

$$R_i = \left(\frac{1}{U_{o,halfclean}} - \frac{1}{U_{o,clean}}\right)\frac{r_i}{r_o} \quad (2\text{-}26)$$

The external fouling factor (R_0) can then easily be written in terms of the internal (R_i) and combined (R_f) fouling factors by re-arranging equation (2-16):

$$R_0 = R_f - \frac{R_i r_o}{r_i} \quad (2\text{-}27)$$

The values for R_f and R_o can be replaced in equation (2-27) and re-written more elegantly in the form as given below:

$$R_o = \frac{1}{U_{o,fouled}} - \frac{1}{U_{o,halfclean}} \quad (2\text{-}28)$$

One should take note that the way R_f is used and defined as zero thickness makes the inherent assumption that the convective heat transfer coefficient on the outside and inside of the tube stays the same. This will not be the case since the inner diameter and hence velocity in the tube as well as the roughness changes. Both of these can lead to an increase in heat transfer coefficient. In the initial stages of fouling this can have a larger effect on the overall heat transfer coefficient and the amount of heat transfer that takes place, than the additional resistance of the fouling layer. This leads to the measurement of negative fouling factors as has been reported by a number of authors and discussed in detail by Crittenden and Alderman in two separate publications [19] [20].

This raises the obvious question if this effect should be compensated for or incorporated in the determination of the fouling factor (R_f). Due to the definition and derivation of R_f as shown above, it is not required since it is used as a layer with zero thickness in the design equation of a heat exchanger (2-15), (2-17). It must however be noted that the fouling factor determined in this way is not an exact representation of the actual fouling resistance. The fouling factor includes the negative effects of the conduction through the fouling layer as well as the positive effects of the increase in heat transfer coefficient inside the tube.

It is for these reasons that the terminology “fouling factor” is preferred and not “fouling resistance”. For the purposes of this work “fouling factor” will be used to describe the combined effect of the fouling and “fouling resistance” will be used to only describe the conductive resistance due to the fouling layers.

2.4.5 Forced Convection in the circular tube

To determine the resistance to heat transfer of the internal boundary layer the internal heat transfer coefficient h_i needs to be determined. There are a number of correlations available to do this. Some of these correlations will be given and discussed in this section.

One of the most well-known correlations is the Dittus-Boelter equation first published in 1930. It is given by [1] as:

$$Nu = 0.023 Re^{\frac{4}{5}} Pr^{n} \tag{2-29}$$

With n = 0.3 for cooling and n = 0.4 for heating. The range of applicability and uncertainty of the Dittus-Boelter Equation is:

$$0.7 \leq Pr \leq 160$$

$$Re \geq 10000$$

$$\frac{L}{d_i} \geq 10$$

$$Uncertainty/Error \approx 25\%$$

Where:

$$Re = \frac{\rho V d_i}{\mu} \tag{2-30}$$

$$Nu = \frac{h_i d_i}{k} \tag{2-31}$$

The Sieder-Tate Equation is an improvement on the Dittus-Boelter equation since it takes into account the change in viscosity between the bulk fluid temperature and the surface temperature. This does require an iterative process to solve since the viscosity factor will change as the Nusselt number change. It is given by [1] as:

$$Nu = 0.027 Re^{\frac{4}{5}} Pr^{\frac{1}{3}} \left(\frac{\mu}{\mu_s}\right)^{0.14} \tag{2-32}$$

The range of applicability and uncertainty of the Sider-Tate Equation is:

$$0.7 \leq Pr \leq 16700$$

$$Re \geq 10000$$

$$\frac{L}{d_i} \geq 10$$

$$Uncertainty/Error \approx 25\%$$

Gnielinski proposed an equation for smooth tubes that improved the uncertainty as well the range of applicability w.r.t large Reynold numbers and Reynold number in the transition region. The Gnielinski equation is given by [1] as:

$$Nu = \frac{\frac{f}{8}(Re_D - 1000)Pr}{1 + 12.7\left(\frac{f}{8}\right)^{\frac{1}{2}}(Pr^{\frac{2}{3}} - 1)} \tag{2-33}$$

The friction factor term f can be determined from the Moody chart, by solving the Colebrook equation or by an approximation as discussed in section 2.3.2.

The range of applicability and uncertainty of the Gnielinski Equation as given in (2-33) is:

$$0.5 \leq Pr \leq 2000$$

$$3000 \leq Re \leq 5\text{x}10^6$$

$$Uncertainty/Error \approx 10\%$$

The original article published by Gnielinski [21] contained further improvements on equation (2-33). It was enlarged by a factor to take into account the dependence of the heat transfer coefficient on the length of the pipe as well as a term that takes temperature dependent properties into account. VDI Heat Atlas [2] adopted this equation.

$$Nu = \frac{\left(\frac{f}{8}\right)(Re - 1000)Pr}{1 + 12.7\left(\frac{f}{8}\right)^{\frac{1}{2}}\left(Pr^{\frac{2}{3}} - 1\right)}\left[1 + \left(\frac{d_i}{L}\right)^{\frac{2}{3}}\right]K \tag{2-34}$$

With K:

$$K = \left(\frac{Pr}{Pr_w}\right)^{0.11} \; For\ liquid\ with\ 0.05 \leq \frac{Pr}{Pr_w} \leq 20 \quad \text{or} \tag{2-35}$$

$$K = \left(\frac{T_m}{T_w}\right)^{0.45} \; For\ gasses\ with\ 0.5 \leq \frac{T_m}{T_w} \leq 1.5 \tag{2-36}$$

Where f for smooth tubes can be determined from:

$$f = (1.82log_{10}Re - 1.64)^{-2} \tag{2-37}$$

The range of applicability and uncertainty is given as:

$$0.1 \leq Pr \leq 1000$$

$$2300 \leq Re \leq 10^6$$

$$\frac{d_i}{L} \leq 1 \; or \; \frac{L}{d_i} \geq 1$$

$$Uncertainty/Error \approx 20\%$$

The version of the Gnielinski equation is also written in a form where the length term can be replaced by a specific distance on the pipe length. This allows calculation of the local Nusselt number at any specific point along the length of the pipe.

For the purposes of this work, the Gnielinski equation with the length term will be used.

2.4.6 Forced convection in annulus

The external flow for the counter flow heat exchanger shown in Figure 2-7 takes place in an annular space or area between the two concentric tubes or pipes.

The characteristic dimension to be used for such an arrangement is:

$$d_h = d_o - d_i \tag{2-38}$$

The diameter ratio a is given as:

$$a = \frac{d_i}{d_o} \tag{2-39}$$

To determine the resistance to heat transfer of the external boundary layer the external heat transfer coefficient h_o needs to be determined. The following correlation and equations are given in [2] and [22].

$$Nu_m = \frac{\left(\frac{f_{ann}}{8}\right) RePr}{k_1 + 12.7\left(\frac{f_{ann}}{8}\right)^{\frac{1}{2}}\left(Pr^{\frac{2}{3}} - 1\right)}\left[1 + \left(\frac{d_h}{L}\right)^{\frac{2}{3}}\right] F_{ann} \tag{2-40}$$

$$k_1 = 1.07 + \frac{900}{Re} - \frac{0.63}{(1 + 10Pr)} \tag{2-41}$$

The friction factor (f_{ann}) for annular ducts differs from that of circular tubes.

$$f_{ann} = (1.8log_{10}(Re^*) - 1.5)^{-2} \tag{2-42}$$

With

$$Re^* = Re\frac{(1 + a^2)\ln a + (1 - a^2)}{(1 - a^2)\ln a} \tag{2-43}$$

For the heat transfer at the inner wall:

$$F_{ann,i} = 0.75a^{-0.27} \tag{2-44}$$

And for heat transfer at the outer wall:

$$F_{ann,o} = (0.9 - 0.15a^{0.6}) \tag{2-45}$$

The range of applicability and uncertainty of the correlation is given as:

$$0.6 \leq Pr \leq 1000$$

$$10^4 \leq Re \leq 10^6$$

$$0 \leq \frac{d_h}{L} \leq 1 \; or \; 0 \geq \frac{L}{d_i} \geq 1$$

$$Uncertainty/Error \approx Notgiven$$

2.5 Calculation of losses to atmosphere

The theory in this section will be used to determine the losses of the cylindrical test section to atmosphere and the required lagging thickness to minimise these losses.

2.5.1 Natural convection of a cylinder

Natural convection will occur if an object is at a higher temperature than its surroundings. The Churchill and Chu [23] correlation were developed for a horizontal cylinder with natural convection on the outer surface in 1976. It has received widespread use and is recommended by [1].

$$Nu_L = \left[0.6 + \frac{0.387 Ra_D^{\frac{1}{6}}}{\left(1 + \left(\frac{0.559}{Pr}\right)^{\frac{9}{16}}\right)^{\frac{8}{27}}} \right]^2 \tag{2-46}$$

With the Raleigh number being:

$$Ra = \frac{g\beta(T_s - T_\infty)D^3}{\alpha\nu} \tag{2-47}$$

2.5.2 Radiation to atmosphere

Radiation occurs when an object is at a higher temperature than its surroundings. To predict the amount of radiation to atmosphere the following equation for the radiation heat transfer coefficient are given by [1]:

$$h_r = \frac{\varepsilon\sigma(T^4 - T_\infty^4)}{T - T_\infty} \tag{2-48}$$

In cases of atmospheric radiation the assumption $T \approx T_\infty$ can be made. In this case equation (2-48) simplifies to:

$$h_r \approx 4\varepsilon\sigma T_\infty^3 \tag{2-49}$$

3. Literature review

3.1 Fouling introduction

Fouling is defined as “any undesirable deposit on heat exchanger surfaces that increases resistance to heat transmission” [24]. This leads to a loss in thermal capacity of the heat transfer equipment [25]. More than 90% of industrial heat exchanger suffers from fouling problems and must be designed with some allowances [7]. This is normally in the form of extra area to accommodate the loss in performance due to fouling.

In recent times the design of heat exchangers have improved and developed in the following ways:

- Heat transfer correlations for different single phase flow problems and geometries have improved and increased in accuracy and applicability ranges.
- Well proven and accepted methodologies are available for heat exchanger design.
- Computational fluid dynamics simulations can be done for complex flow and heat transfer problems. These are being used more and more in industry due to the fact that it is becoming less and less expensive to do.

All of these improvements are negated when estimated or experience based fouling factors, fouling resistances or safety margins are added to heat exchanger designs. Considerable progress has been made in understanding the subject, but this has unfortunately not resulted in the ability of the designer to predict fouling resistances [26] with most designers still using traditional fouling factors.

Fouling was called “the major unresolved problem in heat transfer” [24] in 1972 by Taborek et al. and although the understanding of the subject has increased dramatically, there is still a margin of truth in that statement as reflected by Muller-Steinhagen [7] in 2011.

3.2 Cost of fouling

To fully understand the problem that fouling presents one must have an appreciation in monetary terms of the scale of the problem. To achieve this, a number of authors have estimated the cost of fouling. Some authors have considered the overall cost of fouling in industry where others have only looked at power plants or specific parts of power plants.

3.2.1 Breakdown of the cost of fouling

The cost of fouling can be broken down into 4 main areas [27][28][29]. These are

- Capital Expenditure: This is typically the increase in surface area to accommodate fouling as well as the additional space and transport requirements.
- Fuel Costs / Energy Costs: This is mostly losses associated with the decrease in thermal efficiency and an increase in pressure drop through heat exchangers.
- Maintenance Costs: Mainly cleaning of equipment.
- Production losses: During planned and unplanned outages for fouling cleaning.

3.2.2 Overall fouling costs to industry

Thackery [30] presented an overview of the costs of heat exchanger fouling in the UK in 1980. Although it is very difficult to get accurate estimates due to the extent of the subject and the lack of available statistics, it was found that fouling costs amount to £300-500 million per annum. This figure was obtained by considering the costs in each of the areas mentioned in section 3.2.1 above.

Pritchard [27] considered the economics of fouling 1988. A specific value for overall fouling costs was not given; instead, specific examples were given to allow the readers to be able to do the fouling costs calculations. The same categories as mentioned above were considered. Two further categories were also added in the form of safety and unfulfilled opportunities.

Garrett-Price et al. [31] considered the cost of fouling in the American Industry. It was found that when a similar approach to Thackery [30] and Pritchard [27] were followed, the estimated cost due to fouling in the United States in 1984 was $8-10 billion.

Müller-Steinhagen et al. [28] did a study on the overall fouling costs in New Zealand industries in 1993. Two approaches were used to determine the cost. The first was similar than Thackery [30], Pritchard [27] and Garret-Price et al. [31]. The second was based on a survey that was done in industry. The first approach gave a result of $30-56 million US dollars. The second approach gave a result of $31-45 million US dollars. Both results are in satisfactory agreement which gives a confirmation of the methodology used.

Müller-Steinhagen [4] gave a summary that includes some of the above work on heat exchanger fouling costs in a table form. The values are given for various countries and are based on 1984 values. The fouling costs as a percentage of gross national products (GNP) are given.

It can be seen from Table 3-1 that for more industrialised countries the value is approximately 0.25% of the GNP. For countries with less industrialised economies, this value comes down to approximately 0.15% of GNP.

Table 3-1: Estimated fouling costs incurred in some countries [4]

Country	Fouling Costs million $US	GNP 1984 billion $US	Fouling Costs % of GNP
UK (1978)	700-930	285	0.2 – 0.33
USA (1982)	3860-7000, 8000-10000	3634	0.12 – 0.22, 0.28 – 0.35
New Zealand	35	23	0.15
Australia	260	173	0.15
West Germany	1533	613	0.25
Japan	3062	1225	0.25
Total Industrial world	26850	13429	0.20

3.2.3 Fouling costs applicable to power plants

Walker et al. [9] studied the economic impacts of condenser fouling in existing thermoelectric power plants. The analysis was done on condenser performance and power output for a representative coal-fired power plant of 550 MW. It was found that the cost from additional fuel and production losses is in the range of $0.4 – 2.2 million (USD 2009).

Zhi-Ming et al. [32] did a study on utility fouling costs of boilers and turbines in China in 2006. The Huaneng Dalian Power Plant is used as a case study and the fouling cost calculated for this plant. The cost is averaged per MW and applied to the total installed capacity of China. The annual fouling cost for a 350 MW unit at the Huaneng Dalian Power Plant is 2.23 Million dollars or 6380.79 dollars per MW. Applied to the total Chinese thermal power plant capacity and calculated as a percentage of GDP it yields estimate 0.168% of the GDP of China. This value agrees well with the values given in Table 3-1.

3.2.4 Environmental aspects of fouling

Very little research focus has been put on the environmental aspects of fouling [33]. Lately due to a larger focus on global warming and CO_2 emissions, SOx and NOx emissions and restrictions in the disposal of chemical wastes; this has come to receive more attention.

Fouling affects the environment in a number of ways as Müller-Steinhagen discussed [33]. These are:

- Additional CO_2 emissions. This is mainly due to reduced heat transfer and heat recovery as well as additional required pumping power. It is estimated that 186 million barrels of crude oil are annually used worldwide to offset the impact of fouling in refinery heat exchangers.
- Discharge of chemical fouling inhibitors to the environment. A widely used mitigation strategy for fouling is the use of chemical additives. Most of these chemicals contain substances that have the potential to be harmful to the environment.

- Discharge of spent chemical cleaning agents or removed deposits. The chemicals or substances used for cleaning as well as the removed deposits need to be treated or disposed of in a manner that is environmentally friendly.

3.2.5 Summary of the cost of fouling

Based on the section above it is clear that fouling presents a major cost impact as well as an impact on the environment. Based on a large amount of research with good correlation one can safely say that the cost of fouling can amount to 0.15% - 0.25% of the specific country's GNP.

3.3 Types of fouling

There are a number of different types of fouling in heat exchangers. These are caused and classified by the underlying mechanisms that cause the fouling. They are individually complex, can often occur simultaneously, increase pressure drop, accelerate corrosion and have negative effects on the heat transfer in the heat exchanger [34]. Many authors and textbooks refer to these types [4] [26], [34]–[37] but the first reference to it found was in 1972 by Taborek et al. [24]. This section will give a brief overview of the different types of fouling as well as references if more detailed information is required.

3.3.1 Particulate fouling

Epstein [38] defined particulate fouling as the accumulation of solid particles suspended in a fluid onto a heat transfer surface. This includes sedimentation of settling particles as well as the deposition of colloidal particles [37]. This type of fouling involves deposition of corrosion products, clay and mineral particles in river water, suspended solids in cooling water, magnetic particles in economisers, deposition of salts in desalination plants and deposition of dust particles in air coolers [39].

3.3.2 Chemical reaction fouling

Chemical reaction fouling is defined as a deposit forming on the heat transfer surface by chemical reactions [35]. The heat transfer surface does not take part in the reaction but can act as a catalyst [39]. Watkinson and Wilson gave a detailed overview of chemical reaction fouling in [40].

3.3.3 Corrosion fouling

Corrosion products formed on a heat transfer surface as a result of a corrosion reaction between the flow stream and the heat transfer surface itself is called corrosion fouling [39][41]. The most

common form is material loss due to wall thinning [37]. Somerscales published an overview article addressing the fundamentals of corrosion fouling [41].

3.3.4 Crystallization or precipitation fouling

Crystalline or precipitation fouling is the crystallisation of dissolved salts from solutions and the subsequent precipitation to the heat transfer surface [39]. It is common in aqueous systems. The general term “scaling” or “scale formation” is used to describe crystalline fouling [42]. Bott discussed the aspects of Crystallisation fouling in [42].

3.3.5 Biological fouling

Biological fouling is the attachment of microorganisms and macroorganisms on heat transfer surfaces [37]. This is generally a problem in water systems. Microbial fouling includes organisms such as algae, fungi, yeasts, and bacteria. Macrobial fouling includes organisms such as clams, barnacles and mussels. Melo and Bott discussed Biofouling in water systems in [43].

3.3.6 Solidification or freezing fouling

Solidification or freezing fouling involves the icing of a liquid on a subcooled heat transfer surface [36]. This can include the formation of ice on a heat transfer surface from cooling of moist air. This typically occurs at low temperatures [39].

3.4 Effects of different parameters on fouling

A number of different factors have an effect on fouling and the formation of the different types of fouling. By taking these factors into account during the design of a heat exchanger the formation of fouling can be minimised. A number of these are inherent in the design of feedwater heaters or are specifically used to reduce fouling.

3.4.1 Properties of fluid

The concentration of the fouling constituents plays a major role in the amount of fouling that will take place [36]. The fluid conditions also play a role [44]. The amount of fouling can be reduced by changing the operating conditions, treating the fluid to prevent corrosion and biological growth or by using additives that can disperse certain fouling materials [34].

In power stations and specifically feedwater heaters demineralised water is used. This is as close to the ideal fluid from a fouling point of view as practically possible.

3.4.2 Flow velocity

Cousineau et al. [45] showed experimentally that thinner fouling layers are experienced at higher flow velocities in tubes. It is typically accepted that higher velocities reduce the amount of fouling that takes place [44]. Velocities on the tube side of heat exchanger are however limited by erosion and on the shell side by flow-induced vibration [34]. The Tubular Exchangers Manufacturing Association (TEMA) standards [34] give different fouling factors for boiler feedwater for velocities lower and higher than 3 ft/s (0.91 m/s). Hasson [36] did, however, state that there are specific cases where higher velocities can promote fouling. An example of $CaCO_3$ scale is given.

The velocities in feedwater heater tubes are typically in excess of 2 m/s. This will reduce fouling formation in the tubes. The velocities on the shell side or outside the tubes are high for the steam phase, but for the liquid phase much lower.

3.4.3 Surface and bulk temperature

Most fouling processes, especially crystallisation and chemical reaction fouling, are affected by temperature [24]. In general, the rate of fouling increases as the temperature increases. Lower temperatures produce deposits that are easier to clean and remove [34].

The temperatures in high-pressure feedwater heater tubes are typically between 120°C and 250°C depending on where in the feedwater heating train the specific heater is installed. The shell side temperatures are higher and enter the heater as superheated steam. Temperature ranges typically from 300°C to 420°C. The high temperatures found in the high-pressure feedwater heaters improve conditions for fouling creation and development.

3.4.4 Material

The primary influence of the selected material is the amount of corrosion and hence corrosion fouling that will take place. In some cases, the tube may also act as a catalyst for fouling reactions [24]. Copper-bearing alloys may be toxic to some organisms found in biological fouling [46].

The tube material in most feedwater heaters is carbon or low alloy steels. In some low-pressure heaters, stainless steel alloys are installed. The carbon and low alloy steels can typically suffer from corrosion when used in the demineralised water environment. Iron oxides in the form of hematite and magnetite are commonly found on feedwater tubes. In some cases these are due to corrosion of the tubes and in other cases it is deposited on the tubes originating from upstream sources.

3.4.5 Surface roughness

The surface roughness of the selected material may play a role. It has been shown that the surface roughness affects the rate of fouling as well as the ease of cleaning once fouling has occurred [34].

The surface roughness of feedwater heater tubes is dependent on the tube manufacturing process. No special measures are taken to improve the surface roughness.

3.4.6 Heat transfer process

The fouling factor for the specific fluid can vary considerably depending on wherever the heat transfer mode is sensible heating, sensible cooling, boiling or condensation [44]. Hasson [36] discussed the effects on deposit formation of sensible heating and boiling phase change heat transfer.

3.5 Design approaches to fouling

There are a number of different approaches to incorporate fouling in the design of heat exchangers. All of these methods add additional heat transfer surface area to the design. The difference is in the way that the amount of additional area is determined. This section gives an overview of the available methods.

3.5.1 Cleanliness factor

The cleanliness factor is defined by the HEI Standards [47] and Somerscales [48] for steam surface condensers as the ratio of the overall heat transfer coefficient of a fouled condenser to the overall heat transfer coefficient of a clean condenser.

This can be expressed as:

$$C_f = \frac{U_{fouled}}{U_{clean}} \tag{3-1}$$

The cleanliness factor is mostly used for large steam surface condensers [49] in the power industry. Cleanliness factors of 0.85 or 0.9 are typically used. This method has a high level approach and is very experienced based. It is not commonly used in industry for heat exchangers other than large surface condensers.

3.5.2 Fouling factor

The fouling factor is a separate thermal resistance of zero thickness that is included in the calculation of the overall heat transfer coefficient as shown in equation (2-13) and (2-15).

The earliest reference to fouling factors was by Sieder (original published work not found) as stated by Somerscales in [48]. Sieder presented various fouling factors. The origin of this data was not indicated. In 1941 the first edition of the Tubular Exchanger Manufacturers Association standards or commonly referred to as TEMA [34] was published. TEMA recommended a number of fouling factors [34][50]. The exact origin of these fouling factors is unknown [48]. Chenoweth reported after discussions with some of the original members of the committee that these values where experienced based and was selected before any scientific investigation into fouling was done [44].

In recent years the use of fouling factors has become quite controversial [51]. This is due to a number of problems with the use of fouling factors. Muller-Steinhagen [7], Epstein [35], Shilling [52] and Bennet [51] discussed some of these problems. A summary is given below:

- Published fouling factors often do not reflect true performance and can lead to oversized or underperforming heat exchangers.
- When this method was created, the uncertainty associated with heat exchanger design methodology as well as the determination of heat transfer coefficients was high. The fouling factor thus combined fouling and uncertainty and acted as a general “safety factor”. The use of fouling factors can thus result in duplication of this uncertainty effects.
- The origin and operating conditions on which the fouling factors are based are not necessarily known.
- It is well known that fouling is time dependent. It is not known after which operating time the given fouling resistances are reached. The fouling factors thus impose a static condition on the dynamic nature of fouling [53].
- They do not provide any information or recognise the effect on the fouling factor of operating parameters such as flow velocity, fluid temperature, heat flux, or fluid composition.

In 1990 a joint committee of HTRI and TEMA led by Chenoweth was established to review the TEMA fouling factors. The results are given in [44]. Unfortunately, only minor changes were made and included in later editions of TEMA. This is mainly due to the lack of data from industry [7].

Regardless of the problems associated with the use of fouling factors is it still the most widely used method to incorporate fouling into heat exchanger designs. Epstein [35] called the use of the TEMA fouling factors in 1983 the “current practice” in heat exchanger design. Somerscales stated

in 1990 [48] that: “TEMA fouling factors have been widely, perhaps universally, used to design heat transfer equipment subject to fouling”. According to Muller-Steinhagen in 2011 [7] fouling factors still form the basis of most heat exchanger designs worldwide today. Shilling [52] stated that because the industry has not developed a better method to date (2012) that is suited to all heat exchanger designers, the TEMA fouling factors continues to be used.

This method is also used in the design of feedwater heaters in Eskom. The fouling factors used are as prescribed by the Heat Exchanger Institute (HEI) standards for closed feedwater heaters [6].

3.5.3 Design margin

This approach assigns additional heat transfer surface area and does not use any fouling or cleanliness factors [49].

Bennett et al. [51] and Nesta et al. [46] proposed the addition of 0 - 20% excess area. This is, however, dependant on a number fouling mitigation factors. These fouling mitigation factors are general guidelines that need to be applied in heat exchanger design to prevent the formation of fouling to some degree.

There are a few shortcomings with this design method as discussed by Shilling in [52]. The first is the fact that the method is applied to the overall heat exchanger and not to each individual stream. The second is that a large part of the method is experienced base which is highly dependent on the specific heat exchanger or industry where this experience was obtained.

3.5.4 Risk-based design

The risk-based design method uses risk analysis to determine the required design margin or fouling factors to be used in the specific heat exchanger. The method is described by Shilling et al. in [54].

It considers the three main areas of uncertainty in heat exchanger design and assigns certain probabilities to each of these. Specific probabilities are assigned specific scores. The three areas considered are heat transfer correlation errors, fouling, and operational uncertainty. Consequences are also considered on a cost basis and a score assigned. Both the probabilities and consequence is evaluated in a risk matrix and a specific risk level given. Suggested actions and safety factors are then provided for the different risk levels.

Although this method seems like a good approach to heat exchanger design, no proof was found of the implementation or widespread use of it.

3.5.5 Resistance factor

The resistance factor method is a new method proposed by Shilling [52] in 2012. It aims to address some of the problems and shortcomings associated with the fouling factor method.

It is well known that the fouling factor method does not add additional surface area consistently for different overall heat transfer coefficient values. The fouling factors tend to penalise higher overall heat transfer coefficients more than lower overall heat transfer coefficients. This can be clearly seen in Table 3-2 below. A fouling factor of 0.00018 m²K/W was used on each flow stream which equates to R_f of 0.00036 m²K/W

Table 3-2 Excess surface area for various Heat exchangers [4]

Application	Clean Overall heat transfer coefficient	Excess Area
Gas / Gas shell and tube heat exchanger	50 W/m²K	1.8 %
Liquid / Gas shell and tube heat exchanger	150 W/m²K	5.4 %
Liquid / Liquid shell and tube heat exchanger	1000 W/m²K	36 %
Liquid / Liquid plate and frame heat exchanger	3000 W/m²K	108 %
Water cooled shell and tube steam condenser	4500 W/m²K	162 %

The resistance factor is added to the calculation of the overall heat transfer coefficient as follows:

$$\frac{1}{U_o} = \frac{r_o(R_{factor})_o}{h_i\, r_i} + \frac{r_0 \ln\frac{r_o}{r_i}}{k_w} + \frac{(R_{factor})_i}{h_o} \qquad (3\text{-}2)$$

What the resistance factor adds is an additional margin or safety factor to the internal and external heat transfer coefficient. The result is that the additional surface area added is done much more consistently through the range of overall heat transfer coefficients. This is illustrated in Figure 3-1 below.

Typical values of the resistance factor are 1.1 to 1.2 depending on the fluid. This method was still under development by the *HTRI's exchanger design margin task force* at the time that the article was published. It does states that they aim to develop resistance factors for all the fluids found in the TEMA fouling factor tables. When these values become available for different heat exchangers and fluid types this method does have the potential for widespread use.

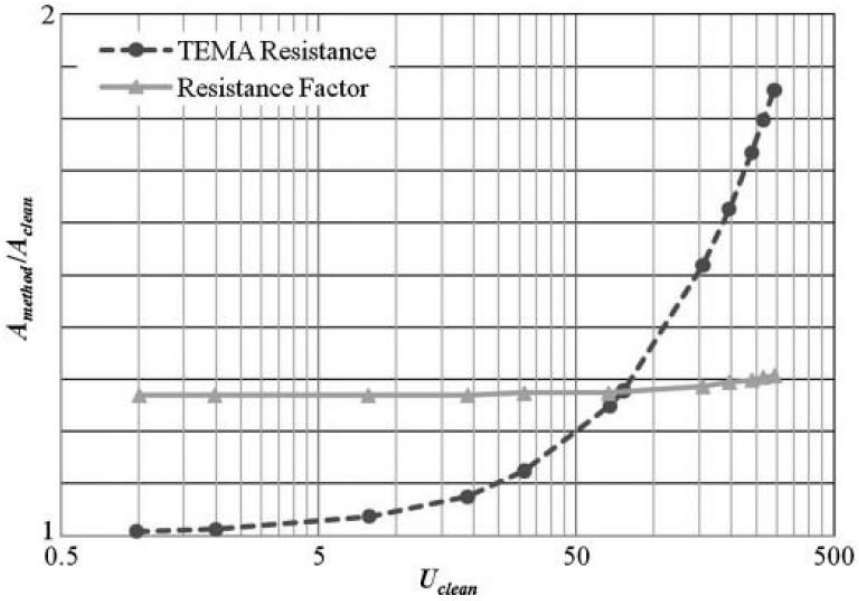

Figure 3-1: Comparison of fouling factor and resistance factor method for a range of U values [52]

3.5.6 Design approaches to fouling summary

Much work has been done to create models for fouling deposition that predict the fouling rates vs. time for different fouling mechanisms. Unfortunately, none of the numerous fouling models have found their way into practical heat exchanger design in industry [7]. The main reasons for this are that these models are normally based on ideal fluids and conditions and are seldom very accurate in predicting the fouling rates in industrial applications. The mechanisms involved in fouling creation are just too complex, dependant on to many variables and always act in combination with other fouling mechanisms.

Of all the approaches mentioned, the fouling factor method and to a lesser degree, the cleanliness factor method remains the only approaches that have received widespread use. None of these are scientific in its approach and both are largely based on experience. Regardless, these methods have been developed and evolved over time to give satisfactory results for specific applications. There is however room for improvement, specifically in the amount of plant-specific data available.

3.6 Heat transfer measurement methodology

This section presents and discusses previous experimental work that has been done to determine the amount of heat transfer that takes place in a specific experimental set-up. These experiments are typically used to determine certain heat transfer coefficients or resistances. The focus is on the experimental set-up and not necessarily the results that were obtained. Work has also been published where authors discuss the different methods available to achieve the above.

This is by no means a comprehensive review since a large amount of work has been done in this field. It does, however, give a good overview and is sufficient to identify required patterns and trends. These patterns and trends are discussed in the latter parts of the section.

3.6.1 Heat transfer measurement for fouling

Jose et al. [55] studied the fouling resistance and fouling rates of geothermal brine in Mexico. This was done by passing the fouling fluid through the tubes of a number of heat exchangers. Two of these were of the shell and tube type containing multiple tubes and two others were of the annular type with one tube in a pipe. Different tube materials were used in the different heat exchangers. Demineralised water was used as a cooling fluid on the outside of the tubes. The flow, inlet, and outlet temperatures were measured for each heat exchanger and the overall fouling factor was calculated at different time intervals as per equation (2-19). See Figure 3-2 for test section of annular arrangements.

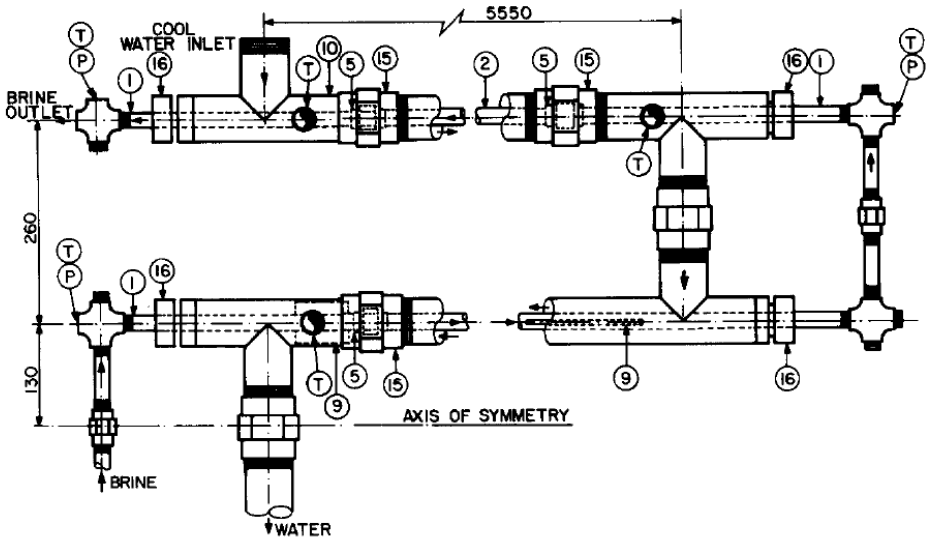

Figure 3-2: Double pipe heat exchanger test section as used by [55]

Agbisit et al. [56] studied the surface fouling tendencies of corn wet-milling water. An annular fouling probe was used with an electric resistance heated concentric rod inside a tube. The fouling liquid flowed outside the heater in an annulus. The test section is shown in Figure 3-3. The inner surface temperature of the inner tube was measured and the outside surface temperature of the inner tube calculated. The energy was determined from the power supplied to the heater. The surface temperature and bulk fluid temperature was used to calculate the fouling factor as per equation (2-20).

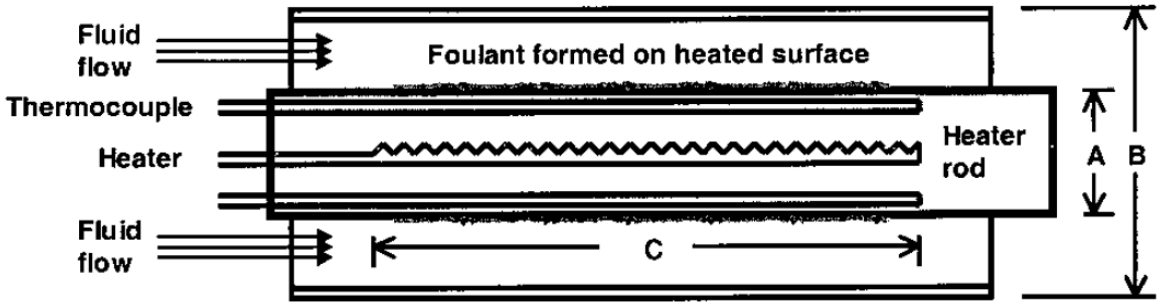

Figure 3-3: Annular fouling probe [56]

Abu-Zaid [57] studied the effect of water fouling on tubes. The experimental setup consisted of a tube heated electrically from the inside with electric resistance heaters. Water flowed outside the tube in an annulus. The setup is similar to that depicted in Figure 3-3. A glass outer pipe was used to allow visual observations. Surface thermocouples were installed at two different locations on the tube. At the same locations, thermocouples were placed in the water stream. The temperatures, as well as the energy input into the electric heaters, were measured before and after fouling took place. This allowed the calculation of the heat transfer resistance from the fluid inside the tube to the tube wall. This can be compared to the measurement of clean tubes with the difference being the fouling factor. Equation (2-20) was used to determine the fouling factor. The thickness of the deposits was also measured at the two locations. With the thermal resistance known the conductivity of the fouling layers was determined.

Goedecke et al. [58] studied the crystalline fouling resistance for wire matrix inserts. A supersaturated $CaSO_4$ solution was heated and pumped through the tubes of two identical double pipe heat exchangers. Hot water was used as the heating fluid and flowed counter-currently outside the tubes. The first test heat exchanger was equipped with 5 thermocouples to measure wall temperatures and five to measure the bulk temperatures of the water flowing on the outside of the tubes. This was measured at the same positions to allow the determination of local resistance. For the second test heat exchanger only bulk properties were measured to be used as a comparison. The Wilson plot method was used to determine the outside heat transfer coefficient for the experimental set-up. Equation (2-20) was used to determine the fouling factor.

Zhenhua et al. [59] did experiments to determine the fouling process of calcium carbonate on heat transfer surfaces during convective heat transfer. A double pipe heat exchanger was used with a copper tube inside a stainless steel tube with a glass insert. Pure hot water flowed inside the test tube and the cooling water which acted as the test liquid outside the tube in the annulus. The flow arrangement was countercurrent. The scale formation occurred on the outside of the tube. Inlet and outlet pressure, bulk temperature and flow rates were measured. The flow and inlet

temperature was kept constant during the experiments. The amount of heat transferred was calculated with equation (2-7) and the fouling factor by equation (2-19). See Figure 3-4 below.

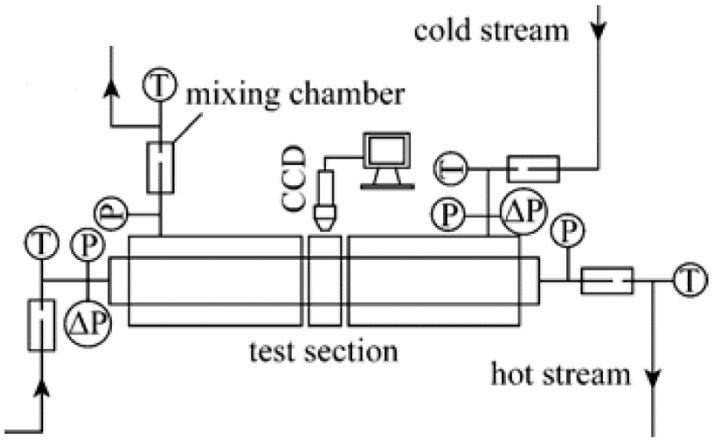

Figure 3-4: Double pipe heat exchanger test section as used by Zhenhua et al. [59]

Chen et al. [60] used a similar experimental setup described above and shown in Figure 3-4 to study the scaling effects of artificial hard water. A new physical fouling model was proposed. The new model compared well with measured results.

Fetkovich et al. [61] [62] developed a novel test apparatus to measure biofouling in seawater at conditions similar to those experienced in Ocean Thermal Energy Conversion (OTEC) plants. A thick-walled copper block was heated with spirally wounded nichrome wire electrical resistance heater. Thermocouples were installed in the copper block. After a certain temperature was reached in the block, the heating was switched off and the temperature decay measured. This can be used to determine the heat transfer resistance and thus the fouling factor. Flow is maintained during normal operation to allow the fouling to form. The transient test is done periodically. Figure 3-5 gives a schematic of the test apparatus.

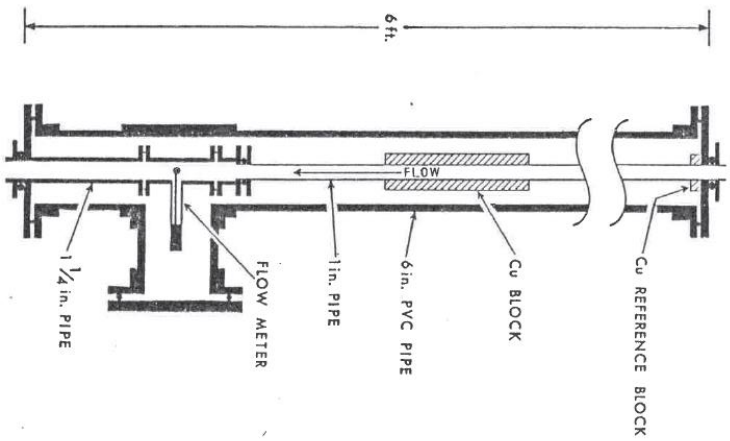

Figure 3-5: Transient test apparatus developed by Fetkovich et al. [61] [62]

Smith [63] used the High Temperature Fouling unit (HTFU) test apparatus at the HTRI to test the fouling propensity of 8 different crude oils. The HTFU consists of an annular test section. A cylindrical cartridge heater probe is installed and centered along the length of the test section. Four thermocouples are installed beneath the outer tube of the heater rod and 90° offsets. The probe is removable for cleaning or to test different materials. A schematic of the diagram is shown in Figure 3-6. Smith did report design issues that were later corrected. Some of these include inconsistent control of bulk fluid properties, change in calibration constant of test apparatus and varying fluid velocities in the annulus test section as proven by CFD studies. Improvements to the mentioned problems were proposed.

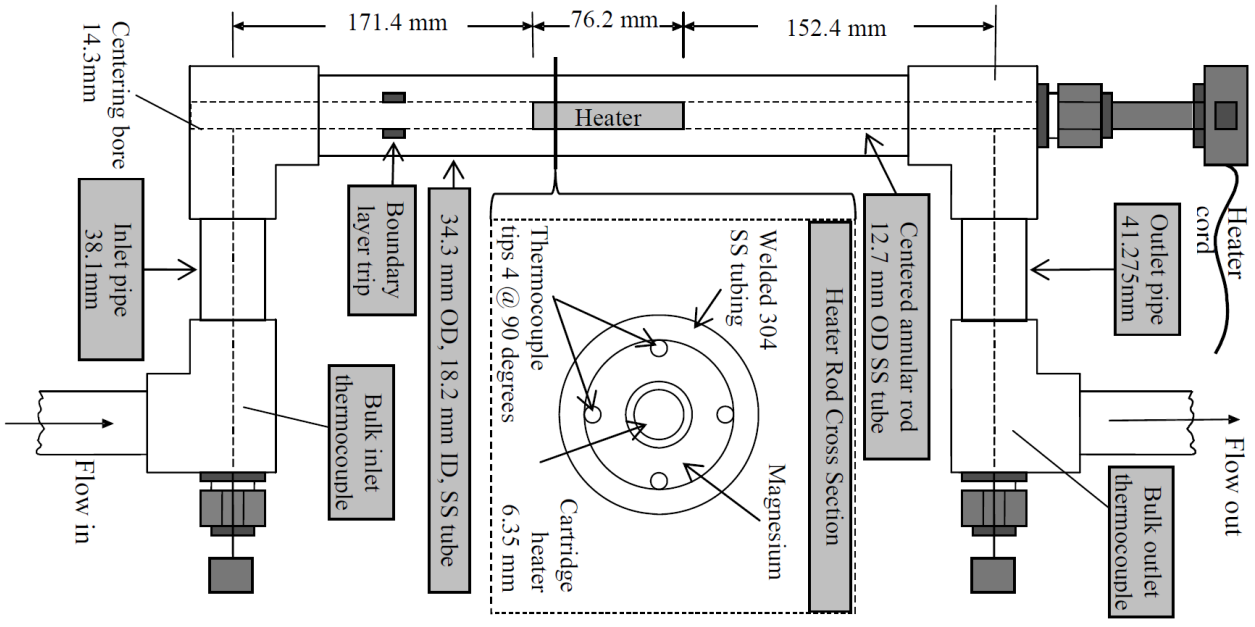

Figure 3-6: HTRI HPTU Annular test section used by Smith [63]

Ratel et al. [64] tested crude oil fouling in shell and tube and plate heat exchangers. The exact details of the experimental set-up are not given. Closed loops linking the different heat exchangers were used. The overall conditions at the inlet and outlet of each heat exchanger were measured. Fouling was evaluated by considering the change in the overall heat transfer coefficient. Both sides of the heat exchangers suffered from fouling. A so-called fouling index was used to compare the different heat exchangers. The fouling index used is similar to the cleanliness factor. The fouling index was defined as the ratio of the fouled overall heat transfer coefficient to the clean overall heat transfer coefficient.

Srinivasan and Watkinson [65] studied the fouling characteristics of Canadian crude oils. An annular electrically heated probe developed by HTRI was used. Details of the test section are shown in Figure 3-7. Heat flow is calculated from the measured voltage. The inlet and outlet

temperatures are measured and the overall heat transfer coefficient calculated for clean and fouled conditions. After each test, the probe is removed, cleaned and reinstalled for the next test.

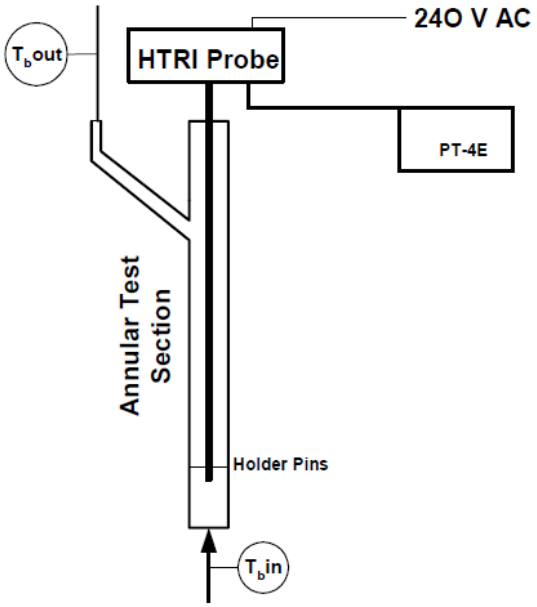

Figure 3-7: HTRI annular fouling probe [65]

Muller-Steinhagen and Branch [66] performed a large number of experiments with New Zealand Forest Products Kraft black liquor. Heat transfer coefficients and fouling rates were measured. This was done under convective and subcooled boiling heat transfer as a function of surface temperature, bulk temperature, velocity, and solids concentration. Results from experiments of two fouling inhibitors were also presented. The heat transfer test section of the experimental set-up used was the HTRI probe with 4 tube wall temperatures as shown in Figure 3-6 but with a layout arrangement similar than that of Figure 3-7. The overall heat transfer coefficient between the tube wall temperature and the bulk fluid temperature was calculated by using equation (2-4). The fouling factor was calculated from the change in this overall heat transfer coefficient for the clean and fouled condition as per equation (2-19).

Heneghan et al. [67] studied the thermal stability and the carbon deposition of different jet fuels. The test rig consist of a large copper block fitted with electrical heaters clamped around a test tube. The copper block heaters heated the tube to maintain a constant tube wall temperature during the experiments. The thermal resistance of the deposits was not tested. After each test, the tube was removed and the amount of carbon deposition physically measured.

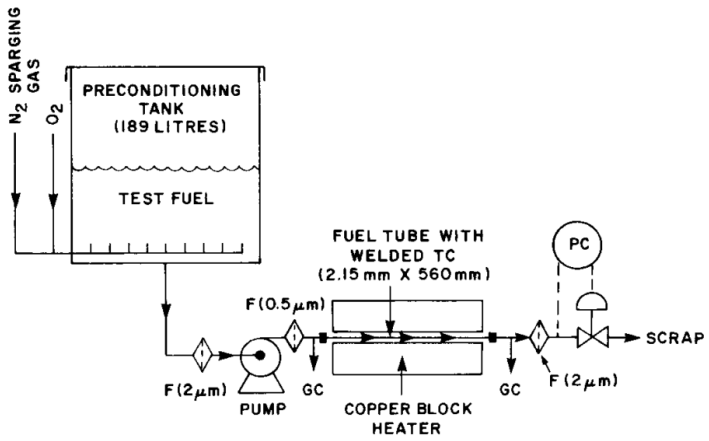

Figure 3-8: Heated copper block experimental arrangement used by Heneghan [67]

Chin et al. [68] used a similar experimental set-up as described above and shown in Figure 3-8 to test the deposits from heated hydrocarbon fuels.

Grant Jones et al. [69] [70] used a similar experimental apparatus as shown in Figure 3-8 to study the insolubilities in a Jet-A fuel.

Marteny et el. [71] studied the decomposition and tendency to form deposits of aircraft fuel. A single heated tube test apparatus was used. The tube was heated by passing electric current through the tube itself. Due to the high electric resistance of the 316 stainless steel, it acts as a resistance heater. The local heat flux achieved is very uniform over the length of the tube since the electrical resistance does not vary significantly with temperature. The internal tube wall temperature was measured along with flow rates, bulk fluid temperatures, and electric heat input. The amount of deposition was measured physically.

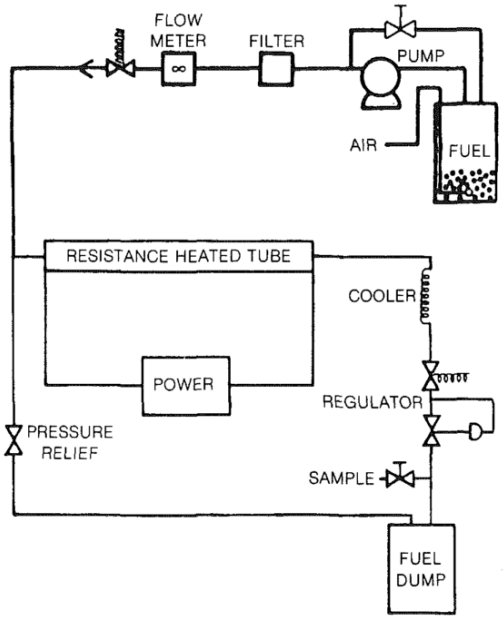

Figure 3-9: Experimental set up used by Marteny et el. [71]

Pahlavanzadeh et al. [72] combined heat transfer enhancement and fouling measurements in one experiment. An experimental study was done on the thermohydraulic and fouling performance of enhanced heat exchanger. A combination of these is logical since a similar experimental set-up is used. Wire coil, wire mesh, and twisted tape inserts were tested. The heat transfer test set-up comprised of two heaters wrapped around and bonded to a large steel cylinder. The steel cylinder was installed around the test tube. Thermocouples are installed at a number of different radiuses in the steel cylinder. The reason given for the use of the steel block is to ensure uniform heat distribution and the calculation of heat flux and surface temperature by using thermocouples at the different radiuses. Bulk temperatures, differential pressure, and the mass flow rate was measured. The internal heat transfer coefficient was calculated by using equation (2-4) between the tube outer surface temp and then bulk fluid temperatures. The fouling resistance was calculated by taking the difference between the fouling internal heat transfer coefficient and the clean internal heat transfer coefficient. See Figure 3-10 for details.

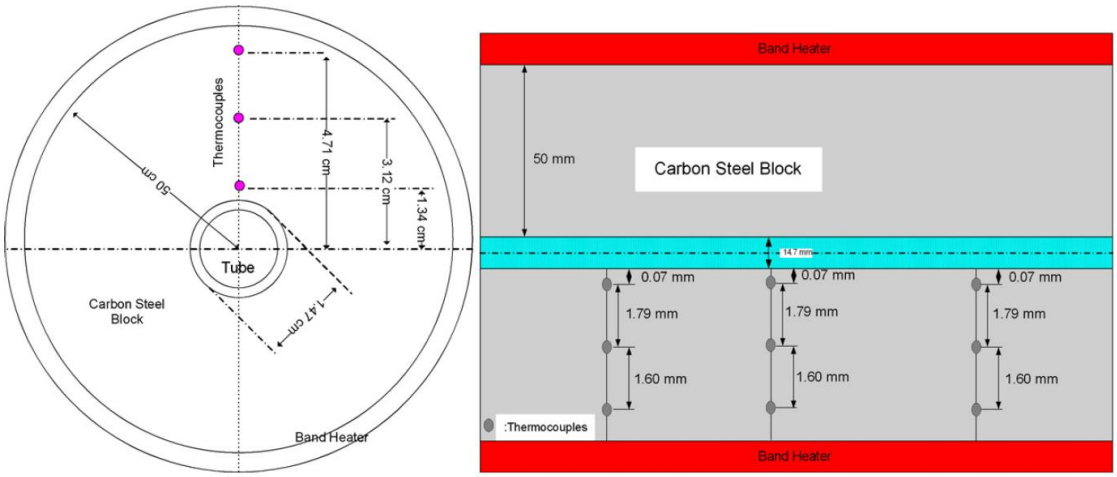

Figure 3-10: Schematic diagram of carbon steel block around the test tube [72]

Hays et al. [73] studied fouling on enhanced tubes. Few details are given of the exact test set-up. There is however sufficient information to determine that the test set-up used is similar to Figure 3-6 and Figure 3-7.

Al-Janbi et al. [74] studied the enhanced heat transfer surfaces under clean and fouled conditions. Flat stainless steel plates with “V” shaped grooves were used. Effect of groove dimensions and orientation was also investigated. The test section was a vertical rectangular duct that contained two parallel plate surfaces. Copper blocks with embedded thermocouples were connected to the flat plates and heated. The heat flux was kept constant and the surface temperature measured. The fouling factor was calculated by the change in overall heat transfer coefficient. The fouling fluid used was calcium sulphate.

Owens [75] developed a fouling measurement device called the LMSC (Lockheed open systems) device. It consists of a tube with a uniform heat flux applied to the tube by means of electric heating tape. The heater power, tube wall temperatures at 8 positions, bulk fluid temperatures and fluid velocities were measured. The change in wall temperature for a clean and fouled tube with the other parameters held constant was used to determine the fouling resistance. The method proposed by Kline and MacClintock [76] was used for uncertainty analysis.

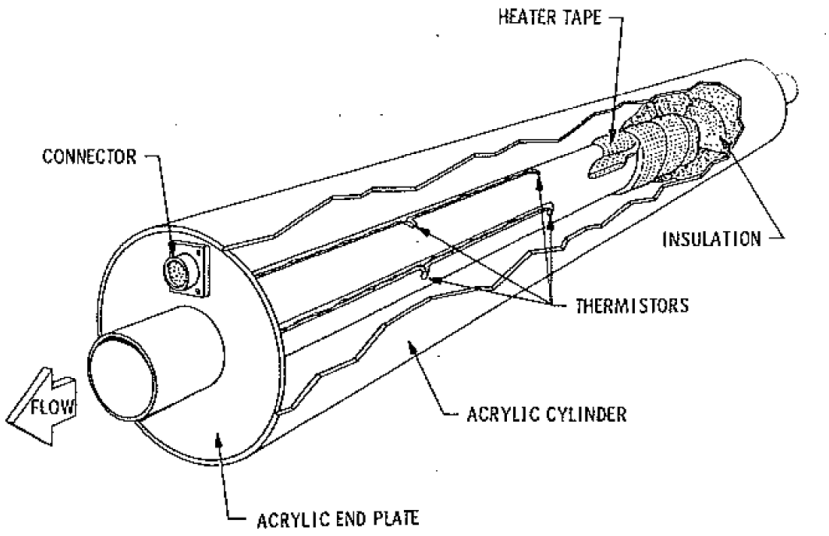

Figure 3-11: LMSC tube fouling measurement device used by Owens [75]

Four types of fouling measurement apparatus designed, build and operated by HTRI are briefly shown and discussed by Fischer et al. [17]. The first is the stationary fouling unit used for laboratory experiments. It uses indirect electrical heating for three parallel test sections. Each test section consists of heavy walled tubes that have heating rods place in longitudinal flutes along the circumference. Thermocouples are embedded in the tube wall. See Figure 3-12.

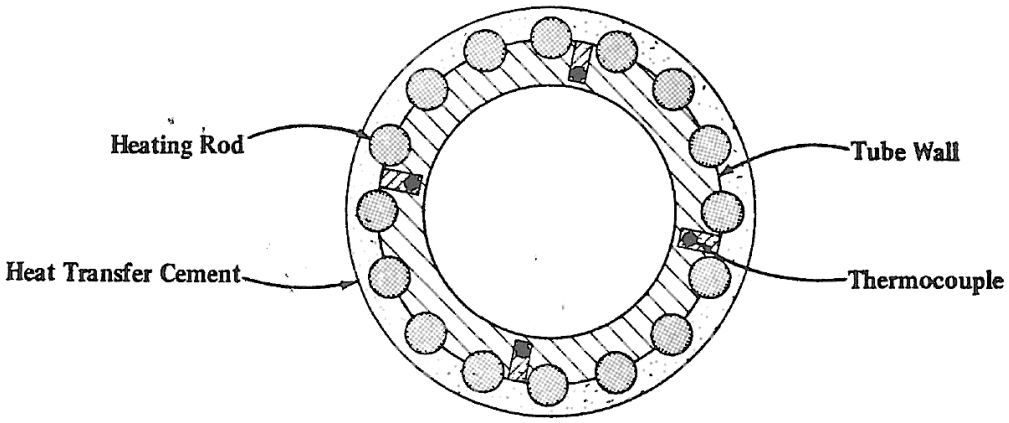

Figure 3-12: HTRI stationary fouling unit [17]

The second is the portable fouling research unit (PFRU) that was developed for field operations. The PFRU are similar than the test facilities used by Smith [63] as shown in Figure 3-6 and Srinivasan and Watkinson [65] as shown in Figure 3-7. The third test unit is called the tube side fouling research unit (TFRU) and was designed to measure fouling inside a tube that is heated by condensing vapour. Fouling factor, in this case, is determined by overall measurements.

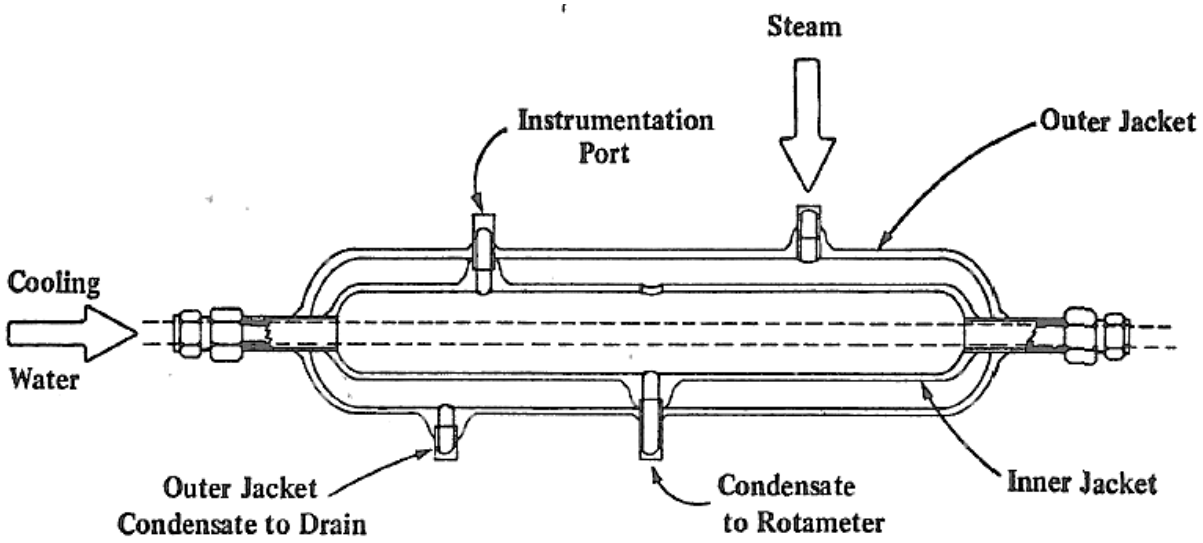

Figure 3-13: HTRI tube side fouling research unit (TFRU) [17]

The last of the four is the shell side research unit (SFRU) that was designed to measure fouling in complex geometries found on the shell side of shell and tube heat exchangers. Hot water is used and sensible heating fluid. Overall measurements are taken and overall resistances calculated. Two heat exchangers with more than 100 tubes are used. Each has different baffles spacing and arrangements.

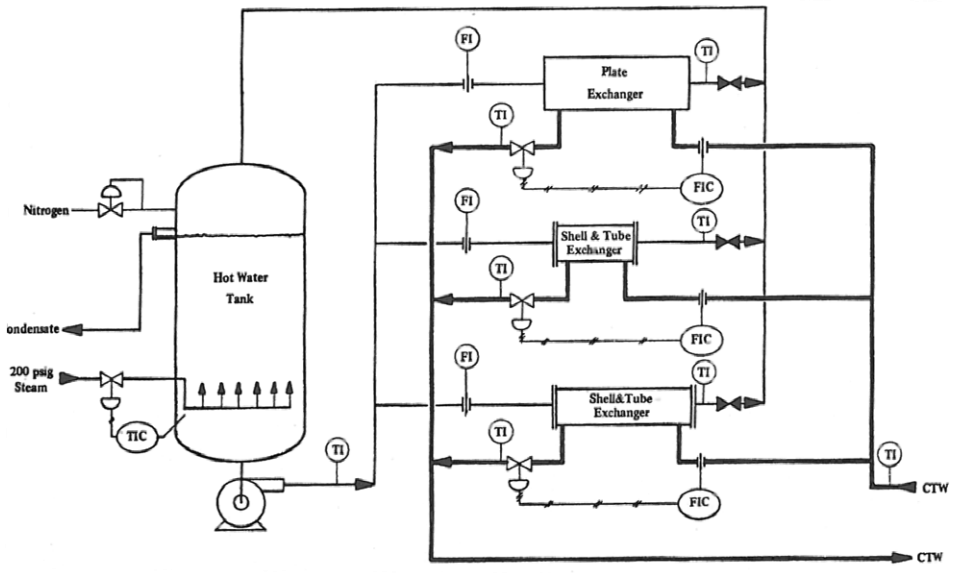

Figure 3-14: Shell side fouling research unit (SFRU) [17]

3.6.2 Heat transfer measurement for enhanced heat transfer

Eiamsa-ard et al. [77] studied the heat transfer enhancement of twisted tape inserts in tubes. Air was passed through a tube that was electrically heated from the outside under uniform heat flux conditions. Airflow, inlet, and outlet temperatures were measured. Local temperatures were measured on the outside of the tube at 15 different positions. The average heat transfer coefficient was calculated by using the area, wall temperature, bulk temperature and overall energy gain by the air. The uncertainties were calculated according to the methods described in [76].

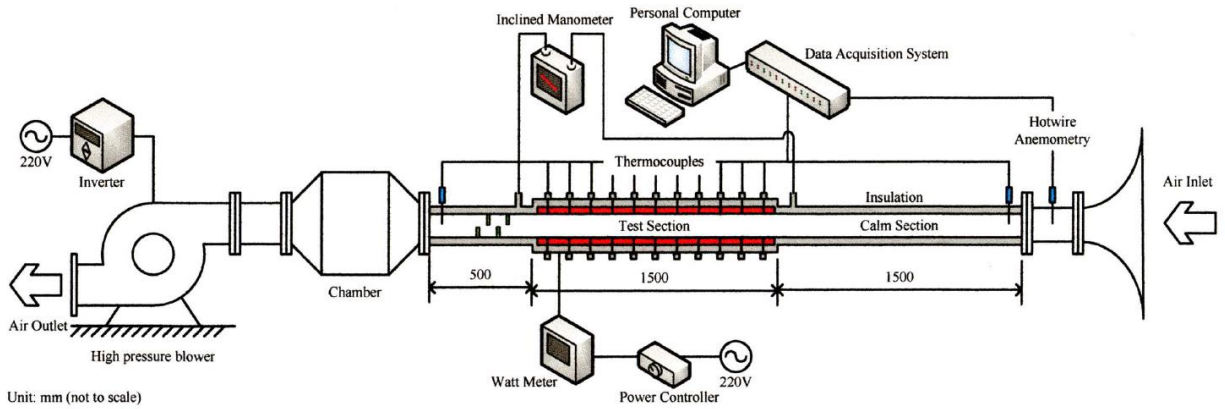

Figure 3-15: Experimental setup used by Eiamsa-ard et al. [77]

Bhuiya et al. [78] studied the enhancement of heat transfer in a tube fitted with perforated strip inserts. A similar experimental set-up as shown in Figure 3-15 and Figure 3-16 was used. A tube was spirally wounded with Nichrome wire. A current was passed through the wire and it was used to heat the tube. The tube inner wall temperature was measured close to the inner tube surface. Air was passed through the tube. The convective heat transfer coefficient inside the tube was calculated using the bulk fluid, surface temperatures and energy used by the electric heater.

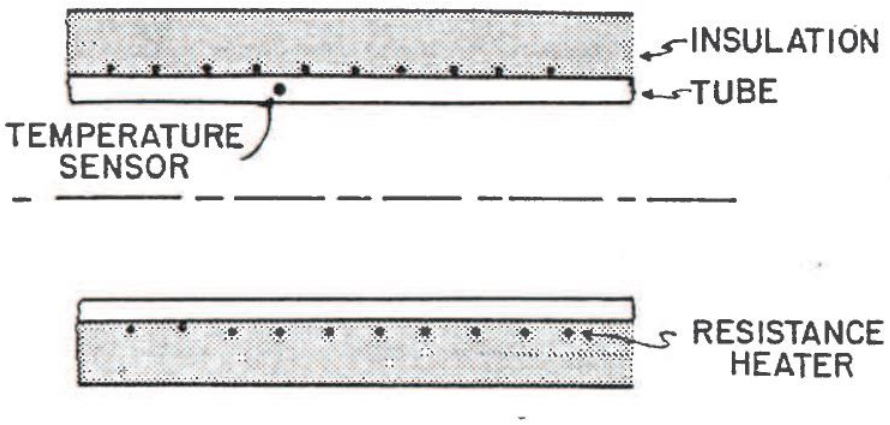

Figure 3-16: Experimental setup where tube are fitted with spirally wounded electric resistance heater [79]

Zeinali Heris et al. [80] experimentally investigated the heat transfer enhancement of a Cu/Water nano-fluid. The nano-fluid was passed through a tube and heated with condensing steam in a double pipe heat exchanger. This created a constant temperature boundary condition on the tube outside wall. The tube wall temperature was measured at 10 different locations. Along with the wall temperatures the inlet temperature, outlet temperature and flow rate of the nano-fluid were measured. This was used the calculated the nano-fluid heat transfer coefficients. See Figure 3-17 for experimental set-up.

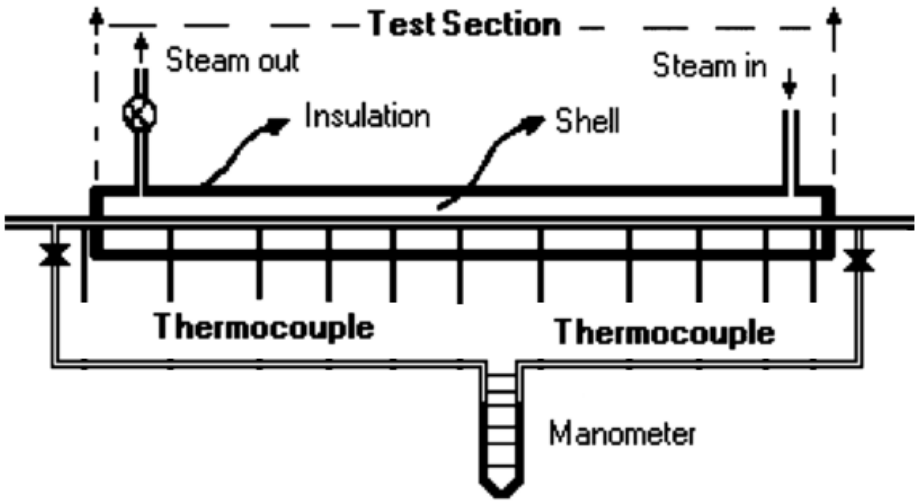

Figure 3-17: Experimental setup used by Zeinali Heris et al. showing condensing steam in double pipe heat exchanger [80]

Cui et al. [81] studied the heat transfer enhancement of W-Type spirally fluted tubes. An experimental setup similar than the one used by Zeinali Heris et al. [80] as depicted in Figure 3-17 was used. The set-up consisted of condensing steam and hence constant temperature boundary conditions on the outside of a tube in a double pipe heat exchanger. Uncertainty analysis was done according to the method described by Moffat [82].

Saha et al. [83] studied the heat transfer characteristics a tube enhanced with different types of twisted tape inserts. A similar heat transfer test section to what is shown in Figure 3-16 was used.

Xuan et al. [84] studied the convective heat transfer characteristics and flow features of nanofluids. A similar heat transfer test section than what is shown in Figure 3-16 was used.

Eiamsa-ard et al. [85] studied the heat transfer and flow friction of different twisted tape inserts. The experimental set-up consisted of a double pipe heat exchanger using hot and cold water on the two sides and is similar to the set-up depicted in Figure 3-17 with the only difference being that local wall temperature measurements were not taken, only bulk temperatures. Uncertainty analysis was done in accordance with ASME PTC 19-1 [86].

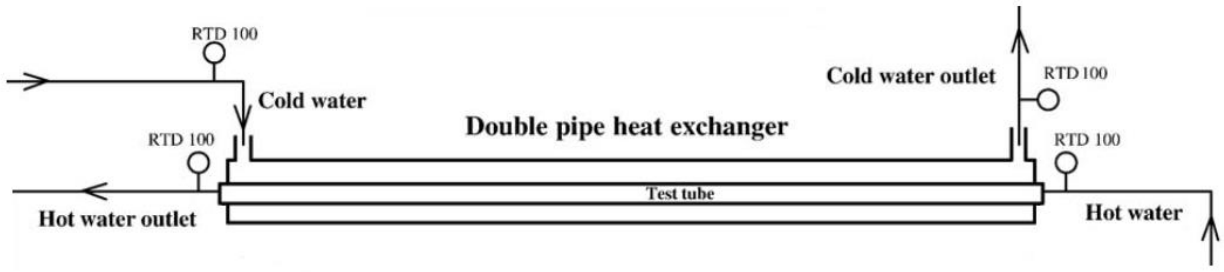

Figure 3-18: Test section as used by Eiamsa-ard et al. [85]

Syam Sundar et al. [87] experimented on the Al_2O_3 nano-fluids in a circular tube with twisted tape inserts. The heat transfer section used was similar than depicted in Figure 3-16.

3.6.3 Heat transfer measurement of tube coatings

Goodenough [88] tested the thermal conductivity of condenser coatings in 2013 as part of a master's degree at the University of Stellenbosch. The experimental set-up consisted of a pipe in pipe or annular type heat exchanger that tested single condenser tubes in the coated and uncoated conditions. The results of the tests were used to determine the conductivity of the applied coatings. Hot water was used for heating purposes. Overall measurements were taken during steady states conditions. The test section used as well as a schematic of the test facility is shown below.

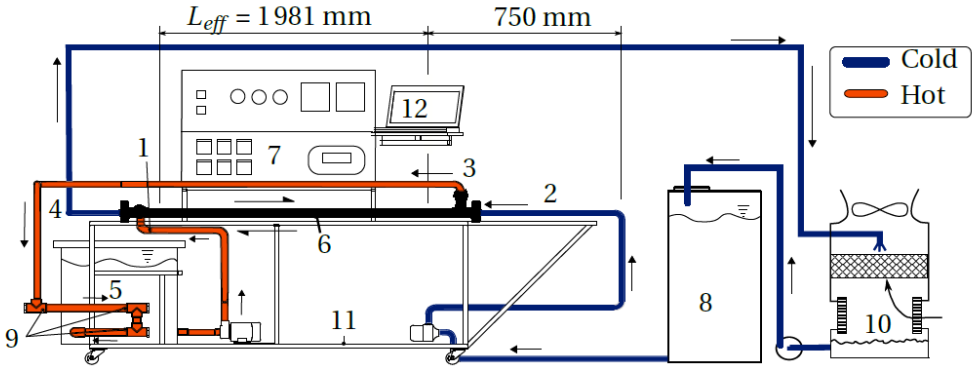

Figure 3-19: Schematic diagram of test rig used by Goodenough[88]

3.6.4 Reviews, comparisons, and recommendation of testing devices

Fischer et al. [17] published a paper in 1977 in an attempt to give guidance to industry on a unified approach to experimental fouling studies. It was recommended that the overall fouling factor is

determined by equation (2-19) and (2-20). Both local and overall measurement and calculation techniques are discussed. It is stated that local measurement gives reliable results for both small fouling resistances and low heat fluxes. Overall measurements are recommended for complex geometries but cautioned against due to the possibility of large errors when the area, fouling resistance or heat flux is small. Heating methods discussed include sensible fluid, condensing vapour, direct electrical and indirect electrical.

Suitor et al. [89] presented a paper in 1977 on the history and status of fouling research. Experimental apparatus formed part of the review. Three categories were identified. This included the type of test section, type of heating and type of measurement. The types of test sections were tubular, annular and unique designs which included hairpin shaped tubes, helical test sections and actual tube bundles in heat exchangers. Heating of the test section included electrical, steam and sensible heating fluid. Measurements were classified as direct or indirect. Direct included local measurement and allowed the calculation of local properties and for indirect only bulk properties was measured and calculated.

Knudson [79] presented a now classic and well-known paper in 1979 that gives a very good overview of apparatus and techniques that can be used for the measurements of fouling. The characteristics and techniques used by various authors are given. Specific test devices using various combinations of these techniques are given and discussed in detail. The combinations considered as well as the comparison are shown in tabular format.

Owens [75] compared three different test facilities in 1986. The first was the “LMSC facility” as shown in Figure 3-11, the second was called the “CMU facility” as used by Fetkovich [61], [62] and shown in Figure 3-5 and the third was a double pipe heat exchanger similar to Figure 3-18 and revered to as “Indirect”. Owens stated that comparison was difficult since the different test apparatuses were at different phases of their development when the comparison was done. Nevertheless, a simple ranking system was presented as shown in Table 3-3.

Table 3-3: Comparison of test facilities by Owens [75]

	LMSC Facility	**CMU Facility**	**Indirect Facility**
Power	1	1	2
Accuracy	1	2	3
Complexity	1	2	3
System Cost	1	3	2
Data Reduction	1	3	2
Developmental Status	2	1	-
Inlet temp variation	1	2	2
Tube Replacement	3	2	1
Fouling Factor	Local	Average	Average

Chenoweth [90] presented a very thorough overview of liquid fouling monitoring equipment in 1988. It included research units, measurement approaches as well as commercial online fouling monitors. The type of test sections that were considered included annular, single tube, transient measurement, multiple tubes, coiled wire and test sections without heat transfer that measures the change in pressure drop. Heating methods discussed included sensible fluid heating, condensing vapour, direct electrical and indirect electrical. The relationships and equations required to calculate the thermal resistance are given. Equation (2-19) is recommended. The possibility of negative fouling factors using this approach as mentioned in section 2.4.4 is discussed.

Bennett et al. [18] published a paper from the HTRI Crude Oil Fouling Task Force. The aim of this paper was to give recommendations to ensure crude oil research is standardised and the research that is done are industrially relevant. Although it is specifically focused on crude oil fouling and fouling rates, a number of the recommendations are relevant to the current work. The following are applicable recommendations:

- Test section to be used is described as the HTRI Annular test set-up as shown in Figure 3-6.
- Test section should be vertically orientated.
- A minimum of 20 pipe diameters before flow reached the annulus test section.
- Fully developed flow must be reached before the test section.
- Instrumentation should be installed outside the test section to ensure instrumentation stays clean.
- Calibration of all instruments must be done regularly.
- Contact thermal resistances may change over time and should be tested regularly.
- Test set-up should be checked and verified by comparing experimentally determined heat transfer coefficients with well-established heat transfer correlations.
- Test apparatus and equipment should be carefully maintained between experiments. Fouling factor must be calculated using equation (2-20).
- The use of equation (2-20) implies that local fouling resistances or factors must be calculated.

3.6.5 Summary of reviewed experiments

The following table gives a summary of the experiments that were reviewed:

Table 3-4: Summary fouling experiments from literature

Reference	Purpose of experiments	Type of test section	Type of heating	Local / Overall	Measurements Taken	Data Analysis
Jose et al. [55]	Fouling resistance and fouling rates of brine	Shell and tube / Annular	Sensible heating	Overall	Flow, temp. and pressure of each steam	Equation (2-19)
Agbisit et al. [56]	Surface fouling tenancies from corn wet-milling water	Annular	Indirect Electric Heating	Local	Wall surface temp, Bulk temp, Electric heat input.	Equation (2-20)
Abu-Zaid [57]	Fouling resistance and conductivity of water fouling	Annular	Indirect Electric Heating	Local	Wall surface temp, Bulk temp, Electric heat input.	Equation (2-20)
Goedecke et al. [58]	Crystalline fouling resistance for wire matrix inserts	Tubular	Sensible heating	Local and Overall	Flow, Wall surface temp, Bulk temp	Equation (2-20)
Zhenhua et al. [59]	Calcium Carbonate fouling during convective heat transfer	Tubular	Sensible heating	Overall	Flow, temp. and pressure of each steam	Equation (2-7) and (2-19)
Fetkovich et al. [61] [62]	Seawater biofouling of OTEC power plants	Thick wall copper block transient test - Tubular	Indirect Electric Heating	Overall	Temperature decay through thick copper block, flow rate, inlet, and outlet temp.	Transient equation
Smith [63]	Fouling propensity of 8 different crude oils	Annular – HTRI Probe	Indirect Electric Heating	Local	Wall surface temp, Bulk temp, Electric heat input.	Equation (2-20)
Ratel et al. [64]	8 different crude oils	Shell and Tube, Plate heat exchangers	Sensible heating	Overall	Flow, temp. and pressure of each steam	Not reported.
Srinivasan et al. [65]	Canadian Crude oils	Annular – HTRI Probe	Indirect Electric Heating	Overall	Bulk inlet and outlet temp, Electric heat input.	Equation (2-19)
Heneghan et al. [67]	Carbon deposition of different jet fuels	Tubular	Indirect Electric Heating	N/A	Wall surface temp, Bulk temp, Electric heat input.	Physical measurement
Chin et al. [68]	Deposits from heated hydrocarbon fuels	Tubular	Indirect Electric Heating	N/A	Amount of Carbon deposits measured	Physical measurement
Grant Jones et al. [69] [70]	Insoluble in a Jet-A fuel	Tubular	Indirect Electric Heating	N/A	Amount of Carbon deposits measured	Physical measurement
Muller-Steinhagen & Branch [66]	Experiments with New Zealand Forest Products Kraft black liquor	Annular – HTRI Probe	Indirect Electric Heating	Local	Wall surface temp, Bulk temp, Electric heat input.	Equation (2-4) and (2-19)
Marteney et el. [71]	Decomposition and tendency to form deposits of aircraft fuel	Tubular	Direct Electric Heating	N/A	Wall surface temp, Bulk temp, Electric heat input, Amount deposits	Physical measurement
Hays et al. [73]	Fouling on enhanced tubes	Annular – HTRI Probe	Indirect Electric Heating	Local	Wall surface temp, Bulk temp, Electric heat input.	Equation (2-20)
Al-Janbi et al. [74]	Fouling on flat enhanced heat transfer surfaces on flat plates	Flat plates	Indirect Electric Heating	Local	Wall surface temp, Bulk temp, Electric heat input.	Equation (2-20)
Owens [75]	LMSC fouling measurement device	Tubular	Indirect Electric Heating	Local	Wall surface temp, Bulk temp, Electric heat input.	Equation (2-20)
Fischer et al. [17]	HTRI stationary fouling unit	Tubular	Indirect Electric Heating	Local	Wall surface temp, Bulk temp, Electric heat input.	Equation (2-20)
Fischer et al. [17]	HTRI portable fouling research unit (PFRU)	Annular – HTRI Probe	Indirect Electric Heating	Local	Wall surface temp, Bulk temp, Electric heat input.	Equation (2-20)
Fischer et al. [17]	HTRI tube side fouling research unit (TFRU)	Tubular	Condensing steam	Overall	Flow, temp. and pressure of each steam	Adaptation of Equation (2-4)
Fischer et al. [17]	HTRI shell side research unit (SFRU)	Shell and tube heat exchanger	Sensible heating	Overall	Flow, temp. and pressure of each steam	Equation (2-19)
Eiamsa-ard et al. [77]	Heat transfer enhancement of twisted tape inserts in tubes	Tubular	Indirect Electric Heating	Local	Wall surface temp, Bulk temp, Electric heat input.	Adaptation of Equation (2-4)
Bhuiya et al. [78]	Heat transfer enhancement in a tube fitted with a perforated strip	Tubular	Indirect Electric Heating	Local	Wall surface temp, Bulk temp, Electric heat input.	Adaptation of Equation (2-4)

Zeinali Heris et al. [80]	Heat transfer enhancement of a Cu/Water nano-fluid	Tubular	Condensing steam	Local	Wall surface temp, Bulk temp, Electric heat input.	Adaptation of Equation (2-4)
Cui et al. [81]	Heat transfer enhancement of W-Type spirally fluted tubes	Tubular	Condensing steam	Local	Wall surface temp, Bulk temp, Electric heat input.	Adaptation of Equation (2-4)
Saha et al. [83]	Heat transfer enhancement of different types of twisted tape inserts	Tubular	Indirect Electric Heating	Local	Wall surface temp, Bulk temp, Electric heat input.	Adaptation of Equation (2-4)
Xuan et al. [84]	Convective heat transfer characteristics and flow features of nanofluids	Tubular	Indirect Electric Heating	Local	Wall surface temp, Bulk temp, Electric heat input.	Adaptation of Equation (2-4)
Eiamsa-ard et al. [85]	Heat transfer and flow friction of different twisted tape inserts	Tubular	Sensible heating	Overall	Flow, temp. and pressure of each steam	Adaptation of Equation (2-4)
Syam Sundar et al. [87]	Heat transfer of Al2O3 nano-fluids in a circular tube with twisted tape inserts	Tubular	Indirect Electric Heating	Local	Wall surface temp, Bulk temp, Electric heat input.	Adaptation of Equation (2-4)
Good-enough[88]	To determine the thermal conductivity of condenser tube coatings	Annular	Sensible heating	Overall	Flow, temp. and pressure of each steam	Adaptation of Equation (2-14) and (2-15)

3.6.6 Classification and identification of reviewed experiments

Clear trends can be observed in the type of experiments used by different researchers. These trends can be used to create different categories to group experimental apparatus. A number of researchers have done similar categorisations. The trends observed from the literature review and from the work done by others [17][79][89][90] were used to create the categories of test apparatus. The options available in each category are given below and summarised in Table 3-5.

1. Type of test section: The type of test section is determined by the geometry of the test section. Flow inside a tube is considered *tubular*, flow outside the tube as *annular*, shell and tube heat exchangers with multiple tubes as *heat exchangers* and *flat plates* are self-explanatory.
2. Type of heating: The type of heating is determined by how the energy is applied to the test section. Heating by means of another flowing fluid is referred to as *sensible heating*. *Direct electric heating* is where the tube itself is used as a resistance heater. *Indirect electric heating* is a type of heater wrapped around a tube or placed inside a tube. *Condensing steam* is self-explanatory.
3. Experimental state: Is determined by whether the measurements are taken during a steady state or transient process.
4. Measurements and Calculation: If only bulk properties are measured and overall resistances of coefficients calculated it is referred to as *overall*. If wall temperatures and fluid temperatures are measured at specific locations and resistances or coefficients for that specific location calculated it is referred to as *Local*.

Table 3-5: Options in each category of experimental apparatuses

Test Section Geometry			
Tubular	Annular	Flat plate	Heat Exchanger
	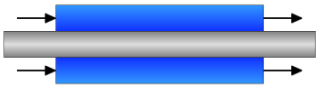		
Types of heating			
Sensible fluid	Condensing steam	Indirect electric heating	Direct electric heating
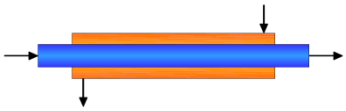	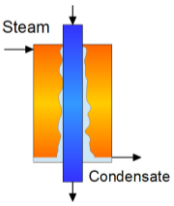	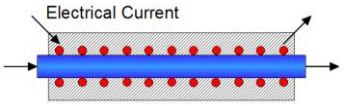	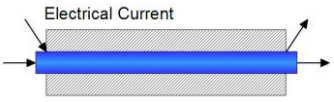
Experimental State		**Measurement & Calculation**	
Steady State	Transient	Overall	Local
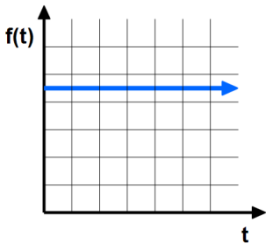	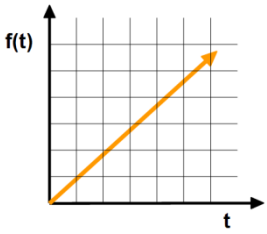		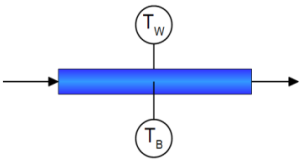

From the above categorisation and literature review, there are a number of combinations that can be identified and are commonly used. The selection of the best concept for this work is done in section 4.4.

Table 3-6: Common Test Sections

Common Test Sections – Descriptions and Figures	
1. Annular Geometry, indirect electric heating (Figure 3-6 and Figure 3-7) 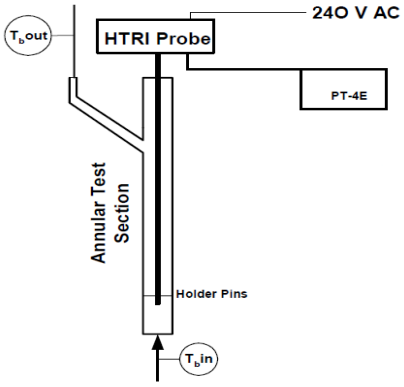	2. Thin-Walled Tube, indirect electric heating (Figure 3-16) 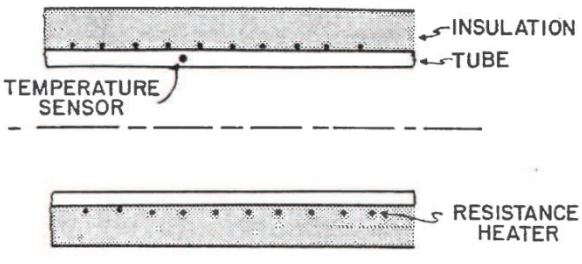

3. Thick Walled Tube, indirect electric heating (Figure 3-10)

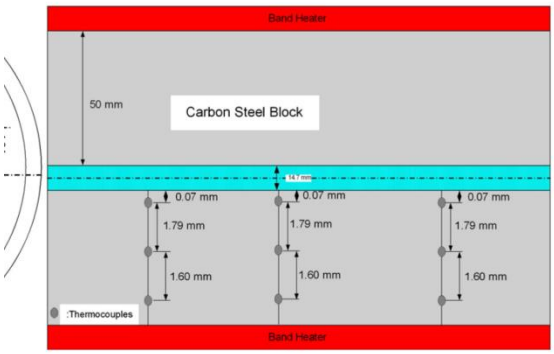

4. Thick Walled Tube, transient technique (Figure 3-5)

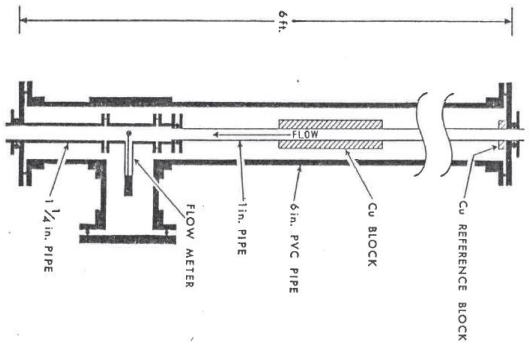

5. Annular or Circular tube geometry, direct electric heating (Figure 3-9)

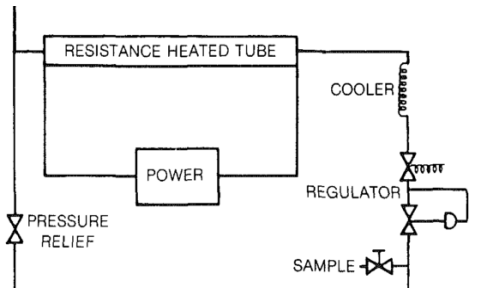

6. Annular or Circular tube geometry, sensible heating (Figure 3-4)

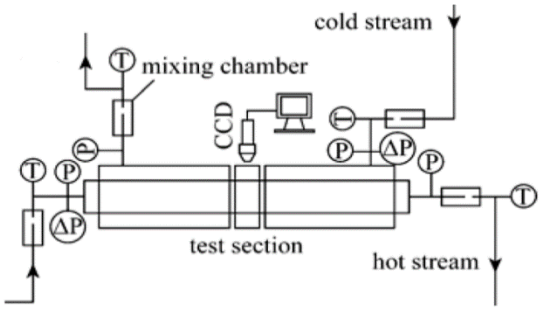

7. Annular or Circular tube geometry, condensing vapour (Figure 3-13)

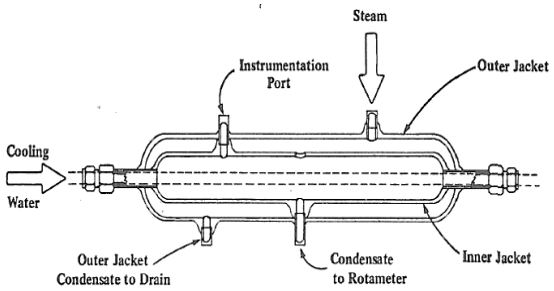

8. Complex Geometries (Heat Exchangers, Figure 3-14)

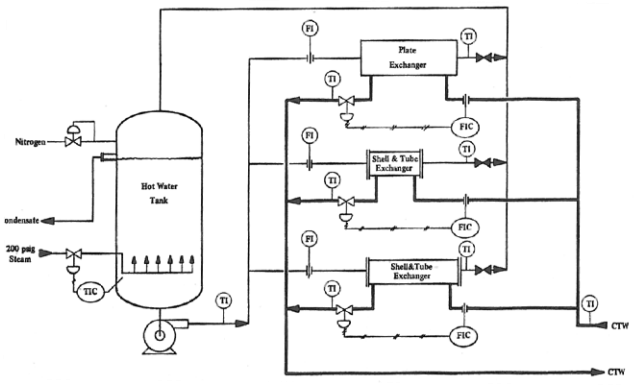

3.7 Uncertainty of measurement

3.7.1 Introduction

When a result, or measurement, is presented the quality of the result or measurement must be defined. Uncertainty analysis provides a methodical approach to estimating this quality [91]. Kline and McClintock [76] defined uncertainty as "a possible value the error might have". In most circles, it is not acceptable to provide any experimental results without describing and discussing the uncertainties involved with the results [82].

In 1993 the Journal of heat transfer published a policy [92] giving guidance on estimating uncertainty. This was done to ensure conformity in the presentation of experimental data and also to raise the awareness of authors on the importance of uncertainty analysis and reporting. The American Society of Mechanical Engineers (ASME) published ASME PTC 19.1 [86] that describes test uncertainty and the determination thereof.

The following section will give an overview of uncertainty analysis for single measurements as well as the uncertainty propagation of these measurements to a result.

Different symbols and definitions are used by different authors to describe uncertainty analysis. For the purposes of this work, the definitions and symbols from ASME PTC 19.1 [86] will be adhered to.

3.7.2 Errors and uncertainty

Every measurement taken has some error associated with the measurement. This results in a difference between the measured value (X) and the true value (X_{true}). This difference is called the total error (δ).

$$X_{true} = X + \delta \tag{3-3}$$

The total error consists of 2 components. That is the random error and systematic error. Random error is the portion of the total error that varies randomly through the test duration. Systematic error is the portion of the total error that remains constant through the duration of the test. Both these errors can be seen in Figure 3-20.

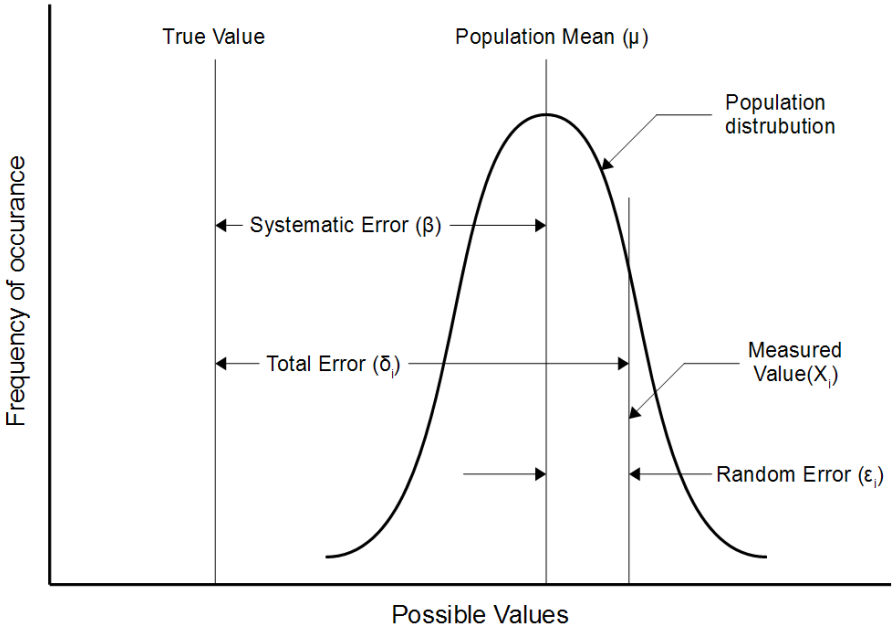

Figure 3-20: Measurement Errors [86]

Since it is impossible to know the true value, it is impossible to know the true error. Only the expected limits of the error can be estimated. This estimate is an assigned value called the uncertainty [91]. The uncertainty describes an interval about the measured value within which it is suspected that the true value will fall within a stated probability.

Figliola [91] summarised it as follows: Errors is a property of the measurement, uncertainty is a property of the result and uncertainty analysis is the process of identifying, quantifying and combining of errors.

The total uncertainty in the measurements is a combination of the random uncertainty caused by the random error and the systematic uncertainty caused by the systematic error. When combined it is referred to as combined or overall uncertainty.

Moffat [82] gave a good concise way to describe this uncertainty of each variable. This is given by:

$$X_i = X_i(measured) \pm \delta X_i \qquad (95\%) \tag{3-4}$$

Interpretation of the above statement is as follows:

- The best estimate of X_i is $X_i(measured)$.
- There is a uncertainty related to X_i that may be as large as δX_i.
- The probability of the uncertainty related to X_i to be smaller than δX_i is 95%, which is then called the confidence level.

The journal of mass and heat transfer uncertainty policy [92] suggests that all uncertainty evaluations must be performed at a confidence level of 95%. ASME PTC 19.1 [86] indicates 95% as accepted practice. For the purposes of this work, 95% will also be used.

3.7.3 Random uncertainty

Random uncertainty is the interval of which the mean of the results would fall if the experiment was repeated many times under the same conditions based on a certain confidence limit [92]. It is thus an estimation of the lack of repeatability that is caused by unsteadiness and stochastic processes. The random uncertainty is also referred to as the precision limit.

For a normally distributed population and a large sample size where N ≥ 30 the random uncertainty can be defined as follows:

$$S_{\bar{X}} \pm t s_{\bar{X}} \tag{3-5}$$

With $\bar{X}$ the sample mean,

$$\bar{X} = \frac{\sum_{j=1}^{N} X_j}{N} \tag{3-6}$$

$s_{\bar{X}}$ the random standard uncertainty,

$$s_{\bar{X}} = \frac{s_X}{\sqrt{N}} \tag{3-7}$$

s_X the sample standard deviation,

$$s_X = \sqrt{\sum_{j=1}^{N} \frac{(X_j - \bar{X})^2}{N-1}} \tag{3-8}$$

and t the coverage factor or so-called Student's t variable as described below.

According to ASME PTC 19.1 [86] a high number of measurements collected during a test is beneficial for the following reasons:

- It improves the sample mean as an estimation of the population mean.
- It improves the sample standard deviation as an estimation of the population standard deviation.
- It reduces the value of the random uncertainty of the sample mean.

Typically 30 measurements are considered sufficient. For the purposes of this work, a minimum of 50 measurements will be taken for each test.

3.7.4 Systematic uncertainty

The systematic uncertainty is also referred to as the bias limit. The systematic uncertainty is an estimate of the fixed or constant error [92]. In successive measurements, the value of the fixed error does not change. They are constant and can therefore not be observed from collected test data. By increasing the number of measurements, the value of the systematic uncertainty will not change. It can thus be difficult to determine or estimate the systematic uncertainty.

Figliola [91] gave some methodologies to estimate the systematic uncertainty. This includes calibration, interlaboratory comparisons, judgement, and experience. ASME PTC 19.1 [86] gives possible sources as published information, special data and engineering judgement. The most common source of uncertainty values is calibration and OEM or supplier data sheets. The systematic uncertainty are thus not calculated, but determined by any of the mentioned methods.

3.7.5 Combined and expanded uncertainty of a measurement

The combined uncertainty is the total uncertainty in the measurements. It is a combination of the random and systematic uncertainty. The combined uncertainty is calculated as follows:

$$u_{\bar{X}} = \sqrt{(s_{\bar{X}})^2 + (b_{\bar{X}})^2} \tag{3-9}$$

With

$s_{\bar{X}}$ = the random uncertainty and

$b_{\bar{X}}$ = the systematic uncertainty

The expanded uncertainty of the measurement mean is the combined uncertainty at a defined level of confidence.

$$U_{\bar{X}} = tu_{\bar{X}} \tag{3-10}$$

For a 68% confidence interval, the student's multiplier t is equal to 1, and then the expanded uncertainty is equal to the combined uncertainty. For applications where a 95% confidence level is required, t is equal to 2.

3.7.6 Error sources

Errors and thus uncertainties in measurements can be grouped by different sources. These following sources were identified by Figliola [91] and ASME PTC 19.1 [86].

- Errors due to the test article or instrumentation installation
- Data Acquisition Errors
- Data Reduction Errors

- Calibration Errors
- Errors due to methods and other effects

3.7.7 Uncertainty of a result

In most instances, the required result is not directly measured. It is rather a function of more basic measurements like temperature, pressure and mass flow. Each of the measurements has a certain uncertainty associated with it. These different uncertainties need to be propagated to the result. This is done by using the functional relationship between the measurements and the result. The effect of the propagation can be approximated by the Taylor series method [86]. The estimation of the uncertainty of a calculated result is done as follows:

The result R is expressed in terms of a number of independent variables $\bar{X}$

$$R = f(\bar{X}_1, \bar{X}_2, \dots, \bar{X}_i) \tag{3-11}$$

With subscript *i* indicating the total number of variables involved in R and $\bar{X}$ the average value of each of the variables.

The random uncertainty of the result will be

$$s_R = \left[\sum_{i=1}^{N} \left(\frac{\partial R}{\partial X_i} s_{\bar{X}_i}\right)^2\right]^{\frac{1}{2}} \tag{3-12}$$

And similarly the systematic uncertainty of the result will be:

$$b_R = \left[\sum_{i=1}^{N} \left(\frac{\partial R}{\partial X_i} b_{\bar{X}_i}\right)^2\right]^{\frac{1}{2}} \tag{3-13}$$

The combined uncertainty of the result can then be found by taking the root-sum-square of both the random and systemic uncertainty.

$$u_R = \sqrt{(s_R)^2 + (b_R)^2} \tag{3-14}$$

When combining and simplifying equation *(3-12)*, *(3-13)* and (3-14) u_R can be written as:

$$u_R = \sqrt{\sum_{i=1}^{N} \left(\frac{\partial R}{\partial X_i} s_{\bar{X}_i}\right)^2 + \sum_{i=1}^{N} \left(\frac{\partial R}{\partial X_i} b_{\bar{X}_i}\right)^2} \tag{3-15}$$

And the expanded uncertainty of the result as

$$U_R = t u_R \tag{3-16}$$

With the t the student's multiplier with values as mentioned previously.

3.7.8 Correlated systematic uncertainty

A special case of the propagation of systematic uncertainties can be found when the systematic uncertainties are correlated. There are many situations where the measured quantities may not be independent. Examples include using the same instruments for different measurements or if different instruments are calibrated against the same calibration standard.

For this work measurements from the same instruments are used to determine the final result. These measurements are 100% correlated. Correlated systematic uncertainty is thus applicable and will be used.

In these cases the systematic uncertainty of the results will be [91]:

$$b_R = \left[\sum_{i=1}^{N}\left(\frac{\partial R}{\partial X_i} b_{\bar{X}_i}\right)^2 + 2\sum_{i=1}^{L-1}\sum_{j=i+1}^{L}\frac{\partial R}{\partial X_i}\frac{\partial R}{\partial X_j} b_{\bar{X}_i\bar{X}_j}\right]^{\frac{1}{2}} \tag{3-17}$$

Where index j is a counter equal to *i + 1* and

$$b_{\bar{X}_i\bar{X}_j} = \sum_{h=1}^{H}\left(b_{\bar{X}_i}\right)_h\left(b_{\bar{X}_j}\right)_h \tag{3-18}$$

Where H is the number of elemental errors that are correlated between X_i and X_j and h is a counter for each correlated error. Examples of correlated systematic uncertainty calculations are given in [86] and [91].

3.7.9 Determining uncertainty

The following flow chart describes the determination of the uncertainty of a result that consists of a function with *i* measured variables with each measured variable having *k* random and *k* systematic errors associated with the measurement. Factor *j* is equal to *i + 1*.

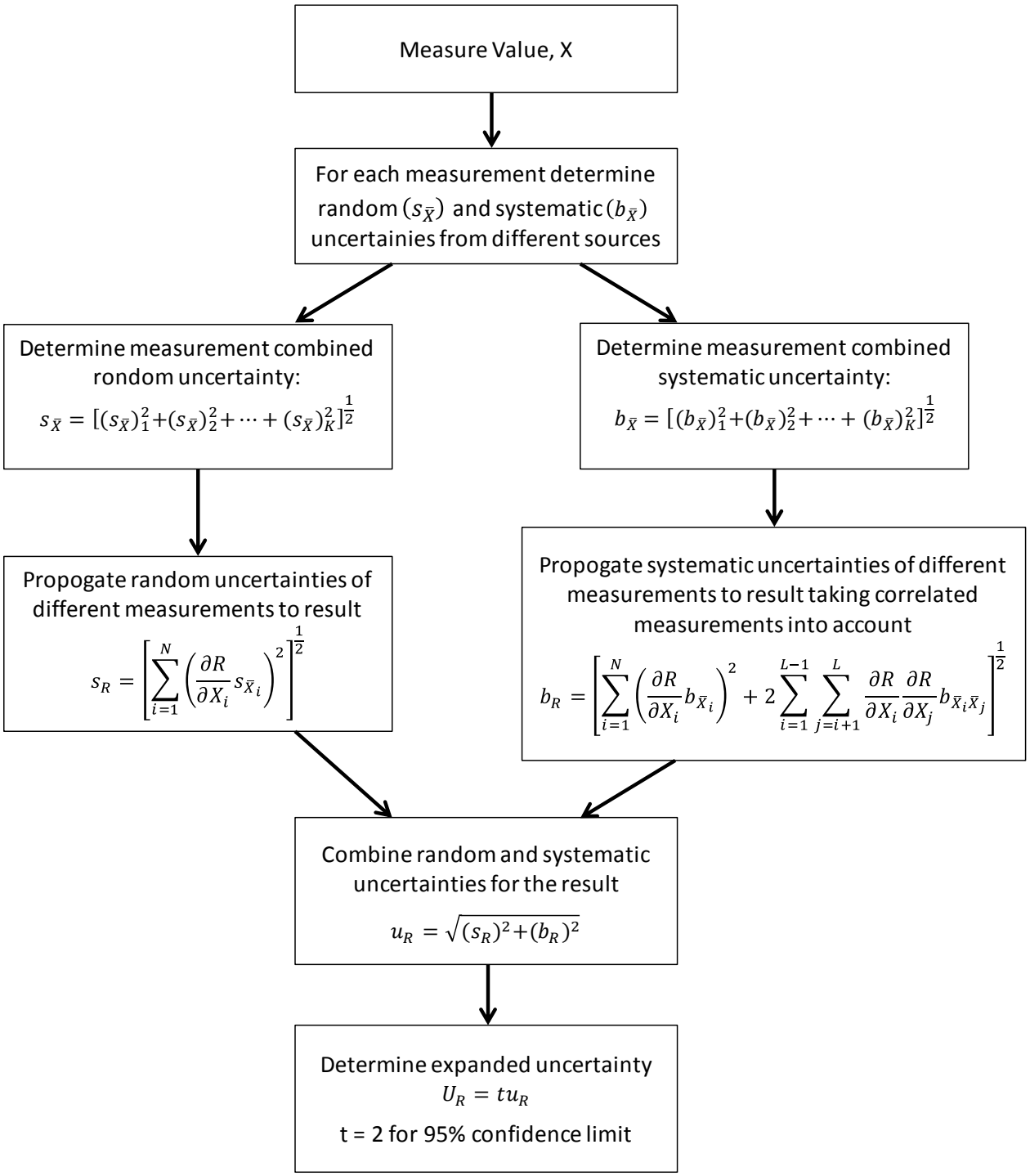

3.8 Calibration

3.8.1 Calibration introduction

Calibration is defined by [86] as “the process of comparing the response of an instrument to a standard instrument over some measurement range”. Holmon [93] stated that the importance of

calibration cannot be overemphasized since it is calibration that firmly establishes the accuracy of instruments. The calibration process usually involves the comparison of the instrument measurement that is being calibrated with a known value. This known value can be one of the following:

- A fixed temperature point like the melting point of ice.
- Another highly accurate instrument.
- A process that contains multiple measurements.

Typically the calibration standard or method has a known certified uncertainty associated with it. SANAS are often used in South Africa for these certifications. ASME PTC 19.1 [86] provides two methods where the uncertainty of an instrument can be determined via calibration. These are:

- In-spec calibration uncertainty.
- Calibration constant or curve uncertainty calculations.

3.8.2 In-Spec calibration uncertainty

In-spec calibration refers to a process where an instrument either passes or fails an inspection or calibration. The measurement uncertainty of an instrument determined to be "in-spec" is calculated as follows:

$$U_{95,IS} = 2\left[(b_{SD})^2 + \left(\frac{U_I}{2}\right)^2\right]^{\frac{1}{2}} \tag{3-19}$$

Where

$\mathrm{U}_{95,\mathrm{IS}}$ = In-Spec Calibrated Uncertainty

b_{SD} = The systematic standard uncertainty of the calibration standard

U_I = Manufacturers quoted instrument uncertainty or accuracy specification for the instrument under calibration. It is assumed to be 95% with infinite degrees of freedom

3.8.3 Calibration constant or curve uncertainty calculations

When a calibration constant or curve is a result of the calibration the following procedure is followed to determine the calibration uncertainty.

$$U_{95,Cal} = 2\left[\left(b_{R,Cal}\right)^2 + \left(s_{\bar{R},cal}\right)^2\right]^{\frac{1}{2}} \tag{3-20}$$

Where

$U_{95,Cal}$ = Simplified calibration uncertainty for the instrument

$b_{R,Cal}$ = Systematic standard uncertainty of the calibration standard. It is the combination of the calibration standard's systematic and random uncertainties into the systematic uncertainty of the instrument under calibration

$s_{\bar{R},cal}$ = Random standard uncertainty of the calibration

$s_{\bar{R},cal}$ can be determined from the standard estimate of error (SEE):

$$s_{\bar{R},cal} = \frac{SEE}{\sqrt{N_{cal}}} \tag{3-21}$$

And

$$s_{R,cal} \approx SEE = \left[\frac{\sum_{i=1}^{N}\left(Y_i - Y_{i_c}\right)^2}{N-K}\right]^{\frac{1}{2}} \tag{3-22}$$

Where

K = number of curve-fit coefficients

N = number of data points used to calculate SEE

N – K = Degrees of freedom

Y_i = ith data value in the calibration corresponding to X_i

Y_{i_c} = Y_i value of the curve fit corresponding to X_i

For the purposes of this work this method will be used for the determination of the uncertainty of the temperature measurement system.

3.9 Temperature measurement

Temperature is a multiple input for the determination of the fouling factor. It is thus critical that temperature is accurately measured. This section will discuss and compare the most common types of temperature measurement.

There are a number of temperature sensors that are used. From these Thermocouples (T/Cs) and resistance temperature detectors (RTDs) and are the most common [94] and applicable to the current work.

3.9.1 Thermocouples

A thermocouple is a temperature measurement device consisting of two electrical wires that are made of dissimilar materials and joined at both ends. Each end is typically referred to as a junction. The end exposed to the process fluid is referred to as the hot junction. The other end is called the cold or reference junction. This reference junction is outside the process fluid at a known temperature. It is at this end where the voltage is measured.

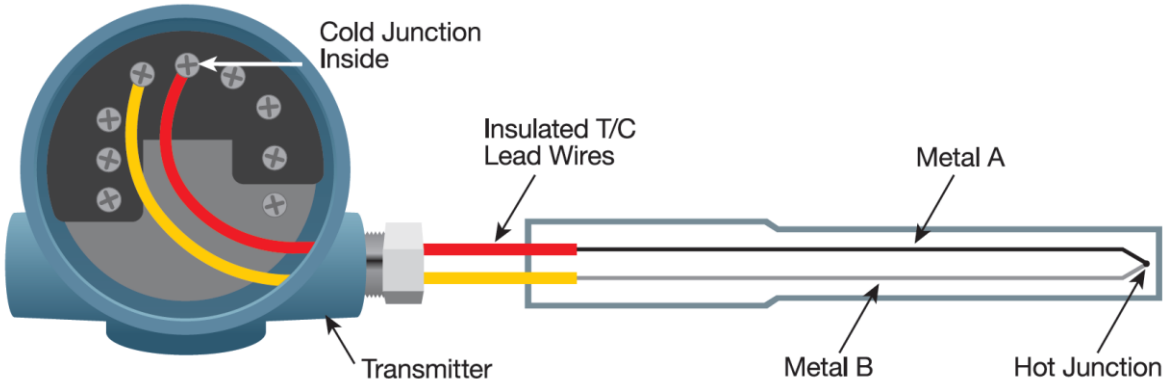

Figure 3-21: Thermocouple [94]

The working of a thermocouple is based on the Seeback effect [95]. The Seeback effect refers to the generation of voltage or EMF in an open electrical circuit due to a difference in temperatures between junctions in the circuit [91]. The voltage measured at the cold junction is proportional to the difference in temperature between the hot and the cold junction [94]. The linearity of the temperature voltage relationship is dependent on the combination of metals used in the thermocouple. The voltage that is measured is only an indication of the difference in temperature between the hot and the cold junction. To know the temperature of the hot junction and thus the process the temperature at the cold junction must be known. This can typically be done by means of an ice bath with a reference temperature of 0°C. That is however not practical on a commercial scale. Most manufacturers of thermocouples install built-in reference junction compensation in the form of thermistor or RTD temperature measurement [91].

Thermocouples are a common choice for temperature measurements [96]. This is mainly due to their self-energization, low cost, relatively simple design and construction, small size and if well protected their resistance to its surroundings. The measured voltages are small, typically 40µV for every 1°C but instruments can commonly display readings with 0.1°C resolution [95]. Uncertainty in temperature measurements when using thermocouples ranges from ±1°C to as low as ±0.1°C [91].

Thermopiles are multiple-junction thermocouples. The main purpose is to amplify the output of the circuit. Thermocouple output voltages are very low and one of the main uncertainties is the measurement of these low voltages. By using multiple thermocouples the voltage is amplified and can be measured more accurately. Thermopiles are also useful to measure temperature differentials. Figure 3-22 shows two different arrangements of a number of thermocouples used as thermopiles.

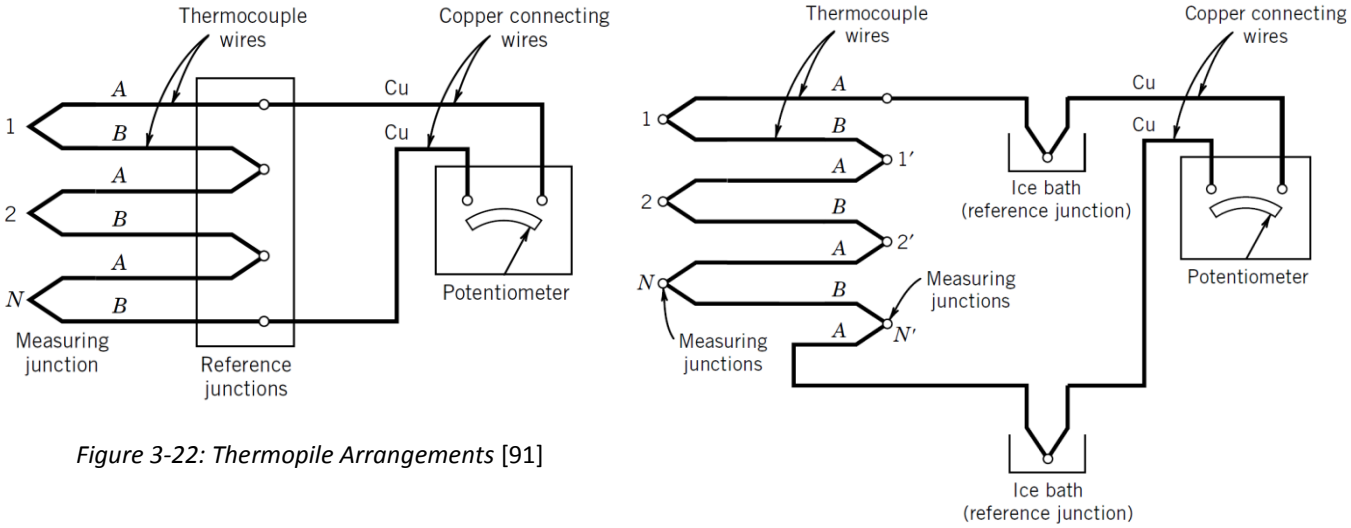

Figure 3-22: Thermopile Arrangements [91]

3.9.2 Resistance temperature detectors (RTD)

The electrical resistance of a metal increases as the temperature increases. This is known as resistivity [94]. By measuring the resistance of a specific material the temperature to which that metal is exposed to can be determined. RTD sensors are manufactured from wire, film, chips or beads that are usually placed in a protective sleeve. The resistive material can be nickel, copper or platinum. The most common of these is platinum [91]. This is due to its high accuracy, good repeatability, excellent linearity over a wide range and large change in resistivity per degree of temperature change [94].

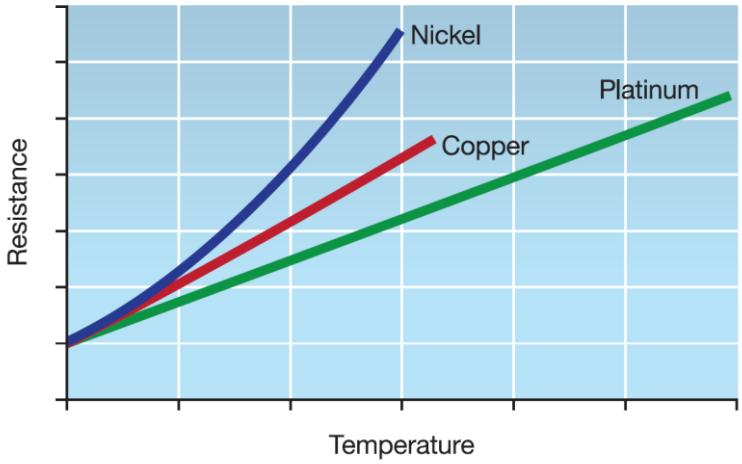

Figure 3-23: Resistance change vs temperature change for common RTD materials [94]

Pt100 is a specific RTD where platinum is used and the resistance is approximately 100 Ω at 0°C. Figure 3-24 shows the change in resistance for Pt100 sensor.

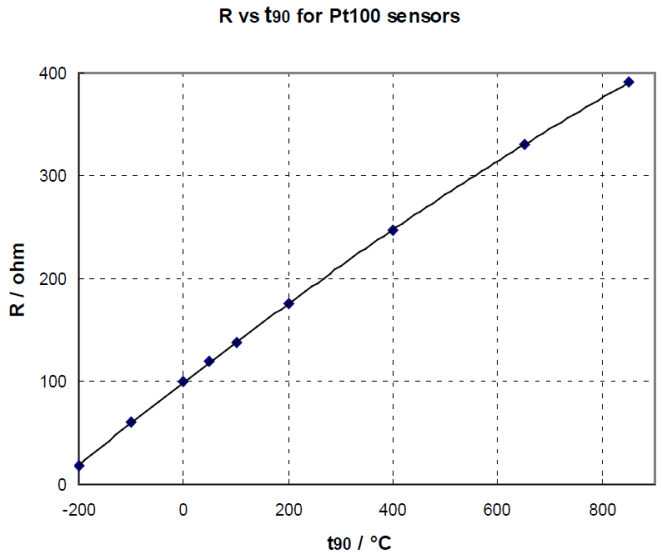

Figure 3-24: Change in resistance with temperature of a Pt100 sensor [95]

According to Figliola [91], by properly constructing an RTD and correctly measuring its resistance, uncertainties in temperature measurement can be as low as ±0.005°C. Rusby [95] reports that Pt100 sensors can be as accurate as ±0.01°C over a limited temperature range of -100°C to +250°C. According to Childs [96] the achievable uncertainty for industrial platinum resistance thermometers is generally in the order of ±0.01°C to ±0.2°C over a range of 0°C to 300°C.

Industrial platinum resistance thermometer sensors are standardised in BS EN 60751[97]. Different tolerance classes are given, each with a difference in tolerance or accuracy. The different classes can be seen in Table 3-7 below. The standard allows for special tolerance classes. These special classes are constructed as multiples or fractions of class B. One such a class that is commonly available is a special class called 1/10 DIN. This class uses the tolerances of class B divided by 10. Table 3-7 shows this is the most accurate class available.

Table 3-7: BS EN 60751 Tolerance Classes and Special Class 1/10 DIN

Tolerance Class	Tolerance Values [°C]
AA	$\pm$ 0.1 + 0.0017|T|
A	$\pm$ 0.15 + 0.002|T|
B	$\pm$ 0.3 + 0.005|T|
C	$\pm$ 0.6 + 0.01|T|
1/10 DIN	$\pm$ 0.03 + 0.0005|T|

Note the tolerance value is given as a function of temperature (T)

3.9.3 Thermistors

Thermistors consist of a ceramic semiconductor whose resistance is sensitive to temperature [96]. The word thermistor is derived from *thermally* sensitive *resistors* [91]. The resistance of thermistors decreases rapidly with temperature which is in contrast with the small increase with temperature of RTDs [91]. Where RTD have a linear change in resistance thermistors have a highly nonlinear change in resistance with temperature. Thermistors are well suited for use in small probes [95] and are generally used when high sensitivity, ruggedness or fast response times are required [91], the level of uncertainty is less critical [96] and when non-linear electrical processing, such as having a microprocessor, are available.

The uncertainty of thermistors can be as low as ±0.01°C to ±0.001°C, but for commercial applications, it is typically in the order of ±1°C [96].

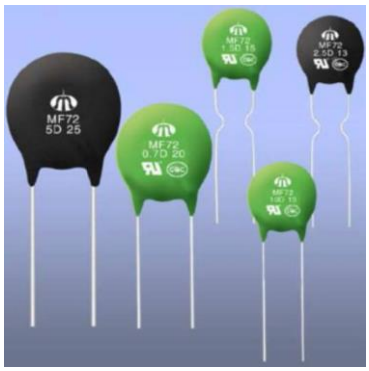

Figure 3-25: Thermistors for use in current limiting circuits [95]

3.9.4 Comparison and application

Three types of temperature measurement sensors are discussed above. The following table provides a direct comparison.

Table 3-8: Comparison of thermocouples and RTDs (adapted from [96] *and* [98]*)*

Property / Criteria	Thermocouples	RTD (Pt100, wire wound)	Thermistor
Cost	Low	High	Low
Range	-270°C to 2300°C	-240°C to 900°C	-100°C to 300°C
Uncertainty	Medium	Low	Low
Accuracy	Low (1°C common)	High (0.03°C common)	Medium (<1°C)
Stability	Low	Medium	Good to Medium
Repeatability	Fair	Excellent	Medium
Response	Medium to Fast	Medium	Medium to fast
Linearity	Fair	Good	Low
Physical Size	Small to large	Medium to Small	Small to medium

For the purposes of this work, RTD temperature measurement sensors will be used. Due to availability and standardisation, the Pt100 sensors and more specifically Class 1/10 DIN will be selected for this work.

3.10 RTD measurement system

Section 3.8 confirmed the RTD temperature measurement as the preferred technology type to be used for this work. It is however clear that in an RTD probe, the temperature is not actually measured. The actual measurement that is made is resistance (Ω). This is converted mathematically to a temperature reading. For high accuracy measurement, this is done externally to the probe. This section will discuss in more detail the different parts of an RTD temperature measurement system, how resistance is measured and some factors that affect the accuracy of RTD temperature measurement.

3.10.1 Constituents of an RTD measurement system

A typical RTD measurement system consists of the probe or sensor (Figure 3-26 on the left) and the data logger or data acquisition system (Figure 3-26 on the right). The probe contains the resistance element that changes with temperature and should be inserted into the flow path or connected to the equipment where the temperature must be measured. The data logger is where the actual measurement takes place. Typically data loggers can measure voltage and current and do the conversion to temperature. They can be connected to a PC, network or DCS to interface with a software system where data analyses or control functions can be carried out. The data logger or data acquisition system looks slightly different for industrial applications and are commonly referred to as the transmitter. Some data loggers can supply the current that allows the resistance measurement, for others an external current source must be used.

Figure 3-26: RTD Probe and data logger [99]

3.10.2 Resistance measurement and factors affecting it

The foundation of resistance measurements is Ohm's law [100]. If a constant current is supplied to a resistance and the potential difference is measured across the resistance, the actual resistance in ohm (Ω) can be easily calculated. This current is typically referred to as the supply, excitation or sensing current. For the purposes of this work sensing current will be used.

A typical way to measure the resistance is in a two-wire configuration. The sensing current is supplied and the voltage measured through the same set of wires. In this case, the actual resistance measured includes the resistance of the supply wires and can lead to errors. If large resistances are measured this can be neglectable, but for the small resistance measurement it can be significant, especially if long wires are used.

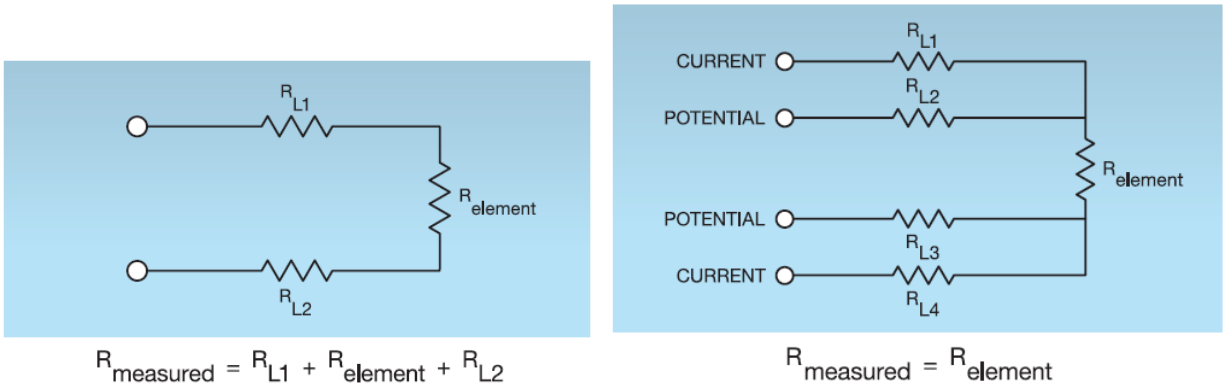

Figure 3-27: Two wire and four wire resistance measurement configurations [94]

A more accurate way is to use a 4 wire configuration. In this case, the current is supplied and the voltage measured with a different set of wires. In this case, the voltage is only measured across the resistance element, as there is virtually no current flowing through the sensing wires. To avoid the lead resistance errors as described, accurate RTD sensors are typically used in the 4 wire configuration [98].

Self-heating is caused when the sensing/excitation or supply current is passed through the sensor resistance. Heating is caused by the I^2R principle contained in Joule's law [94]. For this reason, the sensing current should be kept as low as possible. In most modern instrument this current is typically 200 to 250 μA [94][98]. This minimises the self-heating effect. This error should, however, be taken in to account for high accuracy measurements.

3.11 Flow measurement

The mass flow is an important input in most process calculations. This also applies to the current work. To accurately determine the number of variables the mass flow must be known.

There are a number of different methods that are used in industry to do flow measurement. These are grouped in a number of ways. The selected grouping, as well as the most common types in each group, is presented in Figure 3-28 below. Each of these groups will be examined, discussed and compared in this section.

The turndown ratio is an important parameter when considering flow meters. It is an indication of the rangeability of a specific flow meter. The turndown ratio is the ratio of the maximum and minimum flow that can be measured accurately.

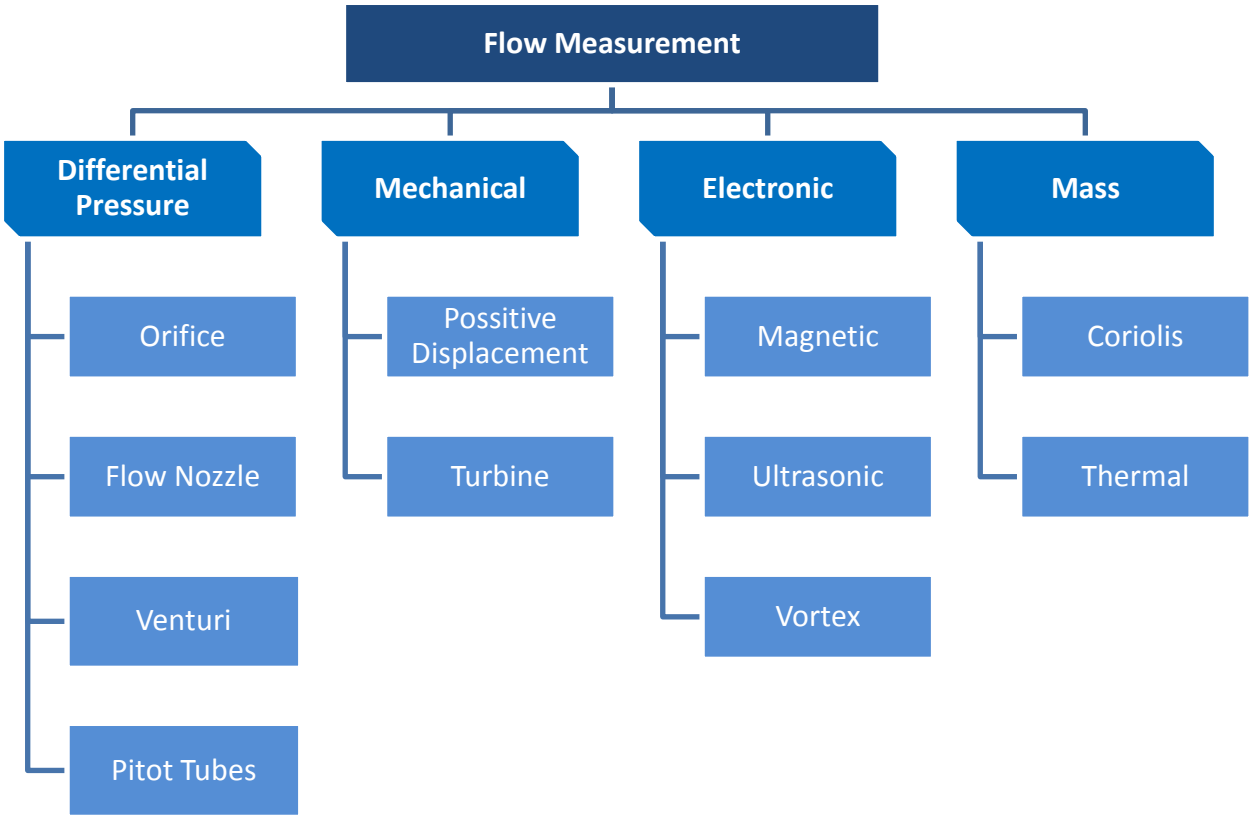

Figure 3-28: Common flow measurement groups and technologies

3.11.1 Differential pressure flow measurement devices

Differential pressure flow meters have been in use for several centuries. Pitot tubes were first used in 1732 and venturis in 1797. Flow nozzles were used in the late 1800s and orifice flow meters started appearing in commercial application in the early 1900s [101].

The differential pressure device consists of a restriction in the flow stream. This restriction results in a measurable differential pressure. If the dimensions of the restriction are known the mass flow rate can be calculated.

The differential pressure relates to the flow rate through the restriction by application of Bernoulli's equation [101]. The equation, however, assumes the area of the restriction to be the flow area. This is not the case with the minimum flow area or the "vena contracta" being smaller than that of the actual area of the restriction. This is accounted for by applying a "coefficient of discharge" which is a function of the restriction dimensions, the pressure measurement points, and the Reynolds number. The coefficient of discharge relates the actual flow rate to the theoretical flow rate [102] and are typical 0.6 – 0.7. The standards used for flow measurement typically give empirical equations to calculate the coefficient of discharge.

There are a number of different types of devices that are grouped as differential pressure measurement devices. These are shown below:

Table 3-9: Differential Pressure Flow Measurement devices [103][104]

Orrifce	Flow Nozzle
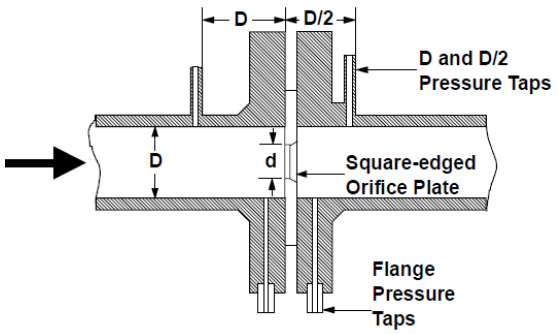	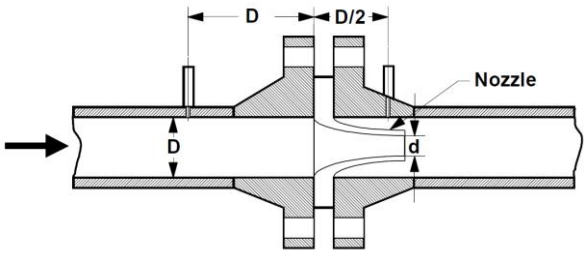
Venturi tube	**Pitot Tube**
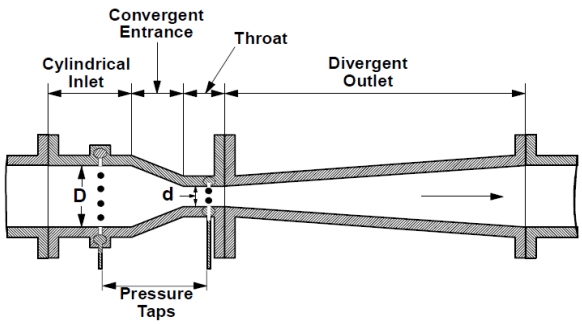	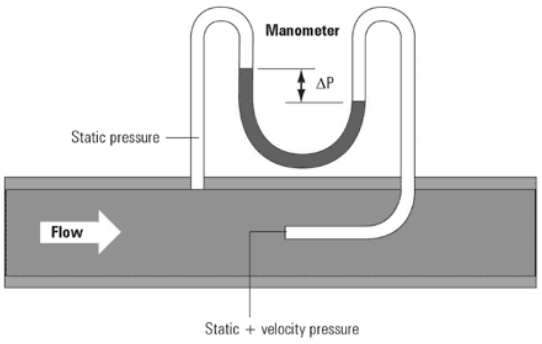

The orifice is simplest, most common and least expensive of these [103]. Orifice meters typically have turndown ratios of 1:4 or 1:5 [105]. The rangeability is thus low. Typical uncertainties are given by LaNasa [101] for concentric square-edged orifice meters. These are shown in Table 3-10.

Table 3-11 gives the advantages and disadvantages of differential pressure flow meters.

Table 3-10: Typical Uncertainty values for concentric square-edged orifice meters [101]

Reynolds Number	Uncertainty [%]
100000	0.58
50000	0.59
10000	0.7
5000	0.84
4000	Not Recommended

Table 3-11: Advantages and disadvantages of differential pressure meters

Advantages	Disadvantages
Well documented and developed	Limited Range of application for a single device
A number of industry standards are available	Additional pressure loss in line
Simple Design and Construction	Long straight length section required before device
High Reliability	Limited Range of Reynolds numbers
Low Cost	Low turndown ratios
Easy to maintain	

3.11.2 Mechanical flow measurement devices

Mechanical flow measurement devices use an arrangement of moving parts. This is typically done in one of two ways [106].

This first is known as positive displacement flow meters. It measures the flow bypassing isolated known volumes of the fluid through a series of chambers or gears. These chambers or gears act as volumes or “buckets” that are constantly filled and emptied. To prevent intermittent operation there are normally multiple volumes that are alternated between. By counting the number of volumes that are being filled and emptied and with the volume known the flow can be determined. Each type of positive displacement meter uses a different means of isolating and counting these volumes. Positive displacement flow meters can achieve accuracies of ±0.1% with turndown ratios of a 100:1 although 15:1 are common [106].

The second is by means of free turning turbine or rotor that is mounted coaxially in the flow path. The fluid imparts an angular velocity to the turbine or rotor that creates rotation. This rotation is proportional to the flow rate [101]. Turbine flow meters can achieve accuracies of ±0.5% for turndown ratios of 10:1 or ±2% for turndown ratios of 25:1 [105].

Table 3-12 shows some of the different types and Table 3-13 gives the advantages and disadvantages of mechanical flow measurement devices.

Table 3-12: Mechanical Flow measurement devices [106]

Single Piston - Reciprocating	Rotating Lobe	Rotating Impeller
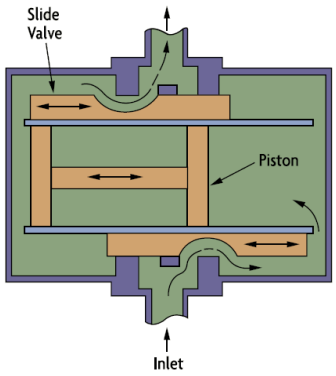	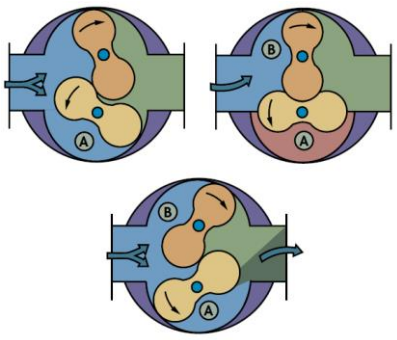	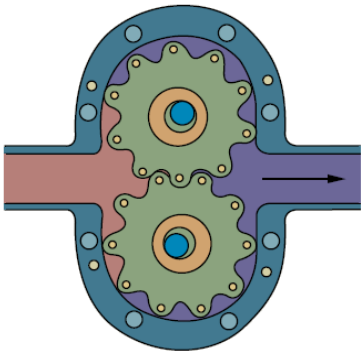
Rotating Valve	**Turbine - Impeller**	**Turbine – Paddle Wheel**
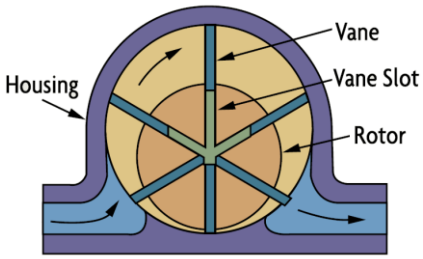	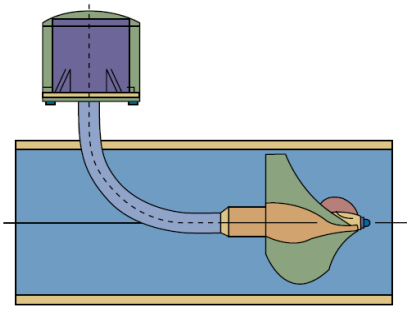	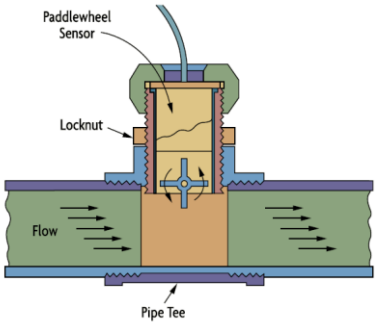

Table 3-13: Advantages and disadvantages of mechanical flow measurement devices

Advantages	Disadvantages
Operating principle easy to understand Very good range ability Good accuracy Accuracy not affected by pulsating flow No minimum upstream pipe lengths required for positive displacement types	Pressure temp ranges are limited Expensive for larger sizes Maintenance cost are high Sensitive to particles in the fluid. Process fluid must be clean

3.11.3 Electronic flow measurement devices

In this section electromagnetic, ultrasonic and vortex type flow measurements devices will be discussed. These types are not exclusively electronic, but all of it consist of no or very few moving parts and are made possible by recent advances in the fields of electronics.

Although grouped together, the principles and operating mechanisms are significantly different. In this section, each type will be discussed independently.

Electromagnetic flow meters

The operating principle of electromagnetic flow meters is based on Faraday's law of electromagnetic induction [103]. Faraday's law states that a voltage will be induced in a conductor moving in an electric field [107].

The electromagnetic flowmeters consist of a nonmagnetic pipe or tube with a pair of magnetic coils and a pair of electrodes protruding into the pipe or tube. If a conductive fluid flows through a pipe with a magnetic field created by the coils a voltage is developed across the electrodes.

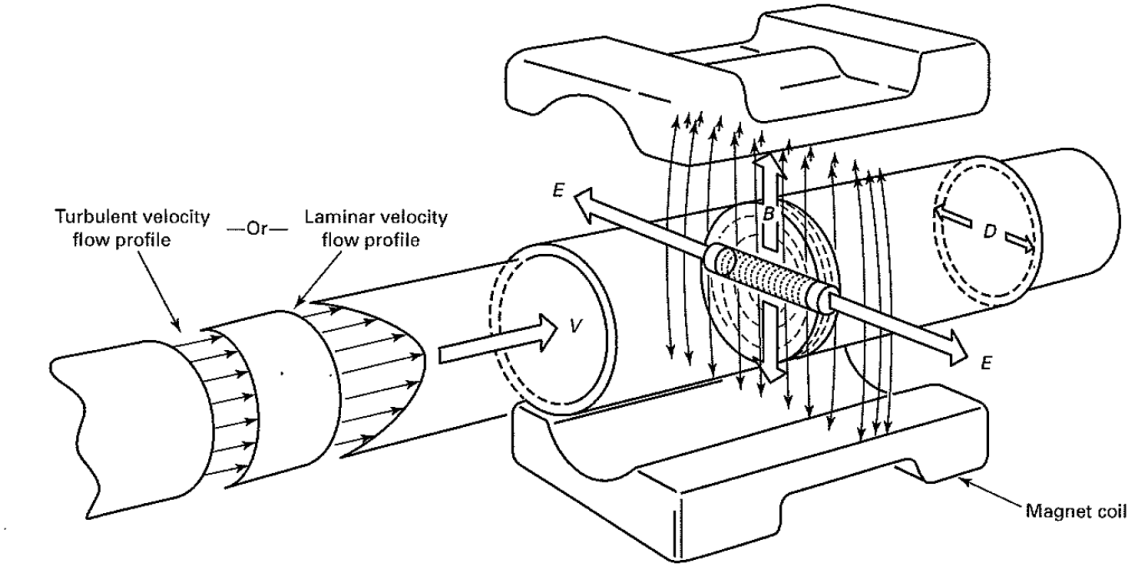

Figure 3-29: Electromagnetic Flowmeter [107]

Due to the nature of operation, the fluid used must be electrically conductive. Early electromagnetic meters required a minimum fluid conductivity of 1-5 microsiemens. Newer designs can accommodate fluids with conductivities of 0.05 – 0.1 microsiemens [106].

Magnetic flowmeters are very versatile and can measure flow velocities of clean, dirty, corrosive, erosive and slurries provided the fluid conductivity is within the required limits. They are full bore which means very little to no additional pressure loss. Typical accuracies range between ±0.2% – ±1% with turndown ration of 10:1 to 30:1 [106]. Flow velocities typically need to exceed 0.3 m/s. Lower velocities can be measured but accuracy is reduced.

Table 3-14: Advantages and disadvantages of electromagnetic flow measurement devices

Advantages	Disadvantages
Very versatile Not affected by change in densities and viscosities Full bore – No additional pressure drop Very Good accuracy Bi directional Can be used for fluids and slurries	High Costs Fluid needs to have certain minimum conductivity Cannot be used for gas applications Air or steam entrainment provides inaccurate readings

Ultrasonic flow meters

The speed that sound waves propagate through a fluid is dependent on the fluid's density. If the density is kept constant the ultra-sonic passage time or reflection can be used to determine the fluid velocity. There are two main different methods used ultrasonic flow measurement. The first uses a transit time method and the second uses Doppler effect [103].

For the transit time method, two transducers are installed on opposite sides of the pipe in such a way that the sound waves traveling between them are at a 45° angle with the flow direction. The time the sound takes to reach to the second transducer is used to determine the speed of the sound. This value represents the inherent speed of sound plus a contribution due to the fluid velocity. A simultaneous measurement is made in the opposite direction. From the measurements made the fluid velocity and hence the volume or mass flow rate is determined. The transit time method works well in most fluids but can be sensitive to entrained gas or solids that scatter the sound waves between the transducers.

The second type uses the Doppler Effect. In this case, two transducers elements are also used but mounted on the same side of the pipe. A sound wave of constant frequency is transmitted into the fluid. Solids or entrained gas bubbles reflects the sound wave back to the receiver transducer. The Doppler principle dictates that there will be a shift in frequency when there is a relative motion between transmitter and receiver. The relative motion of the reflecting bodies suspended in the fluid compressed the sound waves. The new frequency measured is compared with the original frequency. The difference is proportional to the flow velocity in the pipe. Unlike the transit time meter, the Doppler meters require suspended solids or entrained gas in the fluid to be able to measure the fluid velocity.

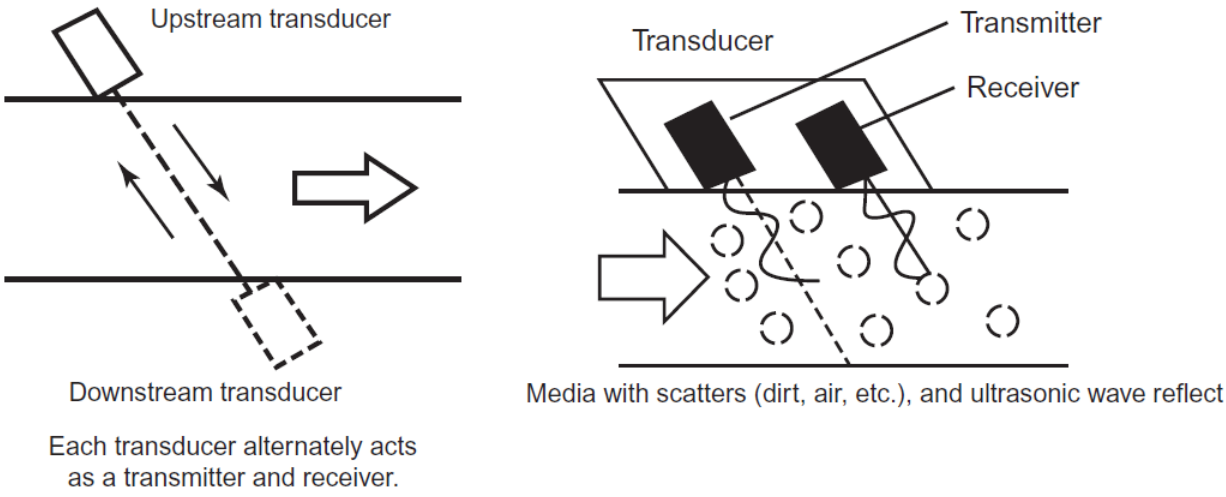

Figure 3-30: Transit time and Doppler type Ultrasonic flow meters [101]

Ultrasonic flow meters required very little maintenance and can easily be scaled to large pipes without a significant increase in costs. They are bi-directional and are full bore with no additional pressure drop in the system. Low velocities and half full pipes or ducts should be avoided. Ultrasonic flow meters can have accuracies of ±2% with turndown ratios of 20:1 [105].

Table 3-15: Advantages and disadvantages of ultrasonic flow measurement devices

Advantages	Disadvantages
No additional pressure drop	High initial cost
Simple Installation	Doppler type does not work for clean fluids
Low installation cost	Transit time type requires clean fluids
High rangeability	Straight lengths required before measurement
No moving parts, low maintenance requirements	Power required for operation

Vortex flow meters

The operation of vortex flowmeters is based on the Von Karman effect [101]. The Von Karman effect states that flow will alternatively shed vortices from one side and then the other over a non-streamlined body (also called a bluff body) in the flow path. These vortices are proportional to the flow velocity and create areas of fluctuating pressure [103] that can be measured or detected by a sensor. A good typical example is a flag on a flagpole. The wind sheds of the flag pole that acts as the bluff body and causes vortices which lead to the ripples in the flag.

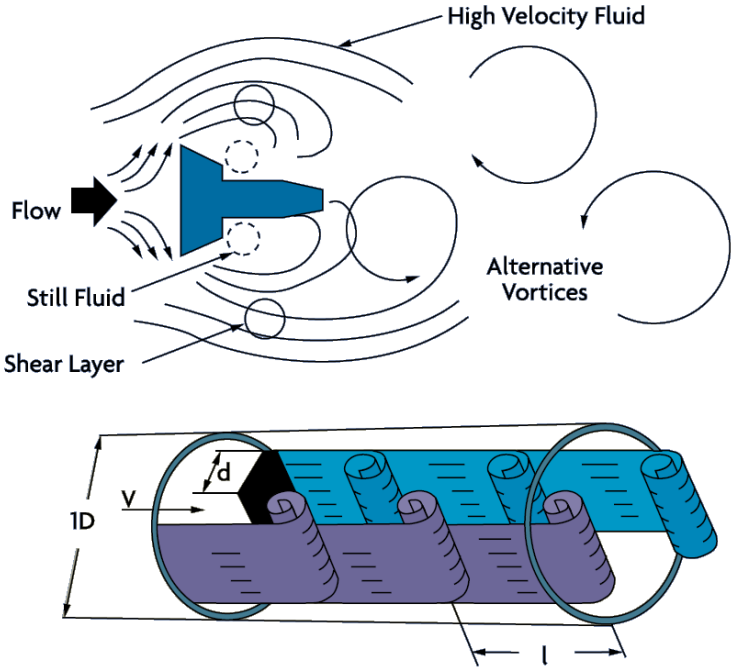

Figure 3-31: Operating principle of vortex flow meters [106]

Vortex shedding meters are best suited for fluids with high velocities in excess of 80 m/s [105]. According to Omega [106] Vortex meters has a turndown ratio of 20:1 for gas and steam service and 10:1 for low viscosity liquid applications. Inaccuracies of ±0.5% up to ±1% can be achieved for Reynolds number higher than 30000. At Reynolds numbers of less than 10000 errors can be become as large as ±10%. Vortex meters are not suited to any fluids that can cause any build up that can affect the shape of the bluff body.

Table 3-16: Advantages and disadvantages of vortex flow measurement devices

Advantages	Disadvantages
Relatively wide rangeability	Long pipe straight lengths required before meter
Installation cost moderate	Only sizes below 200 NB
Simple installation	Not suitable for low Reynolds numbers
No moving parts	Only suitable for clean fluids

3.11.4 Mass flow measurement devices

Most flow meters measure velocity or volume flow and calculate the mass flow based on the density of the fluid. The density is often determined from the pressure and temperature of the fluid which adds additional uncertainties. Mass flow meters measure the mass flow directly.

Coriolis mass flow meters

This type of mass flow measurement device normally has one or more bent or U-shaped vibrating tubes in the fluid stream. If a fluid is passed through the tubes a twisting motion is introduced and the resonant frequency changes. The combination of the twist and the frequency is measured and used to determine the mass flow.

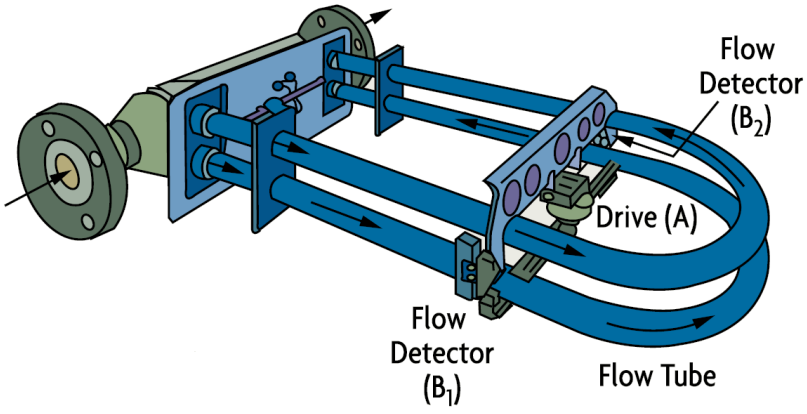

Figure 3-32: Coriolis type mass flow meter [106]

Coriolis flow measurement devices can be used to simultaneously measure the mass flow, density, and temperature of a fluid [108]. They can provide accuracies of ±0.1 – 2%. and have a good rangeability of up to 100:1 [106]. Errors are caused by air or gas pockets in the fluid stream and

these should be avoided. Typically Coriolis type flow meter has a higher pressure loss due to the smaller sizes of the measurement tubes.

Table 3-17: Advantages and disadvantages of Coriolis flow measurement devices

Advantages	Disadvantages
Very Good accuracy High rangeability Can be used on liquids, gasses and slurries No straight pipe lengths required No moving parts	Only available up to 150 NB Special installation requirements to prevent vibration High capital cost Deposits or erosion can lead to errors

Thermal mass flow meters

Thermal mass flow meters operate mainly in one of two ways. The first is by introducing a known amount of energy or heat to a flow stream and measuring the change in temperature. The second is by measuring the amount of input energy required to maintain a constant temperature on a probe or a delta temperature between two probes. Figure 3-33 shows the second type. This device maintains a constant temperature difference between the two probes shown and measure the amount of input energy required. This is used to calculate the mass flow.

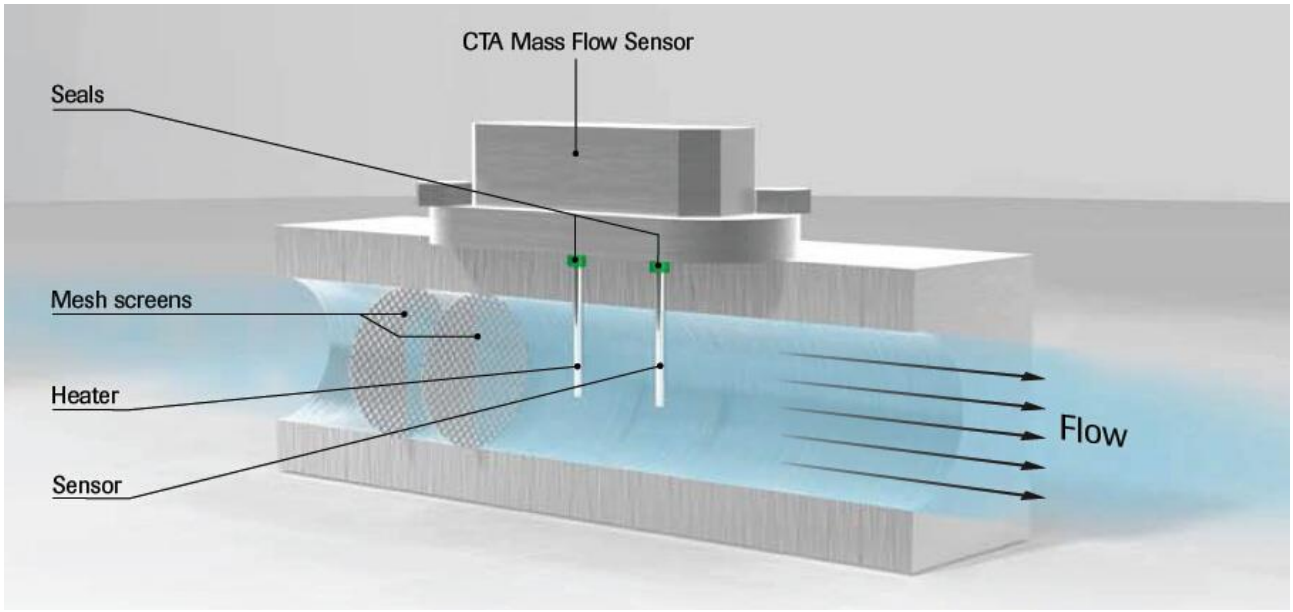

Figure 3-33: Thermal mass flow meter [109]

Thermal mass flow meters are best used for dry gas flow measurement [105]. High rangeability is provided at 10:1 up to 100:1 with accuracies between 1% and 2%. There are however limitations in the form of condensing vapour on the probes as well as scale built up that will adversely affect the measurements.

Table 3-18: Advantages and disadvantages of Thermal flow measurement devices

Advantages	Disadvantages
Good accuracy High rangeability No moving parts Low-pressure drop	Deposits can lead to errors Condensation on probes lead to errors Can only be used a limited amount of fluid types Variation in specific heat of fluid cause errors Limited industrial use

3.11.5 Comparison of flow measuring devices

A number of different groups and types of flow measuring devices have been reviewed and discussed in the previous sections. Each group and types are used for different applications and have different advantages and disadvantages.

The different measuring devices are summarised in the table below based on selected criteria that are deemed important for the current work. The summary was adapted from a publication by Spirax Sarco [105]. All flow meters below can be used for liquid applications.

As with the temperature measurement, accuracy is the highest priority when selecting a flow measurement technology for this project. From the table below it can be seen that the positive displacement, electromagnetic and Coriolis type flow meters are the most accurate. Due to the high amount of moving parts and thus failure and maintenance issues, the positive displacement meters are not considered suitable for this work. The Coriolis and Electromagnetic type flow meters are preferred, and the final selection will be made based on cost and availability.

Table 3-19: Comparison of different type so flow meters

Type of meter	Turndown Ratio (Rangeability)	Accuracy	Cost
Orifice Plate	4:1	±3%	Low
Pitot Tubes	4:1	±5%	Low
Positive displacement	15:1	±0.1%	High
Turbine	10:1 / 25:1	±2% / 0.5%	Low
Electro magnetic	20:1	±0.3%	Medium
Ultrasonic	20:1	±2%	High
Vortex Shedding	10:1 – 20:1	±0.5% - ±1%	Medium
Coriolis	100:1	±0.1% - ±2%	High
Thermal Mass	100:1	±1%	Medium

3.12 Cleaning of tubes

A very important aspect of the tests is the cleaning of the tubes and the removal of the fouling layer for subsequent tests. There are a number of common cleaning methods used to clean heat exchanger tubes in industry and specifically in Eskom. The most common of those will be provided and discussed below. After the discussions, a conclusion will be made on which cleaning technique will be best suited for this work.

Take note that the information given below was gathered from personal discussions with specialised Eskom personnel, K Northcott and A.F du Preez.

3.12.1 Chemical cleaning

Chemical cleaning is a process where specific chemical compositions are used to remove fouling or scaling layers from heat exchanger tubes. The chemical compositions are selected based on the type of fouling or scaling as well as the heat exchanger tube material. The chemicals are typically circulated through the tubes for a certain time period. Chemical cleaning has been done very successfully in Eskom [110]. Care must however be taken when this type of cleaning is done since severe damage can be caused to equipment if an incorrect chemical is used for the tube material or if the cleaning process is not done correctly. An advantage of proper chemical cleaning is that the selected chemicals only attack the fouling or scaling layers and do not affect the tube material. A major disadvantage is the fact that it is expensive to do and requires specialised storage, circulation and disposal equipment. Chemical cleaning is not considered practical on small scale applications.

3.12.2 Abrasive blast cleaning

Abrasive blast cleaning, commonly known as sandblasting, is a mechanical process where an abrasive material at a high velocity is blown against a surface to remove contaminants. Abrasive cleaning is commonly used to remove corrosion and fouling products from most types of metal surfaces. It is also commonly used for surface preparation when protective coatings are applied to the heat exchanger and condenser tubes. It can also be used to clean the tubes of heat exchangers. A major advantage of abrasive blast cleaning is that it is a very common method and a number of suppliers have workshops that specialises in this. The tube can easily be taken to such a workshop to be cleaned without the requirements of equipment transport and set-up costs.

Care must be taken when abrasive cleaning is used. Incorrect blasting media or travel time during blasting can result in tube wall material loss in heat exchanger tubes. Unlike chemical cleaning, blasting cleaning does not differentiate between fouling or scaling products and the tube material.

Northcott [111] did however show that the amount of wall loss is very low (less than 50 µm) when using the correct blasting media during tests done on brass condenser tubes. Brass is softer than the materials typically found in feedwater heater tubes. The amount of wall loss on feedwater heater tubes is expected to be less than that of brass. For the purposes of this work wall loss induced by abrasive blast cleaning will be considered neglectable.

3.12.3 High-pressure water jet cleaning

High-pressure water jet (HPWJ) cleaning involves the use of high pressure (1000 bar) water sprayed through a nozzle on to a surface to remove unwanted substances. It has been used extensively and successfully in Eskom to clean condensers and heat exchangers. In recent years this has become the preferred way to clean condensers in Eskom. It is however not a very common method and specialised equipment and personnel are required. There is also a safety element involved due to high working pressure involved. It is not practical or cost-effective to be done on a small scale as required by this work.

3.12.4 Mechanical cleaning

Mechanical cleaning entails a mechanical removal process using some type of rotating brush. This can be done by means of a wire brush installed on a grinder or a drill for outside cleaning or by means of specialised spiral brushes for internal cleaning. No data was readily found on the amount of tube material removed by means of mechanical cleaning but it was found that this process is extensively used in industry for heat exchanger cleaning. Tests were done on sample tubes and the amount of tube material lost could not be accurately determined by a calibrated vernier which indicates that it is very little. That combined with the fact that the good conductivity of the tube material has very little effect on the actual heat transfer makes this a viable cleaning method.

Hovland et al. [112] did tests using mechanical scraper type tube cleaners that is blown through condenser tubes. It was found that the wall loss was between 0.002286 mm and 0.0127 mm for copper nickel materials. It was mentioned that for harder materials like stainless steel it will be significantly less.

3.12.5 Summary

Cleaning techniques have been reviewed and discussed. From the above discussions, it is clear that only abrasive blast and mechanical cleaning is considered a feasible, practical option for cleaning the tube samples.

4. Experimental facility

The previous chapters described the problem associated with fouling and gave a large amount of theory and background w.r.t fouling. All the theory and background can now be applied to specify and design an experimental test rig that can accurately measure the fouling factor. In this section the following will be discussed and addressed for the experimental facility or test rig:

- Fouling Test Methodology.
- Required accuracy.
- Selection of test concept.
- Technical requirements and specification.
- Process design.
- Component selection.
- Budget.
- Manufacturing.
- Calibration of Instrumentation.
- Commissioning.

Although actual feedwater heaters have water on the one side and condensing steam on the other, does the working fluid not have an effect on the measurement of the fouling factor. For the purposes of this work water will be used as the working medium for the complete test rig.

4.1 Fouling test methodology

Fouling factors cannot be measured directly. Before the test rig can be specified and designed, the exact methodology to determine the fouling factors must be clearly established.

The definition of the fouling factor discussed in section 2.4.4 and given in equation (4-1) is used to accomplish this. It showed that the fouling factor is a function of the clean and fouled overall heat transfer coefficient. The fouling factor is this determined as follows:

$$R_f = \frac{1}{U_{o,fouled}} - \frac{1}{U_{o,clean}} \tag{4-1}$$

The purpose of the test rig is thus to measure the overall heat transfer coefficient. This can be done with a counterblow heat exchanger. By combining equation (2-5), (2-6) and (2-9) the value of the overall heat transfer coefficient can be written in terms of variables that can be measured on a test rig.

$$U_o = \frac{\dot{m}_{CL} c_{p,CL} \left(T_{CL,out} - T_{CL,in}\right) ln\left[\frac{\left(T_{HL,out} - T_{CL,in}\right)}{\left(T_{HL,in} - T_{CL,out}\right)}\right]}{A\left(T_{HL,out} - T_{CL,in} - T_{HL,in} + T_{CL,out}\right)} \quad (4\text{-}2)$$

The purpose of the tests is however to determine the overall (R_f), external (R_o) and internal (R_i) fouling factors of a heat exchanger tube. This cannot be done with just two tests. Three separate tests must be thus done and the overall heat transfer coefficient must be determined in each test.

From the three tests, three values for the overall heat transfer coefficient are determined:

- U_{fouled}
- $U_{halfclean}$
- U_{clean}

These are used to determine the different fouling factors.

- The combined fouling factor as shown in equation (4-1) above.
- The internal fouling factor derived similarly to R_f, but with $R_o = 0$ given in terms of tube inside area as it is used in heat transfer calculations:

$$R_i = \left(\frac{1}{U_{o,halfclean}} - \frac{1}{U_{o,clean}}\right)\frac{r_i}{r_o} \quad (4\text{-}3)$$

- And the external fouling factor, written in terms of tube outside area is:

$$R_o = \frac{1}{U_{o,fouled}} - \frac{1}{U_{o,halfclean}} \quad (4\text{-}4)$$

By using this method to determine the overall heat transfer coefficient and hence the fouling factors, the result becomes independent of the heat transfer coefficients on both the inside and the outside of the test tube. The reason for this is that the heat transfer coefficients effectively cancel out since the overall heat transfer coefficients are subtracted. To ensure that they do cancel out, the tests must be repeated with the exact same process conditions. If this is not the case the heat transfer coefficients will be different between the different tests (clean, half clean and fouled) and will not cancel out. The following test parameters must thus be kept exactly the same for each of the 3 tests done on every tube:

- Cold loop mass flow.
- Hot loop mass flow.
- Hot loop inlet temperature
- Tube orientation.

There is thus no reliance on the calculation of heat transfer coefficients during the testing process and the calculation of the result. That makes the design of the test section simpler since it is not critical to achieve fully developed or perfect annular flow.

The steps in the testing process are given in Figure 4-1.

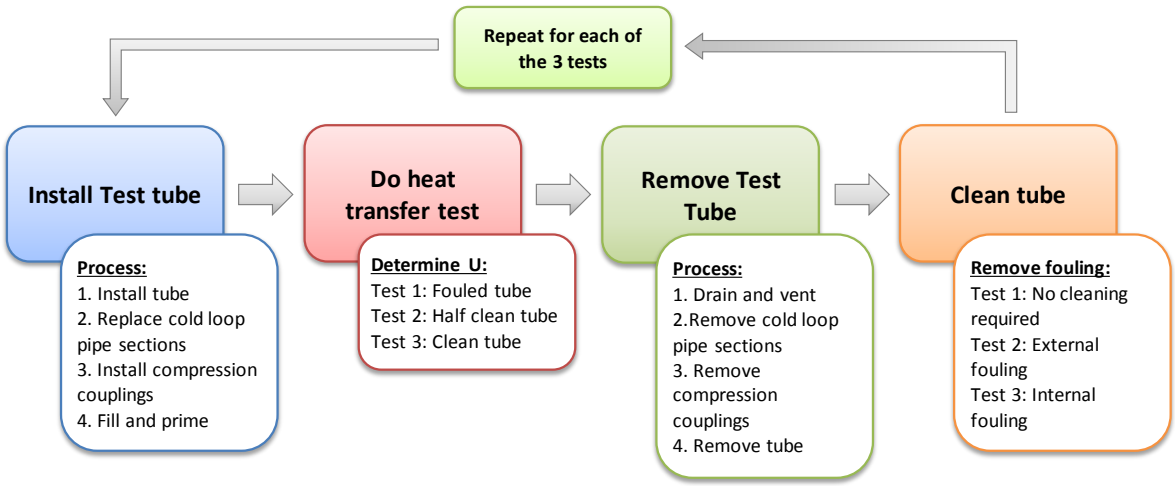

Figure 4-1: Experimental Methodology Flowchart

4.2 Uncertainty design and specification

Accuracy or the uncertainty associated with the result is a critical part of any experiment or test rig. Section 3.7 went into detail on how the uncertainty of a result is determined. During the design of the experiment, the uncertainty can already be predicted to a certain extent. Design or specification choices made during the design phase can have an effect on the uncertainty of the result. Some of these choices applicable to the current work include:

- Evaluation and computation of raw data. This includes the equations used and application there off in determining the result.
- Accuracy of temperature measurements.
- Accuracy of flow measurements.

The design and specification can thus not be done independently of the uncertainty analysis. The purpose of this section is to show how the required uncertainty of the experimental set-up was determined.

4.2.1 Required uncertainty

Due to the high cost and safety risks associated with feedwater heaters there are many standards that govern the design, manufacture and performance testing of feedwater heaters. One of these standards is ASME PTC 12.1 [113]. This is the performance and test code for closed feedwater

heaters. It gives guidance on the measurement uncertainty required for the different instrumentation used for performance testing. This can be seen in Table 4-1 below.

Table 4-1: Maximum Uncertainty values for feedwater heater performance testing [113]

Flow Rates		Pressure		Temperature	
Feedwater at heater	±1%	Desuperheater ΔP	±1%	Steam inlet	±0.56°C
Drains	±1%	Steam inlet	±0.25%	Drains inlet	±0.14°C
		Feedwater inlet	±2%	Drains outlet	±0.14°C
		Feedwater ΔP	±1%	Feedwater inlet	±0.14°C
		Drains cooler ΔP	±1%	Feedwater outlet	±0.14°C

Since the main purpose of a feedwater heater is to heat the feedwater the uncertainty given for the feedwater inlet and outlet temperatures will be used. This is given by the code as ±0.14°C.

The uncertainty of the results of the measured fouling factor must be small enough that the uncertainty of the fouling factor does not have an effect in excess of 0.14°C on the feedwater inlet or outlet temperature. If this can be achieved the uncertainty of the fouling factor will be insignificant and will not have a measurable effect on the performance of the feedwater heater if implemented.

An internal Eskom accepted and used feedwater heater analysis tool was used to run a number of simulations on a typical Eskom feedwater heater. The base fouling factor used in the simulations was the fouling factors as described in the HEI standards [6]. These include fouling factors for the outside and the inside of the tubes. The HEI fouling factor was multiplied by values between 0 and 2. That means that 0 represents a clean heat exchanger, 1 the standard HEI fouling factor and 2, double the HEI fouling factor. The results are given in Figure 4-2. The blue line indicates the decrease in feedwater outlet temperature and the orange line the increase in the distillate drains i.e. condensed steam outlet temperature.

From the calculation results it can be seen that for a 0.14°C decrease to the feedwater outlet temperature the fouling factors must be increased as per the values in Table 4-2 below. Clear differentiation should however be made between the relative and absolute values. Compared to the HEI fouling factors a relative uncertainty of 8% is required. That is a good indication; but for the required specification the absolute values of the change in fouling factor will be used.

Table 4-2: Required increase in fouling factors for an increase of 0.14°C to the feedwater outlet temperature

Description	HEI Fouling Factors [m²K/W]	Increased fouling factor [m²K/W]	Δ fouling factor [m²K/W]	% Increase
Internal fouling factor	3.52E-05	3.8E-05	4.23E-06	8
External fouling factor	5.28E-05	5.71E-05	2.82E-06	8
Overall fouling factor	1.07E-04	1.07E-04	7.92E-06	8

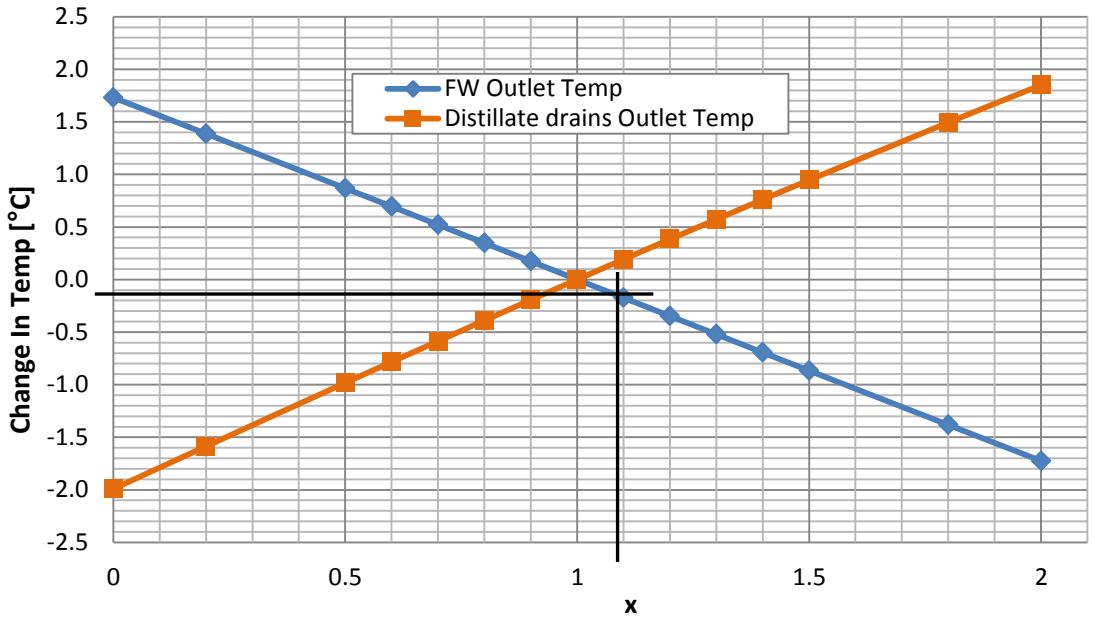

Figure 4-2: Change in outlet parameters with change in fouling factors for a typical Eskom feedwater heater

4.2.2 Uncertainty analysis to determine instrument specification

An uncertainty analysis was done to determine the required accuracy or uncertainty of the instruments that will be used. At this stage in the design process, a number of assumptions had to be made. The hot loop inlet temperature was taken as 95°C instead of 60°C that was eventually used. Lower mass flows rates was also used in the analysis as what was eventually selected. The values were selected in such a way that the calculated fouling factor will be similar to the HEI [6] values. There were also assumptions w.r.t to the random uncertainty of the instruments. These are not available on supplier's data sheets and are dependent on the number of measurements taken. For this reason, the uncertainty analyses were done for a combined uncertainty i.e. the random and systematic uncertainty used together.

The analysis showed that for the assumed operating conditions, a combined uncertainty of 0.1°C on temperature measurements and a combined uncertainty of 0.5% on the mass flow meters, an overall uncertainty of 6.58E-06 m^2K/W on the overall fouling factor will be achieved. This is lower than the required values given in Table 4-2. This was considered acceptable and the instrument uncertainties were specified as such.

Table 4-3: Uncertainty analysis results to determine instrument specification

Calculated Overall Fouling Factor	Calculated Absolute Uncertainty	Calculated Relative Uncertainty
9.7E-05 m^2K/W	6.58E-06 m^2K/W	6.8 %

4.3 Technical requirements and specifications

Before equipment can be designed the design parameters and the specification of the design must be well defined. This section will provide detailed requirements that the design of the test rig must adhere to.

4.3.1 Location and facilities

The experimental set-up must be built at the Flow laboratory at the Eskom RT&D facilities in Rosherville, Johannesburg.

The facilities at Eskom RT&D include a 2 megalitre water reservoir that feeds a water tower such that it can provide a constant water head of 20 meters. Both the water tower and the water reservoir are open to atmosphere. This existing equipment can be utilised in the following ways:

- Water tower to be used to supply water at constant pressure to the test rig. By doing this fewer pumps and pumping power will be required.
- At least one water stream used in the experiment will be heated. Typically this stream needs to be cooled again to enable the re-use of the working fluid. By using the large water reservoir, cooling is not required since the limited amount of energy that will be added to the reservoir while the experiment is taking place will have a negligible effect on the temperature of the water in the reservoir.

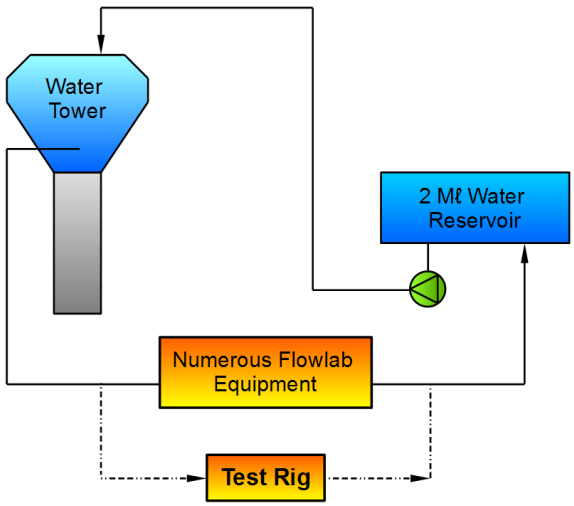

Figure 4-3: Test Rig connection to existing equipment and infrastructure

4.3.2 Operating and design pressure and temperature

The design pressure must be sufficient to accommodate the maximum pressure that can be delivered from the water tower. Using a static head of 20 m and a density of water at room

temperature the operating pressure must be at least 200 kPa(g). Standard practice in the specific laboratory is to use components with a PN 10 pressure rating. At room temperature, this is a design pressure of 1000 kPa(g). To ensure uniformity in interchangeability with the rest of the components in the laboratory this convention will be adhered to.

The operating temperature for the hot stream must be as high as possible and the cold stream as low as possible. The higher the temperature differential, the higher the temperature driving force and the higher the amount of heat transfer. This will allow more energy to be transferred with higher and lower outlet temperatures respectively for the hot and the cold stream. The higher the temperature differentials, the more accurately it can be measured.

Since additional cooling will lead to an increase in cost, the temperature of the cold stream can only be as low as room temperature.

The hot stream is heated. The temperature of the hot stream must be kept below boiling point at atmospheric pressure due to the following reasons:

- The pressure equipment regulations (PER) [114] are part of the Occupational health and safety act (OHS Act) [115]. The PER governs all pressure equipment used in South Africa that is designed for a pressure equal to or greater than 50 kPa(g). Compliance to the PER entails additional cost, quality requirements, inspections, and reviews. There are however some equipment and systems that are excluded. One of these is water distribution systems that operate below its boiling temperature at atmospheric conditions. This is 100°C at sea level and approximately 95°C in the Highveld area and Johannesburg.
- The PER refers to SANS 347 [116]. SANS 347 contains a classification system that classifies regulated equipment into different hazard categories. The higher the hazard category, the higher the safety risk is posed by the equipment and the more stringent the requirements that must be adhered to. The categorisation of piping is done based on the pipe size, the design pressure in the line and the hazard category of the fluid contained in the line. For the same pipe size and design pressure, a higher category will be assigned to a dangerous-gas than a non-dangerous liquid. Water above its boiling point at atmospheric pressure is classified as steam and hence a dangerous gas. This will result in a higher hazard category, more stringent requirements and higher cost.
- When water is pressurised it can be heated to a temperature higher than it's boiling point at atmospheric pressure. For example water at 200 kPa(a) can be heated to 120°C without boiling or changing phase to steam. The problem with this is that if this water is released to atmosphere in the form of a leak it will partially flash to steam. This is considered a safety risk in a laboratory environment and must be avoided.

Based on the reasons given above the design temperature of the hot stream will be selected as 70°C with an operating temperature of 60°C.

The following table summarizes the selected design pressure and temperature for both the hot and the cold stream.

Table 4-4: Summary of design and operating parameters

Fluid Stream	Design Pressure	Maximum Permissible Operating Pressure (MPOP)[1]	Design Temperature	Operating Temperature
Cold Stream	1000 kPa(g)	200 kPa(g)	50°C	21°C
Hot Stream	1000 kPa(g)	200 kPa(g)	70°C	60°C

[1]Although the maximum operating pressure can reach 200 kPa, the actual operating pressure will be significantly lower during normal operating conditions. Most of the static head is expected to be lost across the first control valve.

4.3.3 Allowable velocity in piping

The required pipe size in any design is determined by the maximum allowable velocity in the line. The higher the allowable velocity, the higher the pressure drop and hence the required pumping power will be. The lower the allowable velocity the larger the required pipe diameter and hence the capital cost of the piping system will be.

Different values for this allowable velocity exist that is considered good engineering practice. For flow in water lines, this value is typically 2 – 3 m/s and can go as high as 5 m/s in piping systems where expensive material is used. This is considered the optimum point where a balance is reached between the capital costs of the piping and the pumping power cost throughout the life of the piping system. Since a constant head water tower will be used to supply the test rig the required pumping power is not required to be taken into account. The selected velocity can be higher to reduce the pipe size and reduce capital cost. Based on this a maximum allowable velocity in the piping system of 5 m/s is selected.

It must be noted that the actual pressure drop through the system is limited by the available static head. The design must ensure that the required flow rate is achieved with the available static head which may lead to much lower velocities.

4.3.4 Allowable velocity in test tube

The velocity in the test section needs to resemble the velocity in an actual feedwater heater tube as close as possible. The reasons for this are to achieve similar Reynolds numbers since surface roughness or fouling roughness in this case affects the heat transfer. The HEI standards for feedwater heaters [6] gives guidance on the maximum allowable velocities in feedwater heater tubes for different tube materials. An extract of the standard can be seen in Table 4-5. The velocity in the test tube must comply with the HEI standards.

Table 4-5: HEI [6] Allowable Tube Velocities

Tube Material	Velocity [ft/s]	Velocity* [m/s]
Stainless Steel	10	3
70-30 Nickel Copper	10	3
Copper Nickel (70-30, 80-20, 90-10)	9	2.75
Low Alloy Steel	9	2.75
Admiralty and Copper	8.5	5.6
Carbon Steel	8	2.45

* Values were rounded during conversion

Due to the different tube sizes that will be tested the velocity in the test tube must be adjusted according to each tube size. This will have to be done by means of a control valve that will have to be included in the cold water loop.

4.3.5 Temperature rise across the test tube

The temperature rise across the test tube must be such that sufficient temperature differential measurement is possible. The specified value for the temperature rise across the test tube was selected as 5-10°C.

4.3.6 Material requirements

Material selection is typically based on the operating temperature and the materials strength at the operating temperature. Due to the low temperature of both the hot and the cold loop a carbon steel material is sufficient. Welded, seamless or galvanised piping can be used.

For fittings and elbows, either threaded fittings or compression fittings can be used. Welded fittings are not required due to the low temperature and pressure, but can be used if preferred.

4.3.7 Pressure vessel design requirements

If any pressure vessels are required the design code used will be PD 5500 or ASME VIII Division 1. The vessel must comply to all requirements of the design code as well as the OHS Act [115] and the PER [114].

4.3.8 Flange selection

A number of different flanges codes are available. These provide standard dimensions and pressure ratings for flanges that are commonly used. Pressure and temperature tables for different materials are also available that enables flange selection without the need for extensive flange calculations. The flange codes to be used for the test rig can either be BS EN 1092 or ASME B16.5.

4.3.9 Instrumentation Requirements

Temperature measurement

The temperature measurement will have a significant effect on the accuracy of the experiment. To ensure that the uncertainty associated with the result is within the acceptable limits as discussed in section 4.2 a very small margin of uncertainty can be allowed on the temperature measurement. As discussed in section 3.8 are RTD type temperate measurement sensors are the most accurate type. Of these, the Pt100 sensors are the most readily available and the most cost-effective. This type must be used with a specified accuracy/uncertainty of 0.1°C.

Flow measurement

The flow rate in both the cold stream and the hot stream of the experimental set-up must be accurately measured. The reason for this is as follows:

- To accurately determine the amount of heat and energy transfer
- To provide feedback to enable the control of the velocities in both the cold and the hot loop.

According to the uncertainty analysis done of the design in section 4.2.2 a required uncertainty of 0.5% is required. From the literature review done on flow meters in section 3.10, it can be seen that only two types of flow measurement instruments comply with these criteria. These are the electromagnetic and Coriolis type flow meters. Any of these two types can be used. The Coriolis type is more accurate but does come at a significantly higher price.

4.3.10 Test tube requirements

The experimental facility must be able to tests tube sizes that cover the full range of feedwater heater tubes found in the Eskom fleet. The range of feedwater heater tubes in the Eskom fleet is 14 mm outer diameter with a wall thickness of 1.2 mm up to a 26.9 mm outer diameter with a wall thickness 3.2 mm. This information was obtained from a survey by the author of all the installed feedwater heaters in the Eskom fleet.

The facility must be designed in such a way that a test tube can be easily removed and a new test tube installed with a limited amount of effort and modification. The operator must be able to remove and install a new tube within a time period of 10 minutes.

The length of the test tube must be 2400 mm. This specific length was selected due to the fact that these lengths are readily obtainable, can be easily extracted from feedwater heater shells, can be easily transported in normal vehicles and can be handled by a single person. Only 2000 mm of the test tube will be inside the test section and exposed to heat transfer.

The facility must be able to test a range of different materials. The most common materials are 15Mo3, 16 Mo3, different grades of Carbon Steel, different grades of Stainless steel (typically 304 and 316), Titanium (typically ASTM SB 338 Grade 2) and Brass.

4.3.11 Drain Requirements

Sufficient drains must be fitted to allow draining for tube removal during the testing process. Isolation valves used in conjunction of the drains must allow only draining of the specific areas that will be opened when the test tube are removed and re-installed.

The facility will only be used on an intermittent basis. All piping sections must be fitted with low point drains to ensure the complete piping system and water heater can be drained and dried for storage.

4.3.12 Insulation requirements

The test section must be insulated to prevent losses to atmosphere. Mineral wool with galvanised plate cladding is commonly used in Eskom. This can be difficult to install. Thermalflex polyethylene foam lagging comes in pre-manufactured pipe sections and will be easier to use and install. The required thickness is determined in section 4.5.4.

4.3.13 Summary of technical requirements and specifications

Table 4-6: Summary of Technical requirements and specification

Description	Requirement
Location	Flow laboratory, Eskom RT&D, Johannesburg
Design Pressure	1000 kPa
Operating Pressure	200 kPa
Design Temperature	100°C
Piping allowable Velocity	Max 5 m/s
Test Section tube allowable velocity	As per HEI standards. See Table 4-5
Test Tube temperature rise – Cold loop	8-10°C
Flow Control	Control valve required in cold loop to ensure required velocity in the test section for different tube sizes.
Material Requirements	Welded, Seamless or galvanised carbon steel, PTFE
Fittings	Screwed or compression fittings
Pressure Vessel Design code if required	PD 5500 / ASME VII Div 1
Flange Design and Selection Code	BS EN 1092 / AMSE B16.5
Temperature Measurement Instrumentation	RTD sensors with a required accuracy of 0.1°C
Flow Measurement	Electromagnetic or Coriolis type with a required accuracy of 0.5%

Test Tube Sizes	14 mm OD to 26.9 mm OD.
Test Tube Length	2400 mm
Test tube size change	Switch between different tube sizes to be done with minimal effort and modification within 10 minutes.
Drain requirements	Drains to be fitted at all low points in the system.
Lagging and Cladding of test section	Polyethylene foam in preformed pipe sections.

4.4 Selection of test section concept

The test section is the main and thus most important part of the test rig. The remainder of the test rig and the system will be designed and selected around the test section. In section 4.1 the specification is given for the required test facility. In section 3.6.6 a list of typically used test sections of experimental arrangements was given. Input from both these sections was used to determine the optimum test section concept for the test rig.

4.4.1 Mandatory Requirements

There are criteria from the technical specification that are mandatory and must be complied to. All test sections of experimental arrangement concepts will first be evaluated using these criteria. Only the test section concepts that comply with the criteria will be evaluated further. The mandatory criteria are:

- The range of test tubes that the facility must be able to accommodate (14 mm OD to 27 mm OD).
- The removal and replacement tube must be done within the specified time frame.
- Range of materials to be tested.

Table 4-7: Mandatory evaluation criteria

	Test Section Arrangement (refer to Table 3-6)	Range of tube sizes	Ease of tube installation	Range of materials
1	Annular Geometry, indirect electric heating (Figure 3-6 and Figure 3-7)	Yes	Yes	Yes
2	Thin-Walled Tube, indirect electric heating (Figure 3-16)	Yes	No	Yes
3	Thick Walled Tube, indirect electric heating (Figure 3-10)	No	No	Yes
4	Thick Walled Tube, transient technique (Figure 3-5)	No	No	Yes
5	Annular or Circular tube geometry, direct electric heating (Figure 3-9)	Yes	Yes	No
6	Annular or Circular tube geometry, sensible heating (Figure 3-4)	Yes	Yes	Yes
7	Annular or Circular tube geometry, condensing vapour (Figure 3-13)	Yes	Yes	Yes
8	Complex Geometries (Heat Exchangers)	Yes	No	Yes

From the above, it can be seen that test sections that comply with all the mandatory criteria are arrangement concept 1, 6 and 7. For the remainder of the document and for ease of further evaluation these will be referred to as arrangement concept **a**, **b** and **c** respectively.

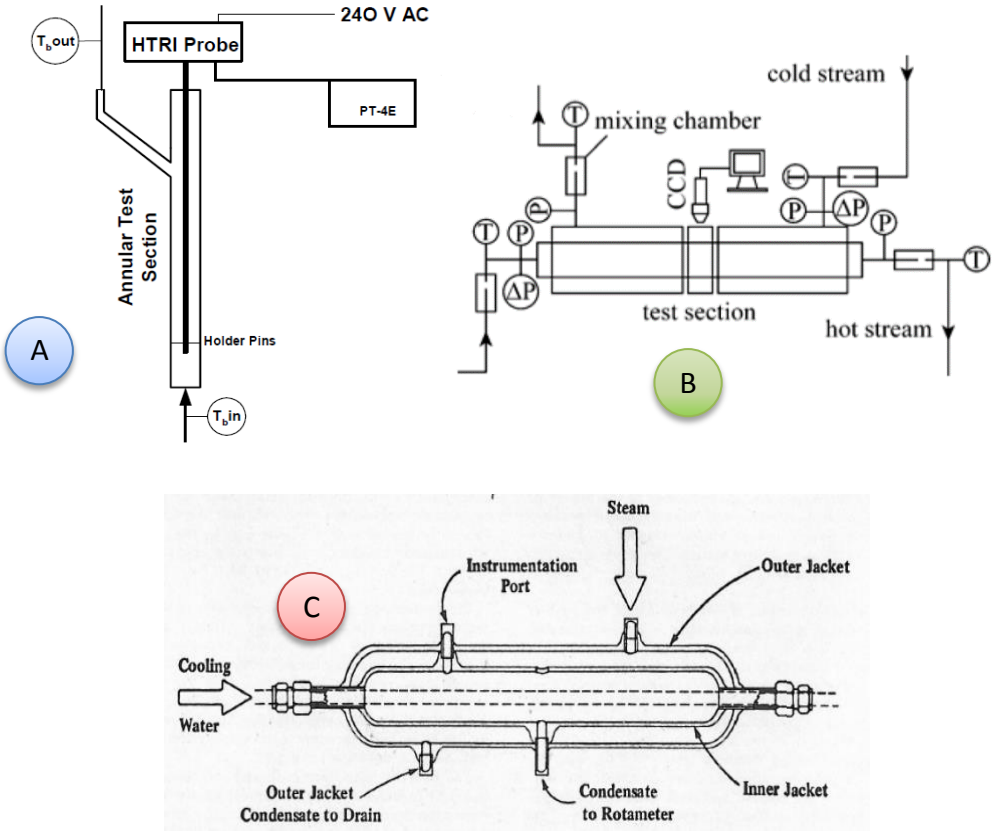

Figure 4-4: Concept a, b and c

4.4.2 Pairwise evaluation

It can be difficult to evaluate different alternatives at once where there are a number of available options. It is however simpler to compare two options with each other and determine which is superior for specific criteria. A pairwise evaluation does exactly that. The best option score 1, the other option 0 and if they are equal both score 0.5. The results are then captured and evaluated in matrix form.

Five different criterions were used to compare the different concepts. These are:

- Amount of measurements.
- Cost to build.
- Time to build.
- Flow patterns to be evaluated as a result of geometry or fluid type. Complex geometries and condensing fluids will be scored lower.
- Controllability of the test facility.

Before the evaluation can be done the weighting of each criterion must be determined. Pairwise evaluation can also be used for this and follows the same principle described above. The results of the weightings are given in Table 4-8.

Table 4-8: Criteria Weightings

	Amount of Measurements	Cost to build	Time to build	Flow patterns to be evaluated	Control of test facility	Row Total (Rank)	Weight	
Amount of Measurements	-	0.5	0.5	1	1	3	30	%
Cost to build	0.5	-	1	0	1	2.5	25	%
Time to build	0.5	0	-	0	1	1.5	15	%
Flow patterns to be evaluated	0	1	1	-	0.5	2.5	25	%
Control of test facility	0	0	0	0.5	-	0.5	5	%
					Total	10		

The results of the pairwise evaluation done on the different concepts are shown in evaluation matrixes below.

Criteria 1:
Amount of Measurements
Less ranks higher

	Concept a	Concept b	Concept c	Rank
Concept a	-	1	1	2
Concept b	0	-	1	1
Concept c	0	0	-	0

Criteria 2:
Cost to build
Less ranks higher

	Concept a	Concept b	Concept c	Rank
Concept a	-	0.5	1	1.5
Concept b	0.5	-	1	1.5
Concept c	0	0	-	0

Criteria 3:
Time to build
Less ranks higher

	Concept a	Concept b	Concept c	Rank
Concept a	-	0	1	1
Concept b	1	-	1	2
Concept c	0	0	-	0

Criteria 4:
Flow patterns to be evaluated
Less ranks higher

	Concept a	Concept b	Concept c	Rank
Concept a	-	0	1	1
Concept b	1	-	1	2
Concept c	0	0	-	0

Criteria 5:
Control of test facility
Less ranks higher

	Concept a	Concept b	Concept c	Rank
Concept a	-	0.5	1	1.5
Concept b	0.5	-	1	1.5
Concept c	0	0	-	0

Figure 4-5: Pairwise Evaluation Results Matrixes

The weighting is shown in Table 4-8 and the scores shown in Figure 4-5 are then combined and the final score as well as ranking determined for each concept. This can be seen in Table 4-9.

Table 4-9: Pairwise evaluation result

	Amount of Measurements	Cost to build	Time to build	Flow patterns to be evaluated	Control of test facility	Weighted Score	Rank
Weight	*30%*	*25%*	*15%*	*25%*	*5%*	-	-
Concept a	2	1.5	1	1	1.5	1.45	2
Concept b	1	1.5	2	2	1.5	1.55	1
Concept c	0	0	0	0	0	0	3

Concept **b** achieved the highest score and was ranked number 1. Concept **b** or test section arrangement concept **6**, as previously called, is the selected concept and will be used for the test section and test rig design.

It can be noted that concept **a** and concept **b** scored similarly and that concept **c** fell out completely. The reason for this is the complex nature involved with the use of condensing steam. It is difficult and expensive to create and control and not suited for the purposes of this work.

The selected concept (**b**) is an annulus or pipe in pipe type heat exchangers. These can be used in a parallel or counter flow configuration. For the purposes of this work the counter flow configuration as used. This allows more heat transfer and higher temperature gains as required in the specification in section 4.3.5.

4.5 Process design

The process design deals with the sizing and selection of the test section and the main components required for the process requirements to the test section. Different design cases will be evaluated that is considered representative of all the required and specified scenarios.

4.5.1 System description

Figure 4-6 indicates the piping and instrumentation diagram (P&ID) that includes all piping and instrumentation required for the test section and overall test rig. Take note that the numbering system used in the P&ID will be used throughout the document going forward.

The test facility will consist of two main loops. The first is the cold loop indicated in blue on the P&ID. The cold loop is supplied from the constant head water tower situated outside the facility (P1). The water supplied by the cold loop flows through the test tube and increases in temperature through the test section (E2). The cold loop is fitted with a control valve (V6) as well

as flow (I1), temperature (I5-6) and pressure measurement (I3). The cold loop discharges to the main water tank situated outside of the laboratory (P8).

The second is the hot loop. The hot loop is used to heat the water in the test section. Initially, a once through hot loop was considered. This resulted in approximately 50 kW heating capacity required that would have been lost when the water was returned to the main tank. To avoid this, the hot loop was changed to a re-circulation loop. It is fitted with a water heater that also acts as a tank with an approximate heating capacity of 20 kW (E1). The water heater is fitted with temperature measurement probe (I9) that sends a signal to a thyristor controller that controls the temperature in the water heater. A vent to atmosphere (P11) is fitted on the water heater. The purpose of this is to create a fixed pressure point in the loop as well as to ensure no pressure build-up in the water heater. A small pump (E3) circulates the flow through the test section and back to the water heater. Similar to the cold loop, the hot loop is also fitted with a control valve (V7) as well as flow (I2), temperature (I7-8) and pressure measurement (I4).

A filling line is installed on the water heater (P5). The filling line is supplied from the water tower and can be used to fill the water heater and the hot loop before the test facility is put in service.

A number of isolation valves at various positions are installed (V1-5). These are to isolate different parts of the system when not in use, to facilitate the removal and re-installation of test tubes and to replace/repair certain equipment without having to drain the complete system

A number of small drains are installed in the system (P9-10). This will typically be used when a new test tube is installed or when testing for a specific period has been completed and the test facility needs to be shut down and preserved.

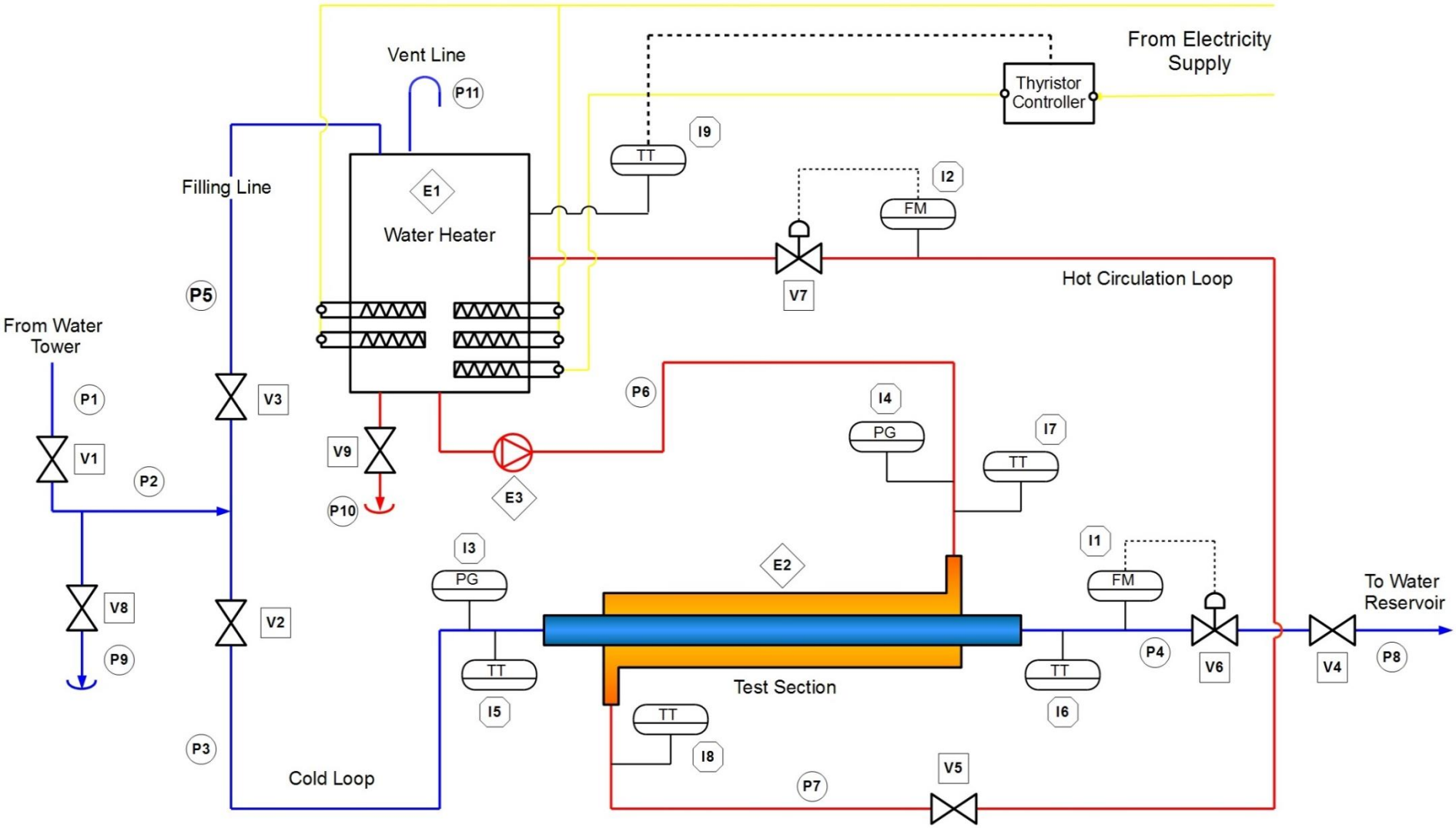

Figure 4-6: Test Rig Piping and Instrumentation Diagram

4.5.2 Process design calculations

The purpose of the process design is to size and select all the different equipment in the system. The main equipment includes the piping, water heater, control valves, pump, and the test section. Since all these components influence each other a detailed model of the complete system must be developed. A software package called Flownex was used to develop the process model. Flownex is a thermal flow package that solves flow and heat transfer problems. The specifications and technical requirements set out in section 4.4 and the P&ID showed in Figure 4-6 was used as the input for the process model.

The following are included in the process model and can be seen in Figure 4-7 and Figure 4-8:

- Details of the test section and test tube geometry included in the Flownex model via a Microsoft Excel component.
- The boundary conditions are the constant head, water tower at the inlet and the water reservoir at the outlet.
- Pipe Sizes of both the cold and the hot loop.
- Mass flow rates at different positions in the system.
- Control valve sizes and control valve position in the form of a slide bar for both the hot and the cold loop control valves.
- Details of the heat transfer and heat transfer coefficients that will take place in the test section. The heat transfer correlation for the annulus was included as a script in Flownex. See section 4.5.3.
- Pump curve of the selected pump as well as the position on the pump curve that indicates the system resistance of the hot loop.

To ensure the equipment are sized and selected correctly for all possible scenarios different design cases need to be considered. In this case, it was deemed sufficient if two design cases are considered. The first is for the maximum tube size. This will lead to the maximum required flow and heating input. The second is for the minimum tube size. This will lead to the minimum required flow and heating input. The logic behind the selection of the design cases is such that if the test set-up can perform as required for the maximum and minimum cases and sufficient controls are implemented all possible cases in between will be catered for. The results of design case 1 and 2 are given below.

Results: Design Case 1 - Tube OD: 27 mm, Tube wall thickness 3.2 mm.

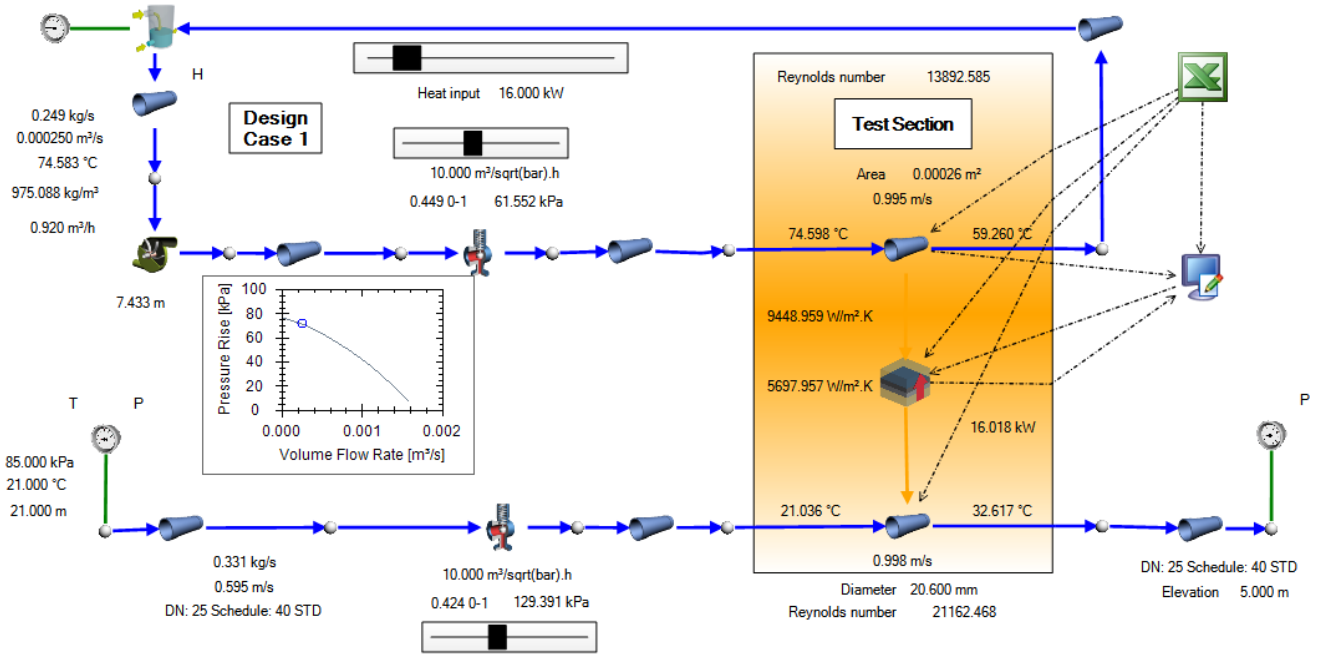

Figure 4-7: Process model for design case 1

Results: Design Case 2 - Tube OD: 14 mm, Tube wall thickness 1.27 mm.

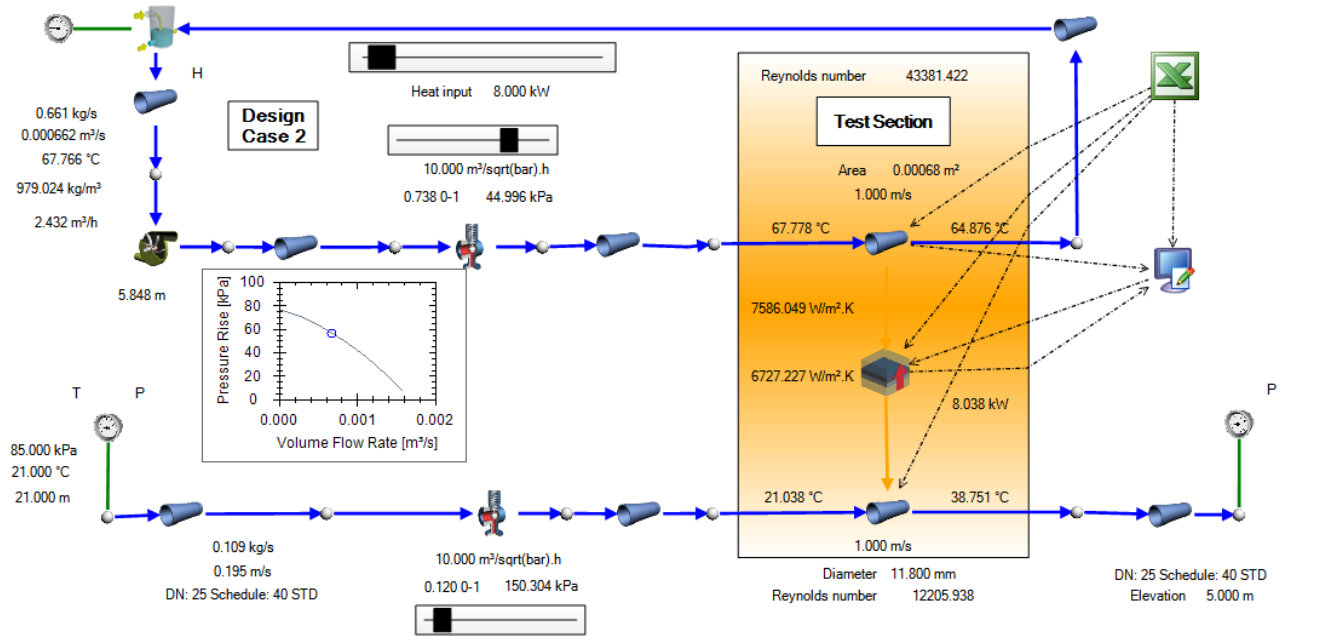

Figure 4-8: Process model for design case 2

A summary of the results for the main equipment is given below. A further detailed discussion of the component selection is done in section 4.6.

Table 4-10: Summarised results of main equipment and parameters from Process models

Equipment	Required Size / Expected parameters	
	Design Case 1	**Design Case 2**
Piping	Selected Size: 25 NB Velocity: 0.6 m/s	Selected Size: 25 NB Velocity: 0.2 m/s
Pump	Required Flow: 0.92 m³/h Required Head: 7.5 m	Required Flow: 2.43 m³/h Required Head: 6 m
Hot Loop Control Valve	Selected Cv: 10 Pressure Drop: 61.5 kPa Percentage Open: 45%	Selected Cv: 10 Pressure Drop: 45 kPa Percentage Open: 74%
Cold Loop Control Valve	Selected Cv: 10 Pressure Drop: 129.3 kPa Percentage Open: 42%	Selected Cv: 10 Pressure Drop: 150.4 kPa Percentage Open: 12%
Water Heater	Heating Capacity: 16 kW	Heating Capacity: 8 kW
Temperatures	Hoot Loop Inlet: 74.5°C Hoot Loop Outlet: 59.2°C Cold Loop Inlet: 21°C Cold Loop Outlet: 32.6°C	Hoot Loop Inlet: 67.7°C Hoot Loop Outlet: 64.8°C Cold Loop Inlet: 21°C Cold Loop Outlet: 38.7°C

The different design cases are accommodated well with the selected equipment with minor changes and control required when the 2 design cases are compared. The design will easily allow all possible design cases between the selected cases.

The velocities in the piping as well as in the test tube are significantly lower than what was allowed for in the specification. Reasons for this are discussed in section 4.6.1.

4.5.3 Flownex model verification

To ensure the Flownex process models given above are accurate and can be used for the design going forward one design case was verified with hand calculations performed in Mathcad. Two main differences were initially found.

The first was a slight difference in the fluid properties. The reason for this is that different methods are used to determine the fluid properties. Flownex uses a table interpolation scheme from the NIST database and Mathcad uses the analytical form of the IAPWS-IF97 properties. Flownex also uses the average static properties and the verification calculation used average total properties. Since these changes are very small and insignificant these will be accepted as is.

The second was the heat transfer coefficient in the annulus part of the test section. There was a significant difference between the Flownex and Mathcad model. Upon further investigation, it was found that Flownex uses a similar heat transfer coefficient correlation for the annulus than that for a straight pipe with limited modifications possible by the user. Although similar, the correlation used is not in line with the latest state of the art correlations used in industry and as given in the

literature study in section 2.4.6. To ensure the correct correlation is used the Flownex model was adjusted by using a script. With these changes made the calculated heat transfer coefficients for both models were in relatively good agreement. Most importantly, the final result, which are the calculated heat transfer, are in very good agreement.

See Table 4-11 below for comparison of the main parameters. See Appendix A for full Mathcad verification calculations.

Table 4-11: Flownex model and verification calculations comparison

Parameter Description	Flownex Model	Mathcad Verification Calculations	Percentage Difference*
Cold Loop Heat Transfer Coefficient	5561.3 W/m².K	5712.28 W/m².K	2.64
Hot Loop Heat Transfer Coefficient	8691.74 W/m².K	8306.45 W/m².K	-4.64
Cold Loop Outlet:	31.37°C	31.28°C	-0.29
Hoot Loop Outlet:	54.89°C	54.98°C	0.16
Heat Transfer	14.28 kW	14.27 kW	-0.07

*Between Mathcad calculation and Flownex model

4.5.4 Required insulation thickness

Any object at a higher temperature than that of its surroundings will suffer from some sort of heat loss to the surroundings. To ensure the results are as accurate as possible it is imperative that a minimum amount of energy is lost to atmosphere during any given test. Even a small amount of energy lost can have an effect on the results. The effect will also be unknown since it cannot be readily quantifiable.

A calculation was done to determine the required insulation or as commonly called, lagging thickness. Input conditions used were the following:

- Hot loop inlet temperature of 70°C and outlet temperature 60°C. This is considered the highest normal operating temperatures.
- Test tube mass flow of 0.661 kg/s and annulus mass flow of 0.25 kg/s was used. This is rounded values from the process design model for design case 1 as described in section 4.5.3.
- Since the test rig will be installed in a closed workshop, only natural convection was considered. The correlation used is well-accepted in industry and recommend by most textbooks. See section 2.5 for details.
- Thermal radiation to atmosphere was also considered. For calculation purposes, a worst case emissivity of 1 was used. This will result in the maximum amount of radiation heat loss.

- Thermaflex polyethylene foam lagging is the preferred choice of the lagging. A conductivity of 0.042 W/mK was used in accordance with the supplier technical data sheet [117]. The temperature effect on the conductivity is small and was ignored due to the small operating temperature range.
- The properties of air were determined using correlations from [118].

The results obtained can be seen in Table 4-12. As expected is there a reduction in energy loss as the lagging thickness increases. The effect of the amount of energy loss was also calculated in terms of temperature loss in the cold loop for design case 1. The amount of energy lost is very low. Reasons for these are:

- The combined natural convection and radiation heat transfer coefficient on the outside of the test section is very low.
- Relatively low temperatures are present in the test section.
- The area of the test section is small.

Table 4-12: Energy loss to atmosphere with change in lagging thickness

Lagging Thickness	Energy lost	Surface Temperature	Cold loop Temp reduction
0 mm	108.7 W	70 °C	0.1C
50 mm	12.41 W	22.8 °C	0.012 °C
100 mm	8.804 W	21.8 °C	0.008 °C
150 mm	7.39 W	21.4 °C	0.007 °C

Based on the results a lagging thickness of 50 mm is selected. That will ensure the surface is below 50 °C as required by internal Eskom standards as well as reduce the energy loss to atmosphere to acceptable margins.

4.6 Component selection

The following section provides details of all the main components. Different methods were used to finalise the different components.

- Some components were designed in detail.
- The requirements for some components were specified and designed and built by others.
- Some components were selected and bought “off the shelf”.

4.6.1 Piping

Piping forms an integral part of any plant with the main function being to connect the different equipment in the system. 25 NB piping was selected for all lines. The actual velocity in the lines is

significantly lower than the allowable velocities given in section 4.3.3. The reasons for this are as follows:

- The first is related to the temperature rise across the test section. A value of 5-10°C was specified. Higher velocities improve the heat transfer coefficients and hence the amount of heat transfer, but in this specific system, it also decreases the amount of temperature increase across the test tube in the cold loop. The decision was made that the temperature rise across the test tube takes preference and the velocities were decreased.
- The pressure drop is directly related to the square of the velocity. If the velocity doubles, the pressure drop increases 4 fold. Since only a limited amount of static pressure is available from the water tower the losses in the piping needs to be minimised. By doing this, most of the pressure drop occurs over the control valve which increases the flexibility of the test rig to accommodate different size tubes and operating scenarios.
- Most of the piping currently installed in the Flow laboratory is 25 NB. For connectivity, interchangeability, spare keeping, and seamless integration the decision was made to use the same size.

For piping materials, two options were considered. The first is galvanised piping. These are very commonly used and standard in the Flow laboratory where the test set-up will be constructed. The second is PTFE piping. PTFE piping does not corrode and will completely eliminate the risk of contamination of corrosion products on the test tubes. Galvanised piping is selected for standardisation purposes. The risk of contamination will be reduced by including a flushing procedure of the test set-up before each test is carried out.

The table below shows all the main lines in the test set-up.

Table 4-13: Piping List

No on P&ID	Description	Line Size
P1	Supply line from water tower	25 NB
P2	Test Rig Supply line	25 NB
P3	Cold loop supply	25 NB
P4	Cold loop discharge	25 NB
P5	Water Heater Filling line	25 NB
P6	Hot loop supply	25 NB
P7	Hot loop discharge	25 NB
P8	Discharge to water tank	25 NB
P9	Cold loop inlet drain	25 NB
P10	Hot Loop Drain	25 NB
P11	Water Heater Vent	25 NB

4.6.2 Water heater

The heating capacity of the water heater was determined for each of the design cases. For design case 1 and 2, the required heating capacity is 16 kW and 8 kW respectively.

The selected water heater was manufactured with 5 X 4 kW elements for a total heating capacity of 20 kW. Control is done in an on/off configuration for 4 of the 5 elements. The 5th element is controlled by a thyristor controller with input from a temperature probe in the water heater

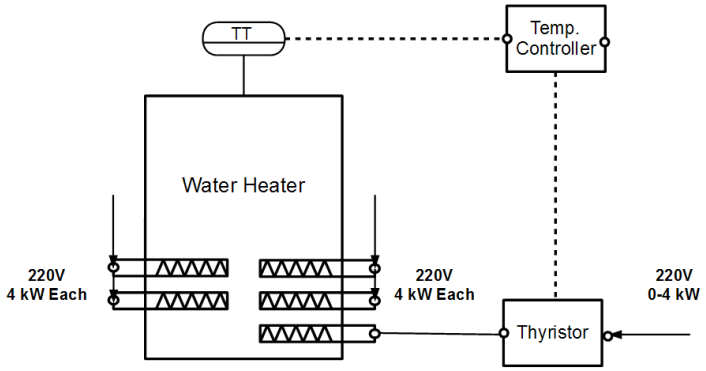

Figure 4-9: Water heater temperature control diagram

The water heater is fitted with a vent to ensure it remains at atmospheric conditions and to provide a constant pressure point in the hot loop. A low-level drain, as well as level indication in the form of a stand pipe is included for the water heater.

To save cost a standard type heater from Heat Transfer Engineering based in Johannesburg was procured. The design pressure of the heater is 600 kPa and it is designed generally in accordance with ASME VIII Div 1. Its hazard category according to SANS 347 is SEP. The water heater has a capacity of 300 liters. This is the standard capacity of the supplier based on their standard tooling and manufacturing methods.

Details of the water heater are available upon request or in a file at the test rig.

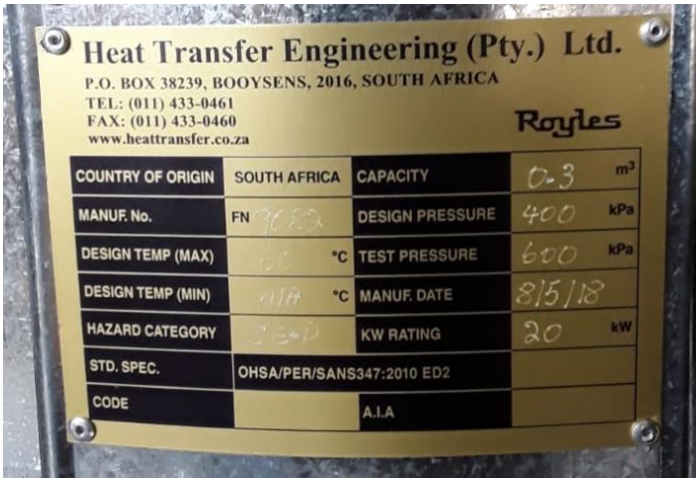

Figure 4-10: Water heater nameplate

4.6.3 Test section

The test section was designed to accommodate all the tube sizes in the identified range. A 32 NB Sch 80 pipe manufactured from A106 Gr B material was selected as the outside shell of the test section. This pipe has a 32.5 mm inner diameter and a 42.2 mm outer diameter. Sealing between the test tube and test section is done by means of a custom compression coupling welded to the test section on either side. A custom compression nut is used to compress the seal. Two sizes of the compression nuts are used. The first is for tube sizes 14 – 21 mm and the second is for tube sizes 21-27 mm. A specific custom made seal and washer will be used for each tube size. Details of the custom compression seal can be seen in Figure 4-12. Two 25 NB nozzles are installed on the test section shell. These are the inlet and outlet of the hot loop configured in a counter flow arrangement. As mentioned in section 4.1 is ideal annular flow in the test section not critical. The overall heat transfer coefficient is determined from measurements and the governing equation for heat transfer, not heat transfer correlations.

The test section is fitted with a flanged connection in the center to provide access if required or to install additional support in case the test tube sags. The flanges are 32 NB, ASME B16.5, Class 150, slip on flanges, manufactured from SA-105 material. The test section is fitted with 4 supports that are bolted to the test rig frame. See Appendix B for detail design drawings.

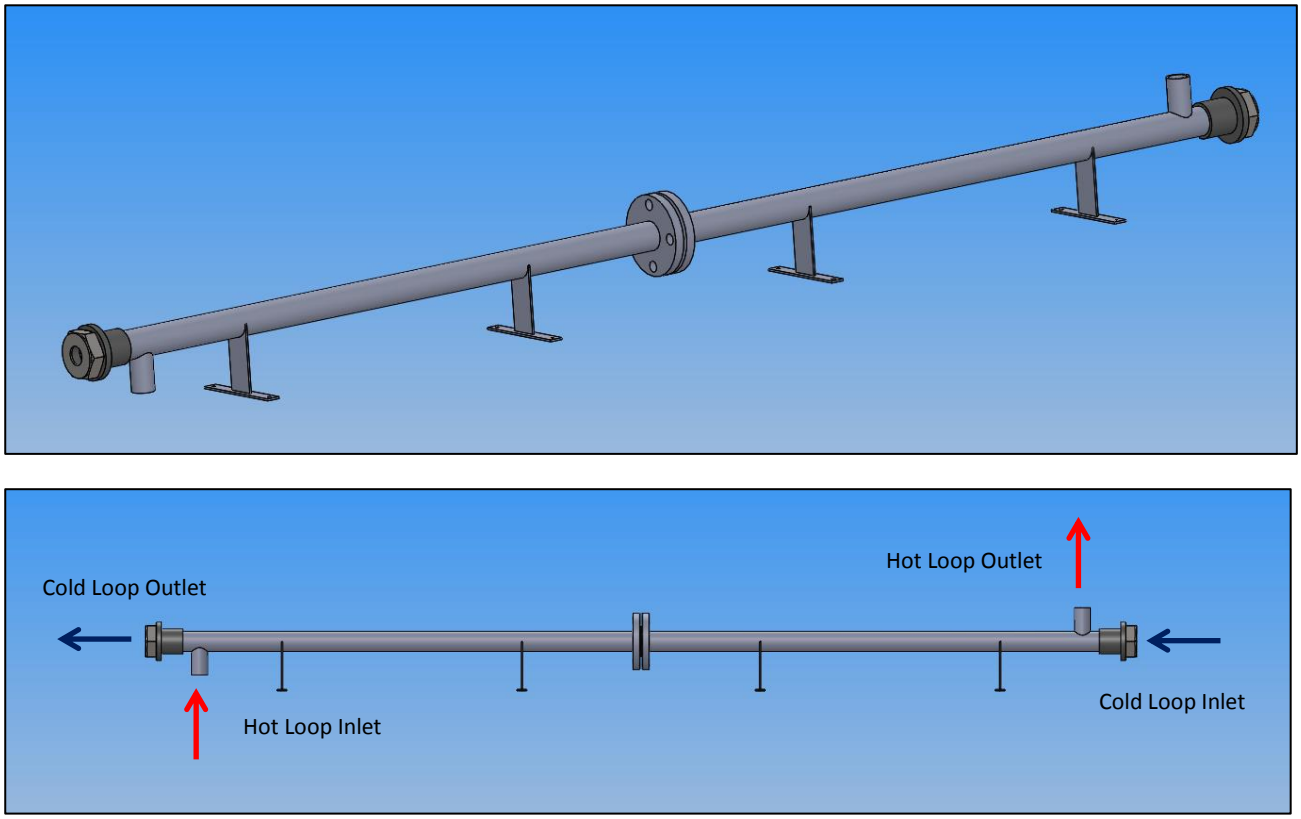

Figure 4-11: Test Section Assembly and Flow Direction

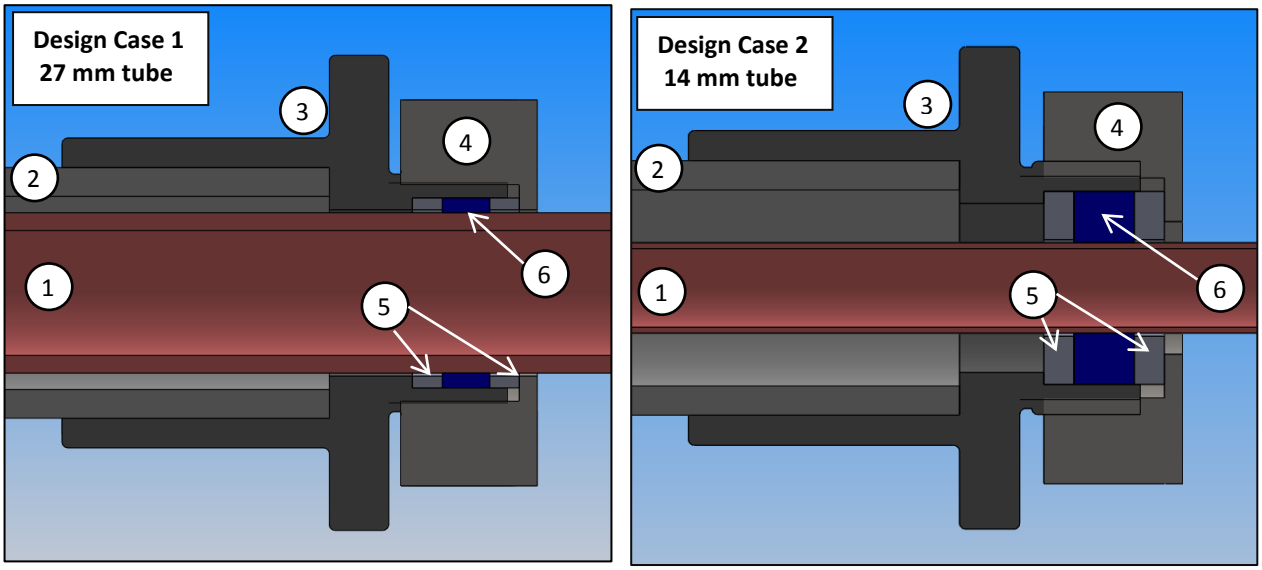

1	Test Tube	2	Test Section Shell	3	Custom Coupling
4	Compression Nut	5	Washer x 2	6	Rubber Seal

Figure 4-12: Custom compression coupling that seals between the test tube and test section

4.6.4 Test tube to inlet pipe connection

The test tube water inlet and water outlet connection must be able to connect the 25 NB water inlet and outlet pipes to the range of tube sizes. No standard couplings that can accommodate such a wide range of sizes are available. A custom compression coupling similar in principle than shown in Figure 4-12 was designed and will be used. The sizes are adjusted accordingly. The coupling does not provide a smooth transition from the pipe to the test tube. This is however not considered a problem for the following reasons:

- The test section inlet is approximately 200 mm from the connection pipe. This distance will allow sufficient time to reach fully developed turbulent flow.
- As mentioned in section 4.1 is the determination of the overall heat transfer coefficient and hence the fouling factor is not dependant on the calculation of heat transfer coefficients if the same flow conditions are used.

4.6.5 Re-circulation pump

The re-circulation pump is a small pump that circulates the water through the test section and the water heater in the hot loop. The pump is only required to provide sufficient head to overcome the resistance in the hot loop. The required flow from the process model for design case 1 is 0.25 kg/s or 0.9 m^3/h and for design case 2 it is 0.66 kg/s or 2.38 m^3/h.

Note that the pump curves show a head of 60-80 kPa which equates to approximately 6-8 m of water head. That is high for a simple system as the hot loop, but most of the pressure drop occurs due to the throttling of the control valves. Since it is a small pump with low power consumption it

was not necessarily sized and selected to operate at its best efficiency point. It was however sized and selected that excess capacity is provided in case it is required.

The selected pump is a Grundfos UPS 25-80. It is designed for 10 bar and 100°C, it has 3 different speed settings and operates with 220V, 50Hz supply. The maximum power output is 165W. The pump curve is shown in Figure 4-13. The pump data sheet is available upon request or in a file at the test rig.

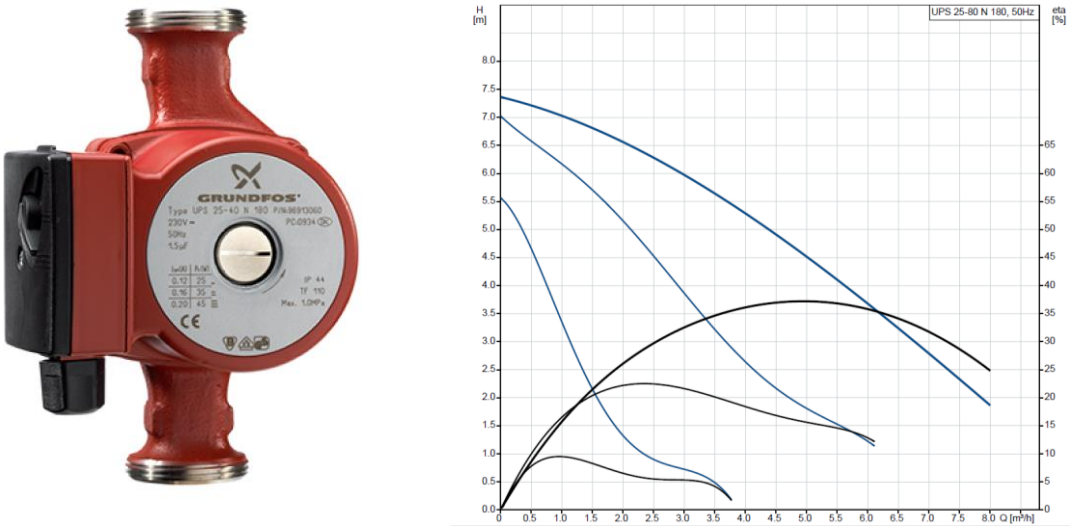

Figure 4-13: Grundfos UPS 25-80 Image and Pump Curve

4.6.6 Valves

25 NB Tekflo full bore ball valves were selected for all isolation and drain valves. These are fitted with 1" BSPT connections.

Two control valves are used, one for the hot loop and one for the cold loop. The process model was used to determine the required capacity of the control valves to accommodate all possible design cases. A maximum Cv of 10 was selected for both valves with an equal percentage characteristic. Due to funding constraints, the actual control valves used did not conform to these specifications. Instead, 25 NB Manual Tekflo brass gate valves were used for control. These are also fitted with 1" BSPT connections.

Figure 4-14: Tekflo Brass gate valve and Tekflo Ball Valve

A summary of the selected valves can be seen in Table 4-14 below.

Table 4-14: Valve List

No on P&ID	Description	Purpose	Type and make of valve	Actuator	Pressure Rating
V1	Water supply isolation valve	Isolation	Tekflo Ball	Manual	PN 10
V2	Cold loop inlet isolation valve	Isolation	Tekflo Ball	Manual	PN 10
V3	Water heater filling valve	Isolation	Tekflo Ball	Manual	PN 10
V4	Cold loop outlet isolation valve	Isolation	Tekflo Ball	Manual	PN 10
V5	Hot loop outlet isolation valve	Isolation	Tekflo Ball	Manual	PN 10
V6	Cold loop control valve	Control	Tekflo Gate	Manual	PN 10
V7	Hot loop control valve	Control	Tekflo Gate	Manual	PN 10
V8	Cold loop drain valve	Drain	Tekflo Ball	Manual	PN 10
V9	Hot loop drain valve	Drain	Tekflo Ball	Manual	PN 10

4.6.7 Layout

The layout was done in a skid based approach. The complete test rig will be built on a single frame that can be easily moved if required. All equipment is installed on the frame. The frame is approximately 3.2 m long and 1.2 m wide. An inlet and outlet water connection is provided. The drains will be routed into a manifold connected to the laboratory drains. Sufficient straight pipe lengths are provided before the flow measurement devices. All valves and instrumentation are installed to provide easy access for the operator. A data capture and analysis station are provided next to the skid that includes a computer, the temperature measurement modules, the hardware required to capture the data and the control of the system.

Tubes must be easily removable for cleaning or to test different tube samples. To accomplish this, the outlet section of the cold loop is fitted with union couplings and adjustable pipe supports that can easily be loosened. This will allow the outlet section of the cold loop to be removed. Once that is removed the currently installed tube can be withdrawn from the test section and a new test or cleaned test tube can be installed. See Appendix B for detail design drawings of the frame.

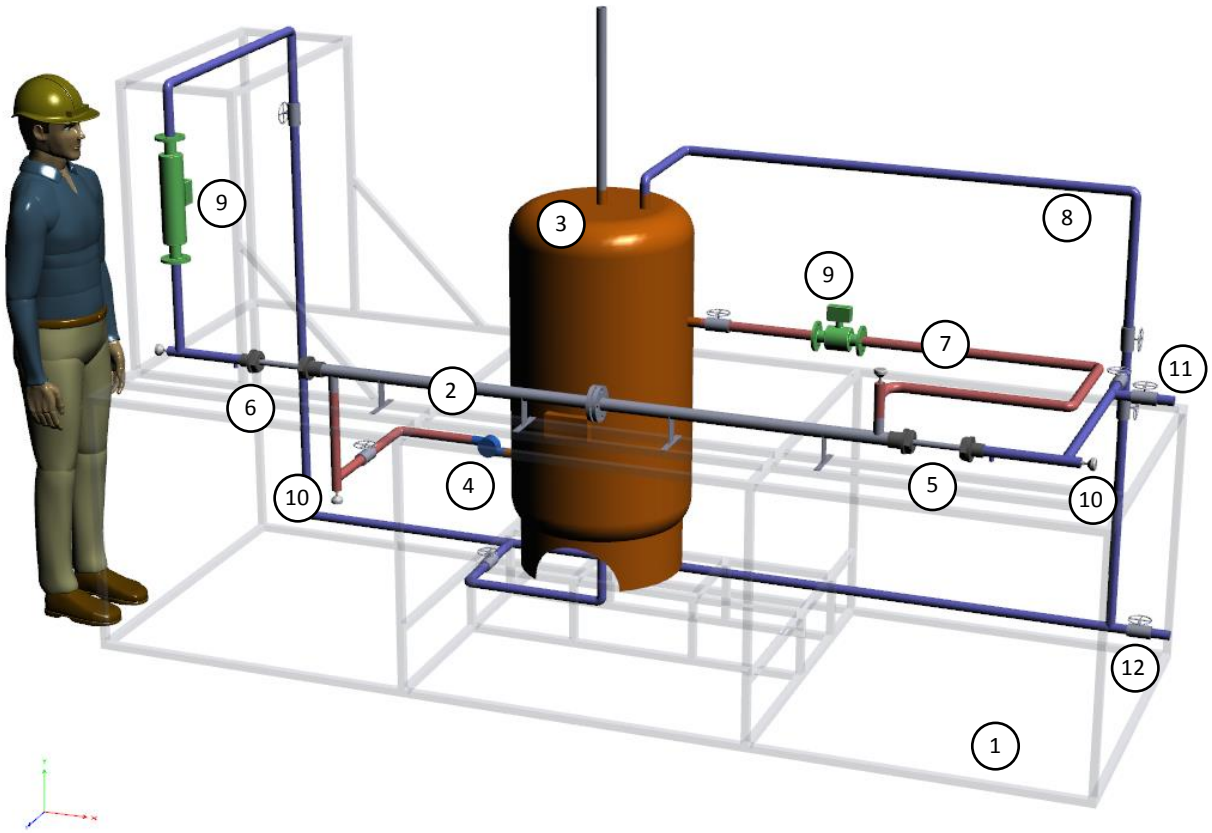

1	Frame	5	Cold Loop Inlet	9	Flow Measurement
2	Test Section	6	Cold Loop Outlet	10	Temperature Measurement
3	Water Heater with vent	7	Hot Loop	11	Test Rig Water Supply
4	Hot Loop Circulation Pump	8	Water Heater Filling Line	12	Water Discharge

Figure 4-15: Test Set-up layout

4.6.8 Flow measurement

Both electromagnetic and Coriolis type flow meters comply with the specified required accuracy. Both of these types are however very expensive. Fortunately one of each type is available in the Flow laboratory for use.

A 25 NB, Endress and Hauser, ProMass 63F, Coriolis type mass flow meter was used for the cold loop. The meter was installed in a vertical position to ensure full bore flow for all load cases. This flow meter has a specified accuracy of 0.1%. The meter provides a 4-20mA signal output and has an adjustable range. For the test rig, 0 - 1.2 kg/s will be used. According to the technical information published by Endress and Hauser [119], the accuracy of the meter is as follows:

$$\pm 0.10\% \pm [(\text{zero stability} / \text{flowrate}) \times 100]\ \%\ \text{of flow rate}$$

For the 25 NB bore meter, the zero stability is given as 0.9 kg/h. For the typical flow rates, the test rig will operate at 0.5 kg/s, so the accuracy is approximately 0.15% of the measured mass flow.

A 15 NB, Endress and Hauser, ProMag 33A electromagnetic type volume flow meter will be used for the hot loop flow measurement. The flow meter also provides a 4-20mA signal output and has

an adjustable range. For the test rig, 0 - 1.2 kg/s will be used. According to the Endress and Hauser datasheet [120], the specified accuracy is ± 0.5%.

Since the systematic uncertainty is a percentage of flowrate it is re-calculated for every individual case.

Table 4-15: Flow measurement list

No on P&ID	Description	Type	Measurement Unit	Range	Systematic Uncertainty (for 0.5 kg/s)
I1	Cold loop flow meter	Coriolis	kg/s	0 – 1.5 kg/s	0.15%
I2	Hot loop flow meter	Electromagnetic	kg/s	0 – 2 kg/s	0.5%

Figure 4-16: Endress and Hauser ProMass Coriolis and ProMag Electromagnetic flow meters

4.6.9 Temperature measurement

The temperature measurement system constitutes a number of parts. These are the following:

- Temperature probes.
- Data logger / Voltage Measurement.
- Current Source.

The temperature probes selected are RTD, PT 100, 1/10 DIN spec, 4 wire probes. These were manufactured by Temperature Controls. The specified accuracy of the 1/10 DIN probes was given in section 3.9.2 as:

$$\pm (0.03 + 0.0005|T|)$$

So for the typical working temperature of the test rig, the probe uncertainty will be:

Table 4-16: 1/10 DIN temperature measurement probes systemic uncertainty

Temp	Probe Systematic Uncertainty [°C]
20	0.04
30	0.045
40	0.05
50	0.055
60	0.06
70	0.065

A PicoLog ADC-24 high-resolution data logger borrowed from the Flow laboratory was used to measure the voltage. The data logger has a voltage measurement accuracy of 0.2%.

The current is supplied by a 1 mA current source that was custom built by the Flow laboratory personnel. The resistance is calculated from the voltage and current by the Pico interface program. Due to the custom nature of the current source the uncertainty values are not available. For this reason, the uncertainty of the temperature measurement system could not be determined to from the different error sources that make up the system. The uncertainty of the temperature measurement system can only be determined by means of the calibration of the complete system. Details can be seen in section 4.9.2.

The resistance value is then transferred to Excel via the VBA interface where the conversion from resistance to temperature is done using a polynomial equation.

Photographs of the temperature measurement system can be seen in section 4.8.

Table 4-17: Temperature measurement list

No	Description	Type	Unit	Range
I5	TS cold loop inlet temperature	RTD, PT 100, 1/10 DIN	°C	0 – 100°C
I6	TS cold loop outlet temperature	RTD, PT 100, 1/10 DIN	°C	0 – 100°C
I7	TS hot loop inlet temperature	RTD, PT 100, 1/10 DIN	°C	0 – 100°C
I8	TS hot loop outlet temperature	RTD, PT 100, 1/10 DIN	°C	0 – 100°C

4.6.10 Pressure measurement

The pressure measurement is used to determine the fluid properties of the hot and the cold loop. At the working temperatures and pressures and with water as the working fluid, the pressure has a very small effect on the properties. For this reason and due to budget constraints no required accuracy is specified for the pressure measurement gauges. Small uncertainties on the measurement will have a neglectable effect on the results. Standard industrial pressure gauges are used. The pressure gauges were supplied by Transducer Technology. They have a dial size of 63 mm and a ½" BSP bottom mounted connection. The gauges are glycerine filled and have a range of 0-4 bar.

Table 4-18: Pressure Measurement List

No	Description	Type	Measurement Unit	Range
I3	TS cold loop inlet pressure	Manual gauge	kPa(g)	0 – 400 kPa
I4	TS cold loop outlet pressure	Manual gauge	kPa(g)	0 – 400 kPa

Figure 4-17: Installed Pressure gauges

4.6.11 Data acquisition

Data acquisition is done with a VBA interface in Excel. A custom program was created with the help of the Flow laboratory personal to capture the data and run the actual tests. The program includes the following functionality:

- Interface and capture readings from all instrumentation.
- Provide trends of measurement to assist in determining if steady state has been achieved.
- Adjust reading sample time.
- Run predefined tests. A typical single test contains 50 readings. 8 tests make up a combined test.
- Calculate among other things the actual heat transfer, theoretical heat transfer, LMTD, overall heat transfer coefficients.

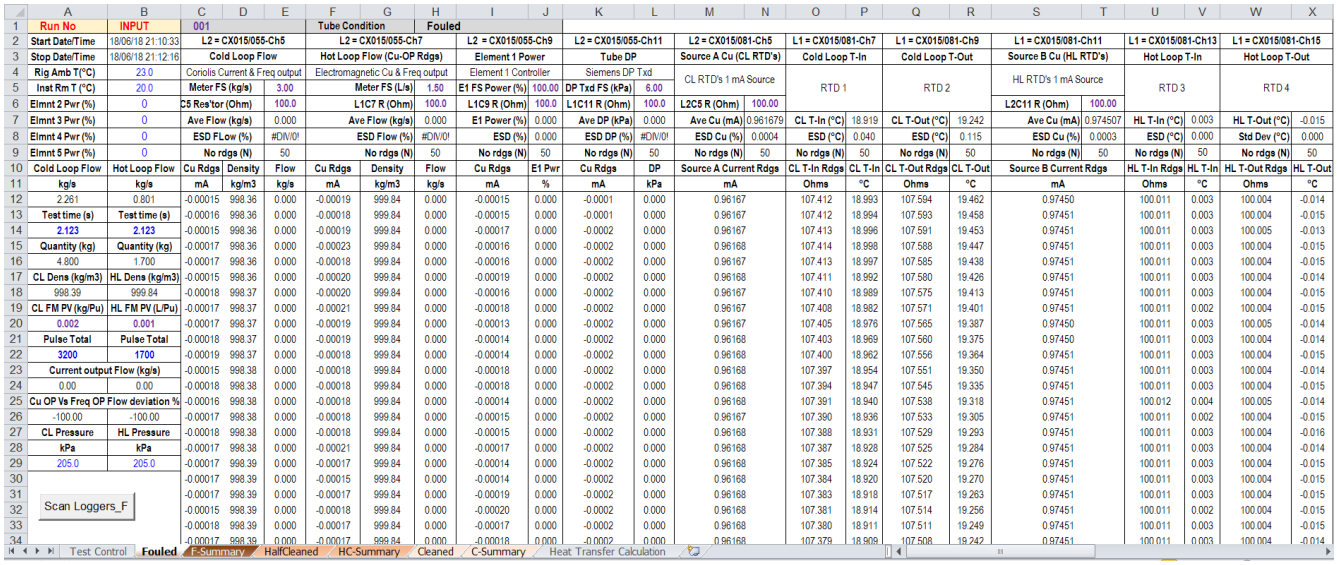

Run No	INPUT	001			Tube Condition		Fouled																	
Start Date/Time	18/06/18 21:10:33	L2 = CX015/055-Ch5			L2 = CX015/055-Ch7			L2 = CX015/055-Ch9		L2 = CX015/055-Ch11		L2 = CX015/081-Ch5		L1 = CX015/081-Ch7		L1 = CX015/081-Ch9		L1 = CX015/081-Ch11		L1 = CX015/081-Ch13		L1 = CX015/081-Ch15	
Stop Date/Time	18/06/18 21:12:16	Cold Loop Flow			Hot Loop Flow (Cu-OP Rdgs)			Element 1 Power		Tube DP		Source A Cu (CL RTD's)		Cold Loop T-In		Cold Loop T-Out		Source B Cu (HL RTD's)		Hot Loop T-In		Hot Loop T-Out	
Rig Amb T(°C)	23.0	Coriolis Current & Freq output			Electromagnetic Cu & Freq output			Element 1 Controller		Siemens DP Txd		CL RTD's 1 mA Source		RTD 1		RTD 2		HL RTD's 1 mA Source		RTD 3		RTD 4	
Inst Rm T (°C)	20.0	Meter FS (kg/s)		3.00	Meter FS (L/s)		1.50	E1 FS Power (%)	100.00	DP Txd FS (kPa)	6.00													
Elmnt 2 Pwr (%)	0	C5 Res'tor (Ohm)		100.0	L1C7 R (Ohm)		100.0	L1C9 R (Ohm)	100.0	L1C11 R (Ohm)	100.0	L2C5 R (Ohm)	100.00					L2C11 R (Ohm)	100.00					
Elmnt 3 Pwr (%)	0	Ave Flow (kg/s)		0.000	Ave Flow (kg/s)		0.000	E1 Power (%)	0.000	Ave DP (kPa)	0.000	Ave Cu (mA)	0.961679	CL T-In (°C)	18.919	CL T-Out (°C)	19.242	Ave Cu (mA)	0.974507	HL T-In (°C)	0.003	HL T-Out (°C)	-0.015	
Elmnt 4 Pwr (%)	0	ESD FLow (%)		#DIV/0!	ESD Flow (%)		#DIV/0!	ESD (%)	0.000	ESD DP (%)	#DIV/0!	ESD Cu (%)	0.0004	ESD (°C)	0.040	ESD (°C)	0.115	ESD Cu (%)	0.0003	ESD (°C)	0.000	Std Dev (°C)	0.000	
Elmnt 5 Pwr (%)	0	No rdgs (N)		50	No rdgs (N)		50	No rdgs (N)	50	No rdgs (N)	50	No rdgs (N)	50	No rdgs (N)	50	No rdgs (N)	50	No rdgs (N)	50	No rdgs (N)	50	No rdgs (N)	50	
Cold Loop Flow	Hot Loop Flow	Cu Rdgs	Density	Flow	Cu Rdgs	Density	Flow	Cu Rdgs	E1 Pwr	Cu Rdgs	DP	Source A Current Rdgs		CL T-In Rdgs	CL T-In	CL T-Out Rdgs	CL T-Out	Source B Current Rdgs		HL T-In Rdgs	HL T-In	HL T-Out Rdgs	HL T-Out
kg/s	kg/s	mA	kg/m3	kg/s	mA	kg/m3	kg/s	mA	%	mA	kPa	mA		Ohms	°C	Ohms	°C	mA		Ohms	°C	Ohms	°C
2.261	0.801	-0.00015	998.36	0.000	-0.00019	999.84	0.000	-0.00015	0.000	-0.0001	0.000	0.96167		107.412	18.993	107.594	19.462	0.97450		100.011	0.003	100.004	-0.014
Test time (s)	Test time (s)	-0.00016	998.36	0.000	-0.00018	999.84	0.000	-0.00015	0.000	-0.0001	0.000	0.96167		107.412	18.994	107.593	19.458	0.97451		100.011	0.003	100.004	-0.015
2.123	2.123	-0.00015	998.36	0.000	-0.00019	999.84	0.000	-0.00017	0.000	-0.0002	0.000	0.96167		107.413	18.996	107.591	19.453	0.97451		100.011	0.003	100.005	-0.013
Quantity (kg)	Quantity (kg)	-0.00017	998.36	0.000	-0.00023	999.84	0.000	-0.00016	0.000	-0.0002	0.000	0.96168		107.414	18.998	107.588	19.447	0.97451		100.011	0.003	100.004	-0.015
4.800	1.700	-0.00017	998.36	0.000	-0.00018	999.84	0.000	-0.00016	0.000	-0.0002	0.000	0.96167		107.413	18.997	107.585	19.438	0.97451		100.011	0.003	100.004	-0.015
CL Dens (kg/m3)	HL Dens (kg/m3)	-0.00015	998.36	0.000	-0.00020	999.84	0.000	-0.00019	0.000	-0.0002	0.000	0.96168		107.411	18.992	107.580	19.426	0.97451		100.011	0.003	100.004	-0.014
998.39	999.84	-0.00018	998.37	0.000	-0.00020	999.84	0.000	-0.00016	0.000	-0.0002	0.000	0.96167		107.410	18.989	107.575	19.413	0.97451		100.011	0.003	100.004	-0.015
CL FM PV (kg/Pu)	HL FM PV (L/Pu)	-0.00017	998.37	0.000	-0.00021	999.84	0.000	-0.00018	0.000	-0.0002	0.000	0.96167		107.408	18.982	107.571	19.401	0.97451		100.011	0.002	100.004	-0.015
0.002	0.001	-0.00017	998.37	0.000	-0.00019	999.84	0.000	-0.00013	0.000	-0.0002	0.000	0.96167		107.405	18.976	107.565	19.387	0.97450		100.011	0.003	100.005	-0.014
Pulse Total	Pulse Total	-0.00018	998.37	0.000	-0.00019	999.84	0.000	-0.00014	0.000	-0.0002	0.000	0.96168		107.403	18.969	107.560	19.375	0.97450		100.011	0.003	100.004	-0.014
3200	1700	-0.00019	998.37	0.000	-0.00018	999.84	0.000	-0.00014	0.000	-0.0002	0.000	0.96168		107.400	18.962	107.556	19.364	0.97451		100.011	0.003	100.004	-0.015
Current output Flow (kg/s)		-0.00015	998.38	0.000	-0.00018	999.84	0.000	-0.00018	0.000	-0.0002	0.000	0.96168		107.397	18.954	107.551	19.350	0.97451		100.011	0.003	100.004	-0.014
0.00	0.00	-0.00018	998.38	0.000	-0.00018	999.84	0.000	-0.00018	0.000	-0.0002	0.000	0.96168		107.394	18.947	107.545	19.335	0.97451		100.011	0.003	100.004	-0.015
Cu OP Vs Freq OP Flow deviation %		-0.00016	998.38	0.000	-0.00018	999.84	0.000	-0.00014	0.000	-0.0002	0.000	0.96168		107.391	18.940	107.538	19.318	0.97451		100.012	0.004	100.005	-0.014
-100.00	-100.00	-0.00017	998.38	0.000	-0.00018	999.84	0.000	-0.00015	0.000	-0.0002	0.000	0.96167		107.390	18.936	107.533	19.305	0.97451		100.011	0.002	100.004	-0.015
CL Pressure	HL Pressure	-0.00018	998.38	0.000	-0.00018	999.84	0.000	-0.00015	0.000	-0.0002	0.000	0.96168		107.388	18.931	107.529	19.293	0.97451		100.011	0.003	100.004	-0.016
kPa	kPa	-0.00017	998.38	0.000	-0.00021	999.84	0.000	-0.00017	0.000	-0.0002	0.000	0.96168		107.387	18.928	107.525	19.284	0.97451		100.011	0.003	100.004	-0.014
205.0	205.0	-0.00017	998.39	0.000	-0.00017	999.84	0.000	-0.00014	0.000	-0.0002	0.000	0.96168		107.385	18.924	107.522	19.276	0.97451		100.011	0.003	100.004	-0.015
		-0.00017	998.39	0.000	-0.00015	999.84	0.000	-0.00014	0.000	-0.0002	0.000	0.96168		107.384	18.920	107.520	19.270	0.97451		100.011	0.003	100.004	-0.015
Scan Loggers_F		-0.00017	998.39	0.000	-0.00017	999.84	0.000	-0.00019	0.000	-0.0002	0.000	0.96168		107.383	18.918	107.517	19.263	0.97451		100.011	0.003	100.004	-0.015
		-0.00015	998.39	0.000	-0.00018	999.84	0.000	-0.00020	0.000	-0.0002	0.000	0.96168		107.381	18.914	107.514	19.256	0.97451		100.011	0.002	100.004	-0.015
		-0.00018	998.39	0.000	-0.00017	999.84	0.000	-0.00017	0.000	-0.0002	0.000	0.96168		107.380	18.911	107.511	19.249	0.97451		100.011	0.003	100.004	-0.015
		-0.00017	998.39	0.000	-0.00017	999.84	0.000	-0.00018	0.000	-0.0002	0.000	0.96168		107.379	18.909	107.508	19.242	0.97451		100.011	0.003	100.004	-0.014

Test Control | Fouled | C-Summary | HalfCleaned | HC-Summary | Cleaned | C-Summary | Heat Transfer Calculation

Figure 4-18: Screenshot from data acquisition program

4.7 Budget

A detailed budget for the test rig was created. Two budgets and the actual spend are shown and discussed.

The first is the estimated budget before construction started. This was obtained from budget quotes from suppliers of the main equipment. Assumptions were made w.r.t. lower cost items. The initial budget is high. The main reason for this is the highly accurate instrumentation that is required. The price of instrumenting increases exponentially as the associated uncertainty decreases. Flow measurement is a good example. A 25NB electromagnetic flow measurement device cost approximately R 50 000. This will provide an accuracy of ±0.3%. A 25NB Coriolis type flow measurement device can decrease the accuracy to ±0.1% but it cost approximately R 150 000.

With the current financial constraints experienced by Eskom, the budget will not be released. For this reason, a second budget was created. This purpose of this is to build the test rig within the lowest possible budget by utilising lower accuracy instrumentation and by using instrumentation and components available in the Flow laboratory. This will increase the achievable uncertainty on the result. If in future the situation changes and funding becomes available the instrumentation can easily be replaced and the uncertainty reduced if required.

After the test rig was completed the actual amount spent was calculated. The actual spent compares very well with the reduced budget.

Table 4-19: Test Rig Construction Budget

Component Description	Required Quantity	Low Uncertainty Budget	Actual Budget	Actual Spend	Notes
Test Section	1	R 2 000	R 2 000	R 663	
Water Heater	1	R 12 000	R 12 000	R 12 950	
Pump	1	R 5 000	-	-	Borrowed from Flow lab.
Control Valves	2	R 40 000	R 500	R 380	Manual control valves used
Flow Meters	2	R 200 000	-	-	Borrowed from Flow lab.
Temp. Measurement - Probes	4	R 6 000	R 6 000	R 6 808	
Temp. Measurement - Data Acquisition	1	R 80 000	-	-	Borrowed from Flow lab.
Pressure Measurement	2	R 2 000	R 2 000	R 1 932	
Valves, pipes, fittings and flanges	-	R 8 000	R 7 500	R 7 462	
Steel for frame	-	R 2 000	R 2 000	R 1 958	
Control System and PC Interface	1		-	R 159	
Special Tools	-	R 2 000	R 2 000	R 2 100	
Consumables during manufacture	-	R 1 000	R 1 000	R 870	
Calibration - Temp.	-	R 12 000	-	-	Done at no cost for Flow lab.
Calibration - Flow	-	R 12 000	-	-	Done at no cost by Flow lab.
Electric Installation	-	R 25 000	-	-	Done on Flow lab. budget
Lagging	N/A	-	-	R 491	Excluded in initial estimations
	Total Cost	R 409 000	R 35 000	R 35 773	

4.8 Manufacturing

The manufacturing of the test rig was completed approximately 6 months after the work started. All mechanical work was done in-house by the author and Flow laboratory personnel.

A number of problems were encountered that had to be solved. This included:

- The feet of the water heater was not built according to the supplied drawing. This necessitated frame modifications that were not part of the initial design.
- Temperature probes supplied with BSPP thread instead of BSPT like the rest of the piping and fittings. This was solved by manufacturing custom connections for the probes that allowed connection of BSPP to BSPT thread.
- Due to the large weight of the flow meters more supports were required than what was allowed for in the design. Additional pipe supports and frame modifications had to be done.
- Numerous issues were experienced with pipe threading and pipe threading tools. Welding showed to be easier and less time-consuming. A number of connections initially planned to be threaded connections was welded.
- Electrical installation was more complicated than anticipated. Also, the certification requirements in terms of the issuing of an electrical Certificate of Compliance (COC) for the

installation were not initially considered. After a number of problems and delays were experienced this was outsourced and completed by external contractors.

The following section shows selected photographs of the manufacturing process. See descriptions below for each photo.

Table 4-20: Manufacturing photographs and descriptions

No.	Description	
1	Completed and painted frame. Take note that additional piping supports strictures were added later	
2	Custom design and manufactured compression couplings	
3	Installation of water heater using overhead crane	
4	Installation of hot loop circulation pump and associated valves and piping	
5	Custom manufactured connections for temperature probes	
6	Adjustable pipe support to allow change removal/installation of the test tube	
7	Test Rig in final position	
	a	Removable Pipe section for tube removal/installation.
	b	Test Section.
	c	Local isolation switches for heating elements.
	d	Splash plate to prevent water in event of a leak to come in contact with electrical elements.
	e	Rear of instrument panel
8	Instrumentation Panel	
	a	Data Logger – Temperature probes
	b	Data Logger – Flow Meters
	c	Current Source for temperature probes
	d	Manual water heater element switches
	e	Water heater thyristor and temperature controller
	f	Selected displays


1

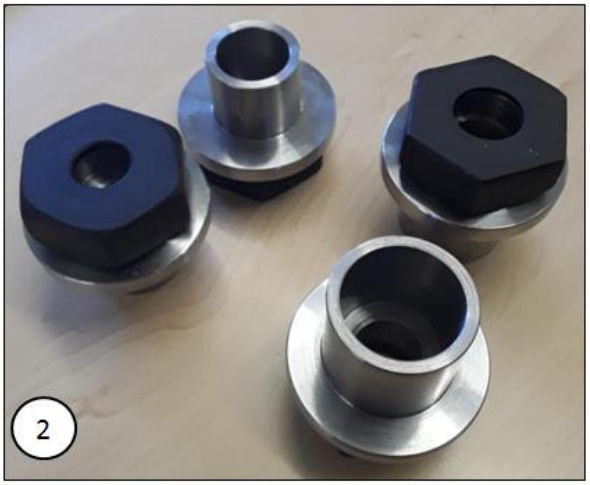
2


3


4


5


6


e
c
b
a
d
7

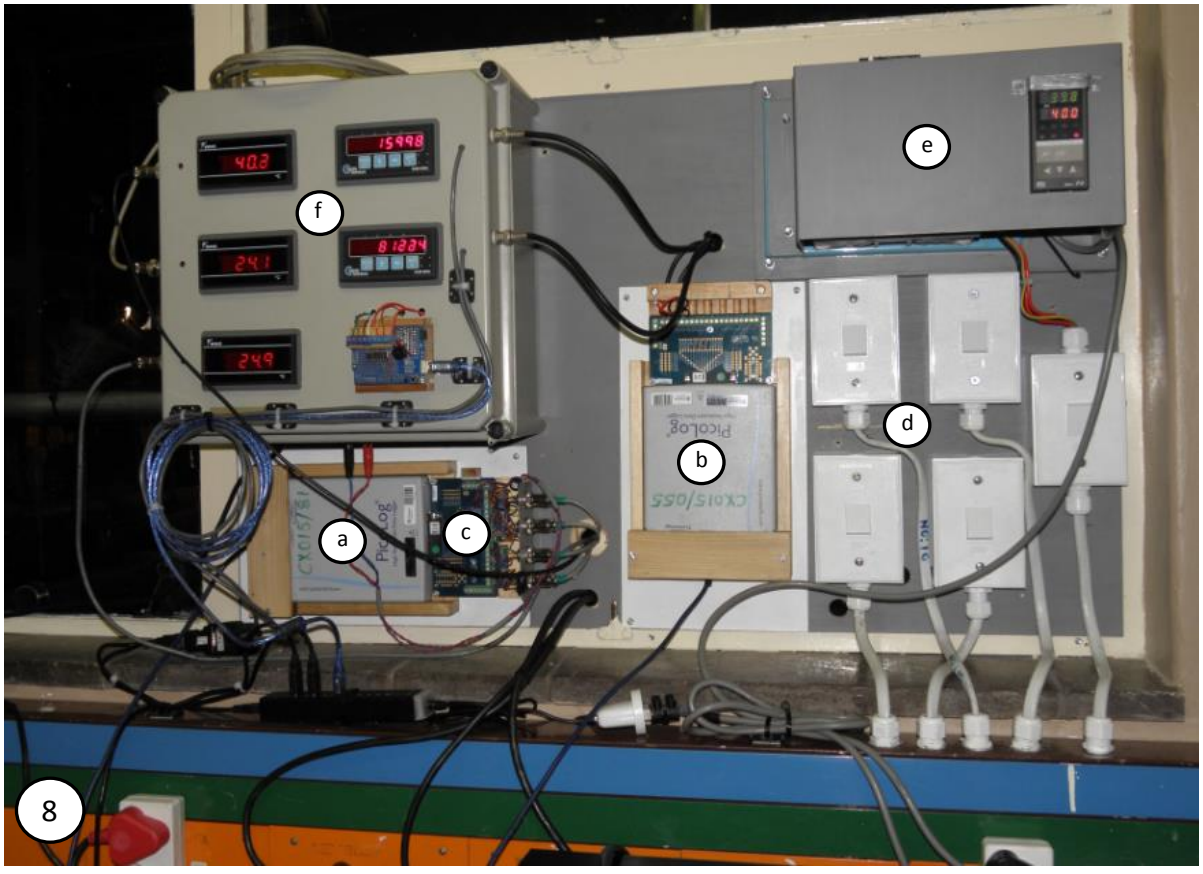
e
f
d
b
a
c
8

4.9 Calibration of instrumentation

The flow meters as well as the temperature measurement system were calibrated. The calibration data with the certification of calibration laboratories was used to determine the uncertainty of the instruments in accordance with the methodology described in section 3.8.

4.9.1 Flow meters

Flow calibration facilities are available in the Flow laboratory. These facilities are certified in accordance with SANAS to 0.5% flow accuracy. To ensure the best possible calibration is done both flow measurement devices were calibrated in-situ. Additional connections were installed to allow the flow to be routed to the calibration equipment. The calibration done was not used to determine the measurement uncertainty of the flow meters, but as a confirmation that both measured correctly. This could be done since data for each flow meter is available from the supplier. The specified systematic uncertainties for both flow meters were used as given in section 4.6.8.

Figure 4-19: Additional connections for in-situ flow calibration of the electromagnetic flow meter (left) and Coriolis flow meter (right)

4.9.2 Temperature measurement system

The temperature measurement system consists of a number of components. This includes the temperature probes, the connecting wires, the current source and the data logger that measures the voltage. Each of these components has an uncertainty associated with it. The uncertainty of the probes and data logger is available from supplier data sheets and international standards. The uncertainty of the connecting wires can be calculated. The current source was custom built. There is thus no uncertainty value available. The best possible calibration is achieved when the complete

temperature measurement system is calibrated. The complete system was removed and taken to a SANAS accredited calibration laboratory where each of the 4 temperature measurements was calibrated. The image below in Figure 4-20 shows the calibration set-up used.

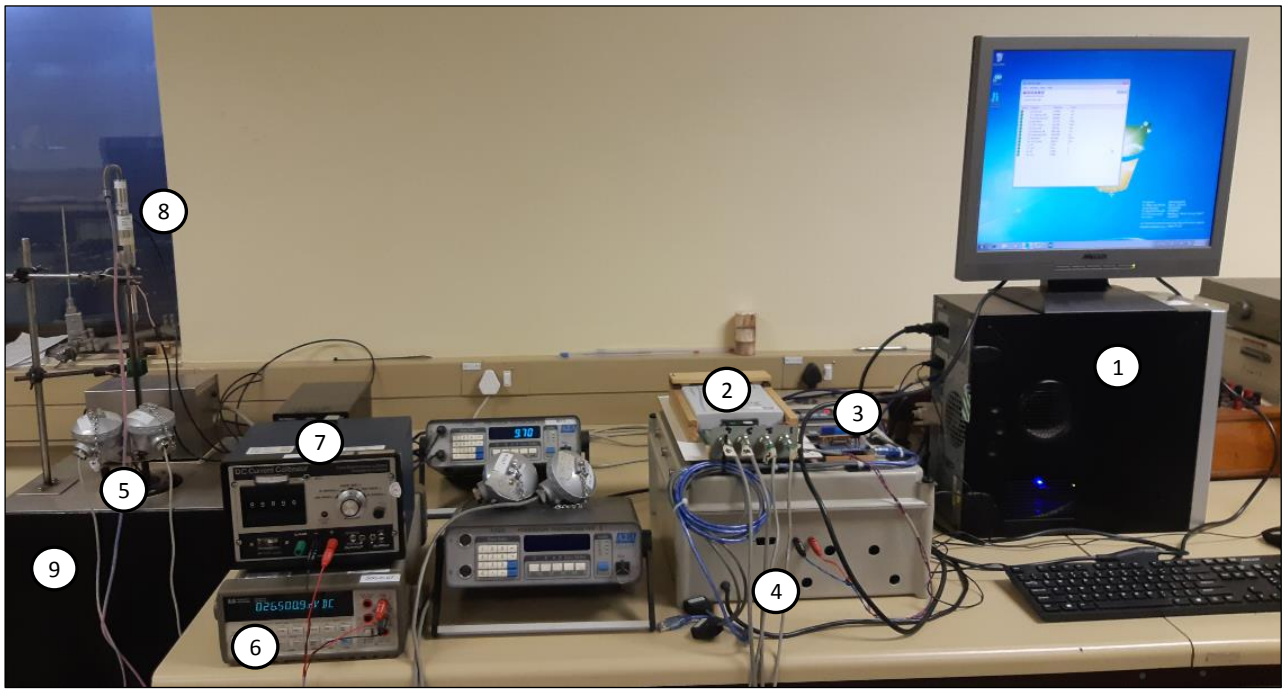

Equipment Being Calibrated			
1	Data Acquisition Computer	4	4 wire connections
2	Data logger / Voltage Measurement	5	RTD Probes currently being calibrated
3	Current Source		
Equipment used for calibration			
6	Voltage Measurement	8	Calibration probe
7	Current Source	9	Adjustable Temperature Bath

Figure 4-20: Temperature measurement system calibration

The calibration process determined the resistance in Ω of the RTD sensor for a given reference temperature. These values were used to generate a 3rd order polynomial fit. The difference between calculated temperature and the reference temperature is given as ΔT. The result of the calibration is given Table 4-21 below. An example of a calibration certificate is available in Appendix C.

It should be noted that the calibration certificates also contain curve fits. It was found that a better curve fit could be achieved by the author. These were used and are the reason for the difference between Table 4-21 and the actual calibration certificates.

Table 4-21: Temperature Calibration Data

Cold Loop In				Cold Loop Out			
Reference Temp [°C]	Resistance [Ω]	Calculated Temp [°C]	ΔT[1] [°C]	Reference Temp [°C]	Resistance [Ω]	Calculated Temp [°C]	ΔT[1] [°C]
0.022	100.040	0.0238	-0.0018	0.010	99.997	0.0094	0.0006
10.016	103.908	10.0098	0.0063	10.016	103.900	10.0176	-0.0016
19.990	107.786	19.9966	-0.0066	19.990	107.782	19.9881	0.0019
34.927	113.581	34.9243	0.0027	34.927	113.582	34.9276	-0.0006
55.900	121.670	55.9003	-0.0003	55.900	121.678	55.8998	0.0002
Hot Loop In				**Hot Loop Out**			
Reference Temp [°C]	Resistance [Ω]	Calculated Temp [°C]	ΔT[1] [°C]	Reference Temp [°C]	Resistance [Ω]	Calculated Temp [°C]	ΔT[1] [°C]
0.022	99.973	0.0180	0.0040	0.022	100.015	0.0186	0.0034
10.016	103.886	10.0262	-0.0102	10.016	103.927	10.0241	-0.0081
19.990	107.766	19.9844	0.0056	19.990	107.805	19.9869	0.0031
34.927	113.562	34.9236	0.0034	34.927	113.591	34.9225	0.0045
54.827	121.240	54.8313	-0.0043	54.827	121.263	54.8316	-0.0046
69.937	127.031	69.9354	0.0016	69.937	127.061	69.9354	0.0016

1: ΔT = Reference Temp – Calculated Temp

By using the curve fit temperature differentials (ΔT) given above, the certified calibration uncertainty of the calibration laboratory of ±0.1°C and methodology described in section 3.8 the systematic uncertainty of each of the 4 temperature measurement systems was determined. The values are given at 95% confidence level.

Table 4-22: Temperature measurement systematic uncertainty

No	Description	Systematic Uncertainty [°C]
I5	Cold loop inlet temperature	0.100185
I6	Cold loop outlet temperature	0.100014
I7	Hot loop inlet temperature	0.100204
I8	Hot loop outlet temperature	0.100145

Table 4-21 shows that good curve fits were achieved with low ΔT values. This indicates that the temperature measurements compared well with the calibration measurements. This can also be seen in Table 4-22 where the calculated systematic uncertainties are all close to 0.1°C. The certified uncertainty of the calibration laboratory is clearly the controlling factor in the uncertainty of the calibrated temperature measurements.

This leads to the conclusion that it might be worthwhile considering a re-calibration at a calibration laboratory with a better-certified uncertainty. Unfortunately are there very few laboratories in South Africa that are certified at values lower than 0.1°C and as can be expected, do this comes at a very high premium. It will not be done for this work but is definitely something that can be considered going forward.

4.10 Commissioning

Before the test rig can be used it must be commissioned. The commissioning process entails the testing and verification of all components to ensure it functions according to the design. The commission process took approximately 2 months which was significantly longer than expected. A number of issues were found that had to be corrected and in some cases repaired. A large amount of time was spent in the Excel computer interface to ensure the data is captured in an acceptable manner that can easily be used.

The following tests and optimisations were done during the commissioning process:

- Flushing of the hot and cold loop to ensure all debris is removed.
- Leak test on the complete system.
- Testing and running the circulation pump under hot and cold conditions.
- Testing and optimising the flow control valves on the hot loop and the cold loop.
- Testing the water heater with and without flow.
- Testing the custom compression couplings to ensure tight seals.
- Testing all instrumentation and ensuring the displayed values are from the correct instrument.
- Optimisation the Excel computer interface with the input for the different instrumentation.
- Optimising the test sequence and the way the test data is captured.
- Testing and optimising the thyristor controller that controls the output temperature from the water heater. For this, two temperature probe locations were investigated. The first location was in the heater and the second in the heater outlet after the pump. Results showed that better control i.e. a smaller temperature control range (defined as max measured temerature minus minimum measured temeprature) of 0.2°C are achieved with the temperature probe installed in the heater. This can be seen in Figure 4-21.

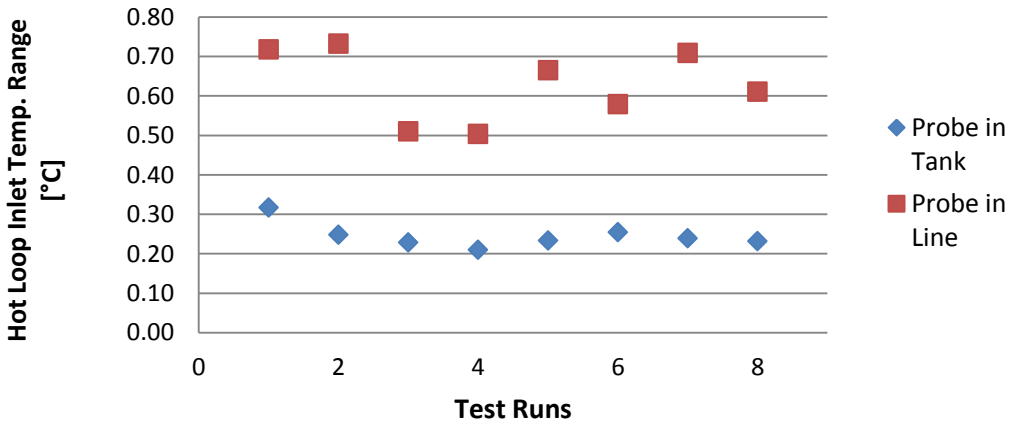

Figure 4-21: Graph of hot loop inlet temperature control range

4.11 Data Reduction

The parameters provided in Table 4-23 are measured and used in the calculation of the overall heat transfer coefficient and eventually the fouling factors for each test tube. Some of these are measured directly and others are converted from the base measurements with the Excel data acquisition program.

The hot loop volume flow is measured in m³/h and converted in Excel to kg/s based on average hot loop temperature and the density determined from the analytical formulations of IAPWS-IF97.

For the temperature measurements the resistance of the Pt 100 probe are measured. This is converted to temperature in °C using 3rd order polynomial equation with the constants obtained from calibration that was done as described in section 4.9.

Table 4-23: Measure and converted parameters

Description	Symbol	Actual Measured value	Converted and used measured value
Cold loop inlet temperature	$T_{CL,in}$	Resistance [Ω]	Temperature [°C]
Cold loop outlet temperature	$T_{CL,out}$	Resistance [Ω]	Temperature [°C]
Hot loop inlet temperature	$T_{HL,in}$	Resistance [Ω]	Temperature [°C]
Hot loop outlet temperature	$T_{HL,out}$	Resistance [Ω]	Temperature [°C]
Cold loop mass flow	$\dot{m}_{CL}$	Mass flow [kg/s]	Mass flow [kg/s]
Hot loop mass flow	$\dot{m}_{HL}$	Volume flow [m³/h]	Mass flow [kg/s]

To ensure lower random uncertainties and lessen the effect of outliers it was decided with the help of the Eskom RT&D Flow laboratory personal based on previous experience that each test should be done in the following way:

- Each individual test consists of the average of 50 measurements taken each 4 seconds for total test duration of 3 minutes and 20 seconds.
- Each combined test consists of the average value of 8 individual tests.
- The final result for each test thus consists of 8 x 50 = 400 measurements.

This can be seen visually in the Figure 4-22.

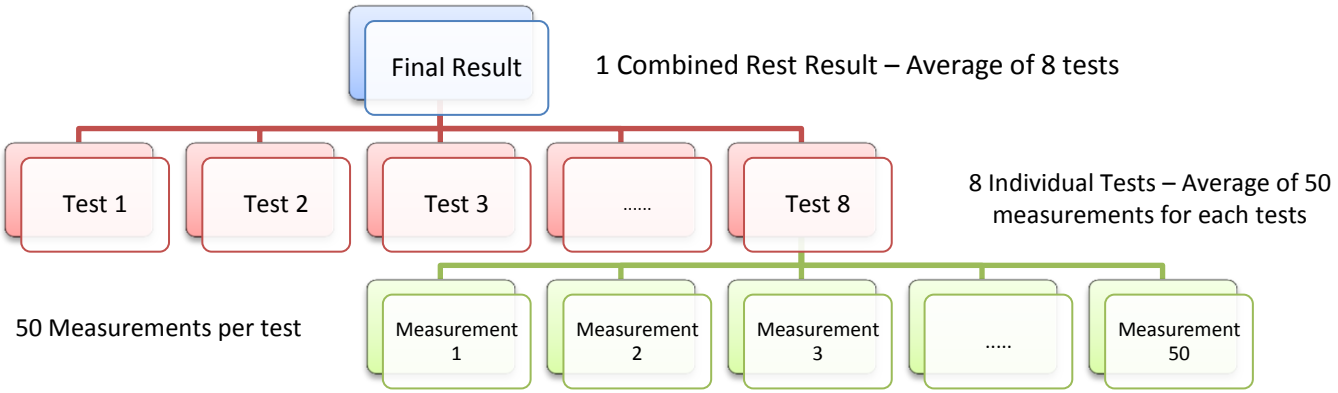

Figure 4-22: Composition of tests

Once the measurements has been taken and converted the following parameters are calculated for each test. Take note that the heat transfer values are just used as an indication of when testing can start as explained in section 5.1.

- Cold loop heat transfer (Q_{CL}) using equation (2-6)in [kW].
- Hot loop heat transfer (Q_{HL}) using equation (2-7) in [kW].
- Cold loop specific heat capacity $(C_{p.CL})$ using the analytical formulations of IAPWS-IF97 based on average cold loop temperature in [kJ/kg.K].
- Hot loop specific heat capacity $(C_{p.HL})$ using the analytical formulations of IAPWS-IF97 based on average hot loop temperature in [kJ/kg.K].
- Overall heat transfer coefficient based on outside diameter (U_o) using equation (4-2) in [W/m².K].

Once the three tests for each condition have been completed the following is available:

- Overall heat transfer coefficient based on the tube outside diameter $(U_{o,fouled})$ for the fouled condition.
- Overall heat transfer coefficient based on outside diameter $(U_{o,halfclean})$ for the half clean condition.
- Overall heat transfer coefficient based on outside diameter $(U_{o,clean})$ for the clean condition.

The overall heat transfer coefficient is then converted to the three fouling factors:

- The combined fouling factor (R_f) as shown in equation (4-1) measured in [m².K/W].
- The internal fouling factor (R_i) as shown in equation (4-3) measured in [m².K/W].
- The external fouling factor $(\mathrm{R_o})$ as shown in equation (4-4) measured in [m².K/W].

The complete process is shown in the flow chart in Figure 4-23.

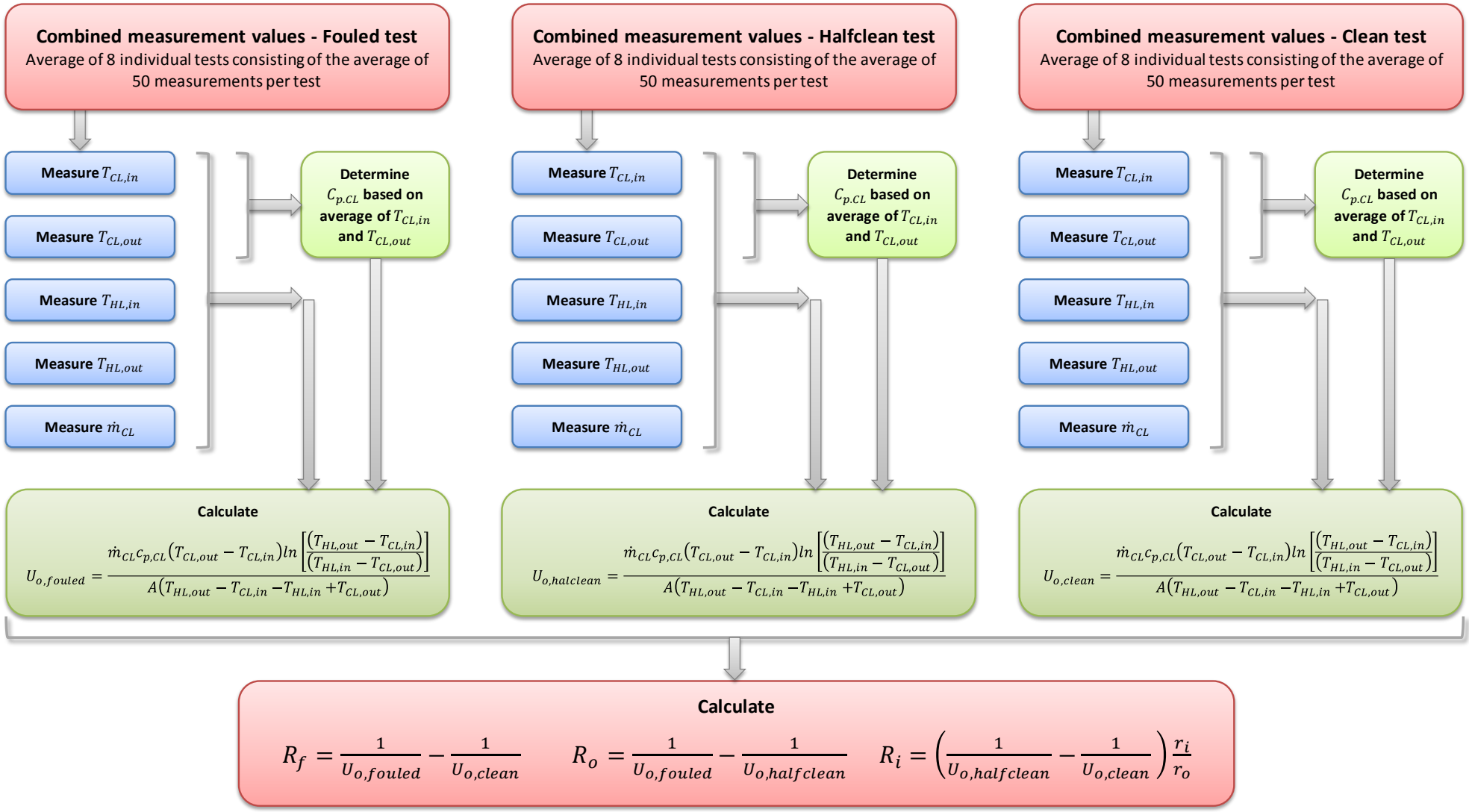

Figure 4-23: Data reduction flowchart

5. Experimental work

The following section provides details and results of the validation tests that were done, the actual test results of the sample tubes and examples of the uncertainty calculations.

5.1 Test rig validation

A number of validation tests were done on the test rig. The main reason for these tests is to show the results can be trusted and provide a high level of confidence in the results.

The validation tests were done with a test tube installed. The material of the test tube is ASTM SB 338 Grade 2 material. That is a titanium alloy used for heat exchanger tubes. Titanium was selected to ensure no corrosion takes place during commissioning and testing. The size of the test tube is 19 mm OD with a 1.2 mm wall thickness.

Each test consists of 50 instrument readings taken over a period of approximate 4 minutes. Typically, 8 tests are done at a time. The rig is run for a minimum of 15 minutes before testing starts. After this time the energy balance between the hot side and the cold side is evaluated. If the measured values are within 2% of each other, it is accepted that a steady state heat transfer rate have been reached and testing can start. Since the calculation of the two heat transfer rates for each side of the heat exchange include the inlet and outlet temperature as well as the mass flows is this considered a good representation of the overall steady state conditions.

5.1.1 Hot Loop and Cold Loop adiabatic tests

The first validation tests that were done were an adiabatic test on the cold as well as the hot loop. The purpose of these tests was as follows:

- To prove that the inlet and outlet temperature measurement on each loop measures within their uncertainty limits of the temperature measurement system i.e. cross-check between the different instruments.
- To determine the amount of losses to atmosphere. From previous calculations in section 4.5.4, this is expected to be negligible.

For each test, the flow in the loop not being tested was drained and isolated i.e. a mass flow rate of 0 kg/s.

The cold loop was tested at the water reservoir temperature. The results of the cold loop test are given in Figure 5-1 below. For all tests done on the cold loop, the inlet and outlet temperatures were within close tolerance. For the test results as shown below an average temperature

differential of 0.006°C was obtained when subtracting the inlet temperature from the outlet temperature. This is considered exceptionally good and well within the instrument measurement uncertainties.

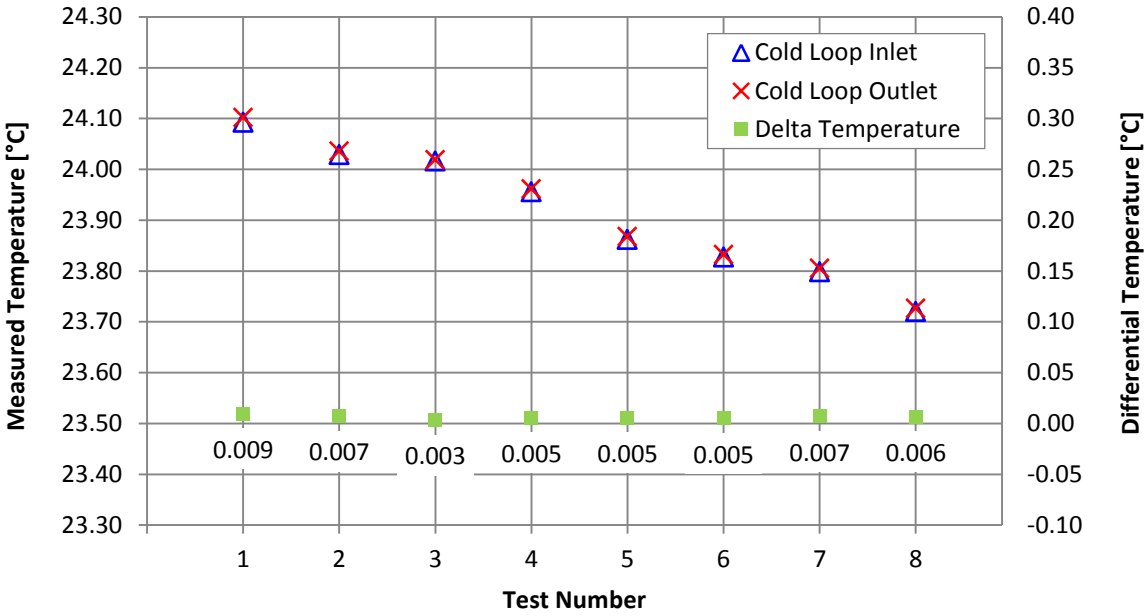

Figure 5-1: Cold Loop adiabatic validation test results

The hot loop was tested at both the reservoir temperature and the operating temperature. For the reservoir temperature of 21 – 25°C, good results, similar to those depicted for the cold loop in Figure 5-1, were obtained. The test done at a operating temperature of approximately 60°C indicated a systematic error between the inlet and outlet probe of 0.02 - 0.04°C. This error seems to change or drift between different test days or ambient conditions. In each of the cases, the outlet probe had the higher reading which rules out losses to atmosphere. These errors are within the limits of the instrument measurement systematic uncertainty given in section 4.9.2 above.

No funding was available for re-calibration of the hot loop temperature measurement system to attempt to reduce or eliminate this error. It is not expected that re-calibration will solve the problem due to the small error involved. In fact, the error is so small that it is well outside the capability of the installed temperature measurement system or most calibration laboratory capabilities. Since it is a systematic error, it is possible to compensate for it, but since it seems to change from day to day a new compensation test will have to be done on a daily or hourly basis. It was decided not to do that since additional sources of uncertainty can easily be introduced into the system.

The results of the hot loop, hot test are given in Figure 5-2 below.

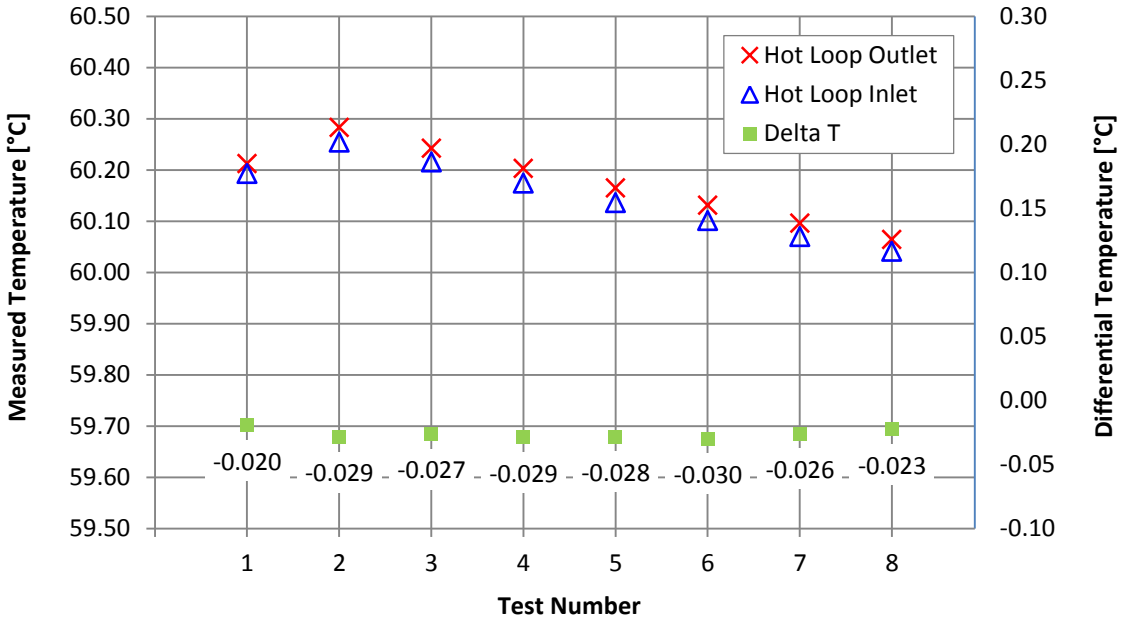

Figure 5-2: Hot Loop adiabatic validation test results

5.1.2 Energy balance comparison

The next validation test was an energy balance comparison. The heat gained by the cold loop and the heat lost by the hot loop should be equal if losses are negligible as was predicted in section 4.5.4 and confirmed above. The energy balance comparison test proves this by comparing the difference in heat transfer between the cold loop and the hot loop between different tests. The results are given as the percentage difference between the cold loop and the hot loop heat transfer. This is calculated as follows:

$$\%\, difference = \frac{Q_{CL}}{Q_{HL}} \text{ x } 100 \; - 100 \tag{5-1}$$

Numerous energy balance tests were done. It was found that the energy balance is relatively sensitive to the process conditions and sufficient time must be given to ensure a steady state is reached. The *% difference* between all tests done was between 0.7% and 3.5%. The results given in Table 5-1 below is for a combined test made up of 8 individual tests done at conditions that will typically be used during the fouling tests and indicates a *% difference* of approximately 2%. Uncertainties were calculated as described in 5.3.1.

Table 5-1: Energy Balance Test Results

Description	Test Run		1	2	3	4	5	6	7	8	Avg.
CL Heat Transfer	Q_{CL}	kW	13.97	13.94	13.88	13.98	13.98	13.97	13.99	13.99	13.96
CL Expanded Uncertainty	$U_{Q,CL}$	%	2.302	2.302	2.302	2.302	2.304	2.302	2.301	2.302	2.302
HL Heat Transfer	Q_{HL}	kW	13.69	13.65	13.59	13.68	13.70	13.71	13.73	13.72	13.68
HL Expanded Uncertainty	$U_{Q,HL}$	%	3.288	3.302	3.245	3.308	3.454	3.288	3.281	3.372	3.317
% difference - CL to HL	%Q	%	2.03	2.16	2.15	2.19	2.03	1.88	1.91	2.00	2.04

It can be seen that the cold loop heat transfer is constantly more than the hot loop heat transfer. The difference is relatively constant. This point to a systematic measurement error between the two loops. Visually this is clear in Figure 5-3. It is also clear that all errors bars overlap. This shows that all values are well within the uncertainty limits of each result and are acceptable.

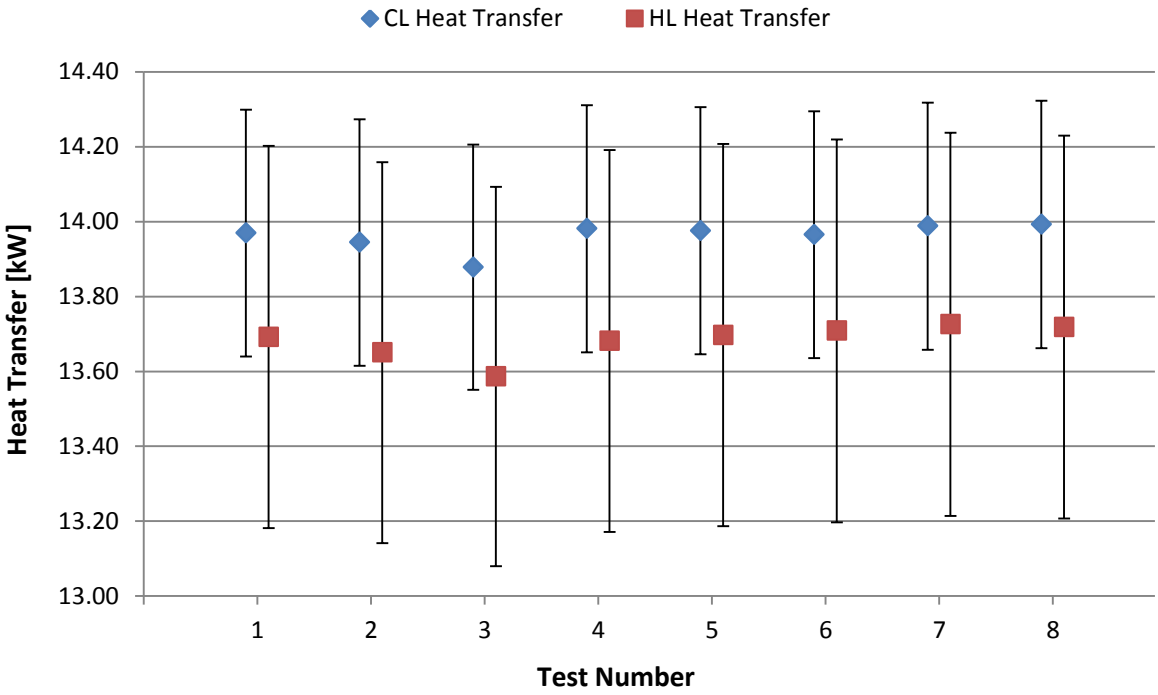

Figure 5-3: Heat Transfer Comparison of cold and hot loop

5.1.3 Measured and calculated heat transfer comparison

A comparison was done between the actual measured heat transfer and the calculated theoretical heat transfer. The uncertainty on both the measured results and the heat transfer correlations used were taken into account.

The correlations used were as per section 2.4.5 and 2.4.6. The uncertainty associated with the Gnielinski heat transfer correlation for forced convection inside tubes is given as ±20% (see equation (2-34)). The uncertainty for forced convection in an annulus, also by Gnielinski, is not that clearly defined in the original paper [22]. It does, however, mention comparison with most results is within 5%. For the purposes of this work 5% will be used, although it seems relatively low.

The theoretical heat transfer was calculated for 3 cases. These are:

- Per standard correlations.
- Nusselt number+20% for heat transfer inside the tube and Nusselt number +5% for heat transfer outside the tube in the annulus.

- Nusselt number -20% for heat transfer inside the tube and Nusselt number -5% for heat transfer outside the tube in the annulus.

The verification consisted of 8 individual tests done at the same flow and inlet temperature conditions. These are conditions that will typically be used during the actual tests. As expected, the results of the 8 tests are very similar. The measured values compare well with the calculated values with significant overlap in the uncertainty ranges. This is better than expected. As mentioned and can be seen from the test section arrangement, are the flow patterns in the annulus section not expected to be fully annular and developed. The Gnielinski correlation (2-40) used does make provision for this and takes it into account. According to the measurements it does so very successfully for this specific case.

The calculated values are determined in a similar way as the example calculations in Appendix A.

Table 5-2: Results of measured and theoretical heat transfer

Calculated Values	Test Run		1	2	3	4	5	6	7	8	Avg.
CL Heat Transfer	Q_{CL}	kW	13.69	13.65	13.59	13.68	13.70	13.71	13.73	13.72	13.68
CL Expanded Uncertainty	$U_{Q,CL}$	%	2.302	2.302	2.302	2.302	2.304	2.302	2.301	2.302	2.302
Calculated Heat Transfer	Q_{Calc}	kW	13.77	13.75	13.69	13.78	13.78	13.77	13.79	13.79	13.77
Max Calculated	Q_{Max}	kW	14.80	14.77	14.71	14.80	14.81	14.80	14.82	14.82	14.79
Min Calculated	Q_{Min}	kW	12.55	12.53	12.48	12.55	12.56	12.55	12.56	12.57	12.54

The following graph shows the results visually with the uncertainties included as error bars:

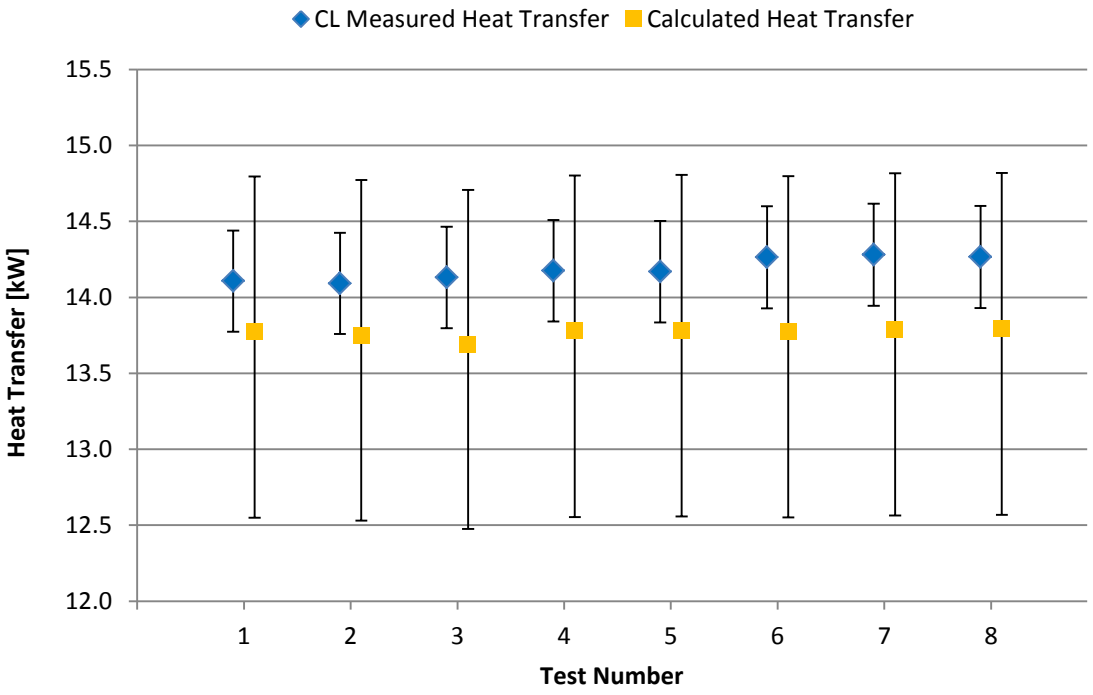

Figure 5-4: Measured and calculated heat transfer comparison

5.1.4 Repeatability tests

The repeatability associated with the test rig is considered one of the most important of the validation tests. The reason for this is that multiple tests will be done on every test tube in different fouling states to determine the final result. For the theory on the calculation of the fouling factor to apply, the inlet conditions i.e. temperature and mass flow must be the same for each test. Details of this and the testing process are given in section 4.1.

To test and document the repeatability of the test rig the following process was followed:

1. The titanuim commissioning tube was installed.
2. Inlet temperature, hot loop flow and cold loop flow was set. The control valve on both the hot loop and cold loop were opened fully. This provides highly repeatable mass flows. The hot loop inlet temperature was set at 60°C. This and the other test parameters are given in Appendix D.
3. The rig was run for approximately 15 minutes at the set conditions to ensure that all metal components were at temperature and that steady state conditions had been reached.
4. The overall heat transfer coefficient of the tube was tested. 8 individual tests were done and the average of the results, referred to as the combined test results, was determined.
5. The tube was removed from the test rig, dried, wiped with a cloth and reinstalled.
6. The process was repeated 5 times.

Initially, the repeatability between the 5 tests, taken as a deviation of the overall heat transfer coefficient from the mean, was between 4% and 6%. This was not considered sufficient and worse than the anticipated capability of the test rig. The process was repeated a couple of times with similar results. An investigation was done to determine how the repeatability could be improved.

The most significant change between tests is the connection of the custom compression couplings to the tubes. Modifications were done to the custom compression couplings to improve the repeatability. These included the improved alignment and centering of the tube by using additional custom manufactured spacers. The rubber seals used where changed to a thicker material. Different manufacturing techniques were used to ensure the manufacturing tolerances on the washers are smaller for better alignment. It was also found that not all the tubes are straight. Measures were put in place to ensure the tube is installed in the exact same position and orientation for each test.

After these were completed the repeatability tests were repeated. Three tests were done in the afternoon on the 21st of November 2018. The remaining two tests were done 8 days later in the morning of the 29th of November 2018. The results were satisfactory with repeatability values

below 1%. This is acceptable and considered very good. It is also well within the calculated uncertainty value associated with the overall heat transfer coefficient.

The results are summarised in Figure 5-5. The overall heat transfer coefficient for each test with the calculated uncertainty value, the mean of these tests and the value of the percentage deviation of each test from the mean are shown.

The combined test results of the repeatability tests can be seen in Appendix D. A calculation example of the uncertainty is given in section 5.3.2.

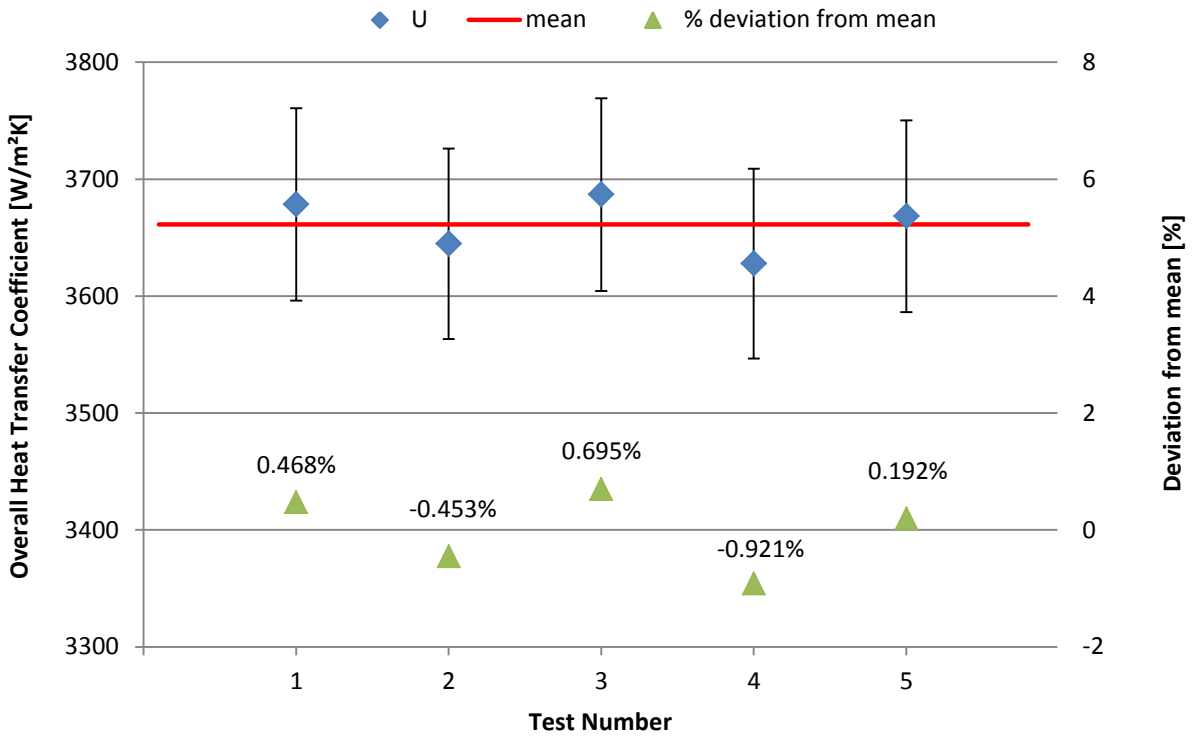

Figure 5-5: Repeatability Test Results Summary

5.2 Test results

Actual feedwater heater tubes were tested. These were obtained from the condensing zone in a Low-Pressure Feedwater Heater that was replaced at one of Eskom's Power Stations. This heater was manufactured in 1981 and was in service in excess of 30 years. The tube samples have a 16 mm OD and 14 mm ID. The tubes were manufactured from SA-249 TP 304L seam welded stainless steel material. Figure 5-6 below shows the removal process in progress.

Figure 5-6: LP Heater Tube Sample Removal

A number of tube samples were removed. 5 viable samples were selected for testing. Only two tubes were tested per a day. This is due to the fact that the testing and cleaning process is repeated 3 times for each tube and is very time-consuming. Table 5-3 below shows the test dates:

Table 5-3: Test Dates and Times

Tube Sample	Test Date	Test Time
LP Heater Tube Sample 1	11 Feb 2019	12:48 - 14:41
LP Heater Tube Sample 2	18 Feb 2019	10:18 – 12:41
LP Heater Tube Sample 3	18 Feb 2019	12:58 – 14:38
LP Heater Tube Sample 4	20 Feb 2019	10:05 – 12:30
LP Heater Tube Sample 5	20 Feb 2019	12:58 – 14:42

Mechanical cleaning by means of a grinder-fitted wire brush was used on the outside of the tubes. Since the outside of the tube is visible it can easily be confirmed that the tube is clean. Internal spiral wound tube cleaning wire brushes, manufactured by Werner Brushes, fitted on a custom made extension rod, were used for the internal cleaning. It is difficult to determine if the internal of the tube actually clean. A few experiments were done on tubes that were not used for testing. These were cleaned and cut open to confirm cleanliness. These showed that if approximately 5 minutes of cleaning is done on each part of the internal surface area, the tubes were sufficiently cleaned. When the actual tubes were cleaned the cleaning time was doubled. This was to ensure the tubes are sufficiently clean if harder fouling substances are present. It is however possible that this can lead to tube material removal. Wall thinning reduction tests was also done and showed

that on the stainless steel tubes the wall loss due to wire brush cleaning this is very small even if it is done for extended periods. The change in tube wall thickness could not be measure with a standard calibrated veneer which confirms that it is neglectable small. Even if a small amount of tube material is removed is it not expected to make a significant difference on the test results. The conduction through the tube wall present very little resistance to heat transfer. Even for a clean tube are the overall heat transfer coefficient is dominated by the internal and external heat transfer coefficients.

Figure 5-7 below shows the following:

a. Grinder fitted wire brush for external cleaning
b. Tube clamped for cleaning and internal tube cleaning extension with spiral wire brush fitted and connected to handheld drill. Allen keys can be seen that were used on the grub screws that hold the brush securely in place.
c. Tube before and after cleaning as well as a spiral wound wire brush. The rubbing on the right of the clean tubes is caused by aluminum end of the brush.

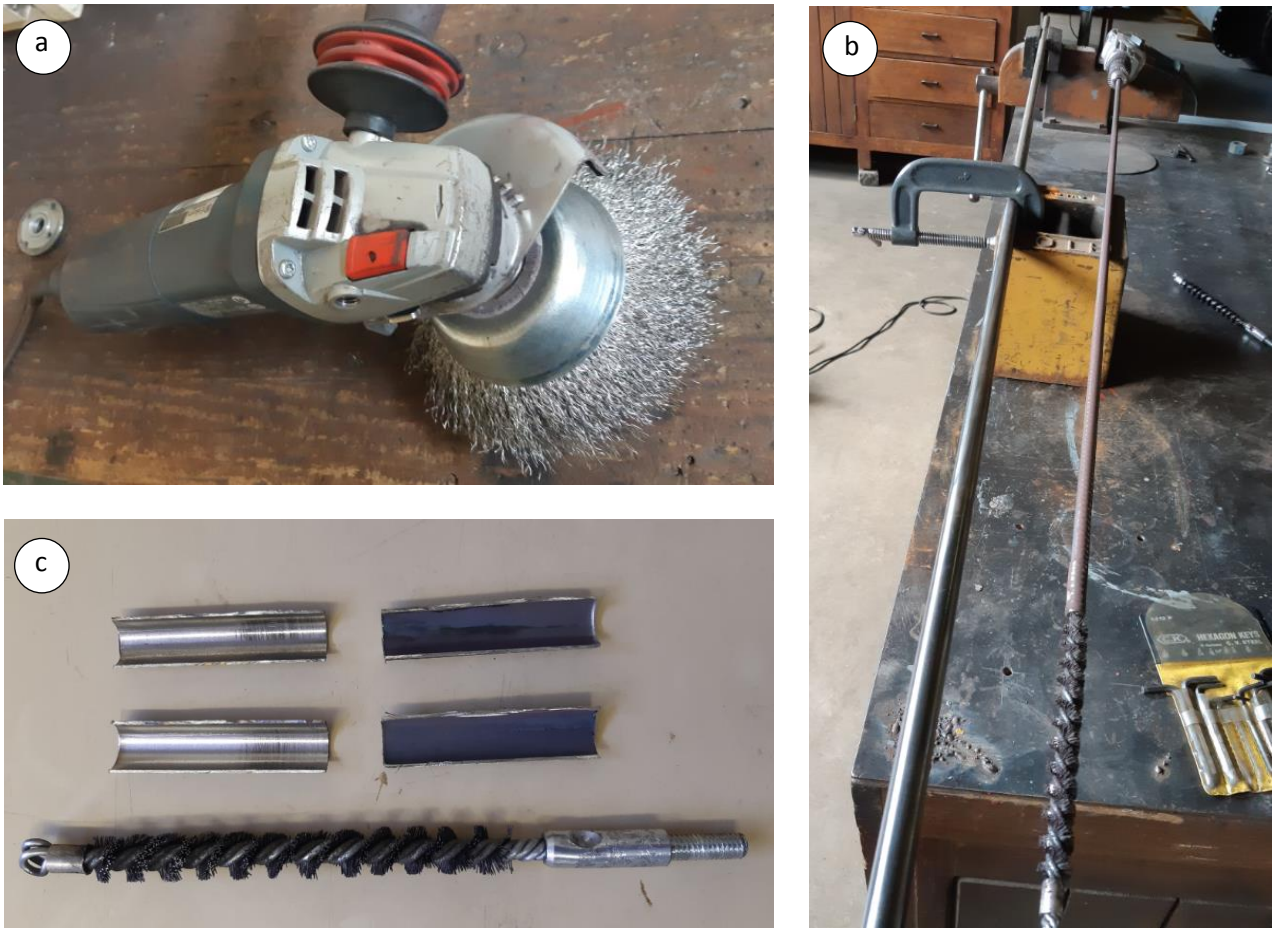

Figure 5-7: Internal and External Tube Cleaning

The test parameters during each test were carefully controlled to ensure that for each of the 3 tests, the same mass flow rates and inlet temperatures were achieved.

In the repeatability tests the flow rates were kept constant by opening both the cold loop and the hot loop control valves fully. This was very successful in providing very repeatable flow rates. For the actual tests the same approach was followed. With the test tubes installed and the head from the water tower, approximately 0.54 kg/s flow is achieved in the cold loop. The pump installed in the hot loop as three speed settings designated as low, medium and high. The speed on the pump is adjusted to change the flow in the hot loop and not the control valve to ensure higher repeatability. It was decided that testing will be done at the high speed setting. For the test tube, this resulted in approximately 0.74 kg/s.

The cold loop inlet temperature should also be the same as for previous tests, but it is not controlled and is dependent on ambient temperature. Throughout the day this temperature remains rather constant due to the large storage tank, if all tests are done within 1 day only small variations will be seen. At the low operating temperatures and the small changes, it is not expected to have a significant effect. For the tests it varied but was typically between 20°C and 23°C. It was however relatively constant between the 3 different test for each tube. The hot loop temperature set point was 60°C. This was achieved within 0.3°C of the set point for all tests.

The average parameters between the 8 individual tests done for each of the tests were:

Table 5-4: Inlet and Outlet Test Parameters

Sample Number	Symbol	Unit	Fouled	Half Clean	Clean
Tube Sample 1					
Cold Loop Mass Flow	m_{CL}	kg/s	0.54	0.54	0.54
Hot Loop Mass Flow	m_{HL}	kg/s	0.74	0.74	0.74
Cold Loop Inlet Temperature	T_{CLI}	°C	22.75	22.69	22.66
Cold Loop Outlet Temperature	T_{CLO}	°C	27.75	27.99	28.13
Hot Loop Inlet Temperature	T_{HLI}	°C	59.99	60.151	60.23
Hot Loop Outlet Temperature	T_{HLO}	°C	56.30	56.32	56.27
Cold Loop Heat Transfer	Q_{CL}	kW	11.49	12.04	12.42
Hot Loop Heat Transfer	Q_{HL}	kW	11.50	11.88	12.31
Tube Sample 2					
Cold Loop Mass Flow	m_{CL}	kg/s	0.54	0.54	0.54
Hot Loop Mass Flow	m_{HL}	kg/s	0.73	0.74	0.74
Cold Loop Inlet Temperature	T_{CLI}	°C	21.12	20.83	20.72
Cold Loop Outlet Temperature	T_{CLO}	°C	26.30	26.34	26.28
Hot Loop Inlet Temperature	T_{HLI}	°C	60.05	60.48	60.28
Hot Loop Outlet Temperature	T_{HLO}	°C	56.18	56.42	56.25

Cold Loop Heat Transfer	Q_{CL}	kW	11.78	12.63	12.64
Hot Loop Heat Transfer	Q_{HL}	kW	11.75	12.55	12.54
Tube Sample 3					
Cold Loop Mass Flow	m_{CL}	kg/s	0.54	0.54	0.55
Hot Loop Mass Flow	m_{HL}	kg/s	0.74	0.74	0.73
Cold Loop Inlet Temperature	T_{CLI}	°C	22.95	23.37	23.31
Cold Loop Outlet Temperature	T_{CLO}	°C	28.05	28.58	28.59
Hot Loop Inlet Temperature	T_{HLI}	°C	59.84	60.06	59.95
Hot Loop Outlet Temperature	T_{HLO}	°C	56.137	56.25	56.06
Cold Loop Heat Transfer	Q_{CL}	kW	11.60	11.86	12.06
Hot Loop Heat Transfer	Q_{HL}	kW	11.44	11.79	11.87
Tube Sample 4					
Cold Loop Mass Flow	m_{CL}	kg/s	0.54	0.54	0.54
Hot Loop Mass Flow	m_{HL}	kg/s	0.73	0.74	0.75
Cold Loop Inlet Temperature	T_{CLI}	°C	21.80	23.63	23.81
Cold Loop Outlet Temperature	T_{CLO}	°C	26.90	28.62	28.84
Hot Loop Inlet Temperature	T_{HLI}	°C	60.11	60.26	60.16
Hot Loop Outlet Temperature	T_{HLO}	°C	56.37	56.65	56.57
Cold Loop Heat Transfer	Q_{CL}	kW	11.56	11.38	11.43
Hot Loop Heat Transfer	Q_{HL}	kW	11.45	11.22	11.25
Tube Sample 5					
Cold Loop Mass Flow	m_{CL}	kg/s	0.54	0.55	0.54
Hot Loop Mass Flow	m_{HL}	kg/s	0.74	0.74	0.74
Cold Loop Inlet Temperature	T_{CLI}	°C	23.79	23.67	23.75
Cold Loop Outlet Temperature	T_{CLO}	°C	25.89	28.89	28.92
Hot Loop Inlet Temperature	T_{HLI}	°C	59.70	60.06	59.81
Hot Loop Outlet Temperature	T_{HLO}	°C	56.03	56.253	56.07
Cold Loop Heat Transfer	Q_{CL}	kW	11.56	11.95	11.74
Hot Loop Heat Transfer	Q_{HL}	kW	11.31	11.74	11.52

From the measured values the overall heat transfer coefficient for each test was calculated using equation (4-2). The results are given below.

Table 5-5: Test Results in terms of overall heat transfer coefficient

Tube Sample	Overall Heat Transfer Coefficient [W/m².K]		
	Fouled	Half Clean	Clean
Tube Sample 1	3471.21	3639.87	3760.96
Tube Sample 2	3407.53	3606.54	3616.26
Tube Sample 3	3551.18	3666.68	3742.82
Tube Sample 4	3392.10	3500.74	3548.26
Tube Sample 5	3648.69	3728.68	3694.30

The overall heat transfer coefficient is then converted to fouling factors as described in section 4.1. The uncertainties for each test at 95% confidence level is calculated and provided next to the result. A full example of the uncertainty calculation can be seen in section 5.3.3 and Appendix E.

Table 5-6: Fouling factor test results and calculated uncertainties

Tube Sample	Fouling Factors [m².K/W]								
	Rf Overall	Absolute uncertainty	Relative uncertainty	Ro External	Absolute uncertainty	Relative uncertainty	Ri Internal	Absolute uncertainty	Relative uncertainty
Sample 1	2.21E-05	±1.21E-06	±5.48%	1.33E-05	±7.73E-07	±5.69%	7.73E-06	±4.36E-07	±5.82%
Sample 2	1.69E-05	±1.02E-06	±6.00%	1.61E-05	±1.00E-06	±6.26%	6.51E-07	±1.98E-07	±24.4%
Sample 3	1.44E-05	±8.98E-07	±6.22%	8.87E-06	±7.27E-07	±8.346%	4.85E-06	±2.94E-07	±5.84%
Sample 4	1.29E-05	±4.43E-07	±3.37%	9.14E-06	±3.71E-07	±4.14%	3.34E-06	±3.23E-07	±8.76%
Sample 5	3.38E-06	±3.22E-07	±8.91%	5.87E-06	±4.32E-07	±7.069%	-2.19E-06	±2.411E-07	±11.04%

Visually Table 5-6 can be expressed as Figure 5-8 with the error bars indicating the uncertainty values. It can be seen that in some cases the error values are so small; the error bars indicated are behind the graph symbol.

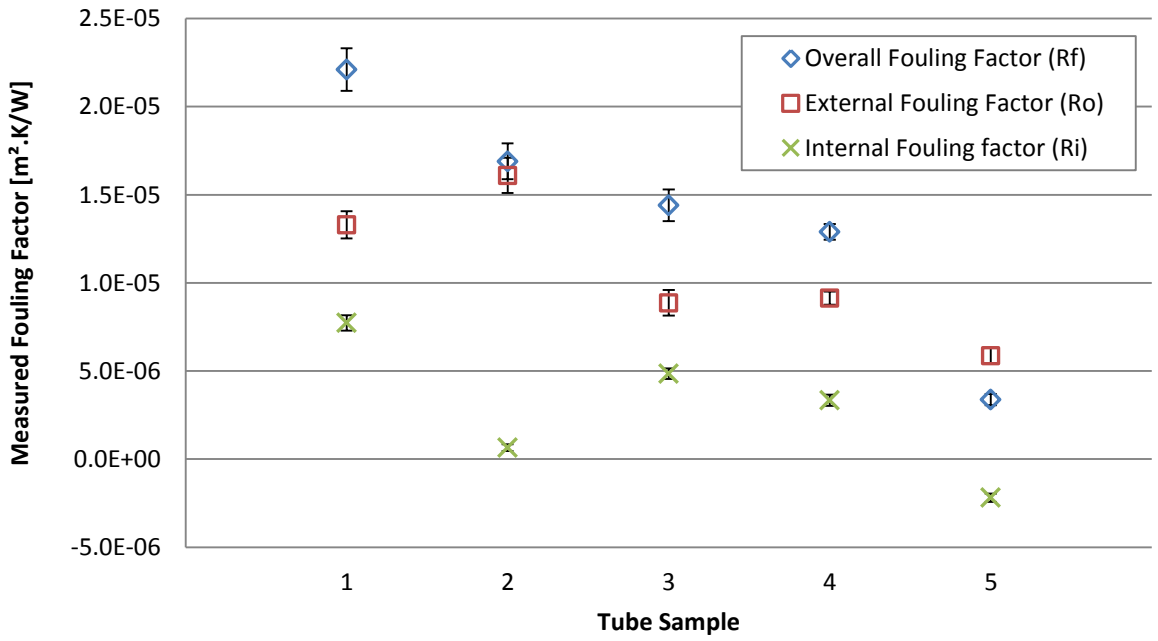

Figure 5-8: Test Results

From Table 5-6 and Figure 5-8 both the absolute and relative uncertainties can be seen. All absolute uncertainties are well within in the specified limits given in Table 4-2. Some of the relative uncertainties do seem high with the highest recorded value as 24.4%. In these cases the measured fouling factors are very low. When the result is a small value, the error becomes a higher percentage of the result.

For tube sample 5 a negative internal fouling factor was measured. This is a well-known phenomenon in literature as discussed in section 2.4.4. It indicates a very thin fouling layer. In these cases, the higher roughness of the fouling layer improves the heat transfer more than the poor conductivity of the fouling layer reduces the heat transfer.

The fouling factors are very small numbers and it is difficult to evaluate in the form given above. To allow better comprehension and analysis of the results it is given as a percentage of the HEI [6] fouling factors in Table 5-7. A similar value than the HEI fouling factor will show as 100%. It can be clearly seen that all measured fouling factors for this specific feedwater heater is significantly lower than the HEI values with the overall fouling factor being only 15% of the HEI value.

The external HEI fouling factors only applies to the de-superheating and subcooling zone, not the condensing zone. According to HEI no fouling allowance is added on the outside of the tubes in the condensing zone. All tested tubes were from the condensing zone. Clear fouling was noted on the external of the tubes which raises a question w.r.t. the HEI approach. This is discussed in section 6.3. The external fouling was also compared to the HEI external fouling factors.

Table 5-7: Test results as a percentage of HEI fouling factors

Tube Sample	Percentage of HEI [6] Fouling factors [%]		
	Rf – Overall	Ro - External	Ri - Internal
Tube Sample 1	23.84	25.27	21.97
Tube Sample 2	18.20	30.65	1.85
Tube Sample 3	15.49	16.79	13.78
Tube Sample 4	13.94	17.32	9.50
Tube Sample 5	3.63	11.13	-6.20
Average	15.02	20.23	8.18

5.3 Uncertainty Results

An uncertainty calculation is done for each validation and fouling test. For most of these, only the uncertainty in relative terms (%) of the result is provided in tabular form as in Table 5-1, Table 5-2, and Table 5-6. The purpose of this section is to provide more in-depth results and details on how these uncertainty values were determined. One of each of the following is provided:

- Heat transfer uncertainty.
- Overall heat transfer coefficient uncertainty.
- Fouling factor uncertainty.

The fouling factor uncertainty calculation is the most complex and the longest due to the amount of variables involved. For this reason a full example calculation is provided in Appendix F. The other are similar, but with fewer variables.

For each of the measured variables, the random uncertainty was calculated as per the methodology provided in section 3.7.3. The systematic uncertainty was used as determined in section 4.9. The uncertainty calculation methodology as described in the flowchart in section 3.7.9 is used for all uncertainty calculations.

The specific heat value (C_p) is commonly used in the calculations. It is however not a measured value but obtained from the steam tables. The uncertainty with this value needs to be included as well. Kim et al [92] stated that the effect of the random uncertainty of typical tabulated values from the steam tables would be neglectable compared to the other random uncertainties. It does, however, have a systematic uncertainty of 0.25-0.5% [92]. The published data of the International Association for the Properties of Water and Steam (IAPWS) [121] indicates a value of 0.3% uncertainty on C_p in the liquid range when their formulations (IF97) are used. For the purposes of this work, 0.5% is used as per first reference.

When all of the different uncertainty calculations given in the following sections are considered, it can be seen that the systematic uncertainty is similar for all temperature measurements. Since it is the same make and model instruments, this is expected. All of them are also at 0.05°C, which is the uncertainty of the calibration standard at 68% confidence level. This is an indication that when the calibration was done, the instruments were a very well matched to the calibration instruments resulting in the uncertainty value of the instruments being almost exactly the same as that of the calibration instruments or calibration standard as discussed in section 4.9.2.

As mentioned, each measurement consists of the combined test of 8 individual tests made up of 50 measurements. If the uncertainty for individual tests is calculated, the 50 measurements of each test are used to determine the standard deviation. For uncertainty calculation of the combined test, the average measured value and standard deviation for the 8 tests are used.

5.3.1 Heat transfer uncertainty

The heat transfer calculation is done in accordance with equation (2-6). Since there are only 3 measured variables and one property from the steam tables in each of the hot and cold loop heat transfer, the uncertainty calculation is relatively simple. The uncertainty analysis given is for test 1 of 8 for the validation test used in section 5.1.2 and 5.1.3. The results for the heat transfer in the cold and the hot loop are given in Table 5-8 and Table 5-9 below.

From the sensitivity factors, it can be seen that the mass flow rate has the biggest influence on the uncertainty of the result. The cold loop uses the highly accurate Coriolis meter and the hot loop the less accurate electromagnetic flow meter. It is for this reason that the uncertainty of the hot loop results is higher than those of the cold loop.

Table 5-8: Cold Loop Heat Transfer Uncertainty Calculation results

Description Cold Loop:	Symbol	Unit	Average Value	Standard Deviation	Random Uncertainty	Systematic Uncertainty	Combined Uncertainty	Expanded Uncertainty[1] (absolute)	Sensitivity Factor[2]
Inlet temp	T_{CLi}	°C	22.860	0.0120	0.00170	0.05	0.05012	0.10024	2.21E+03
Outlet temp	T_{CLo}	°C	29.187	0.0186	0.00269	0.05	0.05008	0.10016	2.21E+03
Flow	m_{CL}	kg/s	0.528	0.0010	0.00014	0.00039	0.00041	0.00083	2.64E+04
Specific heat	Cp_{CL}	kJ/kg.K	4.181	-	-	0.00221	0.00221	0.00441	3.34E+00

Description	Symbol	Unit	Average Value	-	Random Uncertainty	Systematic Uncertainty	Combined Uncertainty	Expanded Uncertainty[1] (absolute)	Expanded Uncertainty[1] (relative %)
Heat Transfer	Q_{CL}	kW	13.968	-	0.00795	0.160448	0.16064	0.32129	2.300

Note 1: Expanded Uncertainty given at 95% confidence level
Note 2: Units do not apply to sensitivity factors

Table 5-9: Hot Loop Heat Transfer Uncertainty Calculation results

Description Hot Loop	Symbol	Unit	Average Value	Standard Deviation	Random Uncertainty	Systematic Uncertainty	Combined Uncertainty	Expanded Uncertainty[1] (absolute)	Sensitivity Factor[2]
Inlet temp.	T_{HLi}	°C	60.019	0.1031	0.01500	0.05	0.05230	0.10460	3.01E+03
Outlet temp.	T_{HLo}	°C	55.462	0.0727	0.01000	0.05	0.05106	0.10212	-3.01E+03
Flow	m_{HL}	kg/s	0.718	0.0040	0.00057	0.00180	0.00189	0.00377	1.91E+04
Specific heat	Cp_{HL}	kJ/kg.K	4.182	-	-	0.00221	0.00221	0.00442	3.28E+00

Description	Symbol	Unit	Average Value	-	Random Uncertainty	Systematic Uncertainty	Combined Uncertainty	Expanded Uncertainty[1] (absolute)	Expanded Uncertainty[1] (relative %)
Heat Transfer	Q_{HL}	kW	13.683	-	0.05468	0.218116	0.22487	0.44973	3.287

Note 1: Expanded Uncertainty given at 95% confidence level
Note 2: Units do not apply to sensitivity factors

5.3.2 Overall heat transfer coefficient uncertainty

The overall heat transfer coefficient is calculated according to equation (4-2). This equation consists of 5 measured variables and one variable from the steam tables. The uncertainty analysis given is for the combined repeatability test 1 as described in section 5.1.4. The results are given in Table 5-10 below.

The results and the sensitivity factors show that the mass flow rate has the biggest influence on the result. It is for this reason that the cold loop flow and thus the cold loop heat transfer is used to determine the uncertainty due to the lower uncertainty of the Coriolis flow meter used in the

cold loop. It can also be noted that the cold loop temperature measurements have a larger influence due to higher sensitivity factors on the result than the hot loop temperature measurement. The reason for this is that the cold loop temperature measurement is effectively used twice in the calculation. This is to determine the amount of heat transfer and to determine the LMTD value. The hot loop temperature measurements are only used to determine the LMTD.

Table 5-10: Overall Heat Transfer Coefficient Uncertainty Calculation results

Description	Symbol	Unit	Average Value	Standard Deviation	Random Uncertainty	Systematic Uncertainty	Combined Uncertainty	Expanded Uncertainty[1] (absolute)	Sensitivity Factor[2]
CL Inlet temp.	T_{CLi}	°C	21.770	0.0101	0.00143	0.05	0.00521	0.01042	-5.11E+02
CL Outlet temp.	T_{CLo}	°C	28.255	0.0283	0.00400	0.05	0.05017	0.10033	6.24E+02
CL Flow	m_{cl}	kg/s	0.527	0.0009	0.00013	0.00179	0.00179	0.00359	6.97E+03
CL Specific heat	Cp_{CL}	kJ/kg.K	4.182	-	-	0.01046	0.01046	0.02091	8.79E-01
HL Inlet temp.	T_{HLi}	°C	59.961	0.1520	0.02100	0.05	0.05433	0.10865	-5.74E+01
HL Outlet temp.	T_{HLo}	°C	55.233	0.1167	0.01700	0.05	0.05288	0.10576	-5.54E+01

Description	Symbol	Unit	Average Value	-	Random Uncertainty	Systematic Uncertainty	Combined Uncertainty	Expanded Uncertainty[1] (absolute)	Expanded Uncertainty[1] (relative %)
Overall Heat Transfer Coef.	U_{out}	$W/m^2.K$	3674.81	-	3.150	41.685	41.804	83.608	2.275

Note 1: Expanded Uncertainty given at 95% confidence level

Note 2: Units do not apply to sensitivity factors

5.3.3 Fouling factor uncertainty

The results given below are for the uncertainty calculation of the overall fouling factor R_f of tube sample 1 as given in section Table 5-6.

The fouling factor R_f is calculated from equation (4-1). It consists of 10 measured variables and 2 calculated variables in the form of c_p from the steam tables. Each of these has a random and systematic uncertainty value associated with it with the exception of c_p that only includes a systematic error.

The same measurements are used twice in the calculation of the fouling factor. This happens when the inverse of the clean overall heat transfer coefficient are subtracted from the inverse of the fouled overall heat transfer coefficient. In this case the systematic uncertainty of the measurements is correlated due to the fact that the same instrumentation is used to measure it. The systematic uncertainty of these measurements is thus exactly the same. Due to the subtraction that takes place and the correlation between them, the systematic uncertainty associated with the temperature measurement cancels out to a large extent. This has a significant

reduction on the uncertainty of the result. Another example of this correlated uncertainties applied to a simple energy calculation in the form of $Q = \dot{m}c_p(T_2 - T_1)$ can be seen in [92].

Similar conclusions with regards to the sensitivity factors and the different flow meters used can be drawn for the fouling factor calculation as for the overall heat transfer coefficient as given in the previous section.

The results of the analysis are given in Table 5-11. The full calculation can be seen in Appendix F.

Table 5-11: Results of fouling factor uncertainty analysis

Description	Symbol	Unit	Avg. Value	Standard Dev.	Random Uncert.	Systematic Uncert.	Combined Uncert.	Expanded Uncert.[1] (absolute)	Sensitivity Factor[2]
Fouled CL Inlet temp	$T_{CL,i,f}$	°C	22.70	0.0140	0.00005	0.0004	0.0004	0.001	5.28E-05
Fouled CL Outlet temp	$T_{CL,o,f}$	°C	27.75	0.0180	0.0007	0.05	0.050	0.10	-6.16E-05
Fouled CL Flow	$m_{CL,f}$	kg/s	0.54	0.0010	0.0009	0.05	0.050	0.10	4.92E-04
Fouled CL Specific heat	$Cp_{CL,f}$	kJ/kg.K	1.18	N/A	N/A	0.0105	0.0105	0.021	-6.90E-08
Fouled HL Inlet temp	$T_{HL,i,f}$	°C	59.99	0.0780	0.0039	0.05	0.0502	0.100	4.44E-06
Fouled HL Outlet temp	$T_{HL,o,f}$	°C	56.30	0.0680	0.0034	0.05	0.0501	0.100	4.32E-06
Clean CL Inlet temp	$T_{CL,i,c}$	°C	22.664	0.0120	0.0006	0.05	0.050	0.10	-4.47E-05
Clean CL Outlet temp	$T_{CL,o,c}$	°C	28.133	0.0170	0.0009	0.05	0.050	0.10	5.28E-05
Clean CL Flow	$m_{CL,c}$	kg/s	0.542	0.0010	0.00005	0.05	0.050	0.100	-5.31E-04
Clean CL Specific heat	$Cp_{CL,c}$	kJ/kg.K	4.180	N/A	N/A	0.01	0.0104	0.021	6.37E-08
Clean HL Inlet temp	$T_{HL,i,c}$	°C	60.230	0.0530	0.0022	0.05	0.0500	0.100	-4.12E-06
Clean HL Outlet temp	$T_{HL,o,c}$	°C	56.268	0.0440	0.0034	0.05	0.0501	0.100	-3.99E-06

Description	Symbol	Unit	Avg. Value	-	Random Uncert.	Systematic Uncert.	Combined Uncert.	Expanded Uncert.[1] (absolute)	Expanded Uncert.[1] (relative %)
Overall Fouling Factor	R_F	m^2.K / W	2.22E-05		9.59E-08	5.99E-07	6.07E-07	1.21E-06	5.48

Note 1: Expanded Uncertainty given at 95% confidence level

Note 2: The units given do not apply to sensitivity factors

6. Discussion and conclusion

The following chapter will provide the discussions, recommendations, and conclusion of the work done.

6.1 Test rig

The test rig that was designed and built performed exceptionally well. With the reduced budget the performance was better than expected. All of the required specifications were met and in most cases exceeded. The hypotheses were confirmed that a well-designed and manufactured test rig can accurately measure the fouling factors found on feedwater heater tube samples.

Initially some issues with the repeatability of the rig were experienced. Modifications were done to successfully address these problems. The rig performed exceptionally well in all the validation tests that were done. All comparative validation test results were well within calculated uncertainty values.

There is room for improvement that can be considered. This includes:

- The Excel user interface may be difficult to understand to someone not familiar with it. More work can be done to make this more user-friendly.
- Currently the hot loop temperature control is done within a range of approximately 0.2°C of its set point. Variations were also observed in the cold loop inlet temperature from the reservoir that was higher than expected. Both of these can be improved. It will however come at a high capital cost. Due to this it is recommended that a sensitivity analyses is done to determine the effect on the final test results of these variations. It is expected to be low.
- Although planned in the initial phases, the differential pressure measurement across the tube was never procured and installed. This was mostly due to funding restrictions. This will add valuable information w.r.t. the roughness and more specifically the roughness changes of the tube between the clean and fouled conditions.
- The configuration of the hot loop outlet RTD probe installation was problematic. It was installed with the probe in an upwards direction. There is no thermo-well fitted with the probe, it is installed into the process fluid and sealed with a compression fitting. If a leak develops at the compression fitting, it leaks into the probe wire connections where it is not visible. This causes a small short circuit between the 4 wires in the probe which leads to incorrect measurements. The error is small, in the order of 0.1 – 0.3°C, so it is difficult to

detect. It does however have a significant impact on the energy balance and the results due to the small temperature differences involved in the measurements.

- Consideration must be given to improving the symmetry between the hot loop inlet and outlet to remove or cancel out flow effects on the temperature measurements. Throughout the tests, there was a small difference in measurement between the two probes on hot loop when the same fluid temp is measured. Although it is within the error range of the probes, it was never explained. Symmetry was suggested, but not confirmed. This will be a small modification and is considered worth doing.
- The mechanical cleaning of the tubes is not ideal. It is very time consuming and although it can safely be said that very little or no tube material is lost, the question remains if the inside of the tubes are really 100% clean. For the 5 tests that were done, new brushes were used for every tube. The internal cleaning brushes are expensive with long lead times and it is not practical to use a new brush for every tube for bulk testing.

  Some of the tubes were cut after the final tests to inspect and confirm the cleanliness. It was visibly clean, but this is also not practical if a large number of tubes need to be tested. Since the tube samples are hard to come by and takes long to test, one does not want to be in a position where a test is completed only to realise afterwards that the tube was not sufficiently cleaned. The cleaning is a critical part of the process and more work and funding are required to improve and give more confidence to this process.

6.2 Test rig uncertainty

The uncertainty on the measured result is important for experimental work. The test rig met all the specified absolute required uncertainties. Some of the relative uncertainties were high, but is due to the small fouling factors measured.

It is not expected that the uncertainties can be significantly improved. This conclusion was made by studying the uncertainty analysis process, the instrumentation available at reasonable costs and the process used to determine the fouling factors. The Coriolis flow meter that was used is considered the best and most accurate flow meter type. It is thus not possible to improve the flow measurement uncertainty. There is room for improvement from a temperature measurement point of view and the calibration there-of. This will however come at a very high cost and will not make a significant difference. Due to the correlated nature of the temperature measurements where the systematic uncertainties from the same instrumentation are effectively subtracted from each other, a large part of the uncertainty associated with the temperature measurement cancels out. Since 400 measurements were used to determine the random uncertainties, little can be gained from a number of measurement points of view. The only room for improvement is in the

operating range. A study can be done to see in which operating range i.e. input conditions and amount of measurement will provide lower uncertainties. The results of such a study are difficult to predict, but there is literature available that shows that improvements can be made in this way [122].

6.3 Results

The results of the measured fouling factors are very promising. The test results confirm that the HEI fouling factors [6] that are being used for feedwater heaters are in this specific case conservative. It also contradicts the HEI recommendations that no fouling factors have to be used on the outside of tubes in the condensing zones. All the tubes tested were from the condensing zone of the specific heater and fouling factors higher than the internal fouling factors were measured. It must be noted that all the tested tubes were from the periphery of the tube bundle which may suffer from more particulate fouling than the tubes deeper into the bundle.

Only 5 tubes were tested from a single heater. This can by no means be considered representative. More testing will have to be done on different tubes, different materials and from different zones in the heater to be able to make meaningful conclusions. The initial results are however very promising and clearly indicates that tube sample collection and testing must continue.

6.4 Conclusion

The only method that has achieved widespread use in industry to accommodate fouling in heat exchanger design is the fouling factor method. The fouling factors in use are however outdated and considered very conservative.

The purpose of this work was to design, build and validate a test rig that can accurately determine the fouling factors on feedwater heater tubes. This was done successfully and the test rig proved to be of acceptable accuracy.

Initial tests were completed and showed promising results. Collection and testing of feedwater heater tube samples must continue. In time a fouling factor database can be developed that will provide sufficient motivation to lower the fouling factors in use that will allow capital saving on the design and construction of new feedwater heaters.

7. List of References

[1] F. P. Incropera, T. L. Bergman, A. S. Lavine, and D. P. DeWitt, *Fundamentals of heat and mass transfer.* 2011.

[2] *VDI Heat Atlas*, Second Edi. Springer-Verlag Berlin Heidelberg, 2010.

[3] "BS EN 13445 - Unfired Pressure Vessels." BSI Standards, 2014.

[4] H. M. Steinhagen, "Fouling : The Ultimate Challenge for Heat Exchanger Design," in *The sixth International Symposium on Transport Phenomena in Thermal Engineering*, 1993, pp. 811–823.

[5] H. Padayachee, "Camden Power Station Unit 6 HPH Tube Evaluation," *RTD/MAT/16*. 2016.

[6] Heat Exchanger Institute, "Standards for Closed Feedwater Heaters 8th Edition." 2009.

[7] H. Müller-Steinhagen, "Heat Transfer Fouling: 50 Years After the Kern and Seaton Model.," *Heat Transf. Eng.*, vol. 32, no. 1, pp. 1–13, 2011.

[8] T. Terranova and I. Gibbard, *Training Course - Powerplant Feedwater Heaters*. Power Plant Engineering, 2006.

[9] M. Walker, I. Safari, and R. Theregowda, "Economic impact of condenser fouling in existing thermoelectric power plants," *Energy*, vol. 44, no. 1, pp. 429–437, 2012.

[10] Eskom, "Integrated report 2016," p. 129.

[11] S. N. Raju and P. D. Kumar, "Analysis of Regenerative System in Steam Power Plant," no. 7, pp. 39–44, 2015.

[12] R. Grosser and G. Bouwer, *Lethabo Turbine and Turbine Plant Training*. 2007.

[13] I. S. Hussaini, S. M. Zubair, and M. A. Antar, "Area allocation in multi-zone feedwater heaters," *Energy Convers. Manag.*, vol. 48, pp. 568–575, 2007.

[14] S. Genić, I. Arandjelović, P. Kolendić, M. Jarić, N. Budimir, and V. Genić, "A Review of Explicit Approximations of Colebrook ' s Equation," *FME Trans.*, vol. 39, no. 2, pp. 67–71, 2011.

[15] D. Zigrang and N. Sylvester, "Explicit Approximations to the Solution of Colebrook's Friction Factor Equation," *AiChE J.*, vol. 28, no. 3, pp. 514–515, 1982.

[16] P. Rousseau and L. Jestin, *Fundamentals of Thermal Fluid Sciences*, Revision 3. Department of Mechanical Engineering, University of Cape Town, 2016.

[17] P. Fischer, J. W. Suitor, and R. B. Ritter, "Fouling Measurement Techniques," *Chem. Eng. Prog.*, vol. 71, no. 7, pp. 66–72, 1975.

[18] C. Bennett, S. Appleyard, and M. Gough, "Industry-Recommended Procedures for Experimental Crude Oil Preheat Fouling Research," *Heat Transf. Eng.*, vol. 27, no. 9, pp. 28–35, 2006.

[19] B. D. Crittenden and N. J. Alderman, "Mechanisms by Which Fouling Can Increase Overall Heat Transfer Coefficients," *Heat Transf. Eng.*, vol. 13, no. 4, pp. 32–41, 1992.

[20] B. D. Crittenden and N. J. Alderman, "Negative fouling resistances: The effect of surface roughness," *Chem. Eng. Sci.*, vol. 43, no. 4, pp. 829–838, 1988.

[21] V. Gnielinski, “New Equations for heat and mass transfer in turbulant pipe and channel flow,” *Int. Chem. Eng.*, vol. 16, no. 2, pp. 359–368, 1976.

[22] V. Gnielinski, “Heat Transfer Coefficients for Turbulant Flow in Concentric Annular Ducts,” *Heat Transf. Eng.*, vol. 30, no. 6, pp. 431–436, 2009.

[23] S. Churchill and H. Chu, “Correlating Equations for Laminer and Turbulant Free Convection from a Horizontal Cylinder,” *Int. J. Heat Mass Transf.*, vol. 18, pp. 1049–1053, 1975.

[24] J. Taborek, T. Aoki, R. B. Ritter, J. . Palen, and J. . Knudsen, “Fouling: The Major Unresolved Problem in Heat Transfer,” *Chem. Eng. Prog.*, vol. 68, no. 2, pp. 59–67, 1972.

[25] J. Knudsen and B. Roy, “Influence of fouling on heat transfer,” in *7th International Heat Transfer Conference*, 1982, pp. 269–287.

[26] E. Schlunder and G. Hewit, Eds., *HEDH - Heat Exchanger Design Handbook*. Hemisphere Publishing, 1983.

[27] A. Pritchard, “The economics of fouling,” *Fouling Sci. Technol.*, pp. 31–45, 1988.

[28] R. Steinhagen, H. Muller-Steinhagen, and K. Maani, “Problems and Costs due to Heat Exchanger Fouling in New Zealand Industries,” *Heat Transf. Eng.*, vol. 14, no. 1, pp. 19–30, 1993.

[29] S. N. Kazi, “Fouling and Fouling Mitigation on Heat Exchanger Surfaces,” *Heat Exch. - Basics Des. Appl.*, no. March, pp. 507–532, 2012.

[30] P. Thackery, “The cost of fouling in Heat Exchanger Plant,” *Effluent Water Treat. J.*, pp. 111–115, 1980.

[31] B. Garrett-Price, S. A. Smith, J. G. Knudsen, W. J. Marner, and J. W. Suitor, *Fouling of Heat Exchangers: Characteristics, Costs, Prevention, Control and Removal*. 1985.

[32] Z. M. Xu, S. R. Yang, S. Q. Guo, H. Zhao, B. Qi, and Z. B. Zhang, “Costs due to utility boiler fouling in China,” *Heat Transf. - Asian Res.*, vol. 34, no. 2, pp. 53–63, 2005.

[33] H. Müller-Steinhagen, M. Malayeri, and P. Watkinson, “Heat Exchanger Fouling: Environmental Impacts,” *Heat Transf. Eng.*, vol. 30, no. 10–11, pp. 773–776, 2009.

[34] *Standards of the Tubular Exchanger Manufacturers Association*, Ninth Edit. 2007.

[35] N. Epstein, “Thinking about Heat Transfer Fouling: A 5 × 5 Matrix,” *Heat Transf. Eng.*, vol. 4, no. 1, pp. 43–56, 1983.

[36] D. Hasson, “Heat Exchanger Fouling, CSIR Report CENG 339,” Pretoria, South Africa, 1980.

[37] K. Thulukkanam, *Heat Exchanger Design Handbook*, Second Edi. 2013.

[38] N. Epstein, “Particulate Fouling fo Heat Transfer surfaces: Mechanisms and Models,” in *Fouling Science and Technology*, 1988, pp. 143–146.

[39] M. M. Awad, “Fouling of heat transfer surfaces,” in *Heat Transfer - Theoretical Analysis, Experimental Investigations and Industrial Systems*, A. Belmiloudi, Ed. Vienna: InTech (Open access Publisher), 2011, p. 666.

[40] A. P. Watkinson and D. I. Wilson, “Chemical reaction fouling: A review,” *Exp. Therm. Fluid Sci.*, vol. 14, no. 4, pp. 361–374, 1997.

[41] E. F. C. Somerscales, “Fundamentals of corrosion fouling,” *Exp. Therm. Fluid Sci.*, vol. 14, no. 4, pp. 335–355, 1997.

[42] T. R. Bott, “Aspects of crystallization fouling,” *Exp. Therm. Fluid Sci.*, vol. 14, no. 96, pp. 356–360, 1997.

[43] L. F. Melo and T. R. Bott, “Biofouling in water systems,” *Exp. Therm. Fluid Sci.*, vol. 14, no. 96, pp. 375–381, 1997.

[44] J. M. Chenoweth, “Final Report of the HTRI/TEMA Joint Committee to Review the Fouling Section of the TEMA Standards,” *Heat Transf. Eng.*, vol. 11, no. 1, pp. 73–107, 1990.

[45] P. G. Cousineau, G. D. Fulford, and P. M. Simmons, “Monitoring fouling using a novel technique,” in *Fouling Science and Technology*, 1988, pp. 77–84.

[46] J. M. Nesta and C. A. Bennett, “Fouling Mitigation By Design,” in *Proceedings of 6th International Conference on Heat Exchanger Fouling and Cleaning - Challenges and Opportunities*, 2005.

[47] Heat Exchanger Institute, “Standards for Steam Surface Condensers 11th edition.” 2012.

[48] E. F. C. Somerscales, “Fouling of Heat Transfer Surfaces: An Historical Review,” *Heat Transf. Eng.*, vol. 11, no. 1, pp. 19–36, 1990.

[49] J. M. Chenoweth, “General Design of Heat Exchangers for Fouling Conditions,” in *Fouling Science and Technology*, 1988, pp. 477–494.

[50] C. Shen, C. Cirone, A. M. Jacobi, and X. Wang, “Fouling of enhanced tubes for condensers used in cooling tower systems: A literature review,” *Appl. Therm. Eng.*, vol. 79, pp. 74–87, 2015.

[51] C. A. Bennett, R. S. Kistler, T. G. Lestina, and D. C. King, “Improving heat exchanger designs,” *Chem. Eng. Prog.*, vol. 103, no. 4, pp. 40–45, 2007.

[52] R. L. Shilling, “Fouling and Uncertainty Margins in Tubular Heat Exchanger Design: An Alternative,” *Heat Transf. Eng.*, vol. 33, no. March 2015, pp. 1094–1104, 2012.

[53] T. R. Bott, *Fouling of heat exchangers*. Elsevier, 1995.

[54] R. L. Shilling, M. P. Rudy, and T. M. Rudy, “Risk-Based Design Margin Selection for Heat Exchangers,” *Heat Transf. Eng.*, vol. 32, no. 3–4, pp. 307–313, 2011.

[55] J. L. Hernandez-Galan and L. Alberto Plauchu, “Determination of fouling factors for shell-and-tube type heat exchangers exposed to los azufres geothermal fluids,” *Geothermics*, vol. 18, no. 1/2, pp. 121–128, 1989.

[56] R. M. Agbisit, V. Singh, J. J. Valenti, M. Kakleas, M. E. Tumbleson, and K. D. Rausch, “Technique to measure surface-fouling tendencies of steepwater from corn wet milling,” *Cereal Chem.*, vol. 80, no. 1, pp. 84–86, 2003.

[57] M. Abu-Zaid, “A New Technique for the Measurement of Fouling on Heat Transfer Surfaces,” *Int. Commun. Heat Mass Transf.*, vol. 19, pp. 117–125, 1992.

[58] R. Goedecke, P. Drögemüller, W. Augustin, and S. Scholl, “Experiments on Integral and Local Crystallization Fouling Resistances in a Double-Pipe Heat Exchanger With Wire Matrix Inserts,” *Heat Transf. Eng.*, vol. 37, no. 1, pp. 24–31, 2016.

[59] Q. Zhenhua, Y. Chen, and C. Ma, “Experimental study of fouling on heat transfer surface during forced convective heat transfer,” *Chinese J. Chem. Eng.*, vol. 16, no. 4, pp. 535–540, 2008.

[60] Y. C. Chen, Z. H. Quan, and C. F. Ma, “Investigation of Fouling Process for Convective Heat Transfer in an Annular Duct,” in *Proceedings of 7th International Conference on Heat Exchanger Fouling and Cleaning - Challenges and Opportunities*, 2007, pp. 215–220.

[61] J. G. Fetkovich, G. N. Grannemann, D. L. Meier, and C. W. Fette, “A Novel Method of Measuring heat transfer Coefficients with High Precision,” in *Twelfth South Eastern Seminar on Thermal Sciences*, 1976.

[62] J. G. Fetkovich, G. N. Grannemann, L. M. Mahalingam, D. L. Meier, and F. C. Munchmeyer, “Studies of Biofouling in Ocean Thermal Energy Conversion Plants,” in *4th Annual Conference on Ocean Thermal Energy Conversion*, 1977.

[63] A. D. Smith, “Analysis of Fouling Rate and Propensity for Eight Crude Oil Samples in Annular Test Section,” in *International Conference on Heat Exchanger Fouling and Cleaning*, 2013.

[64] M. Ratel, Y. Kapoor, Z. Anxionnaz-Minvielle, L. Seminel, and B. Vinet, “Investigation of fouling rates in a heat exchanger using an innovative fouling rig,” in *Proc. Int. Conf. Heat Exchanger Fouling and Cleaning*, 2013, pp. 36–41.

[65] M. Srinivasan and A. P. Watkinson, “Fouling of Some Canadian Crude Oils,” in *Heat Exchanger Fouling and Cleaning: Fundamentals and Applications*, 2003.

[66] H. Müller-Steinhagen and C. A. Branch, “Heat transfer and heat transfer fouling in Kraft black liquor evaporators,” *Exp. Therm. Fluid Sci.*, vol. 14, pp. 425–437, 1997.

[67] S. P. Heneghan, C. R. Martel, T. F. Williams, and D. R. Ballal, “Studies of Jet Fuel Thermal Stability in a Flowing System,” in *International Gas Turbine and Aeroengine Congress and Exposition*, 1992.

[68] J. S. Chin and A. H. Lefebvre, “Influence of Flow Conditions on Deposits From Heated Hydrocarbon Fuels,” in *International Gas Turbine and Aeroengine Congress and Exposition*, 1992.

[69] E. G. Jones and W. J. Balster, “Phenomenological study of the formation of insolubles in a jet-A fuel,” *Energy & Fuels*, vol. 7, no. 6, pp. 968–977, 1993.

[70] E. G. Jones and W. J. Balster, “Surface Fouling in Aviation Fuel: Short- vs LongTerm Isothermal Tests,” *Fuel*, no. April 1985, pp. 610–615, 1995.

[71] P. J. Marteney and L. J. Spadaccini, “Thermal Decomposition of Aircraft Fuel,” *J. Eng. Gas Turbines Power*, vol. 108, no. October 1986, pp. 648–653, 1986.

[72] H. Pahlavanzadeh, M. R. Jafari Nasr, and S. H. Mozaffari, “Experimental study of thermo-hydraulic and fouling performance of enhanced heat exchangers,” *Int. Commun. Heat Mass Transf.*, vol. 34, no. 7, pp. 907–916, 2007.

[73] G. F. Hays, E. S. Beardwood, and S. J. Colby, “Enhanced Heat Exchanger Tubes : Their Fouling Tendency and Potential Cleanup,” in *Proceedings of 6th International Conference on Heat Exchanger Fouling and Cleaning - Challenges and Opportunities*, 2005.

[74] A. Al-Janabi, M. R. Malayeri, and H. Müller-Steinhagen, “Experimental investigation of

crystallization fouling on grooved stainless steel surfaces during convective heat transfer," *Heat Transf. Eng.*, vol. 30, no. 10–11, pp. 832–839, 2009.

[75] W. L. Owens, "A Simple Device for measuring Fouling in a Heat Exchanger Tube," *J. Sol. Energy Eng.*, vol. 108, pp. 135–139, 1986.

[76] S. J. Kline and F. A. McClintock, "Describing uncertainties in single sample experiments," *Mech. Eng.*, vol. 75, pp. 3–8, 1953.

[77] S. Eiamsa-ard, K. Nanan, C. Thianpong, and P. Eiamsa-ard, "Thermal Performance Evaluation of Heat Exchanger Tubes Equipped with Coupling Twisted Tapes," *Exp. Heat Transf.*, vol. 26, pp. 413–430, 2013.

[78] M. M. K. Bhuiya *et al.*, "Heat Transfer and Pressure Drop Characteristics in Turbulent Flow Through a Tube," *Exp. Heat Transf.*, vol. 25, pp. 301–322, 2012.

[79] J. G. Knudsen, "Apparatus and Techniques for Measurement of Fouling of Heat Transfer Surfaces," in *Fouling of Heat Transfer Equipment*, 1981, pp. 57–81.

[80] S. Z. Heris, S. G. Etemad, and M. N. Esfahany, "Convective Heat Transfer of a Cu/Water Nanofluid Flowing Through a Circular Tube," *Exp. Heat Transf.*, vol. 22, pp. 217–227, 2009.

[81] H. Cui, X. Yuan, and Z. Yao, "Experimental Investigation of Heat Transfer and Pressure Drop Characteristics of W-Type Spirally Fluted Tubes," *Exp. Heat Transf.*, vol. 16, no. 3, pp. 159–169, 2003.

[82] R. J. Moffat, "Describing the uncertainties in experimental results," *Exp. Therm. Fluid Sci.*, vol. 1, pp. 3–17, 1988.

[83] S. K. Saha, A. Dutta, and S. K. Dhal, "Friction and heat transfer characteristics of laminar swirl ¯ ow through a circular tube ® tted with regularly spaced twisted-tape elements," vol. 44, no. September 2014, pp. 4211–4223, 2001.

[84] Y. Xuan and Q. Li, "Investigation on convective heat transfer and flow features of nanofluids," *J. Heat Transfer*, vol. 125, no. 1, p. 151, 2003.

[85] S. Eiamsa-ard, C. Thianpong, and P. Promvonge, "Experimental investigation of heat transfer and flow friction in a circular tube fitted with regularly spaced twisted tape elements," *Int. Commun. Heat Mass Transf.*, vol. 33, no. 10, pp. 1225–1233, 2006.

[86] "ASME, PTC 19.1, Measurement Uncertainty," 2013.

[87] L. S. Sundar and K. V. Sharma, "Turbulent heat transfer and friction factor of Al2O3 Nanofluid in circular tube with twisted tape inserts," *Int. J. Heat Mass Transf.*, vol. 53, no. 7–8, pp. 1409–1416, 2010.

[88] J. Goodenough, "Thermal performance evaluation of artificial protective coatings applied to steam surface condenser tubes by," Stellenbosch University, 2013.

[89] J. W. Suitor, W. J. Marner, and R. B. Ritter, "The history and status of research in fouling of heat exchangers in cooling water service," *Can. J. Chem. Eng.*, vol. 55, no. 4, pp. 374–380, 1977.

[90] J. M. Chenoweth, "Liquid fouling monitoring equipment," in *Fouling Science and Technology*, 1988, pp. 49–65.

[91] R. S. Figliola and D. E. Beasley, *Theory and Design for Mechanical Measurements*, Fifth Edit. John Wiley & Sons Inc, 2011.

[92] J. Kim, T. Simon, and R. Viskanta, "Journal of heat transfer policy on reporting uncertainties in experimental measurements and results," *J. Heat Transfer*, vol. 115, no. 1, pp. 5–6, 1993.

[93] J. P. Holman, *Experimental Methods for Engineers*, Eighth Edi. McGraw Hill.

[94] Rosemount and Emerson Process Management, *The Engineer's Guide to Industrial Temperature Measurement*, 2013 Ed. .

[95] R. Rusby, *National Physical Laborotory, Good Practice Guide No . 125, The Beginner's Guide to Temperature Measurement*, September. 2012.

[96] P. R. N. Childs, *Practical Temperature Measurement*. Butterworth-Heinemann, 2001.

[97] "BS EN 60751: Industrial platinum resistance thermometers and platinum temperature sensors," 2008.

[98] Pico Technology, "Improving the accuracy of temperature measurements." [Online]. Available: https://www.picotech.com/library/application-note/improving-the-accuracy-of-temperature-measurements. [Accessed: 20-Nov-2017].

[99] Pico Technology, "Pt100 Platinum Resistance Thermometers." [Online]. Available: https://www.picotech.com/library/application-note/pt100-platinum-resistance-thermometers. [Accessed: 23-Mar-2018].

[100] CAS Data Loggers, "Basic Techniques for Accurate Resistance Measurement," 2014.

[101] P. J. LaNasa and E. Loy Upp, *Fluid Flow Measurement - A Practical Guide to Accurate Flow Measurement*, Third Edit. Butterworth-Heinemann, 2014.

[102] "BS EN ISO 5167: Measurement of fluid flow by means of pressure differential devices inserted in circular cross-section conduits running full." 2003.

[103] Emerson and Rosemount, "Fundamentals of Flow Metering, Technical Data Sheet, 00816-0100-3031." .

[104] Spirax Sarco, "Steam Flow Meters." [Online]. Available: http://pointing.spiraxsarco.com/resources/steam-engineering-tutorials/flowmetering/types-of-steam-flowmeter.asp. [Accessed: 17-Aug-2017].

[105] Spirax Sarco, "Flowmetering." .

[106] Omega, "Transactions in measurement and control, Volume 4, Flow and Level Measurement." 2001.

[107] "ASME PTC 19.5 Flow Measurment." 2004.

[108] ABB, "Industrial Flow Measurement." 2006.

[109] Bronkhorst, "Thermal mass flow measurement." [Online]. Available: http://www.bronkhorst.com/en/products/theory/thermal_mass_flow_measurement/. [Accessed: 21-Aug-2017].

[110] O. Augustyn and A. . du Preez, "240-56030499 Condenser Health Care Guideline." 2016.

[111] K. Northcott and H. Makumbane, "CRD/MAT/06/2522/MT359 Abrasive blast cleaning of

brass tubing." p. 2006.

[112] A. Hovland, D. Rankin, and E. Saxon, "Heat Exchanger Tube Wear By Mechanical Cleaners," *Proc. Jt. Power Gener. Conf.*, 1988.

[113] "ASME PTC 12.1 Closed Feedwater Heaters." 2000.

[114] "Pressure Equipment Regulations." Department of Labour.

[115] "Occupational Health and Safety Act and regulations (85 of 1993)." .

[116] *SANS 347 Categorization and conformity assessment criteria for all pressure equipment*, Edition 2. 2012.

[117] Thermaflex International, "ThermaEco ZZ Technical Datasheet."

[118] John C. Dixon, "Properties of Air," in *The Shock Absorber Handbook*, Second Ed., John Wiley & Sons, Ed. 2007.

[119] Endress and Hauser, "Coriolis Mass Flow Measurement System Promass 63 - Technical Information." .

[120] Endress and Hauser, "Electromagnetic Flow Measuring System Promag 33 - Technical Information." .

[121] W. Wagner, J. Cooper, A. Dittmann, and J. Kijima, "The IAPWS Industrial Formulation 1997 for the Thermodynamic Properties of Water and Steam," *Trans. ASME*, vol. 122, pp. 150–182, 2000.

[122] C. Shen, C. Cirone, and X. Wang, "Uncertainty analysis: Design of a fouling test device for the liquid-to-refrigerant heat exchangers," *Appl. Therm. Eng.*, vol. 85, pp. 148–159, 2015.

Appendix A. Process Design Flownex model Verification Calculations

Flownex Model Verification Calculations

Reference:C:\Users\hallatNJ\Desktop\Masters\1. Dissertation\Mathcad Models\Water-Steam IAPWS-IF97 rev A.3.xmcd

1. Geometric Parameters:

$d_{i.tube} := 20.6mm$

$d_{o.tube} := 27mm$

$d_{i.ann} := d_{o.tube} = 0.027\,m$

$d_{o.ann} := 32.5mm$

$t_{tube} := \frac{d_{o.tube} - d_{i.tube}}{2} = 3.2 \times 10^{-3}\,m$

$d_{h.ann} := d_{o.ann} - d_{i.ann} = 5.5 \cdot mm$

$L := 2m$ Note: Test Tube is 2.4 m long, but only 2 m are included in the annulus section and are subjected to heat transfer

$e_i := 67.5\mu m = 6.75 \times 10^{-5}\,m$ Surface roughness for commercial steel – Value commonly used in Eskom

$e_o := 67.5\mu m = 6.75 \times 10^{-5}\,m$ Surface roughness for commercial steel – Value commonly used in Eskom

Tube Material = 15Mo3

$k_{tube} := 50\,\frac{W}{m \cdot K}$

$A_{ht.i} := 2 \cdot \pi \cdot \left(\frac{d_{i.tube}}{2}\right) \cdot L = 0.129\,m^2$

$A_{ht.o} := 2 \cdot \pi \cdot \left(\frac{d_{o.tube}}{2}\right) \cdot L = 0.17\,m^2$

$A_{flow.i} := \pi \cdot \left(\frac{d_{i.tube}}{2}\right)^2 = 0.00033329\,m^2$

$A_{flow.o} := \pi \cdot \left(\frac{d_{o.ann}}{2}\right)^2 - \pi \cdot \left(\frac{d_{i.ann}}{2}\right)^2 = 0.00025702\,m^2$

2. Process Parameters:

2.1 Tube

$P_{i.tube} := 87.82kPa$

$T_{i.tube} := 21\,°C$

$T_{o.tube.guess} := 31.23\,°C$

$v_i := 1\frac{m}{s}$

$rho_i := \rho_{steam}\left[P_{i.tube}, \frac{\left(T_{i.tube} + T_{o.tube.guess}\right)}{2}, "", "", ""\right] = 996.75\frac{kg}{m^3}$

$mu_i := \mu_{steam}\left[P_{i.tube}, \frac{\left(T_{i.tube} + T_{o.tube.guess}\right)}{2}, "", "", "", ""\right] = 8.679\times 10^{-4}\frac{kg}{m\cdot s}$

$m_i := rho_i \cdot v_i \cdot A_{flow.i} = 0.332\frac{kg}{s}$

$k_i := \lambda_{steam}\left[P_{i.tube}, \frac{\left(T_{i.tube} + T_{o.tube.guess}\right)}{2}, "", "", "", ""\right] = 0.609\cdot\frac{W}{m\cdot K}$

$cp_i := Cp_{steam}\left[P_{i.tube}, \frac{\left(T_{i.tube} + T_{o.tube.guess}\right)}{2}, "", "", "", ""\right] = 4.181\times 10^{3}\frac{m^2}{K\cdot s^2}$

2.2 Annulus

$P_{i.ann} := 90.56kPa$

$T_{i.ann} := 68.5\,°C$

$T_{o.ann.guess} := 55.045\,°C$

$v_o := 1\frac{m}{s}$

$rho_o := \rho_{steam}\left[P_{i.ann}, \frac{\left(T_{i.ann} + T_{o.ann.guess}\right)}{2}, "", "", ""\right] = 982.285\frac{kg}{m^3}$

$mu_o := \mu_{steam}\left[P_{i.ann}, \frac{\left(T_{i.ann} + T_{o.ann.guess}\right)}{2}, "", "", "", ""\right] = 4.538\times 10^{-4}\frac{kg}{m\cdot s}$

$m_o := rho_o \cdot v_o \cdot A_{flow.o} = 0.252\frac{kg}{s}$

$$k_o := \lambda_{steam}\left[P_{i.ann}, \frac{\left(T_{i.ann} + T_{o.ann.guess}\right)}{2}, "", "", "", ""\right] = 0.652 \cdot \frac{W}{m \cdot K}$$

$$cp_o := Cp_{steam}\left[P_{i.ann}, \frac{\left(T_{i.ann} + T_{o.ann.guess}\right)}{2}, "", "", "", ""\right] = 4.184 \times 10^3 \frac{m^2}{K \cdot s^2}$$

3. Heat Transfer Coefficient Calculation

3.1 Internal heat Transfer Coefficient:

$$Re_i := \frac{rho_i \cdot v_i \cdot d_{i.tube}}{mu_i} = 23659.23$$

$$Pr_i := Pr_{steam}\left[P_{i.tube}, \frac{\left(T_{i.tube} + T_{o.tube.guess}\right)}{2}, ""\right] = 5.957$$

$$f_i := \left(1.8 \cdot \log\left(Re_i\right) - 1.5\right)^{-2} = 0.025$$

$$\varepsilon_i := \frac{e_i}{d_{i.tube}} = 3.277 \times 10^{-3}$$

$$f_i := \left(-2 \cdot \log\left(\frac{\varepsilon_i}{3.7} - \frac{5.02}{Re_i} \cdot \log\left(\varepsilon_i - \frac{5.02}{Re_i} \cdot \log\left(\frac{\varepsilon_i}{3.7} + \frac{13}{Re_i}\right)\right)\right)\right)^{-2} = 0.031$$

$$Nu_i := \frac{Re_i \cdot Pr_i \cdot \frac{f_i}{8}}{1 + 12.7 \cdot \sqrt{\frac{f_i}{8}} \cdot \left(Pr_i^{\frac{2}{3}} - 1\right)} = 193.155$$

$$h_i := \frac{Nu_i \cdot k_i}{d_{i.tube}} = 5712.28 \cdot \frac{W}{m^2 \cdot K}$$

3.2 External heat Transfer Coefficient

$$Re_o := \frac{rho_o \cdot v_o \cdot d_{h.ann}}{mu_o} = 11904.55$$

$$Pr_o := Pr_{steam}\left[P_{i.ann}, \frac{\left(T_{i.ann} + T_{o.ann.guess}\right)}{2}, ""\right] = 2.91$$

$$a := \frac{d_{i.ann}}{d_{o.ann}} = 0.831 \qquad F_{ann} := 0.75 \cdot a^{-0.17} = 0.774$$

$$Re_{star} := Re_o \frac{(1+a)^2 \cdot \ln(a) + \left(1 - a^2\right)}{(1-a)^2 \cdot \ln(a)} = 698601.54$$

$$e_o := 67.5\mu m = 6.75 \times 10^{-5} m$$

$$\varepsilon_o := \frac{e_o}{d_{h.ann}} = 0.012$$

$$f_o := \left(1.8 \cdot \log\left(Re_{star}\right) - 1.5\right)^{-2} = 0.012$$

$$f_o := \left(-2 \cdot \log\left(\frac{\varepsilon_o}{3.7} - \frac{5.02}{Re_o} \cdot \log\left(\varepsilon_o - \frac{5.02}{Re_o} \cdot \log\left(\frac{\varepsilon_o}{3.7} + \frac{13}{Re_o}\right)\right)\right)\right)^{-2} = 0.044$$

$$f_{o.flownex} := 0.0455770712$$

$$k_1 := 1.07 + \frac{900}{Re_o} - \frac{0.63}{1 + 10 \cdot Pr_o} = 1.125$$

$$Nu_o := \frac{Re_o \cdot Pr_o \cdot \frac{f_o}{8}}{\left[k_1 + 12.7 \cdot \sqrt{\frac{f_o}{8}} \cdot \left(Pr_o^{\frac{2}{3}} - 1\right)\right]} \cdot F_{ann} = 70.019$$

$$h_o := \frac{Nu_o \cdot k_o}{d_{h.ann}} = 8306.45 \frac{W}{m^2 \cdot K}$$

$$k_o = 0.652 \frac{m \cdot kg}{K \cdot s^3}$$

$d_{h.ann} = 5.5 \times 10^{-3}\,m$

Overall Heat Transfer Coefficient

$$R_o := \frac{d_{o.tube}}{h_i \cdot d_{i.tube}} + \frac{d_{o.tube} \cdot \ln\left(\frac{d_{o.tube}}{d_{i.tube}}\right)}{2k_{tube}} + \frac{1}{h_o} = 4.229 \times 10^{-4} \cdot \frac{m^2 \cdot K}{W}$$

$$U_{o.c} := \frac{1}{R_o} = 2364.709 \frac{W}{m^2 \cdot K}$$

Heat Transfer Governing Equation

$T_{i.ann} = 68.5 \cdot °C$

$T_{i.tube} = 21 \cdot °C$

$T_{o.ann} := 55.045\,°C/°C = 55.045$

$T_{o.tube} := 31.23\,°C/°C = 31.23$

$Q_{clean} := \frac{14000W}{W} = 14000$

Given

$$Q_{clean} = \frac{U_{o.c}}{\frac{W}{m^2 \cdot K}} \cdot \frac{A_{ht.o}}{m^2} \cdot \left[\frac{\left(T_{i.ann}/°C - T_{o.tube}\right) - \left(T_{o.ann} - T_{i.tube}/°C\right)}{\ln\left[\frac{\left(T_{i.ann}/°C - T_{o.tube}\right)}{\left(T_{o.ann} - T_{i.tube}/°C\right)}\right]} \right]$$

$$Q_{clean} = \frac{m_i}{\frac{kg}{s}} \cdot \frac{cp_i}{\frac{m^2}{K \cdot s^2}} \cdot \left(T_{o.tube} - T_{i.tube}/°C\right)$$

$$Q_{clean} = \frac{m_o}{\frac{kg}{s}} \cdot \frac{cp_o}{\frac{m^2}{K \cdot s^2}} \cdot \left(T_{i.ann}/°C - T_{o.ann}\right)$$

$$Result := Find\left(Q_{clean}, T_{o.ann}, T_{o.tube}\right)$$

$$Result = \begin{pmatrix} 1.427 \times 10^4 \\ 54.986 \\ 31.275 \end{pmatrix}$$

$Q_{clean} := Result_0 \cdot W = 14273.7W$

$T_{o.ann.c} := Result_1 \cdot °C = 54.99 \cdot °C$

$T_{o.tube.c} := Result_2 \cdot °C = 31.275 \cdot °C$

$$LMTD := \frac{\left(T_{i.ann}/°C - T_{o.tube}\right) - \left(T_{o.ann} - T_{i.tube}/°C\right)}{\ln\left[\frac{\left(T_{i.ann}/°C - T_{o.tube}\right)}{\left(T_{o.ann} - T_{i.tube}/°C\right)}\right]} = 35.633$$

Clean Tube Results

Tube:

$P_{i.tube} = 87.82 \cdot kPa$

$m_i = 0.332 \frac{kg}{s}$

$v_i = 1 \frac{m}{s}$

Annulus:

$P_{i.ann} = 90.56 \cdot kPa$

$m_o = 0.252 \frac{kg}{s}$

$v_o = 1 \frac{m}{s}$

$T_{i.ann} = 68.5 \cdot °C$

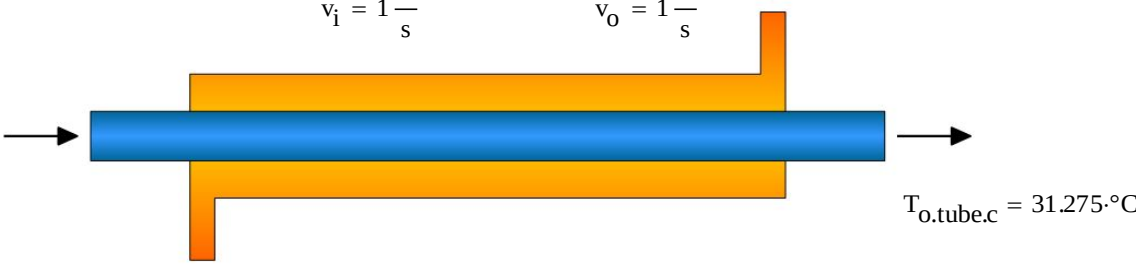

$T_{o.tube.c} = 31.275 \cdot °C$

$T_{i.tube} = 21 \cdot °C$

$T_{o.ann.c} = 54.986 \cdot °C$

$h_i = 5712.28 \cdot \frac{W}{m^2 K}$ $h_o = 8306.45 \cdot \frac{W}{m^2 K}$

$U_{o.c} = 2364.71 \cdot \frac{W}{m^2 K}$ $Q_{clean} = 14.27 \cdot kW$

$d_{i.tube} = 20.6 \cdot mm$

$d_{o.tube} = 27 \cdot mm$

$d_{o.ann} = 32.5 \cdot mm$

$L = 2m$

$A_{ht.o} = 0.17m^2$

Appendix B. Detail Design drawings

This appendix provides the detail design drawings. It includes the following:

- NH-UCT-001 Test Section Coupling
- NH-UCT-002 Inlet pipe Sealing
- NH-UCT-003 Compression nut - 15 mm
- NH-UCT-004 Compression nut - 27 mm
- NH-UCT-005 Test Section
- NH-UCT-006 Frame

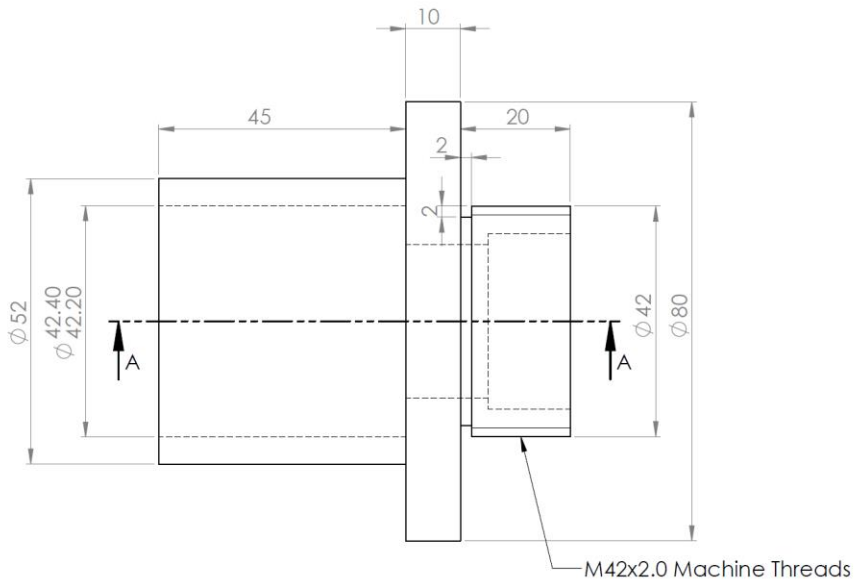

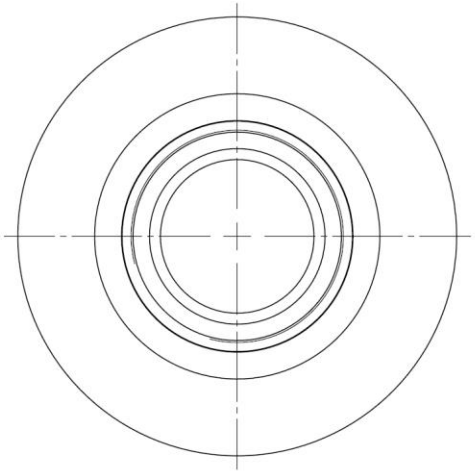

Notes:
1. Design Pressure: 10 bar
2. Design Temperature: 100°C
3. 2 off required
4. Material: Carbon Steel
5. For any queries contact Nicolaas Hallatt at 0845887708.
6. Please confirm material before work start.

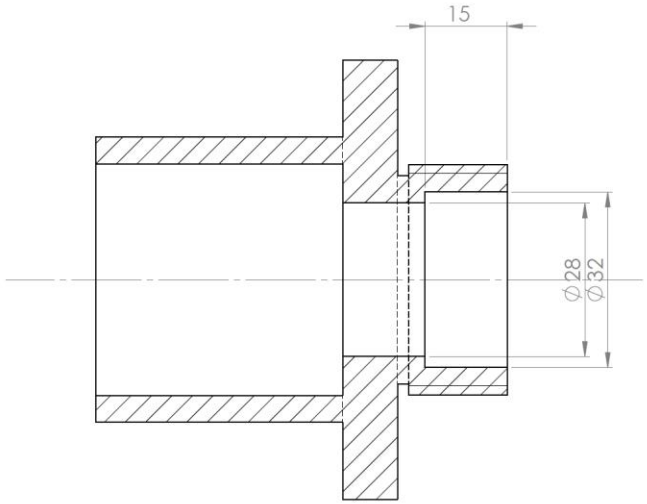

SECTION A-A
SCALE 1.2 : 1

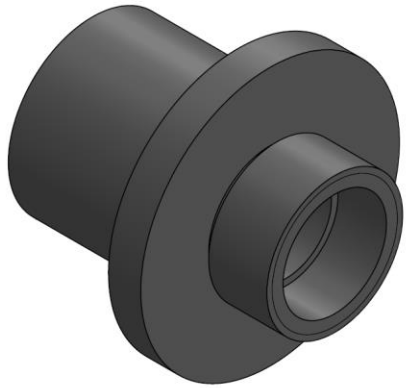

UNLESS OTHERWISE SPECIFIED: DIMENSIONS ARE IN MILLIMETERS SURFACE FINISH: 3.2 µm TOLERANCES: LINEAR: 0.1 mm ANGULAR: N/A	FINISH:				DEBUR AND BREAK SHARP EDGES	DO NOT SCALE DRAWING / REVISION: 0.1
	NAME	SIGNATURE	DATE			
DRAWN	Nicolaas Hallatt		07/11/17			TITLE: Test Section Coupling
CHK'D						
APP'V'D						
MFG						
Q.A				MATERIAL: Carbon Steel		DWG NO. NH/UCT-001 / A3
				WEIGHT:		SCALE:1:1 / SHEET 1 OF 1

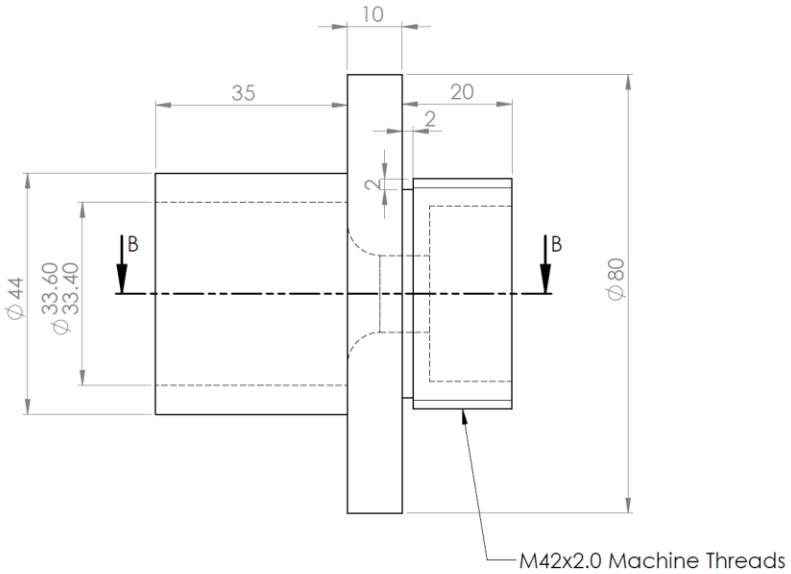

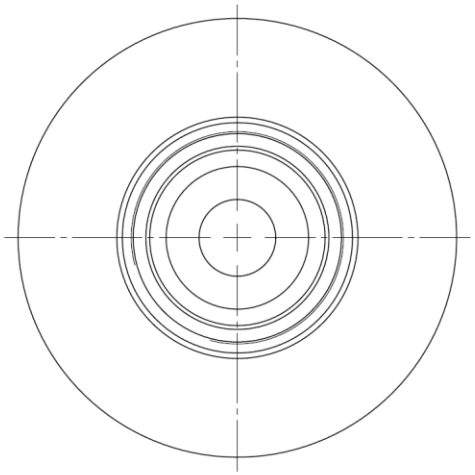

Notes:
1. Design Pressure: 10 bar
2. Design Temperature: 100°C
3. Material: Carbon Steel
4. 2 off required.
5. For any queries contact Nicolaas Hallatt at 0845887708.
6. Please confirm material before work start.

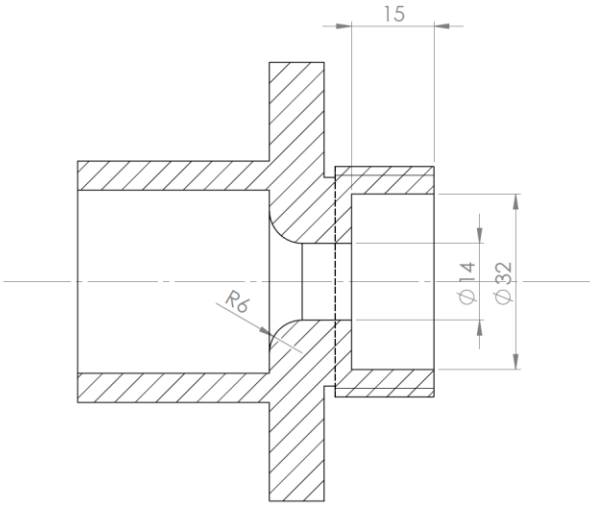

SECTION B-B
SCALE 1.2 : 1

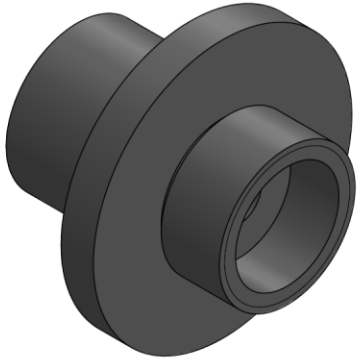

UNLESS OTHERWISE SPECIFIED: DIMENSIONS ARE IN MILLIMETERS SURFACE FINISH: 3.2 µm TOLERANCES: LINEAR: 0.1 mm ANGULAR: N/A	FINISH:	DEBUR AND BREAK SHARP EDGES	DO NOT SCALE DRAWING	REVISION: 0.1
	NAME	SIGNATURE	DATE	TITLE: Pipe Connection Coupling
DRAWN	Nicolaas Hallatt		07/11/17	
CHK'D				
APPV'D				
MFG				
Q.A				
MATERIAL: Carbon Steel				DWG NO. NH/UCT-002 A3
WEIGHT:				SCALE:1:1 SHEET 1 OF 1

Notes:
1. 4 off required
2. Material: Carbon Steel
3. For any queries contact Nicolaas Hallatt at 0845887708.
4. Please confirm material before work start.

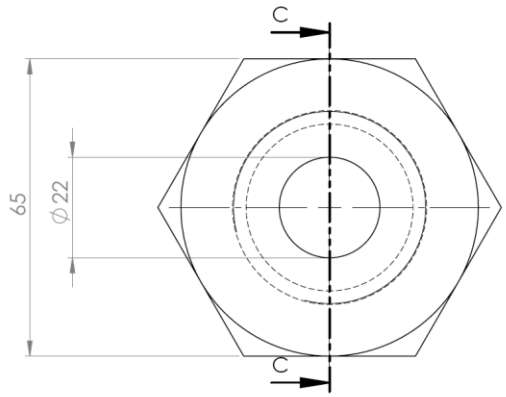

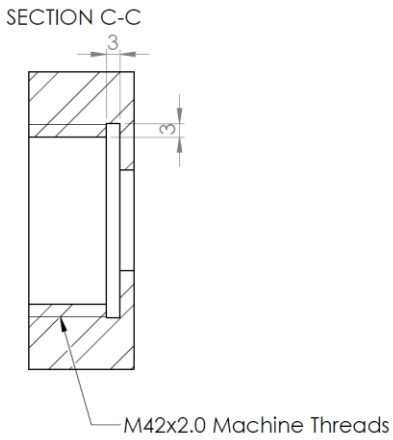

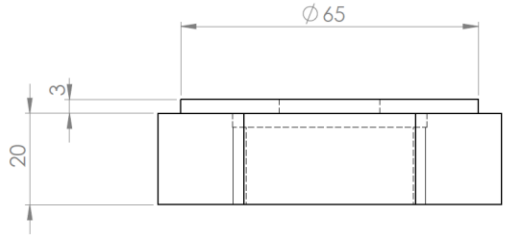

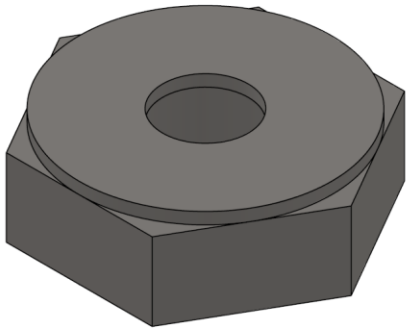

UNLESS OTHERWISE SPECIFIED: DIMENSIONS ARE IN MILLIMETERS SURFACE FINISH: 3.2 µm TOLERANCES: LINEAR: 0.1 mm ANGULAR: N/A		FINISH:		DEBUR AND BREAK SHARP EDGES	DO NOT SCALE DRAWING	REVISION: 0.1
	NAME	SIGNATURE	DATE		TITLE: M42 Compression Nut - 22 mm hole	
DRAWN	Nicolaas Hallatt		07/11/17			
CHK'D						
APPV'D						
MFG						
Q.A				MATERIAL: Carbon Steel	DWG NO. NH/UCT-003	A3
				WEIGHT: 0.47	SCALE:1:1	SHEET 1 OF 1

Notes:
1. 4 off required
2. Material: Carbon Steel
3. For any queries contact Nicolaas Hallatt at 0845887708.
4. Please confirm material before work start.

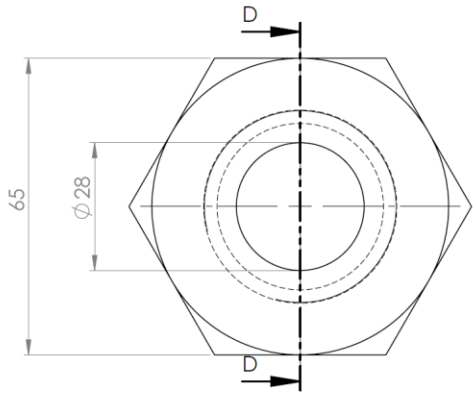

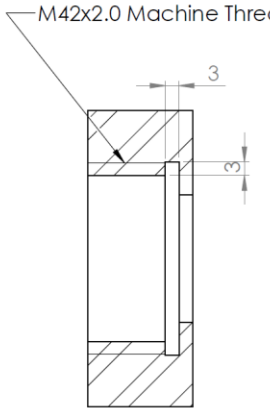

SECTION D-D

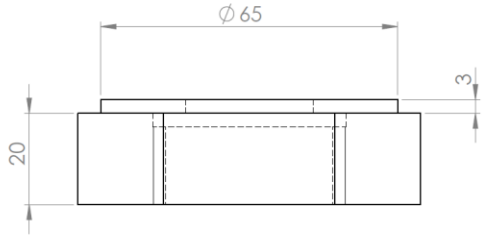

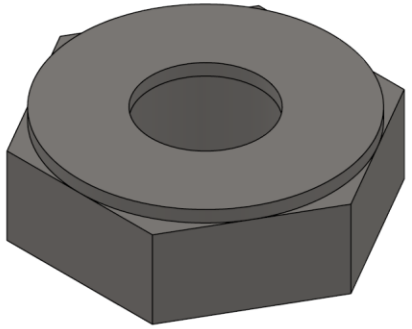

UNLESS OTHERWISE SPECIFIED: DIMENSIONS ARE IN MILLIMETERS SURFACE FINISH: 3.2 µm TOLERANCES: LINEAR: 0.1 mm ANGULAR: N/A		FINISH:		DEBUR AND BREAK SHARP EDGES	DO NOT SCALE DRAWING	REVISION: 0.1
	NAME	SIGNATURE	DATE		TITLE: M42 Compression Nut - 28 mm hole	
DRAWN	Nicolaas Hallatt		07/11/17			
CHK'D						
APPV'D						
MFG						
Q.A				MATERIAL: Carbon Steel	DWG NO. NH/UCT-004	A3
				WEIGHT: 0.46	SCALE:1:1	SHEET 1 OF 1

Item No.	Quantity	Description	Material
1	2000 mm	32NB SCH80 Pipe - 1000 mm each side	A106 Gr B
2	2	32NB AMSE B16.5 Class 150 Slip On Flange	A105
3	1	Gasket, bolts and nuts to suit 2	Rubber
4	60 mm	25NB SCH 40 Pipe	A106 Gr B
5	2	25NB Pipe Socket	Galvinised pipe
6	4	Support 3 mm thick plate	Carbon Steel
7	4	Support 3 mm thick plate	Carbon Steel

Support Dimensions Mirrored Around Centre

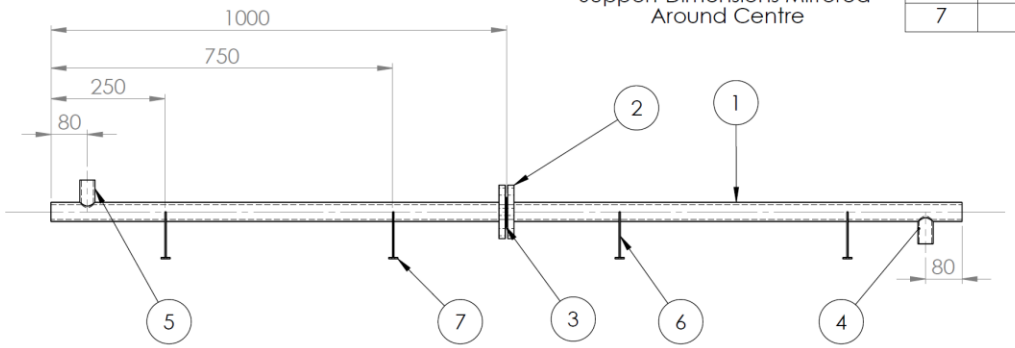

Notes:
1. Design Pressure: 10 Bar
2. Design Temp: 90 °C
3. Fluid: Water
4. SANS 347 Hazard Category: Not Regulated
5. All nozzles in the Set-on configuration
6. Support to be tag-welded
7. Only visual inspection required

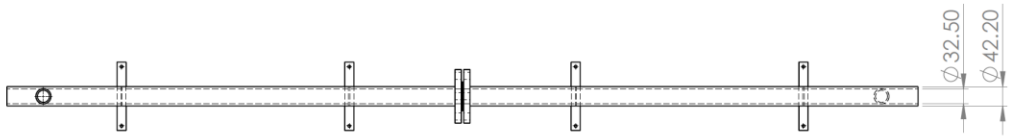

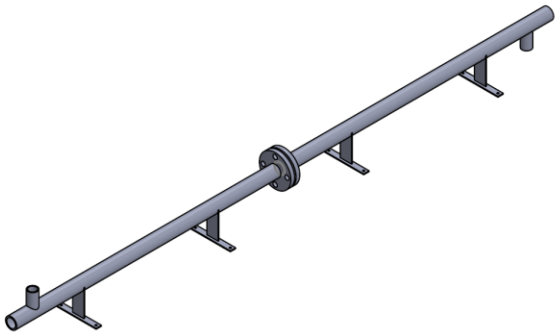

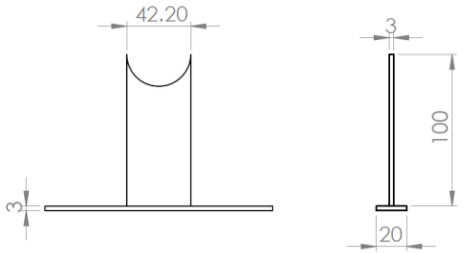

Support Details - 4 off required

UNLESS OTHERWISE SPECIFIED: DIMENSIONS ARE IN MILLIMETERS SURFACE FINISH: TOLERANCES: LINEAR: ANGULAR:		FINISH:			DEBUR AND BREAK SHARP EDGES	DO NOT SCALE DRAWING	REVISION
	NAME	SIGNATURE	DATE			TITLE: Test Section	
DRAWN	N. Hallatt		2018/03/28				
CHK'D							
APP'V'D							
MFG							
Q.A				MATERIAL: See bill of materials		DWG NO. NH/UCT-005	A3
				WEIGHT:		SCALE:1:20	SHEET 1 OF 1

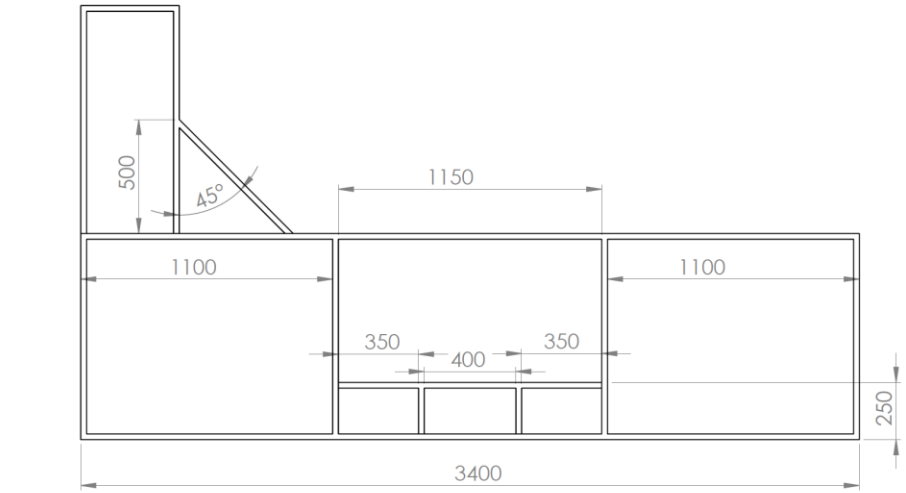

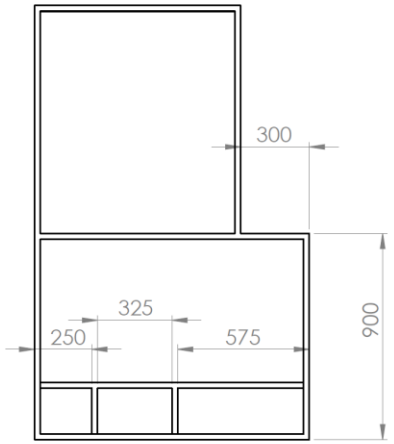

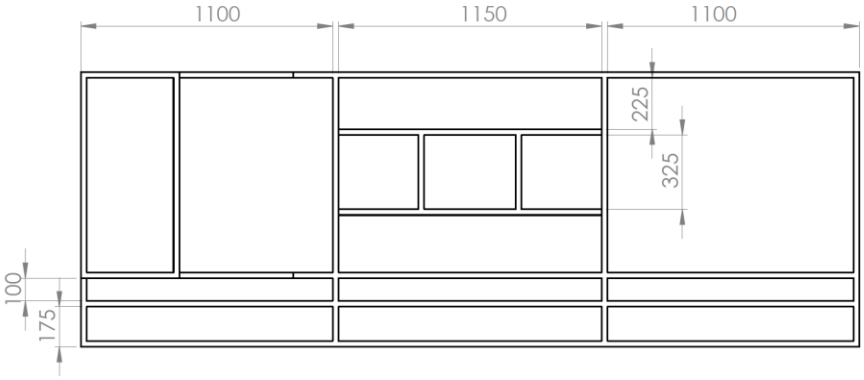

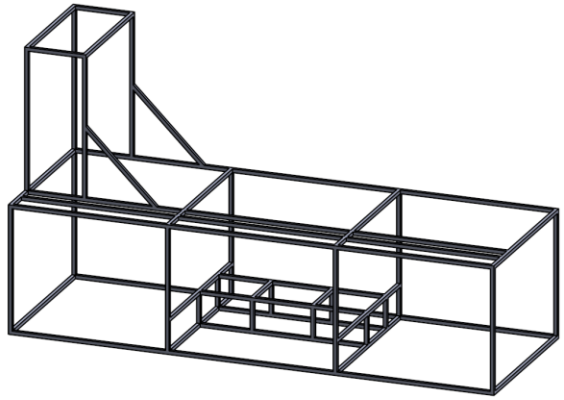

Notes:
1. 25mm x 2 mm square tubing to be used
2. All material to be mild steel
3. All connections to be welded
4. No special weld preps are required
5. Total required material length: 43000 mm
6. Order: 10 x 6000mm lengths
7. Frame to be coated with anti rust primer
8. For any queries contact Nicolaas Hallatt at 084 588 7708

UNLESS OTHERWISE SPECIFIED: DIMENSIONS ARE IN MILLIMETERS SURFACE FINISH: TOLERANCES: LINEAR: ANGULAR:		FINISH:		DEBUR AND BREAK SHARP EDGES	DO NOT SCALE DRAWING	REVISION
	NAME	SIGNATURE	DATE		TITLE: Frame	
DRAWN	NH		18-04-2018			
CHK'D						
APP'D						
MFG						
Q.A				MATERIAL: Mild Steel	DWG NO. NH/UCT-006	A3
				WEIGHT:	SCALE:1:20	SHEET 1 OF 1

Appendix C. Cold Loop inlet Temperature Measurement System Calibration Certificate

All 4 temperature measurement system was calibrated and calibration certificates provided. For practical purposes, only the cold loop inlet calibration certificates are provided.

Unique Metrology
Eskom Research & Innovation Centre
Lower Germiston Road • Rosherville
P O Box 145296 • Bracken Gardens • 1452
Tel: 011 626 3808 • Cell: 083 254 3635 • Fax: 086 610 4196
Web: www.unimet.co.za

sanas Calibration Laboratory
205 306 1406

SANAS ACCREDITED CALIBRATION LABORATORY No 306

TEMPERATURE METROLOGY

CERTIFICATE OF CALIBRATION

Date of issue : 13/09/2018

Certificate No : 1809T8022-1

Technical Signatory

Signature Removed

M Mathieson.

The results of all measurements are traceable to the national measuring standards.

The values in this certificate are correct at the time of calibration. Subsequently the accuracy will depend on such factors as the care executed in handling and use of the device, and the frequency of use. Recalibration should be performed after the period so chosen to ensure that the instrument's accuracy remains within the desired limits.

The South African National Accreditation System (SANAS) is a member of the International Laboratory Accreditation Cooperation (ILAC) Mutual Recognition Arrangement (MRA). This arrangement allows for the mutual recognition of technical test and calibration data by the member accreditation bodies worldwide. For more information on the Arrangement please contact www.ilac.org.

Unique Metrology
Eskom Research & Innovation Centre
Lower Germiston Road • Rosherville
P O Box 145296 • Bracken Gardens • 1452
Tel: 011 626 3808 • Cell: 083 254 3635 • Fax: 086 610 4196
Web: www.unimet.co.za

sanas Calibration Laboratory
205 306 1406

CERTIFICATE OF CALIBRATION

Certificate Number	:	1809T8022-1		
Calibration of a	:	Resistance Thermometer		
Manufacturer & Type	:	PT 100 & Picolog datalogger,		
Serial Number	:	CL-IN & CX015/81		
Calibrated for	:	Eskom Holdings SOC Limited, RT&D, Flow Sciences.		
Procedure Number	:	53-164		
Date of Calibration	:	10/09/2018		
Date of Issue	:	13/09/2018		
Laboratory Environment	:	22.9 °C		
Reference Standards	:	101-S-05	Time Electronics, 609N	S/N 1206L5
	:	101-S-07	Hewlett Packard, 34401A	S/N 3146A70688
	:	306-S-02	Rosemount, PRT	S/N 451

Reference Temperature °C	Indicated Reading Ohms	Equivalent Temperature °C	Correction °C
0.022	100.004	0.010	0.012
10.016	103.908	10.015	0.001
19.990	107.786	19.982	0.008
34.927	113.581	34.933	-0.006
55.900	121.670	55.914	-0.014

The uncertainty of measurement is ± 0.10°C
The reported uncertainty is based on a standard uncertainty multiplied by a coverage factor of k=2, which unless specifically stated otherwise, provides a confidence level of 95%, in accordance with the Guide to the Expression of Uncertainty in Measurement, first edition, 1993.

Comments : The actual uncertainty of measurement was calculated to be 0.041 Degrees C
The laboratories accreditation schedule is proven for ±0.1 dedrees C.

Signature Removed
Calibrated by : M Mathieson Technical Signatory

Unique Metrology
Eskom Research & Innovation Centre
Lower Germiston Road • Rosherville
P O Box 145296 • Bracken Gardens • 1452
Tel: 011 626 3808 • Cell: 083 254 3635 • Fax: 086 610 4196
Web: www.unimet.co.za

sanas Calibration Laboratory
205 306 1406

CERTIFICATE OF CALIBRATION

Certificate Number	:	1809T8022-1		
Calibration of a	:	Resistance Thermometer		
Manufacturer & Type	:	PT 100		
Serial Number	:	CL-IN & CX015/81		
Calibrated for	:	Eskom Holdings SOC Limited, RT&D, Flow Sciences.		
Procedure Number	:	53-164		
Date of Calibration	:	10/09/2018		
Date of Issue	:	13/09/2018		
Laboratory Environment	:	22.9 °C		
Reference Standards	:	101-S-05	Time Electronics, 609N	S/N 1206L5
	:	101-S-07	Hewlett Packard, 34401A	S/N 3146A70688
	:	306-S-15	Rosemount, Series 78 , Pt100	S/N 0661870

PT 100 RESISTANCE Ohms	REFERENCE TEMPERATURE °C
100.004	0.022
107.786	19.990
113.581	34.933
121.670	55.900

Equation constants

Ro =	100.004
a =	-2.2830E-02
b =	2.0332E-02
c =	-4.2250E-02

Measurement check

Measured =	103.900
Ratio =	1.0389
Wr90 =	1.0398
X =	-0.9757
Temp =	9.999
Check	10.016
Diff	-0.017

The uncertainty of measurement is ± 0.10°C
The reported uncertainty is based on a standard uncertainty multiplied by a coverage factor of k=2, which unless specifically stated otherwise, provides a confidence level of 95%, in accordance with the Guide to the Expression of Uncertainty in Measurement, first edition, 1993.

Comments : The customers probe was immersed to constant depth of 70 mm and compared with a reference thermometer during the calibration.

Signature Removed
Calibrated by : M Mathieson Technical Signatory

Appendix D. Repeatabilty Test Results

TEST REFERENCE	Repeatability Test - Summary				**Test Date and Time**			N/A
Tested By	N Hallatt				**No of Tests Completed**			5
Input Values	**Test No.**		**1**	**2**	**3**	**4**	**5**	**Average**
Test Date	TD	-	2018/11/21	2018/11/21	2018/11/21	2018/11/29	2018/11/29	N/A
Start time	s_{tart}	hh:mm	13:41:50	14:18:02	14:56:25	10:39:01	11:20:32	N/A
Stop time	t_{stop}	hh:mm	14:03:31	14:39:42	15:18:05	10:55:28	11:36:45	N/A
Element 1 Power	PE1	kW	3.76	3.76	3.76	3.76	3.76	3.76
Element 2 Power	PE2	kW	0.00	0.00	0.00	0.00	0.00	0.00
Element 3 Power	PE3	kW	3.84	3.84	3.84	3.84	3.84	3.84
Element 4 Power	PE4	kW	3.71	3.71	3.71	3.71	3.71	3.71
Element 5 Power	PE5	kW	2.56	2.49	2.16	2.47	2.01	2.34
Cold Loop Flow	m_{CL}	kg/s	0.527	0.528	0.529	0.523	0.527	0.527
Hot Loop Flow	m_{HL}	kg/s	0.715	0.722	0.719	0.714	0.716	0.717
Cold Loop T-In	T_{CLI}	°C	21.77	21.79	21.81	20.72	20.59	21.34
Cold Loop T-Out	T_{CLO}	°C	28.26	28.21	28.29	27.35	27.27	27.87
Cold Loop ΔT	ΔT_{CL}	°C	6.49	6.41	6.48	6.63	6.68	6.54
Hot Loop T-In	T_{HLI}	°C	59.96	59.87	59.94	59.97	59.96	59.94
Hot Loop T-Out	T_{HLO}	°C	55.23	55.26	55.27	55.17	55.10	55.21
Hot Loop ΔT	ΔT_{HL}	°C	4.73	4.61	4.67	4.80	4.86	4.73
Cold Loop Pressure	P_{CL}	kPa	165.00	165.00	165.00	165.00	165.00	165.00
Hot Loop Pressure	P_{HL}	kPa	105.00	105.00	105.00	105.00	105.00	105.00
Calculated Values	**Test No.**		**1**	**2**	**3**	**4**	**5**	**Average**
Heat Transfer Area	A	m2	0.12	0.12	0.12	0.12	0.12	0.12
CL inlet enthalpy	h_{CLI}	kJ/kg	91.48	91.58	91.65	87.08	86.56	89.67
CL outlet enthalpy	h_{CLO}	kJ/kg	118.60	118.41	118.73	114.82	114.48	117.01
HL inlet enthalpy	h_{HLI}	kJ/kg	251.06	250.68	250.97	251.10	251.04	250.97
HL outlet enthalpy	h_{HLO}	kJ/kg	231.29	231.41	231.46	231.02	230.73	231.18
CL Heat Transfer	Q_{CL}	kW	14.31	14.16	14.33	14.52	14.71	14.40
HL Heat Transfer	Q_{HL}	kW	14.14	13.92	14.04	14.34	14.54	14.20
ΔT at CL inlet	ΔT_{CLI}	°C	33.46	33.47	33.46	34.45	34.50	33.87
ΔT at CL outlet	ΔT_{CLO}	°C	31.71	31.66	31.65	32.62	32.69	32.06
Log Mean ΔT	LMTD	°C	32.58	32.56	32.55	33.53	33.59	32.96
Overall HT Coefficient	$U_{x\,CL}$	W/m^2K	3678.45	3644.67	3686.85	3627.79	3668.26	3661.20
HT Coef. Uncertainty	$U_{R,U}$	%	2.269	2.286	2.281	2.238	2.220	2.259
Ux vs Umean	UDFM	%	-0.47	0.45	-0.70	0.92	-0.19	-
HTC Mean	U_{mean}	W/m^2K	3661.20					

Appendix E. LP Heater Tube Test Sample 1 - Test Results

TEST	LP Heater 3 - Tube 1 - Fouled				**Test Date**		11 February 2019			Page	
Tested By	N Hallatt				**No of Tests**		8			1 of 1	
Input Values	**Test Run**		**1**	**2**	**3**	**4**	**5**	**6**	**7**	**8**	**Avg.**
Start time	$Time_{Start}$	hh:mm	12:48	12:50	12:52	12:54	12:56	12:58	13:00	13:02	N/A
Stop time	$Time_{Stop}$	hh:mm	12:49	12:51	12:54	12:56	12:58	13:00	13:02	13:04	N/A
Test Sect Amb. T	$T_{TS\ amb}$	°C	25.0	25.0	25.0	25.0	25.0	25.0	25.0	25.0	25.0
Test Equip. Amb T	$T_{TE\ amb}$	°C	24.0	24.0	24.0	24.0	24.0	24.0	24.0	24.0	24.0
Element 1 Power	P_{E1}	kW	0.0	0.0	0.0	0.0	0.0	0.0	0.0	0.0	0.0
Element 2 Power	P_{E2}	kW	3.8	3.8	3.8	3.8	3.8	3.8	3.8	3.8	3.8
Element 3 Power	P_{E3}	kW	3.8	3.8	3.8	3.8	3.8	3.8	3.8	3.8	3.8
Element 4 Power	P_{E4}	kW	3.7	3.7	3.7	3.7	3.7	3.7	3.7	3.7	3.7
Element 5 Power	P_{E5}	kW	0.4	0.8	2.0	2.5	2.6	3.1	2.8	1.3	1.9
Cold Loop Flow	m_{CL}	kg/s	0.5	0.5	0.5	0.5	0.5	0.5	0.5	0.5	0.5
Hot Loop Flow	m_{HL}	kg/s	0.8	0.7	0.7	0.7	0.7	0.7	0.7	0.7	0.7
Cold Loop T-In	T_{CLI}	°C	22.7	22.7	22.7	22.7	22.7	22.7	22.7	22.6	22.7
Cold Loop T-Out	T_{CLO}	°C	27.8	27.8	27.7	27.7	27.7	27.7	27.7	27.7	27.7
Cold Loop ΔT	ΔT_{CL}	°C	5.1	5.1	5.0	5.0	5.0	5.0	5.1	5.1	5.1
Hot Loop T-In	T_{HLI}	°C	60.3	59.9	59.7	59.9	59.8	59.8	60.1	60.4	60.0
Hot Loop T-Out	T_{HLO}	°C	56.6	56.3	56.0	56.2	56.2	56.1	56.3	56.6	56.3
Hot Loop ΔT	ΔT_{HL}	°C	3.7	3.7	3.7	3.7	3.7	3.7	3.7	3.8	3.7
Cold Loop Pressure	P_{CL}	kPa	164.0	164.0	164.0	164.0	164.0	164.0	164.0	164.0	164.0
Hot Loop Pressure	P_{HL}	kPa	104.0	104.0	104.0	104.0	104.0	104.0	104.0	104.0	104.0
Calculated Values	**Test Run**		**1**	**2**	**3**	**4**	**5**	**6**	**7**	**8**	**Avg.**
Heat Transfer Area	A	m^2	0.1	0.1	0.1	0.1	0.1	0.1	0.1	0.1	0.1
CL inlet enthalpy	h_{CLI}	kJ/kg	95.5	95.5	95.5	95.4	95.4	95.2	95.2	95.2	95.4
CL outlet enthalpy	h_{CLO}	kJ/kg	116.9	116.6	116.4	116.5	116.4	116.2	116.4	116.5	116.5
HL inlet enthalpy	h_{HLI}	kJ/kg	252.6	251.0	249.9	250.7	250.5	250.3	251.5	253.0	251.2
HL outlet enthalpy	h_{HLO}	kJ/kg	237.1	235.7	234.7	235.3	235.2	234.9	235.9	237.2	235.8
CL Heat Transfer	Q_{CL}	kW	11.7	11.5	11.4	11.4	11.4	11.4	11.5	11.6	11.5
HL Heat Transfer	Q_{HL}	kW	11.7	11.5	11.4	11.5	11.4	11.4	11.6	11.6	11.5
ΔT at CL inlet	ΔT_{CLI}	°C	33.9	33.6	33.3	33.5	33.4	33.4	33.7	34.0	33.6
ΔT at CL outlet	ΔT_{CLO}	°C	32.5	32.2	32.0	32.1	32.1	32.1	32.3	32.7	32.2
Log Mean ΔT	LMTD	°C	33.2	32.8	32.6	32.8	32.8	32.8	33.0	33.3	32.9
Overall HT Coefficient	U_x	W/m^2K	3493.3	3480.6	3472.5	3469.3	3462.4	3467.9	3466.1	3457.7	3471.2
HTC R-R Dev'n	U_{TTTD}	%	NA	-0.36	-0.23	-0.09	-0.20	0.16	-0.05	-0.24	N/A
Ux versus Umean	U_{DFM}	%	0.64	0.27	0.04	-0.06	-0.25	-0.10	-0.15	-0.39	N/A
HTC Mean	U_{mean}	W/m^2K	3471.21								

TEST	LP Heater 3 - Tube 1 - Half Clean				**Test Date**		11 February 2019			Page	
Tested By	N Hallatt				**No of Tests**		8			1 of 1	
Input Values	**Test Run**		**1**	**2**	**3**	**4**	**5**	**6**	**7**	**8**	**Avg.**
Start time	TimeStart	hh:mm	13:44	13:46	13:48	13:50	13:52	13:54	13:56	13:58	N/A
Stop time	TimeStop	hh:mm	13:45	13:47	13:49	13:51	13:53	13:55	13:57	14:00	N/A
Test Sect Amb. T	TTS amb	°C	25.0	25.0	25.0	25.0	25.0	25.0	25.0	25.0	25.0
Test Equip. Amb T	TTE amb	°C	24.0	24.0	24.0	24.0	24.0	24.0	24.0	24.0	24.0
Element 1 Power	PE1	kW	0.0	0.0	0.0	0.0	0.0	0.0	0.0	0.0	0.0
Element 2 Power	PE2	kW	3.8	3.8	3.8	3.8	3.8	3.8	3.8	3.8	3.8
Element 3 Power	PE3	kW	3.8	3.8	3.8	3.8	3.8	3.8	3.8	3.8	3.8
Element 4 Power	PE4	kW	3.7	3.7	3.7	3.7	3.7	3.7	3.7	3.7	3.7
Element 5 Power	PE5	kW	1.8	0.9	0.3	0.3	0.9	2.4	2.5	1.7	1.4
Cold Loop Flow	mCL	kg/s	0.5	0.5	0.5	0.5	0.5	0.5	0.5	0.5	0.5
Hot Loop Flow	mHL	kg/s	0.7	0.7	0.7	0.7	0.7	0.7	0.7	0.7	0.7
Cold Loop T-In	TCLI	°C	22.7	22.7	22.7	22.7	22.7	22.6	22.6	22.6	22.7
Cold Loop T-Out	TCLO	°C	28.0	28.0	28.1	28.1	28.0	27.9	27.9	27.9	28.0
Cold Loop ΔT	ΔTCL	°C	5.3	5.3	5.3	5.3	5.3	5.2	5.3	5.3	5.3
Hot Loop T-In	THLI	°C	60.2	60.3	60.5	60.3	59.9	59.7	60.0	60.3	60.2
Hot Loop T-Out	THLO	°C	56.3	56.5	56.6	56.5	56.1	55.9	56.2	56.4	56.3
Hot Loop ΔT	ΔTHL	°C	3.8	3.8	3.9	3.8	3.8	3.8	3.9	3.9	3.8
Cold Loop Pressure	PCL	kPa	164.0	164.0	164.0	164.0	164.0	164.0	164.0	164.0	164.0
Hot Loop Pressure	PHL	kPa	104.0	104.0	104.0	104.0	104.0	104.0	104.0	104.0	104.0
Calculated Values	**Test Run**		**1**	**2**	**3**	**4**	**5**	**6**	**7**	**8**	**Avg.**
Heat Transfer Area	A	m2	0.1	0.1	0.1	0.1	0.1	0.1	0.1	0.1	0.1
CL inlet enthalpy	hCLI	kJ/kg	95.5	95.4	95.5	95.5	95.4	95.1	95.1	95.1	95.3
CL outlet enthalpy	hCLO	kJ/kg	117.7	117.7	117.9	117.8	117.4	116.9	117.1	117.3	117.5
HL inlet enthalpy	hHLI	kJ/kg	251.9	252.7	253.1	252.7	250.8	249.8	251.3	252.5	251.9
HL outlet enthalpy	hHLO	kJ/kg	235.9	236.6	236.9	236.7	235.0	233.9	235.2	236.3	235.8
CL Heat Transfer	QCL	kW	12.1	12.1	12.1	12.1	12.0	11.8	11.9	12.1	12.0
HL Heat Transfer	QHL	kW	12.0	12.0	12.0	11.9	11.8	11.7	11.8	11.9	11.9
ΔT at CL inlet	ΔTCLI	°C	33.6	33.8	33.8	33.8	33.4	33.2	33.5	33.8	33.6
ΔT at CL outlet	ΔTCLO	°C	32.1	32.3	32.4	32.3	31.9	31.8	32.1	32.4	32.2
Log Mean ΔT	LMTD	°C	32.9	33.0	33.1	33.0	32.7	32.5	32.8	33.1	32.9
Overall HT Coefficient	Ux	W/m2K	3655.8	3651.9	3648.4	3652.5	3642.4	3625.4	3617.5	3625.1	3639.9
HTC R-R Dev'n	UTTTD	%	NA	-0.11	-0.09	0.11	-0.28	-0.47	-0.22	0.21	N/A
Ux versus Umean	UDFM	%	0.44	0.33	0.24	0.35	0.07	-0.40	-0.61	-0.41	N/A
HTC Mean	Umean	W/m2K	3639.87								

TEST	LP Heater 3 - Tube 1 - Clean				**Test Date**		11 February 2019			Page	
Tested By	N Hallatt				**No of Tests**		8			1 of 1	
Input Values	**Test Run**		**1**	**2**	**3**	**4**	**5**	**6**	**7**	**8**	**Avg.**
Start time	TimeStart	hh:mm	14:25	14:27	14:29	14:31	14:33	14:35	14:37	14:39	N/A
Stop time	TimeStop	hh:mm	14:26	14:29	14:31	14:33	14:35	14:37	14:39	14:41	N/A
Test Sect Amb. T	TTS amb	°C	25.0	25.0	25.0	25.0	25.0	25.0	25.0	25.0	25.0
Test Equip. Amb T	TTE amb	°C	24.0	24.0	24.0	24.0	24.0	24.0	24.0	24.0	24.0
Element 1 Power	PE1	kW	0.0	0.0	0.0	0.0	0.0	0.0	0.0	0.0	0.0
Element 2 Power	PE2	kW	3.8	3.8	3.8	3.8	3.8	3.8	3.8	3.8	3.8
Element 3 Power	PE3	kW	3.8	3.8	3.8	3.8	3.8	3.8	3.8	3.8	3.8
Element 4 Power	PE4	kW	3.7	3.7	3.7	3.7	3.7	3.7	3.7	3.7	3.7
Element 5 Power	PE5	kW	1.3	1.2	0.7	0.4	0.2	0.2	0.1	0.1	0.5
Cold Loop Flow	mCL	kg/s	0.5	0.5	0.5	0.5	0.5	0.5	0.5	0.5	0.5
Hot Loop Flow	mHL	kg/s	0.8	0.7	0.7	0.7	0.7	0.7	0.7	0.7	0.7
Cold Loop T-In	TCLI	°C	22.7	22.7	22.7	22.7	22.7	22.6	22.6	22.6	22.7
Cold Loop T-Out	TCLO	°C	28.2	28.1	28.1	28.2	28.1	28.1	28.1	28.1	28.1
Cold Loop ΔT	ΔTCL	°C	5.5	5.5	5.5	5.5	5.5	5.5	5.5	5.5	5.5
Hot Loop T-In	THLI	°C	60.0	60.2	60.2	60.3	60.3	60.3	60.3	60.3	60.2
Hot Loop T-Out	THLO	°C	56.1	56.2	56.3	56.3	56.3	56.3	56.3	56.3	56.3
Hot Loop ΔT	ΔTHL	°C	3.9	3.9	4.0	4.0	4.0	4.0	4.0	4.0	4.0
Cold Loop Pressure	PCL	kPa	164.0	164.0	164.0	164.0	164.0	164.0	164.0	164.0	164.0
Hot Loop Pressure	PHL	kPa	104.0	104.0	104.0	104.0	104.0	104.0	104.0	104.0	104.0
Calculated Values	**Test Run**		**1**	**2**	**3**	**4**	**5**	**6**	**7**	**8**	**Avg.**
Heat Transfer Area	A	m2	0.1	0.1	0.1	0.1	0.1	0.1	0.1	0.1	0.1
CL inlet enthalpy	hCLI	kJ/kg	95.3	95.2	95.3	95.4	95.3	95.1	95.1	95.0	95.2
CL outlet enthalpy	hCLO	kJ/kg	118.2	118.1	118.1	118.3	118.2	118.0	118.0	117.8	118.1
HL inlet enthalpy	hHLI	kJ/kg	251.2	251.9	252.2	252.4	252.5	252.5	252.5	252.3	252.2
HL outlet enthalpy	hHLO	kJ/kg	234.9	235.4	235.6	235.9	235.9	235.9	235.8	235.6	235.6
CL Heat Transfer	QCL	kW	12.4	12.4	12.4	12.4	12.4	12.4	12.4	12.4	12.4
HL Heat Transfer	QHL	kW	12.4	12.3	12.3	12.3	12.3	12.3	12.3	12.3	12.3
ΔT at CL inlet	ΔTCLI	°C	33.4	33.5	33.6	33.6	33.6	33.7	33.7	33.7	33.6
ΔT at CL outlet	ΔTCLO	°C	31.8	32.0	32.1	32.1	32.2	32.2	32.2	32.2	32.1
Log Mean ΔT	LMTD	°C	32.6	32.8	32.8	32.9	32.9	32.9	32.9	32.9	32.8
Overall HT Coefficient	Ux	W/m2K	3795.9	3765.0	3763.8	3761.9	3750.7	3758.7	3749.4	3742.4	3761.0
HTC R-R Dev'n	UTTTD	%	N/A	-0.81	-0.03	-0.05	-0.30	0.21	-0.25	-0.19	N/A
Ux versus Umean	UDFM	%	0.93	0.11	0.07	0.02	-0.27	-0.06	-0.31	-0.49	N/A
HTC Mean	Umean	W/m2K	3760.96								

Appendix F. LP Heater Tube Test Sample 1 - Fouling Factor Uncertainty Calculation

Fouling Factor (R_f) - Uncertainty Analysis

Reference:C:\Users\hallatNJ\Desktop\Masters\1. Dissertation\Mathcad Models\Water-Steam IAPWS-IF97 rev A.3.xmcd

1. Geometric Variables

$L := 2m$

$d_o := 16mm$

$A := \pi \cdot d_o \cdot L = 0.101m^2$

2. Process Variables

$P_{HL} := 105kPa \quad P_{CL} := 165kPa$

$m_{dot.CL.c} := 0.542\frac{kg}{s}$ $\quad$ $m_{dot.CL.f} := 0.543\frac{kg}{s}$

$T_{CL.in.c} := 22.664°C$ $\quad$ $T_{CL.in.f} := 22.698°C$

$T_{CL.out.c} := 28.133°C$ $\quad$ $T_{CL.out.f} := 27.749°C$

$T_{HL.in.c} := 60.230°C$ $\quad$ $T_{HL.in.f} := 59.993°C$

$T_{HL.out.c} := 56.268°C$ $\quad$ $T_{HL.out.f} := 56.300°C$

$$Cp_{CL.c} := Cp_{steam}\left[P_{CL}, \frac{\left(T_{CL.in.c} + T_{CL.out.c}\right)}{2}, "", "", "", ""\right] = 4.18153 \times 10^{3}\,\frac{m^2}{K \cdot s^2}$$

$$Cp_{CL.f} := Cp_{steam}\left[P_{CL}, \frac{\left(T_{CL.in.f} + T_{CL.out.f}\right)}{2}, "", "", "", ""\right] = 4.18161 \times 10^{3}\,\frac{m^2}{K \cdot s^2}$$

$$U_c := \frac{m_{dot.CL.c} \cdot Cp_{CL.c} \cdot \left(T_{CL.out.c} - T_{CL.in.c}\right)}{A \cdot \left(T_{HL.in.c} - T_{CL.out.c} - T_{HL.out.c} + T_{CL.in.c}\right) \ln\left[\frac{\left(T_{HL.in.c} - T_{CL.out.c}\right)}{\left(T_{HL.out.c} - T_{CL.in.c}\right)}\right]} = 3753.849\,\frac{W}{m^2 K}$$

$$U_f := \frac{m_{dot.CL.f} \cdot Cp_{CL.f} \cdot \left(T_{CL.out.f} - T_{CL.in.f}\right)}{A \cdot \left(T_{HL.in.f} - T_{CL.out.f} - T_{HL.out.f} + T_{CL.in.f}\right) \ln\left[\frac{\left(T_{HL.in.f} - T_{CL.out.f}\right)}{\left(T_{HL.out.f} - T_{CL.in.f}\right)}\right]} = 3465.636\,\frac{W}{m^2 K}$$

$$R_f := \frac{1}{U_f} - \frac{1}{U_c} = 2.215 \times 10^{-5} \cdot \frac{m^2 K}{W}$$

3. Evaluation of Partial Derivatives to determine Sensitivity factors

$$\Delta m_{dot.CL.f} := \frac{d}{dm_{dot.CL.c}}\left[\frac{1}{\frac{m_{dot.CL.f} \cdot Cp_{CL.f} \cdot \left(T_{CL.out.f} - T_{CL.in.f}\right)}{A \cdot \left(T_{HL.in.f} - T_{CL.out.f} - T_{HL.out.f} + T_{CL.in.f}\right) \ln\left[\frac{\left(T_{HL.in.f} - T_{CL.out.f}\right)}{\left(T_{HL.out.f} - T_{CL.in.f}\right)}\right]}} - \frac{1}{\frac{m_{dot.CL.c} \cdot Cp_{CL.c} \cdot \left(T_{CL.out.c} - T_{CL.in.c}\right)}{A \cdot \left(T_{HL.in.c} - T_{CL.out.c} - T_{HL.out.c} + T_{CL.in.c}\right) \ln\left[\frac{\left(T_{HL.in.c} - T_{CL.out.c}\right)}{\left(T_{HL.out.c} - T_{CL.in.c}\right)}\right]}}\right] = 4.915 \times 10^{-4}\,\frac{K \cdot s^4}{kg^2}$$

$$\Delta m_{dot.CL.c} := \frac{d}{dm_{dot.CL.f}}\left[\frac{1}{\frac{m_{dot.CL.f}\cdot Cp_{CL.f}\cdot\left(T_{CL.out.f}-T_{CL.in.f}\right)\ln\left[\frac{\left(T_{HL.in.f}-T_{CL.out.f}\right)}{\left(T_{HL.out.f}-T_{CL.in.f}\right)}\right]}{A\cdot\left(T_{HL.in.f}-T_{CL.out.f}-T_{HL.out.f}+T_{CL.in.f}\right)}} - \frac{1}{\frac{m_{dot.CL.c}\cdot Cp_{CL.c}\cdot\left(T_{CL.out.c}-T_{CL.in.c}\right)\ln\left[\frac{\left(T_{HL.in.c}-T_{CL.out.c}\right)}{\left(T_{HL.out.c}-T_{CL.in.c}\right)}\right]}{A\cdot\left(T_{HL.in.c}-T_{CL.out.c}-T_{HL.out.c}+T_{CL.in.c}\right)}}\right] = -5.314\times 10^{-4}\,\frac{K\cdot s^4}{kg^2}$$

$$\Delta T_{CL.in.c} := \frac{d}{dT_{CL.in.c}}\left[\frac{1}{\frac{m_{dot.CL.f}\cdot Cp_{CL.f}\cdot\left(T_{CL.out.f}-T_{CL.in.f}\right)\ln\left[\frac{\left(T_{HL.in.f}-T_{CL.out.f}\right)}{\left(T_{HL.out.f}-T_{CL.in.f}\right)}\right]}{A\cdot\left(T_{HL.in.f}-T_{CL.out.f}-T_{HL.out.f}+T_{CL.in.f}\right)}} - \frac{1}{\frac{m_{dot.CL.c}\cdot Cp_{CL.c}\cdot\left(T_{CL.out.c}-T_{CL.in.c}\right)\ln\left[\frac{\left(T_{HL.in.c}-T_{CL.out.c}\right)}{\left(T_{HL.out.c}-T_{CL.in.c}\right)}\right]}{A\cdot\left(T_{HL.in.c}-T_{CL.out.c}-T_{HL.out.c}+T_{CL.in.c}\right)}}\right] = -4.472\times 10^{-5}\,\frac{s^3}{kg}$$

$$\Delta T_{CL.in.f} := \frac{d}{dT_{CL.in.f}}\left[\frac{1}{\frac{m_{dot.CL.f}\cdot Cp_{CL.f}\cdot\left(T_{CL.out.f}-T_{CL.in.f}\right)\ln\left[\frac{\left(T_{HL.in.f}-T_{CL.out.f}\right)}{\left(T_{HL.out.f}-T_{CL.in.f}\right)}\right]}{A\cdot\left(T_{HL.in.f}-T_{CL.out.f}-T_{HL.out.f}+T_{CL.in.f}\right)}} - \frac{1}{\frac{m_{dot.CL.c}\cdot Cp_{CL.c}\cdot\left(T_{CL.out.c}-T_{CL.in.c}\right)\ln\left[\frac{\left(T_{HL.in.c}-T_{CL.out.c}\right)}{\left(T_{HL.out.c}-T_{CL.in.c}\right)}\right]}{A\cdot\left(T_{HL.in.c}-T_{CL.out.c}-T_{HL.out.c}+T_{CL.in.c}\right)}}\right] = 5.28\times 10^{-5}\,\frac{s^3}{kg}$$

$$\Delta T_{CL.out.c} := \frac{d}{dT_{CL.out.c}}\left[\frac{1}{\frac{m_{dot.CL.f}\cdot Cp_{CL.f}\cdot\left(T_{CL.out.f}-T_{CL.in.f}\right)\ln\left[\frac{\left(T_{HL.in.f}-T_{CL.out.f}\right)}{\left(T_{HL.out.f}-T_{CL.in.f}\right)}\right]}{A\cdot\left(T_{HL.in.f}-T_{CL.out.f}-T_{HL.out.f}+T_{CL.in.f}\right)}} - \frac{1}{\frac{m_{dot.CL.c}\cdot Cp_{CL.c}\cdot\left(T_{CL.out.c}-T_{CL.in.c}\right)\ln\left[\frac{\left(T_{HL.in.c}-T_{CL.out.c}\right)}{\left(T_{HL.out.c}-T_{CL.in.c}\right)}\right]}{A\cdot\left(T_{HL.in.c}-T_{CL.out.c}-T_{HL.out.c}+T_{CL.in.c}\right)}}\right] = 5.283\times 10^{-5}\,\frac{s^3}{kg}$$

$$\Delta T_{CL.out.f} := \frac{d}{dT_{CL.out.f}}\left[\frac{1}{\frac{m_{dot.CL.f}\cdot Cp_{CL.f}\cdot\left(T_{CL.out.f}-T_{CL.in.f}\right)\ln\left[\frac{\left(T_{HL.in.f}-T_{CL.out.f}\right)}{\left(T_{HL.out.f}-T_{CL.in.f}\right)}\right]}{A\cdot\left(T_{HL.in.f}-T_{CL.out.f}-T_{HL.out.f}+T_{CL.in.f}\right)}} - \frac{1}{\frac{m_{dot.CL.c}\cdot Cp_{CL.c}\cdot\left(T_{CL.out.c}-T_{CL.in.c}\right)\ln\left[\frac{\left(T_{HL.in.c}-T_{CL.out.c}\right)}{\left(T_{HL.out.c}-T_{CL.in.c}\right)}\right]}{A\cdot\left(T_{HL.in.c}-T_{CL.out.c}-T_{HL.out.c}+T_{CL.in.c}\right)}}\right] = -6.157\times 10^{-5}\,\frac{s^3}{kg}$$

$$\Delta T_{HL.in.c} := \frac{d}{dT_{HL.in.c}}\left[\frac{1}{\frac{m_{dot.CL.f}\cdot Cp_{CL.f}\cdot\left(T_{CL.out.f}-T_{CL.in.f}\right)\ln\left[\frac{\left(T_{HL.in.f}-T_{CL.out.f}\right)}{\left(T_{HL.out.f}-T_{CL.in.f}\right)}\right]}{A\cdot\left(T_{HL.in.f}-T_{CL.out.f}-T_{HL.out.f}+T_{CL.in.f}\right)}} - \frac{1}{\frac{m_{dot.CL.c}\cdot Cp_{CL.c}\cdot\left(T_{CL.out.c}-T_{CL.in.c}\right)\ln\left[\frac{\left(T_{HL.in.c}-T_{CL.out.c}\right)}{\left(T_{HL.out.c}-T_{CL.in.c}\right)}\right]}{A\cdot\left(T_{HL.in.c}-T_{CL.out.c}-T_{HL.out.c}+T_{CL.in.c}\right)}}\right] = -4.118\times 10^{-6}\,\frac{s^3}{kg}$$

$$\Delta T_{HL.in.f} := \frac{d}{dT_{HL.in.f}}\left[\frac{1}{\frac{m_{dot.CL.f}\cdot Cp_{CL.f}\cdot\left(T_{CL.out.f}-T_{CL.in.f}\right)\ln\left[\frac{\left(T_{HL.in.f}-T_{CL.out.f}\right)}{\left(T_{HL.out.f}-T_{CL.in.f}\right)}\right]}{A\cdot\left(T_{HL.in.f}-T_{CL.out.f}-T_{HL.out.f}+T_{CL.in.f}\right)}} - \frac{1}{\frac{m_{dot.CL.c}\cdot Cp_{CL.c}\cdot\left(T_{CL.out.c}-T_{CL.in.c}\right)\ln\left[\frac{\left(T_{HL.in.c}-T_{CL.out.c}\right)}{\left(T_{HL.out.c}-T_{CL.in.c}\right)}\right]}{A\cdot\left(T_{HL.in.c}-T_{CL.out.c}-T_{HL.out.c}+T_{CL.in.c}\right)}}\right] = 4.444\times 10^{-6}\,\frac{s^3}{kg}$$

$$\Delta T_{HL.out.c} := \frac{d}{dT_{HL.out.c}}\left[\frac{1}{\frac{m_{dot.CL.f}\cdot Cp_{CL.f}\cdot\left(T_{CL.out.f}-T_{CL.in.f}\right)\ln\left[\frac{\left(T_{HL.in.f}-T_{CL.out.f}\right)}{\left(T_{HL.out.f}-T_{CL.in.f}\right)}\right]}{A\cdot\left(T_{HL.in.f}-T_{CL.out.f}-T_{HL.out.f}+T_{CL.in.f}\right)}} - \frac{1}{\frac{m_{dot.CL.c}\cdot Cp_{CL.c}\cdot\left(T_{CL.out.c}-T_{CL.in.c}\right)\ln\left[\frac{\left(T_{HL.in.c}-T_{CL.out.c}\right)}{\left(T_{HL.out.c}-T_{CL.in.c}\right)}\right]}{A\cdot\left(T_{HL.in.c}-T_{CL.out.c}-T_{HL.out.c}+T_{CL.in.c}\right)}}\right] = -3.994\times 10^{-6}\,\frac{s^3}{kg}$$

$$\Delta T_{HL.out.f} := \frac{d}{dT_{HL.out.f}}\left[\frac{1}{\frac{m_{dot.CL.f}\cdot Cp_{CL.f}\cdot\left(T_{CL.out.f}-T_{CL.in.f}\right)\ln\left[\frac{\left(T_{HL.in.f}-T_{CL.out.f}\right)}{\left(T_{HL.out.f}-T_{CL.in.f}\right)}\right]}{A\cdot\left(T_{HL.in.f}-T_{CL.out.f}-T_{HL.out.f}+T_{CL.in.f}\right)}} - \frac{1}{\frac{m_{dot.CL.c}\cdot Cp_{CL.c}\cdot\left(T_{CL.out.c}-T_{CL.in.c}\right)\ln\left[\frac{\left(T_{HL.in.c}-T_{CL.out.c}\right)}{\left(T_{HL.out.c}-T_{CL.in.c}\right)}\right]}{A\cdot\left(T_{HL.in.c}-T_{CL.out.c}-T_{HL.out.c}+T_{CL.in.c}\right)}}\right] = 4.323\times 10^{-6}\,\frac{s^3}{kg}$$

$$\Delta Cp_{CL.c} := \frac{d}{dCp_{CL.c}}\left[\frac{1}{\frac{m_{dot.CL.f}\cdot Cp_{CL.f}\cdot\left(T_{CL.out.f}-T_{CL.in.f}\right)\ln\left[\frac{\left(T_{HL.in.f}-T_{CL.out.f}\right)}{\left(T_{HL.out.f}-T_{CL.in.f}\right)}\right]}{A\cdot\left(T_{HL.in.f}-T_{CL.out.f}-T_{HL.out.f}+T_{CL.in.f}\right)}} - \frac{1}{\frac{m_{dot.CL.c}\cdot Cp_{CL.c}\cdot\left(T_{CL.out.c}-T_{CL.in.c}\right)\ln\left[\frac{\left(T_{HL.in.c}-T_{CL.out.c}\right)}{\left(T_{HL.out.c}-T_{CL.in.c}\right)}\right]}{A\cdot\left(T_{HL.in.c}-T_{CL.out.c}-T_{HL.out.c}+T_{CL.in.c}\right)}}\right] = 6.371\times 10^{-8}\,\frac{K^2\cdot s^5}{m^2\cdot kg}$$

$$\Delta Cp_{CL.f} := \frac{d}{dCp_{CL.f}}\left[\frac{1}{\frac{m_{dot.CL.f}\cdot Cp_{CL.f}\cdot\left(T_{CL.out.f}-T_{CL.in.f}\right)\ln\left[\frac{\left(T_{HL.in.f}-T_{CL.out.f}\right)}{\left(T_{HL.out.f}-T_{CL.in.f}\right)}\right]}{A\cdot\left(T_{HL.in.f}-T_{CL.out.f}-T_{HL.out.f}+T_{CL.in.f}\right)}} - \frac{1}{\frac{m_{dot.CL.c}\cdot Cp_{CL.c}\cdot\left(T_{CL.out.c}-T_{CL.in.c}\right)\ln\left[\frac{\left(T_{HL.in.c}-T_{CL.out.c}\right)}{\left(T_{HL.out.c}-T_{CL.in.c}\right)}\right]}{A\cdot\left(T_{HL.in.c}-T_{CL.out.c}-T_{HL.out.c}+T_{CL.in.c}\right)}}\right] = -6.9\times 10^{-8}\,\frac{K^2\cdot s^5}{m^2\cdot kg}$$

4. Random Uncertainty

4.1 Calculation of Instrument Random Uncertainty

$n := 400$ sd = standard deviation from 400 measurements (8 test x 50 measurements each)

$sd_{m.dot.CL.c} := 0.001\frac{kg}{s}$ $sd_{m.dot.CL.f} := 0.001\frac{kg}{s}$

$sd_{T.CL.in.c} := 0.012\Delta°C$ $sd_{T.CL.in.f} := 0.014\Delta°C$

$sd_{T.CL.out.c} := 0.017\Delta°C$ $sd_{T.CL.out.f} := 0.018\Delta°C$

$sd_{T.HL.in.c} := 0.053\Delta°C$ $sd_{T.HL.in.f} := 0.078\Delta°C$

$sd_{T.HL.out.c} := 0.044\Delta°C$ $sd_{T.HL.out.f} := 0.068\Delta°C$

$$s_{mdot.CL.c} := \frac{sd_{mdot.CL.c}}{\sqrt{n}} = 5 \times 10^{-5}\,\frac{kg}{s} \qquad s_{mdot.CL.f} := \frac{sd_{mdot.CL.f}}{\sqrt{n}} = 5 \times 10^{-5}\,\frac{kg}{K \cdot s}\cdot \Delta°C$$

$$s_{T.CL.in.c} := \frac{sd_{T.CL.in.c}}{\sqrt{n}} = 0.0006 \cdot \Delta°C \qquad s_{T.CL.in.f} := \frac{sd_{T.CL.in.f}}{\sqrt{n}} = 0.0007 \cdot \Delta°C$$

$$s_{T.CL.out.c} := \frac{sd_{T.CL.out.c}}{\sqrt{n}} = 0.0009 \cdot \Delta°C \qquad s_{T.CL.out.f} := \frac{sd_{T.CL.out.f}}{\sqrt{n}} = 0.0009 \cdot \Delta°C$$

$$s_{T.HL.in.c} := \frac{sd_{T.HL.in.c}}{\sqrt{n}} = 0.0027 \cdot \Delta°C \qquad s_{T.HL.in.f} := \frac{sd_{T.HL.in.f}}{\sqrt{n}} = 0.0039 \cdot \Delta°C$$

$$s_{T.HL.out.c} := \frac{sd_{T.HL.out.c}}{\sqrt{n}} = 0.0022 \cdot \Delta°C \qquad s_{T.HL.out.f} := \frac{sd_{T.HL.out.f}}{\sqrt{n}} = 0.0034 \cdot \Delta°C$$

4.2 Calculation of Random uncertainty of the result

$$s_R := \left[\begin{array}{l} \left(\Delta m_{dot.CL.f} s_{m.dot.CL.c}\right)^2 + \left(\Delta m_{dot.CL.c} s_{m.dot.CL.f}\right)^2 + \left(\Delta T_{CL.out.c} s_{T.CL.out.c}\right)^2 + \left(\Delta T_{CL.out.f} s_{T.CL.out.f}\right)^2 + \left(\Delta T_{CL.in.c} s_{T.CL.in.c}\right)^2 \cdots \\ + \left(\Delta T_{CL.in.f} s_{T.CL.in.f}\right)^2 + \left(\Delta T_{HL.in.c} s_{T.HL.in.c}\right)^2 + \left(\Delta T_{HL.in.f} s_{T.HL.in.f}\right)^2 + \left(\Delta T_{HL.out.c} s_{T.HL.out.c}\right)^2 + \left(\Delta T_{HL.out.f} s_{T.HL.out.f}\right)^2 \end{array} \right]^{0.5} = 9.589 \times 10^{-8} \cdot \frac{m^2 \cdot K}{W}$$

$$s_{R.relative} := \frac{s_R}{R_f} = 0.433 \cdot \%$$

5. Systematic Uncertainty

5.1 Calculation of Systematic uncertainty of measurements

All systematic uncertainties are given at 95% confidence limits from their respective sources. It is for this reason that they are divided by two to ensure the values used are at 65% confidence level like the test of the calculation. The final result is then converted back to a 95% confidence level.

$$b_{m.dot.CL.c} := m_{dot.CL.c}\frac{\left[0.1\% + \left[\left(\frac{0.9\frac{kg}{3600s}}{m_{dot.CL.c}}\right)\cdot 100\right]\%\right]}{2} = 0.0004\frac{kg}{s} \qquad b_{m.dot.CL.f} := m_{dot.CL.f}\frac{\left[0.1\% + \left[\left(\frac{0.9\frac{kg}{3600s}}{m_{dot.CL.f}}\right)\cdot 100\right]\%\right]}{2} = 0.0004\frac{kg}{s}$$

$$b_{T.CL.in.c} := \frac{0.100185}{2}\Delta°C = 0.0501K \qquad b_{T.CL.in.f} := \frac{0.100185}{2}\Delta°C = 0.0501K$$

$$b_{T.CL.out.c} := \frac{0.100014}{2}\Delta°C = 0.05K \qquad b_{T.CL.out.f} := \frac{0.100014}{2}\Delta°C = 0.05K$$

$$b_{T.HL.in.c} := \frac{0.100204}{2}\Delta°C = 0.0501K \qquad b_{T.HL.in.f} := \frac{0.100204}{2}\Delta°C = 0.0501K$$

$$b_{T.HL.out.c} := \frac{0.100145}{2}\Delta°C = 0.0501K \qquad b_{T.HL.out.f} := \frac{0.100145}{2}\Delta°C = 0.0501K$$

$$b_{Cp.CL.c} := Cp_{CL.c}\frac{0.5\%}{2} = 0.0105\frac{kJ}{kg\cdot K} \qquad b_{Cp.CL.f} := Cp_{CL.f}\frac{0.5\%}{2} = 0.010454\frac{kJ}{kg\cdot K}$$

5.2 Calculation of Correlation factors

Since the same instruments are used for measurements in the clean and fouled conditions, these are considered 100% correlated.

$$b_{m.dot.CL} := b_{m.dot.CL.c} \cdot b_{m.dot.CL.f} = 1.57 \times 10^{-7} \frac{kg^2}{s^2}$$

$$b_{T.CL.in} := b_{T.CL.in.c} \cdot b_{T.CL.in.f} = 2.509 \times 10^{-3} K^2$$

$$b_{T.CL.out} := b_{T.CL.out.c} \cdot b_{T.CL.out.f} = 2.501 \times 10^{-3} K^2$$

$$b_{T.HL.in} := b_{T.HL.in.c} \cdot b_{T.HL.in.f} = 2.51 \times 10^{-3} K^2$$

$$b_{T.HL.out} := b_{T.HL.out.c} \cdot b_{T.HL.out.f} = 2.507 \times 10^{-3} K^2$$

Since the same tables are used to determine Cp, these are considered 100% correlated.

$$b_{CP} := b_{Cp.CL.c} \cdot b_{Cp.CL.f} = 109.285 \frac{m^4}{K^2 \cdot s^4}$$

5.3 Calculation of Systematic uncertainty of the result

$$b_R := \left[\begin{array}{l} \left(\Delta m_{dot.CL.f} \cdot b_{m.dot.CL.c}\right)^2 + \left(\Delta m_{dot.CL.c} \cdot b_{m.dot.CL.f}\right)^2 + \left(\Delta T_{CL.out.c} \cdot b_{T.CL.out.c}\right)^2 + \left(\Delta T_{CL.out.f} \cdot b_{T.CL.out.f}\right)^2 + \left(\Delta T_{CL.in.c} \cdot b_{T.CL.in.c}\right)^2 \cdots \\ + \left(\Delta T_{CL.in.f} \cdot b_{T.CL.in.f}\right)^2 + \left(\Delta T_{HL.in.c} \cdot b_{T.HL.in.c}\right)^2 + \left(\Delta T_{HL.in.f} \cdot b_{T.HL.in.f}\right)^2 + \left(\Delta T_{HL.out.c} \cdot b_{T.HL.out.c}\right)^2 + \left(\Delta T_{HL.out.f} \cdot b_{T.HL.out.f}\right)^2 \cdots \\ + \left(\Delta Cp_{CL.c} \cdot b_{Cp.CL.c}\right)^2 + \left(\Delta Cp_{CL.f} \cdot b_{Cp.CL.f}\right)^2 + 2 \cdot \Delta m_{dot.CL.f} \cdot \Delta m_{dot.CL.c} \cdot b_{m.dot.CL} + 2 \cdot \Delta T_{CL.in.c} \cdot \Delta T_{CL.in.f} \cdot b_{T.CL.in} \cdots \\ + 2 \cdot \Delta T_{CL.out.c} \cdot \Delta T_{CL.out.f} \cdot b_{T.CL.out} + 2 \cdot \Delta T_{HL.in.c} \cdot \Delta T_{HL.in.f} \cdot b_{T.HL.in} + 2 \cdot \Delta T_{HL.out.c} \cdot \Delta T_{HL.out.f} \cdot b_{T.HL.out} + 2 \cdot \Delta Cp_{CL.c} \cdot \Delta Cp_{CL.f} \cdot b_{CP} \end{array} \right]^{0.5} = 5.993 \times 10^{-7} \cdot \frac{m^2 \cdot K}{W}$$

$$b_{R.relative} := \frac{b_R}{R_f} = 2.705 \cdot \%$$

6. Combined Uncertainty

$$u_R := \sqrt{\left(s_R\right)^2 + \left(b_R\right)^2} = 6.069 \times 10^{-7} \cdot \frac{m^2 K}{W}$$

$$u_{R.relative} := \frac{u_R}{R_f} = 2.74 \cdot \%$$

7. Expanded Uncertainty

$$t_{95} := 2$$

$$U_R := t_{95} \cdot u_R = 1.214 \times 10^{-6} \cdot \frac{m^2 K}{W}$$

$$U_{R.relative} := \frac{U_R}{R_f} = 5.479 \cdot \%$$

Appendix G. Ethics Form

Application for Approval of Ethics in Research (EiR) Projects
Faculty of Engineering and the Built Environment, University of Cape Town

APPLICATION FORM

Please Note:
Any person planning to undertake research in the Faculty of Engineering and the Built Environment (EBE) at the University of Cape Town is required to complete this form **before** collecting or analysing data.The objective of submitting this application *prior* to embarking on research is to ensure that the highest ethical standards in research, conducted under the auspices of the EBE Faculty, are met. Please ensure that you have read, and understood the **EBE Ethics in Research Handbook**(available from the UCT EBE, Research Ethics website) prior to completing this application form: http://www.ebe.uct.ac.za/usr/ebe/research/ethics.pdf

APPLICANT'S DETAILS		
Name of principal researcher, student or external applicant		Nicolaas Hallatt
Department		Mechanical Engineering
Preferred email address of applicant:		Nicolaas.Hallatt@Eskom.co.za
If a Student	Your Degree: e.g., MSc, PhD, etc.,	MSc
	Name of Supervisor (if supervised):	Wim Fuls
If this is a researchcontract, indicate the source of funding/sponsorship		
Project Title		Feedwater Heater Fouling Investigation

I hereby undertake to carry out my research in such a way that:

- there is no apparent legal objection to the nature or the method of research; and
- the research will not compromise staff or students or the other responsibilities of the University;
- the stated objective will be achieved, and the findings will have a high degree of validity;
- limitations and alternative interpretations will be considered;
- the findings could be subject to peer review and publicly available; and
- I will comply with the conventions of copyright and avoid any practice that would constitute plagiarism.

SIGNED BY	Full name	Signature	Date
Principal Researcher/ Student/External applicant	Nicolaas Hallatt	Signature Removed	18/01/2017

APPLICATION APPROVED BY	Full name	Signature	Date
Supervisor (where applicable)	A/Prof Wim Fuls	Signature Removed	2017/1/18
HOD (or delegated nominee) Final authority for all applicants who have answered NO to all questions in Section1; and for all Undergraduateresearch (Including Honours).	Prof T. Bello-Ochende	Signature Removed	19/01/2017
Chair : Faculty EIR Committee For applicants other than undergraduate students who have answered YES to any of the above questions.			